Sources and proxy potential of long-chain diols in marine and continental settings

Julie Lattaud

Members of the reading committee:
Prof. dr. Geert-Jan Brummer
Dr. Vincent Grossi
Prof. dr. Lucas Lourens
Prof. dr. Gert-Jan Reichart
Prof. dr. Jaime Toney

This research has been funded by the European Research Council (ERC) under the European Union's Seventh Framework Program (FP7/2007-2013) ERC grant agreement [339206] to Stefan Schouten. The work was further supported by funding from the Netherlands Earth System Science Center (NESSC) through a gravitation grant (NWO 024.002.001) from the Dutch Ministry for Education, Culture and Science to Jaap S. Sinninghe Damsté and Stefan Schouten.

Cover design Julie Lattaud and Rose Leahy
Printed by Ipskamp
ISBN 978-94-028-1450-7

Sources and proxy potential of long-chain diols in marine and continental settings

Herkomst en proxy-potentieel van langketige diolen in mariene en continentale milieus

(met een samenvatting in het Nederlands)

Les diols à longue chaine marins et terrestres, de potentiels proxies ?

(avec un résumé en français)

Proefschrift
ter verkrijging van de graad van doctor aan de Universiteit Utrecht op gezag van de rector magnificus, prof.dr. H.R.B.M. Kummeling, ingevolge het besluit van het college voor promoties in het openbaar te verdedigen op vrijdag 10 mei 2019 des middags te 2.30 uur

door

Julie Lattaud

geboren op 2 december 1990
te Chalon sur Saône, Frankrijk

Promotoren: Prof.dr. S. Schouten
Prof.dr. J. S. Sinninghe Damsté

Contents

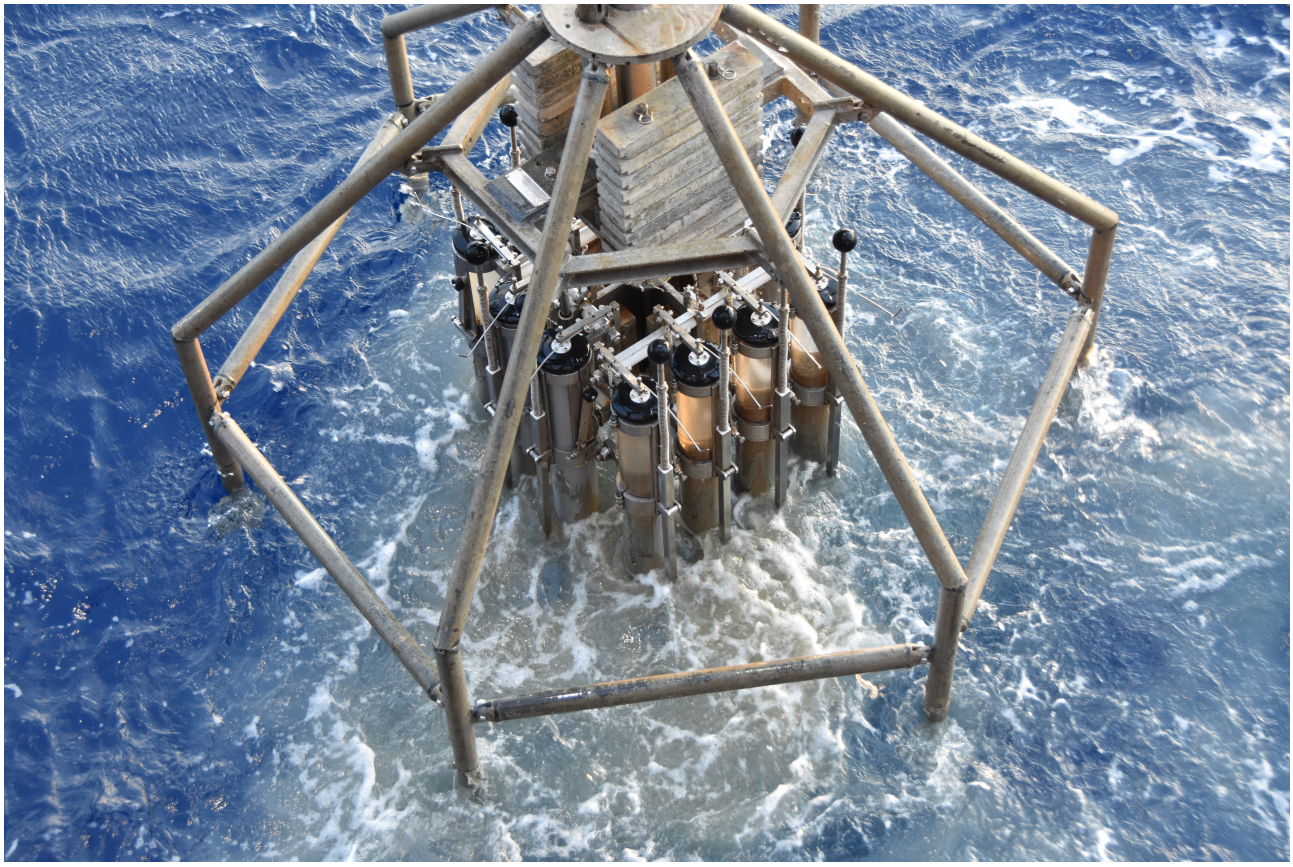

Recovery of multicores, cruise 64PE434, March 2018, credit @Wouter Hooijmans

Summary

Understanding past climate variability is of key importance to better predict future climatic evolution. Models used to predict future climatic changes such as sea-level rise, temperature increase or water-column hypoxia are often tested and validated by their ability to mimic past climate variability due to changes in environmental factors and orbital configurations. As instrumental records are limited in time, geological archives such as tree rings, ice cores and sedimentary records are used. So-called proxies, obtained by the analyses of these sedimentary records, are used to reconstruct past environmental settings and climate change. Paleontological proxies such as the distribution of dinoflagellate cysts, inorganic proxies like stable isotopic compositions of foraminifera shells and organic proxies based on biomarkers represent different types of proxies. The organic ones reflect specific source organisms, their habitats and/or biochemical processes at the time of deposition. However, as these proxies have limitations they have to be studied extensively and new ones need to be developed.

In this thesis the focus is on one class of biomarkers and their potential as proxy: the long-chain diols. These compounds have a long carbon chain with two hydroxyl groups, are often resistant to degradation and can be found in sediments up to 65 million years old. They are widespread common compounds in marine and freshwater environments although their source organism(s) are not well known. In freshwater environments, eustigmatophytes, a group of unicellular phototrophic algae, are probably the main producers, while in the marine realm the sources of just a few long-chain diols are well known. The 1,14-diols are produced by *Proboscia* diatoms and *Apedinella radians*, whereas the source organisms of the other long-chain diols, i.e. 1,13- and 1,15-diols, are unknown.

The relative abundance of long-chain diols varies with sea water temperature, the C_{30} 1,15-diol being more abundant in warmer waters, while the 1,13-diols (C_{28} and C_{30}) are more abundant in colder waters. Following this observation, the Long-chain Diol Index (LDI) has been developed and a calibration curve of this proxy based on the analysis of a large number of surface sediments distributed worldwide permitted the reconstruction of sea surface temperature (SST) in the past. However, due to the lack of knowledge of marine long-chain diol producers and their habitats, the LDI cannot be calibrated using laboratory cultures. Related to this, it is not clear how far back in time the LDI can be applied to reliably reconstruct SST. This lack of knowledge regarding the sources and the controls on long-chain diol distributions in the water column is also severely hampering their application as reliable proxies.

This thesis focuses on understanding what exactly determines long-chain diol distributions, which organism(s) are producing them in marine and freshwater environments, and how they can be reliably used as proxies to reconstruct the past. The thesis is divided into two parts: Part I focuses on long-chain diols in modern marine and freshwater environments and Part II describes the application of long-chain diol proxies.

Part I integrates results of modern long-chain diol distributions determined in present-day settings going from the open ocean to rivers and lakes via coastal margins. In an equatorial cross Atlantic transect, long-chain diols in the water column were dominated by the C_{30} 1,15-diol, in agreement with the presence of relatively warm surface water. However, 18S rRNA analysis suggested that this and other long-chain diols were not derived from in situ production but from dead organic matter, severely hampering lipid/DNA comparisons and the search for their source organisms. Surprisingly, the Amazon plume, representing the western end of the transect, did not seem to impact the marine long-chain diol distributions. To investigate if other rivers and terrestrial organic matter have an effect on marine long-chain diol distributions, four coastal margins influenced by major rivers were examined. The C_{32} 1,15-diol was recognized as an important component of riverine origin. Because other long-chain diols are also partly derived from the rivers, in particular the C_{30} 1,15-diol, the LDI is not properly reflecting SST. Thus, along coastal margins impacted by riverine organic matter, the LDI is not reliable. We therefore developed a tool to assess if the sampling site is influenced by rivers using the fractional abundance of the C_{32} 1,15-diol ($F_{C32\ 1,15}$), which increases upon increasing river impact. We suggest that this

new proxy can be used to trace river influence in past coastal settings (see below).

Since the sources and controls of freshwater diols are not yet well understood in river systems, we studied the Godavari, Danube and Rhine rivers. Long-chain diol concentrations were found to be enhanced in low flow areas such as lakes and side ponds. Therefore, two lakes were investigated, namely temperate Lake Geneva (Switzerland/France) and tropical Lake Chala (Kenya/Tanzania). In Lake Geneva, the long-chain diols were mainly produced from spring to late summer and their relative distributions changed over this period. Their production was enhanced during periods of thermal stratification of the water column. These results were confirmed by the four years sediment trap study of Lake Chala. 18S rRNA analysis of Suspended Particulate Matter (SPM) from Lake Geneva corroborated previous findings that eustigmatophytes produce long-chain diols in freshwater systems. Species related to *Nannochloropsis* spp. were probably responsible for the C_{32} 1,15-diol production during spring, while species related to *Ellipsoidion edaphicum* might have been responsible for the abundance of C_{30} 1,15-diol during summer, although their long-chain diol distributions have not been studied in cultures.

In part II, the new proxy developed to trace river input in shelf seas, $F_{C32\ 1,15}$, as well as other diol proxies were tested and applied to the analyses of several sedimentary cores. A comparison of the $F_{C32\ 1,15}$ with the BIT index (a proxy for river and soil input) in sedimentary cores from the Mozambique Channel, offshore the Zambezi River and in the eastern Mediterranean, offshore the Nile River, showed a close correspondence, further confirming the applicability of $F_{C32\ 1,15}$ to trace river input. Periods during which the results of the two proxies differed corresponded to periods of changes in sources of soil input, indicating that a multi-proxy study allows for a better understanding of erosion processes.

The $F_{C32\ 1,15}$ was also applied to reconstruct the past in a long sedimentary core, covering the last 1.5 million years, from the central Sea of Okhotsk. As observed in the case of the Mozambique Channel and Mediterranean Sea, $F_{C32\ 1,15}$ was mainly driven by changes in sea-level. Its periodicity was dominated by the 100-kyr Milankovitch orbital cycle. This cycle, which is caused by changes in the eccentricity of Earth's orbit, causes changes in the global ice volume and sea levels over such timescales. The LDI temperature proxy was indicative of autumn SST during the Holocene and other interglacials whereas it seemed to reflect summer SST during glacial periods. This shift in glacial/interglacial seasonality was responsible for the lack of a strong periodicity in the LDI record. Furthermore, proxies based on the occurrence of 1,14-diols clearly indicated a periodicity of *Proboscia* diatom productivity over such timescales. The primary productivity in the Sea of Okhotsk was enhanced during deglaciations and was mainly driven by sea ice advance and retreat, as indicated by the dominant 100-kyr periodicity of the 1,14-diols record.

The results described in this thesis allowed for the development of a new diol-based proxy for river input, which, in combination with other proxies, enables a much better understanding of riverine production and transport, and of soil erosion processes. Furthermore, the limitations of previously developed long-chain diol-based proxies are now better recognized. New paleo-reconstructions in both tropical and polar regions have been generated, enabling improved reconstructions of past climatic changes and a potential to better test and validate climate models.

Résumé

Comprendre la variabilité du climat dans le passé est d'une importance capitale pour pouvoir mieux prévoir son évolution dans le futur. Les modèles climatiques utilisés pour prévoir les changements futurs, tels que l'élévation du niveau de la mer, la hausse des températures ou l'augmentation de l'hypoxie dans la colonne d'eau, sont souvent testés et validés en les comparant à des observations obtenues sous les mêmes configurations environnementales et orbitales. Comme les enregistrements instrumentaux sont limités dans le temps, des archives géologiques sont utilisées, telles que les cernes d'arbres, les carottes de glace et les enregistrements sédimentaires. De ces enregistrements sédimentaires sont extraits des proxies qui contiennent des informations climatiques et environnementales. Les proxies peuvent varier en nature, ils peuvent être paléontologiques tels que la distribution de kystes de dinoflagellés, inorganiques comme la composition isotopique de la coquille de foraminifères ou organiques à l'aide de molécules appelées biomarqueurs. Ces derniers sont spécifiques d'un organisme source et/ou d'un processus biogéochimique. Cependant, comme ces proxies ont des limites, ils doivent être étudiés en profondeur et de nouveaux proxies doivent être développés.

Dans cette thèse, l'accent est mis sur une classe de biomarqueurs et leur potentiel en tant que proxy: les diols à longue chaîne. Ces composés possèdent une longue chaîne carbonée et deux groupes hydroxyle, ils sont résistants à la dégradation et peuvent être extraits de sédiment vieux de 65 millions d'années. Ce sont des molécules communes dans les milieux marins et d'eau douce, mais leur(s) organisme(s) source n'est pas bien contraint. En eau douce (lacs, rivières), les eustigmatophytes, algues unicellulaires phototrophes, en sont probablement les principaux producteurs, tandis que dans le milieu marin, les sources de certains isomères sont très bien contraintes. Par exemple, les 1,14-diols sont produits par les diatomées *Proboscia* et les dictyochophytes appartenant à l'espèce *Apedinella radians*, tandis que les organismes sources des autres diols (1,13 et 1,15-diols) sont inconnus. L'abondance relative des isomères des diols varie en fonction de la température de l'eau de mer. Le C_{30} 1,15-diol est plus abondant dans les eaux chaudes, tandis que les 1,13-diols sont plus abondants dans les eaux froides. Suite à cette observation, le Long-chain Diol Index (LDI) a été créé et une courbe d'étalonnage permet de reconstituer la température de la surface de la mer dans le passé. Mais, en raison du manque de connaissances sur les producteurs des diols marins et leurs habitats, le LDI ne peut pas être calibré à l'aide de cultures en laboratoire. De fait, il n'est pas clair dans quelle mesure le LDI peut être appliqué dans le passé pour reconstruire la température de l'eau de mer. Le manque de connaissances sur les sources de ces diols et sur les facteurs contrôlant leur distribution dans la colonne d'eau entrave gravement leur application. Cette thèse vise à comprendre ce qui contrôle la distribution des diols à longue chaîne, quel(s) sont les organisme(s) producteur(s) en milieux marins et d'eau douce, et aussi comment ils peuvent être utilisés comme proxy de manière fiable. Pour atteindre ces objectifs, cette thèse est divisée en deux parties: la première partie se concentre sur les diols à longue chaîne dans des environnements marins et d'eau douce actuels et la deuxième partie porte sur l'application de proxies basés sur les diols dans le passé.

La première partie présente des résultats sur la distribution des diols à longue chaîne dans plusieurs contextes, de l'océan aux rivières et lacs en passant par les marges côtières du monde entier. Dans la colonne d'eau d'un transect transatlantique, les particules organiques en suspension sont dominés par un des isomères, le C_{30} 1,15-diol, ce qui est en accord avec la présence d'eau relativement chaude. Cependant, l'analyse de l'ARNr 18S suggère que les diols à longue chaîne ne proviendraient pas d'une production in situ mais de matière organique morte, ce qui entraverait gravement les comparaisons lipides/ADN et la découverte des organismes sources. La présence du plume amazonien (présent a l'ouest du transect et représentant une grosse quantité d'eau douce) n'influe pas sur le LDI et la reconstruction de la température de l'eau de mer. Pour étudier plus précisément si les rivières, et la matière organique terrestre en général, ont un effet sur la distribution des diols à longue chaîne, nous avons examiné quatre marges côtières sous influence de rivières majeures. Un isomère semble provenir principalement des rivières, le C_{32} 1,15-diol,

mais comme d'autres isomères dérivent aussi partiellement des rivières, en particulier le C_{30} 1,15-diol, le LDI ne reflète pas correctement la température de l'eau de mer. En conclusion, le long des marges côtières sous influence fluviale, le LDI n'est pas fiable. Nous avons développé un moyen d'évaluer si le site d'échantillonnage est influencé par une rivière en utilisant l'abondance relative du C_{32} 1,15 diol, qui augmente avec l'influence de la rivière. Nous suggérons que ce nouveau proxy peut être utilisé pour retracer l'influence des rivières dans le passé.

Etant donné que les sources et les contrôles des diols d'eau douce ne sont pas encore bien compris, des rivières et leurs affluents ont été étudiés : les rivières Godavari, Danube et Rhin. Dans ces rivières et leurs affluents, les concentrations des diols à longue chaîne augmentent dans les zones à faible débit d'eau, comme les lacs de barrage et les étangs. Par conséquent, deux lacs ont été étudiés, à savoir, le lac Léman en milieu tempéré et le lac Chala sous climat tropical. Les résultats indiquent que dans le lac Léman, les diols à longue chaîne sont produits in situ au cours de saisons précises, du printemps à la fin de l'été, et que leur distribution relative change. De plus, leur production est accrue pendant la période de stratification thermique de la colonne d'eau. Ces résultats sont confirmés par l'étude, sur quatre ans, du piège à sédiments du lac Chala. L'analyse de l'ARNr 18S des particules en suspension présentes dans la colonne d'eau du lac Léman confirme des découvertes précédemment publiées selon lesquelles les eustigmatophytes produisent les diols à longue chaîne dans les milieux d'eau douce. Les espèces du genre *Nannochloropsis* sont probablement responsables de la production accrue du C_{32} 1,15 diol au printemps, tandis que les espèces apparentées à *Ellipsoidion edaphicum* pourraient être responsables de l'abondance du C_{30} 1,15 diol en été, bien que la distribution des diols à longue chaîne de cette espèce n'ait pas été étudiée.

Dans la partie II, le nouveau proxy permettant de suivre l'influence des rivières dans les marges continentales, *i.e.* l'abondance du C_{32} 1,15-diol par rapport aux autres diols ($F_{C32\ 1,15}$), ainsi que d'autres proxies basés sur les diols ont été testés et appliqués à plusieurs carottes sédimentaires. Une comparaison du nouveau $F_{C32\ 1,15}$ avec l'indice BIT (indicateur des apports provenant des rivières et des sols, couramment utilisé) dans une carotte sédimentaire de la mer du Mozambique, au large du fleuve Zambèze et dans une carotte provenant de l'est de la Méditerranée, au large du Nile, montre une forte corrélation confirmant l'utilisation du $F_{C32\ 1,15}$ pour tracer l'influence des rivières dans le passé. Les périodes au cours desquelles les deux proxies diffèrent correspondraient à des périodes de changement de source des sols érodés, ce qui indique qu'une étude multi-proxy permettrait de mieux comprendre les processus d'érosion. Le $F_{C32\ 1,15}$ a également été utilisé sur une longue carotte sédimentaire (1,5 million d'années) provenant du centre de la mer d'Okhotsk. Comme pour les carottes de la mer du Mozambique et de la mer Méditerranée, le $F_{C32\ 1,15}$ était principalement contrôlé par les variations du niveau de la mer. Sa périodicité était dominée par un cycle orbital de 100 kyr (caractéristique de l'excentricité définie par Milankovitch) qui régissait le volume des glaces et le niveau de la mer à cette échelle de temps. Le LDI dans cette carotte permettrait de reconstruire la température de surface de la mer en automne au cours de l'Holocène et d'autres périodes interglaciaires, alors qu'il permettrait de reconstruire la température de surface de la mer en été pendant les périodes glaciaires. Ce changement de saisonnalité est probablement à l'origine de l'absence de périodicité significative dans l'enregistrement sédimentaire du LDI. Au contraire, les proxies basés sur les 1,14-diols semblent refléter avec succès la productivité des diatomées *Proboscia*. La productivité primaire dans la mer d'Okhotsk a augmenté au cours des déglaciations et était principalement influencée par les avancées et reculs de la glace de mer, qui étaient dominés par une périodicité de 100 kyr qui est aussi retrouvée dans l'enregistrement des 1,14 diols.

Les résultats de cette thèse ont permis de développer un nouveau proxy basé sur un diol provenant des rivières, qui permet une meilleure compréhension de la production de matière organique et son transport le long des fleuves et, associé à d'autres proxies, des processus d'érosion des sols. En outre, les proxies basés sur les diols précédemment développés sont maintenant mieux compris et leurs limites connues. Enfin, de nouvelles reconstructions paleoclimatiques ont été générées dans des régions tropicales et polaires, ce qui peut être utile pour reconstruire les changements climatiques passés et potentiellement tester des modèles climatiques.

Samenvatting

Inzicht in klimaatvariabiliteit is van groot belang om toekomstige klimaatveranderingen, zoals zeespiegelstijging, temperatuurstijging of zuurstofgebrek in het water, beter te kunnen voorspellen. Modellen die worden gebruikt om klimaatveranderingen te voorspellen, worden vaak getest en aangepast op basis van hun vermogen om klimaatvariabiliteit in het verleden te reconstrueren. Om aan gegevens uit het verleden te komen, worden geologische archieven zoals boomringen, ijskernen en sedimenten gebruikt.

Op basis van deze geologische gegevens worden zogeheten proxy's ontwikkeld. Deze proxy's kunnen gebruikt worden om omgevingsfactoren en klimaatveranderingen te reconstrueren. Verschillende proxy's zijn paleontologische proxy's, zoals de verspreiding van cysten van dinoflagellaten, anorganische proxy's zoals de hoeveelheden van stabiele isotopen in de schelpen van foraminiferen, en organische proxy's zoals de aanwezigheid van bepaalde organische stoffen (biomarkers). De organische proxy's geven informatie over de aanwezigheid van specifieke organismen, hun habitats en/of de biochemische processen op het moment van depositie. Omdat deze proxy's beperkingen hebben, moeten ze uitgebreid worden onderzocht en moeten er nieuwe worden ontwikkeld.

In dit proefschrift ligt de nadruk op één groep van organische stoffen: langeketendiolen. Deze verbindingen hebben een lange koolstofketen met twee hydroxylgroepen. Ze worden niet snel afgebroken en kunnen aangetroffen worden in sedimenten tot 65 miljoen jaar oud. Het zijn veel voorkomende verbindingen in zeewater en zoet water. Helaas is niet altijd bekend welke organismen deze verbindingen maken. In zoet water zijn eustigmatofyten (eencellige fototrofe algen) waarschijnlijk de belangrijkste producenten, terwijl in zee de oorsprong van slechts enkele langeketendiolen bekend is. 1,14-diolen worden geproduceerd door *Proboscia* diatomeeën en *Apedinella radians*, terwijl de producenten van de andere langeketendiolen, zoals 1,13- en 1,15-diolen, niet bekend zijn.

De relatieve hoeveelheden van langeketendiolen variëren met de temperatuur van het water, waarbij het C_{30} 1,15-diol meer aanwezig is in warm water, terwijl de 1,13-diolen (C_{28} en C_{30}) meer aanwezig zijn in koud water. Op basis van deze waarneming is de Long-chain Diol Index (LDI) ontwikkeld. Analyses van een groot aantal topsedimenten wereldwijd maakten het mogelijk om voor deze proxy een kalibratiecurve op te stellen. Zo werd de reconstructie van de zeewatertemperatuur (SST) in het verleden mogelijk. Maar door het gebrek aan kennis van diolproducenten in zee kon de LDI niet worden gekalibreerd met laboratoriumculturen. Ook is niet duidelijk hoe ver terug in de tijd de LDI kan worden toegepast om de SST betrouwbaar te reconstrueren. Dit gebrek aan kennis van de producenten belemmert de toepassing van de LDI als een betrouwbare proxy.

Dit proefschrift gaat over de verspreiding van langeketendiolen in zeewater en zoet water, welke organismen ze produceren en hoe ze betrouwbaar kunnen worden gebruikt als proxy's om het verleden te reconstrueren. Het proefschrift bestaat uit twee delen: Deel I richt zich op langeketendiolen in hedendaagse zee- en zoetwateromgevingen en deel II beschrijft de toepassing van proxy's die gebaseerd zijn op langeketendiolen.

Deel I beschrijft de verspreiding van langeketendiolen in hedendaagse milieus, variërend van open oceanen en kustgebieden tot rivieren en meren. In een equatoriaal Atlantisch transect werden de langeketendiolen in de waterkolom gedomineerd door het C_{30} 1,15-diol, wat te verwachten was omdat het oppervlaktewater warm was. 18S-rRNA-analyse wees er echter op dat deze en andere langeketendiolen niet afkomstig waren van in situ productie, maar van dood organisch materiaal. Hierdoor was het niet mogelijk om te bepalen welk organisme de diolen heeft geproduceerd.

De uitstroom van de Amazone, in het westen van het transect, bleek tegen de verwachting in geen invloed te hebben op de verdeling van de langeketendiolen in zee. Om te onderzoeken of rivieren en/of van het land afkomstige organische stoffen een effect hebben op de diolverdelingen in zee, werden vier kustgebieden in de buurt van grote rivieren onderzocht. Het C_{32} 1,15-diol bleek een belangrijke component in rivierwater te zijn. Aangezien andere diolen, met name het C_{30} 1,15-diol, ook deels afkomstig kunnen zijn uit rivieren, geeft de

LDI de SST niet correct weer. In kustgebieden die beïnvloed worden door organisch materiaal uit een rivier, is de LDI dus niet betrouwbaar.

Daarom hebben we op basis van het C_{32} 1,15-diol een proxy ontwikkeld om te bepalen of kustgebieden worden beïnvloed door rivieren. Deze proxy, $F_{C32\ 1,15}$, is de fractionele hoeveelheid van het C_{32} 1,15-diol en deze neemt toe bij toenemende invloed van de rivier. De nieuwe proxy kan worden gebruikt om de invloed van rivieren nauwkeuriger te bepalen (zie hieronder).

Omdat nog niet goed bekend is welke eustigmatofyten in zoet water diolen produceren, hebben we de rivieren Godavari, Donau en Rijn bestudeerd. De concentraties van langeketendiolen bleken hoog te zijn in water met weinig stroming zoals meren. Daarom werden twee meren onderzocht, namelijk het Meer van Genève (Zwitserland/Frankrijk) en het tropische Chalameer (Kenia/Tanzania). In het Meer van Genève werden de langeketendiolen voornamelijk geproduceerd vanaf de lente tot de late zomer en hun relatieve verdeling in deze periode bleek te veranderen. Tijdens de periode van thermische stratificatie gedurende de zomer ging de productie van diolen door eustigmatofyten omhoog. Deze resultaten werden bevestigd door een vier jaar durend sedimentatie-onderzoek in het Chalameer. 18S rRNA-analyse van gesuspendeerd materiaal uit het Meer van Genève bevestigde eerdere bevindingen dat eustigmatofyten langeketendiolen produceren in zoetwatersystemen. Waarschijnlijk zijn soorten die verwant zijn met *Nannochloropsis* spp. verantwoordelijk voor de productie van het C_{32} 1,15-diol tijdens de lente, terwijl soorten die verwant zijn met *Ellipsoidion edaphicum* mogelijk verantwoordelijk zijn voor de productie van C_{30} 1,15-diol tijdens de zomer. De productie van langeketendiolen is echter niet in culturen bekeken.

Deel II beschrijft hoe de nieuwe proxy ($F_{C32\ 1,15}$) voor het aantonen van rivierinvloed in kustgebieden en andere diolproxy's zijn getest door verschillende sedimentkernen te analyseren. Een vergelijking van de $F_{C32\ 1,15}$ met de BIT-index (een andere indicator voor rivier- en bodeminvloed) in sedimentkernen uit de Straat Mozambique, voor de monding van de Zambezi-rivier, en uit het oostelijke Middellandse Zeegebied, voor de monding van de Nijl, vertoonde een goede overeenkomst en bevestigde daarmee de toepasbaarheid van $F_{C32\ 1,15}$ om rivierinvloed aan te tonen.

Perioden waarin de resultaten van de twee proxy's verschilden, kwamen overeen met perioden van veranderingen in terrestrische invloed, wat aangeeft dat een multi-proxy-studie een beter begrip van erosieprocessen mogelijk maakt. De $F_{C32\ 1,15}$-proxy werd ook toegepast om het verleden te reconstrueren door analyse van een lange sedimentkern uit de Zee van Ochotsk. Deze kern bestreek de afgelopen 1,5 miljoen jaar. Net als in de Straat Mozambique en de Middellandse Zee, werd de $F_{C32\ 1,15}$ voornamelijk bepaald door veranderingen in de zeespiegel. Deze veranderingen zijn een gevolg van de 100.000 jaar durende Milankovitch-cyclus, die wordt bepaald door de excentriciteit van de aardbaan om de zon.

De LDI-proxy wees op herfsttemperaturen tijdens het Holoceen en andere interglacialen en op zomertemperaturen tijdens glaciale perioden. Door dit verschil tussen de interglacialen en glacialen was er geen sterke periodiciteit in de LDI-gegevens te zien. Bovendien geven proxy's gebaseerd op 1,14-diolen een duidelijke indicatie van de productiviteit van Proboscia-diatomeeën. De primaire productiviteit in de Zee van Ochotsk was hoger tijdens interglacialen en werd voornamelijk bepaald door veranderingen in de zeespiegel, zoals blijkt uit de 100.000-jarige periodiciteit van de gegevens van de 1,14-diolen. De resultaten beschreven in dit proefschrift maakten de ontwikkeling mogelijk van een nieuwe proxy om de invloed van rivieren te bepalen. In combinatie met andere proxy's maakt de nieuwe proxy een beter begrip mogelijk van de productie in en het transport door rivieren, en van bodemerosieprocessen. Bovendien worden de beperkingen van eerder ontwikkelde proxy's nu beter herkend. Ten slotte zijn er nieuwe paleoreconstructies in zowel tropische als polaire gebieden uitgevoerd die betere reconstructies van eerdere klimaatveranderingen mogelijk maken en de potentie hebben om klimaatmodellen beter te testen.

Chapter 1

Introduction

1 Reconstructing past environmental changes

The reconstruction of past environmental changes is important to better understand the present climate and to better predict future climate evolution. Over the last decades, climate change has attracted much scientific, economic and societal attention, the more so because human activities are responsible for the on-going global warming observed (Intergovernmental Panel on Climate Change, IPCC 2017). Greenhouse gas concentrations will further increase in the centuries to come to levels not seen since the Paleocene-Eocene Thermal Maximum (Demicco et al. 2003; Smith et al. 2010; Sluijs et al. 2018). The direct and indirect impacts of increasing greenhouse gases on the long term are difficult to predict. Modelling of future climatic evolution is possible but the multiple predicted scenarios need to be tested and validated. Validations of climate change models can be realized by applying these models to past time slices where environmental parameters have been reconstructed using so-called proxies. Proxies are preserved environmental parameters distilled from geological archives that can stand in for direct measurements. Proxies are used to reconstruct paleo-environmental parameters such as sea surface temperature (SST), riverine input, pCO_2, salinity and productivity (e.g. Eglinton and Hamilton 1967; Volkman 1986 Prahl and Wakeham 1987; Rosell-Melé 1998; Pagani 1999; Schouten et al. 2002; Sicre et al. 2002; Hopmans et al. 2004; Rampen et al. 2008, 2012; Castaneda and Schouten 2011). Based on proxy records of appropriate sedimentary archives, past climate changes similar to the present climate change can be reconstructed, enabling a much better understanding of future climate scenarios and validation of present-day climate models. The development of new proxies as well as the refinement of existing ones will result in better and more detailed paleo-climate reconstructions and, therefore, a better understanding of the consequences of the present on-going climate change on both short and long time scales. One class of proxies is based on relatively stable sedimentary lipids called biomarkers, which are indicators for the past presence of certain organisms and consequently for past environmental and climate conditions.

Here, the development and refinement of two organic proxies, for sea surface temperature (SST) reconstructions and for terrestrial input to marine environments, will be discussed.

1.1 SST proxies

The most commonly used organic proxy for SST is the $U^{k'}_{37}$, based on the degree of unsaturation of long-chain alkenones (Fig. 1) produced by several haptophyte algae (De Leeuw et al. 1980; Volkman et al. 1980; Brassell et al. 1986; Prahl and Wakeham 1987). A relative increase of the number of double bonds in the alkenones is indicative for a lower water temperature. The TEX_{86} proxy is also used to reconstruct SST. This index is based on the number of cyclopentyl moieties in glycerol dialkyl glycerol tetraether (GDGT) lipids biosynthetized by Thaumarchaeota in marine environments and depends on water temperature (Schouten et al. 2002). The number of rings increases with increased water temperature to maintain optimal membrane fluidity (Gliozzi et al. 1983, 2002). The $U^{k'}_{37}$ and TEX_{86} proxies, as all proxies, have their limitations as they can be impacted by nutrient limitation, oxic degradation, lateral transport, seasonal production (e.g. Hoefs et al. 1998; Gong and Hollander 1999; Prahl et al. 2003; Sikes et al. 2005; Kim et al. 2009; Rontani et al. 2013) and deep water production of GDGTs and terrigenous input, respectively (Weijers et al. 2007; Huguet et al. 2007; Shintani et al. 2011; Ho et al. 2014; Kim et al. 2015). On the other hand, different SST proxies can be used to better understand climate

change, as for example it enables the reconstruction of seasonal temperatures or temperature of different water depths (e.g. Dos Santos et al. 2010). Thus, multiproxy studies are often performed by combining organic SST proxies and inorganic SST proxies. A very common inorganic SST proxy is the oxygen isotopic ratio ($\delta^{18}O$) of foraminifera shells which can also reflect past sea water temperatures (e.g. Epstein et al. 1953; Shackleton and Opdyke 1973; Erez and Luz 1983).

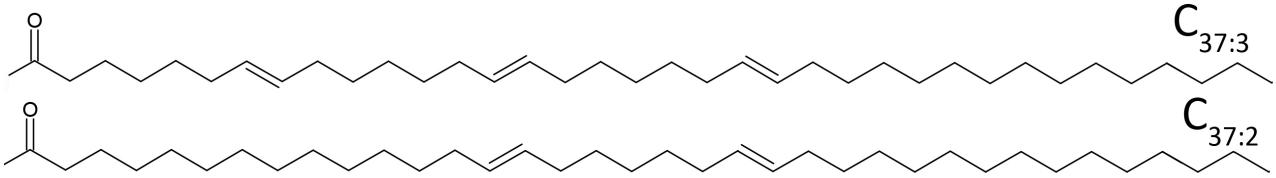

Figure 1: Molecular structures of long-chain alkenones.

1.2 Proxies for terrestrial contribution to marine environments

Terrestrial organic matter (OM) can be differentiated from marine OM using, for example, carbon to nitrogen (C/N) ratios and by the bulk stable carbon isotopic composition ($^{12}C/^{13}C$) of sedimentary OM (e.g., Meyers 1994, Fig. 2). The abundance of N-free macromolecules such as lignin and cellulose in terrestrial plants result in a higher C/N ratio for terrestrial OM compared to OM of aquatic organisms (Hedges et al. 1986). Differences in stable carbon isotopic composition are also used to determine the contribution of terrestrial input to aquatic environments as terrestrial OM is relatively depleted in ^{13}C ($\delta^{13}C$ -28 to -25‰) compared to marine OM ($\delta^{13}C$ -22 to -19‰) (e.g., Hedges et al. 1986). However, both proxies have limitations as the C/N ratio can be biased when plant tissues gain nitrogen during bacterial degradation and when planktonic OM preferentially loses nitrogen over carbon during decay (Hedges et al. 1997). Furthermore, C_4 plants, using a different initial carboxylating enzyme than C_3 plants (i.e. first phosphoenolpyruvate carboxylase instead of Rubisco; Hatch 1992), produce a ^{13}C-enriched OM ($\delta^{13}C$ as low as -15‰; Ehleringer et al. 1997).

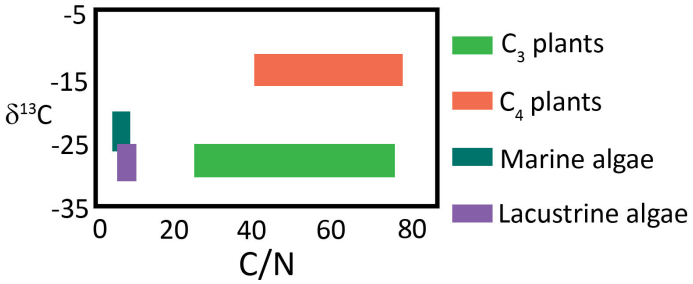

Figure 2: Carbon/nitrogen ratios (C/N) and stable carbon isotopic values of bulk OM (from Meyers 1994).

In addition to bulk proxies like C/N ratio and the isotopic composition of OM, there are many molecular proxies that can be indicative of terrestrial input such as long-chain *n*-alkanes derived from waxes of higher plants (Eglinton and Eglinton 2008, and references cited therein), or methoxy-phenols derived from lignin (Ludwig 1971; Goni et al. 1997). The latter are chemically or pyrolitically released from lignin and suberins and can be source-specific. For example, syringyl phenols are mainly derived from angiosperms. The bacteriohopanepolyol C_{35} adenosylhopanoid is a soil-specific biomarker (Cooke et al. 2008) as it is only produced by soil bacteria and thus can be used for tracing soil erosion and bacterial activity. Branched glycerol dialkyl glycerol tetraethers (brGDGTs) are widely used as soil and riverine biomarkers (e.g. Weijers et al. 2007, 2009; Jonge et al. 2014b). The branched and isoprenoid tetraether (BIT) index indicates the terrestrial contribution to marine environments based on the relative abundance of brGDGTs and crenarchaeol, which is predominantly biosynthetised by marine archaea (Hopmans et al. 2004). However, as before, these biomarker proxies have their limitations, i.e. some long-chain *n*-alkanes are also produced by algae or aquatic macrophytes (Elias et al. 1997; Ficken et al. 2000), lignin and suberin derivatives are difficult to release from sediments and are prone to oxidative degradation

by microorganisms during transport (Goni et al. 1997; Filley et al. 1999; Ward et al. 2013) whereas brGDGT producers are not only soil derived but sometimes also of aquatic origin (Peterse et al. 2009; Sinninghe Damsté 2016).

In addition to the proxies and biomarkers shortly discussed above, long-chain diols are also used to both reconstruct SST and terrestrial contribution to marine ecosystems. The current state of these long-chain diols with respect to sources, biomarker potential and proxy value are discussed hereafter.

2 Discovery of long-chain diols

Long-chain diols are compounds with long unbranched carbon chains (26-36 carbons) and two hydroxyl groups, one at position 1 and one at carbon atom 12 to 16 (Fig. 3). They were first discovered in Unit I (0-3000 yrs BP) and Unit II (3000-7000 yrs BP) of Black Sea sediments by De Leeuw et al. (1981). Later on, Morris and Brassell (1988) and Versteegh et al. (1997) reviewed the occurrence of these lipids and showed that they are widespread in marine sediments ranging in age from the Holocene to the Cretaceous/Paleogene boundary (Fig. 4). The oldest occurrence of long-chain diols is reported from the Geulhemmerberg clay formation (The Netherlands, 65 Ma; Yamamoto et al. 1996). The main long-chain diols encountered in marine sediments are the C_{28} 1,13- and 1,14-diols (Fig. 3a, b), the C_{30} 1,13-, 1,14- and 1,15-diols (Fig. 3c, d, e) and the C_{32} 1,15-diol (Fig. 3f; Morris and Brassell 1988; Versteegh et al. 1997; Gogou and Stephanou 2004; Naafs et al. 2012; Rampen et al. 2012; Dos Santos et al. 2013; Smith et al. 2013; Rodrigo-Gámiz et al. 2014 and reference therein).

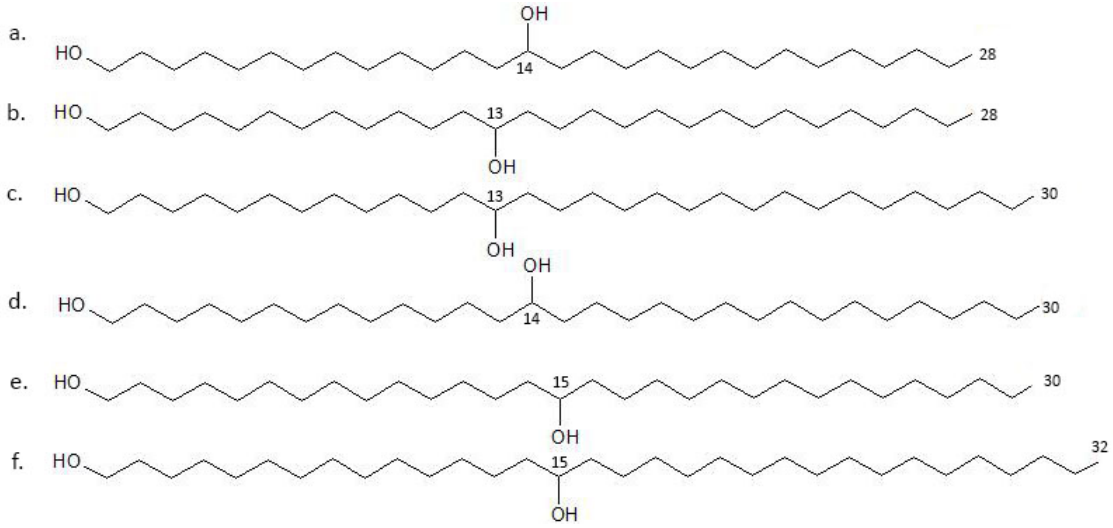

Figure 3: Molecular structures of the most common long-chain diols (a) C_{28} 1,14- (b) C_{28} 1,13- (c) C_{30} 1,13- (d) C_{30} 1,14- (e) C_{30} 1,15- and (f) C_{32} 1,15-diols.

Long-chain diols have also been discovered in lacustrine sediments, first in sediments of Lake Priest Pot by Cranwell et al. (1987) and later on in many lacustrine sediments around the world as reported in Versteegh et al. (1997) and Rampen et al. (2014b) (Fig. 4). They are sometimes the major polar lipids in lake sediments (Castaneda et al. 2011). The dominant diols in lake sediments are the C_{30} 1,15- and C_{32} 1,15-diols (Versteegh et al. 1997; Castaneda et al. 2011; Rampen et al. 2014a and reference cited therein).

3 Origin of long-chain diols

At first, De Leeuw et al. (1981) proposed coccolithophores or bacteria as producers of long-chain diols. But, during their cruise in the Baltic Sea, Morris and Brassell (1988) followed a bloom of cyanobacteria (*Aphanizomenon flos-aquae*) and noticed a high abundance of C_{30} and C_{32} long-chain diols. They, therefore, linked the presence of long-chain diols to the cyanobacterial bloom. However, these diols were not detected in laboratory cultures of the suspected cyanobacterium *A. flos-aquae* (De Leeuw et al. 1992). Volkman et al. (1992) cultured eustigmatophytes (*Nannochloropsis salina*, *Nannochloropsis oculata* and an unnamed species,

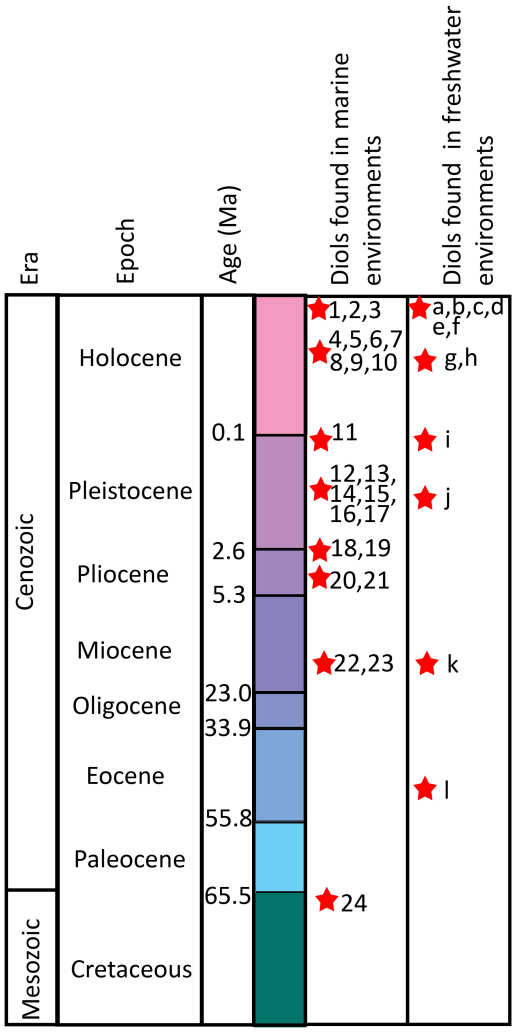

Figure 4: Reports of long-chain diols in marine and lacustrine sediments through time ([1]Shanchun et al. 1994; [2]Smith et al. 2013; [3]Rampen et al. 2014b; [4]de Leeuw et al. 1981; [5]Smith et al. 1983; [6]Morris and Brassell 1988; [7]Middelburg et al. 1993; [8]Willmott et al. 2010; [9]Nieto-Moreno et al. 2013; [10]Rodrigo-Gámiz et al. 2014;[11]Haven et al. 1986; [12]Brassell et al. 1981; [13]Haven et al. 1992; [14]Rampen et al. 2008; [15]Versteegh et al. 2000; [16]Rampen et al. 2012; [17]dos Santos et al. 2013; [18]Comet and Eglinton 1987; [19]Haven et al. 1992; [20]Pancost et al. 2009; [21]Naafs et al. 2012; [22]Yamamoto et al. 1996; [23]Seki et al. 2012; [24]Yamamoto et al. 1996; [a]Cranwell et al. 1987; [b]Robinson et al. 1984; [c]Castaneda et al. 2011; [d]Romero-Viana et al. 2012; [e]Rampen et al. 2014b; [f]Villanueva et al. 2014; [g]Xu et al. 2007; [h]Atwood et al. 2014; [i]Shimokawara et al. 2010; [j]Middelburg et al. 1993; [k]Huang et al. 1995; [l]Zeng et al. 1988)

CS-246, subfamily Monodopsidaceae, family Eustigmatophyceae) and showed the production of long-chain diols by these phototrophic organisms. Ether-bound long-chain alkyldiol-moieties have been detected in the protective cell wall of eustigmatophytes as part of an aliphatic biopolymer, i.e. algaenan (Gelin et al. 1997a), representing 1-2% of the dry biomass. Long-chain diols have subsequently been found in other eustigmatophytes (Table 1), in diatoms (*Proboscia* spp., Sinninghe Damsté et al. (2003), and in dictyochophytes (*Apedinnella radians*, Rampen et al. 2011).

The C_{28-32} 1,13- and 1,15-diols are found in eustigmatophytes, whereas the C_{28-30} 1,14-diols are only found in *Proboscia* diatoms and *Apedinnella radians* (Table 1). A clear correlation has been noted between the fluxes of 1,14-diols and fluxes of *Proboscia* diatoms in sediment traps in the Arabian Sea offshore Oman (Rampen et al. 2007). During periods of upwelling there is a high flux of 1,14-diols and of *Proboscia* valves, whereas during periods of no upwelling 1,14-diols fluxes and *Proboscia* valves are low (Fig. 5). This clearly indicates that, in the marine environment *Proboscia* diatoms are the main producers of 1,14-diols. In contrast, it should be noted that the distribution of 1,13- and 1,15-diols in marine sediments is quite different from their distribution encountered in eustigmatophyte cultures, i.e. the C_{32} 1,15- or $C_{32:1}$ 1,15-diols are the main diols in most of the cultures while the C_{30} 1,15- or C_{30} 1,13-diols are abundant in sediments (for cultures, Volkman et al. 1992, 1999; Méjanelle et al. 2003; Rampen et al. 2014b; for sediments, Morris and Brassell 1988; Versteegh et al. 1997, Gogou and Stephanou 2004; Naafs et al. 2012; Rampen et al. 2012; Dos Santos et al. 2013; Smith et al. 2013; Plancq et al. 2014; Rodrigo-Gámiz et al. 2014 and reference cited therein). This indicates that eustigmatophytes are probably not the main producers of 1,13- and 1,15-diols in marine environments though we have to keep in mind that culture conditions do not always reflect environmental conditions.

Long-chain diols are also present in freshwater environments. Villanueva et al. (2014) showed that the concentrations of 1,13- and 1,15-diols in suspended particulate matter (SPM) of lake Chala (Eastern Africa)

correlates with the abundance of 18S rRNA gene copies of uncultivated eustigmatophytes. The distribution of long-chain diols matches with that of cultures of freshwater eustigmatophytes (Shimokawara et al. 2010; Rampen et al. 2014b): in the Goniochloridaceae and Monodopsidaceae subfamilies the main long-chain diol is the C_{32} 1,15-diol, while members of the Eustigmataceae subfamily are dominated by a mix of C_{28} 1,13-, C_{30} 1,15- and C_{32} 1,15-diols (Table 1). Only some freshwater eustigmatophytes are producing minor amounts of 1,14-diols (Rampen et al. 2014b).

Table 1: Overview of long-chain diols in extant aquatic organisms.
Bold character indicate the major long-chain diols.

Species	Family	Environment	Long-chain diols	Reference
Algae				
Nannochloropsis salina	Eustigmatophyceae	Marine	**C_{32} 1,15**; **$C_{32:1}$ 1,15**; C_{30} 1,15; C_{30} 1,13; C_{31} 1,15, C_{34} 1,15	Volkman et al. 1992; Gelin et al. 1997b
Nannochloropsis oculata	Eustigmatophyceae	Marine	**C_{32} 1,15**; $C_{32:1}$ 1,15; C_{30} 1,15; C_{30} 1,13; C_{31} 1,15; C_{34} 1,15	Volkman et al. 1992
Eustigmatos vischeri	Eustigmatophyceae	Freshwater	**C_{30} 1,15**; C_{28} 1,13; C_{29} 1,13; C_{30} 1,13, 1,16; C_{31} 1,15-1,16; C_{32} 1,15-1,16	Volkman et al. 1999; Rampen et al. 2014b
Vischeria helvetica	Eustigmatophyceae	Freshwater	**C_{32}**; C_{28}; C_{29}; C_{30} ; C_{31}	Volkman et al. 1999
Vischeria punctuate	Eustigmatophyceae	Soil	**C_{30} 1,15**; C_{28} 1,13; C_{29} 1,14; C_{30} 1,13 ; C_{31} 1,15; C_{32} 1,13-1,15	Volkman et al. 1999; Rampen et al. 2014b
Proboscia spp.	Rhizosoleniaceae	Marine	**C_{28} 1,14**; C_{28} 1,13; $C_{28:1}$ 1,14; C_{30} 1,14; $C_{30:1}$ 1,14	Sinninghe Damsté et al. 2003; Rampen et al. 2007
Apedinnella radians	Dictyochophyceae	Brackish	**C_{30} 1,14**; C_{28} 1,14; C_{32} 1,14	Rampen et al. 2011
Nannochloropsis gaditana	Eustigmatophyceae	Marine	**C_{32} 1,15**; C_{28} 1,13; C_{30} 1,11-1,15; C_{31} 1,13-1,16, $C_{32:1}$ 1,15, C_{33} 1,14-1,16, C_{34} 1,13-1,15, $C_{35:1}$ 1,14-1,15, C_{35} 1,14-1,15; $C_{36:1}$ 1,13-1,15, C_{36} 1,15	Méjanelle et al. 2003; Rampen et al. 2014b
Nannochloropsis subterranea	Eustigmatophyceae	Freshwater	**C_{32} 1,15**; C_{30} 1,13-1,15; C_{31} 1,14-1,17	Rampen et al. 2014b
Vischeria stellata	Eustigmatophyceae	Soil	**C_{32} 1,15**; C_{28} 1,13; C_{29} 1,13; C_{30} 1,13-1,15; C_{31} 1,15; C_{32} 1,19; C_{34} 1,19	Rampen et al. 2014b
Chloridella simplex	Eustigmatophyceae	Soil	**C_{32} 1,15**; C_{28} 1,13; C_{29} 1,13; C_{30} 1,13-1,15; C_{31} 13-1,17	Rampen et al. 2014b

Table 1 – *Continued from previous page*

Species	Family	Environment	Long-chain diols	Reference
Goniochloris sculpta	Eustigmatophyceae	Freshwater	**$C_{32:1}$ 1,15**; C_{30} 1,13-1,16; C_{31} 1,13-1,16; C_{32} 1,15-1,16	Rampen et al. 2014b
Microtalis aquatica	Eustigmatophyceae	Freshwater	**C_{32} 1,15**; C_{30} 1,14-1,15; C_{31} 1,14-1,15; $C_{32:1}$ 1,15	Rampen et al. 2014b
Pseudostaurastrum enorme	Eustigmatophyceae	Freshwater	**$C_{32:1}$ 1,15**; C_{28} 1,13-1,14; C_{29} 1,12-1,15; C_{30} 1,13-1,16; C_{32} 1,15	Rampen et al. 2014b
Nannochloropsis oceanca	Eustigmatophyceae	Marine	**C_{32} 1,15**; C_{28} 1,13; C_{29} 1,13; C_{30} 1,13-1,15; C_{31} 1,14-1,16; C_{32} 1,16-1,17	Rampen et al. 2014b

4 Long-chain diol proxies

Until recently, long-chain diols have occasionally been used as proxies for environmental or climate reconstructions. Versteegh et al. (1997) were the first to observe a link between the distribution of long-chain diols and environmental parameters. They reported that the ratio of C_{30} 1,15- and C_{32} 1,15-diols, was higher in environments with higher salinities. Later on this relation was clarified by Rampen et al. (2012) who showed that temperature rather than salinity impacted this ratio. More recently, a variety of proxies have been proposed based on long-chain diols.

4.1 Indices based on 1,14-diols as a proxy for upwelling/high nutrients

Rampen et al. (2008) developed an upwelling proxy based on long-chain 1,14-diols: Diol Index (DI-1). The authors linked the higher flux of 1,14-diols in sediment traps with the bloom of *Proboscia* diatoms in the upwelling zone of the Arabian Sea, offshore Oman (Fig. 5). The 1,14-diols flux was particularly high during the south west monsoon when *Proboscia* diatoms were blooming intensely and the intensity of the upwelling was at its highest (Fig. 5). The DI-1 proxy is the ratio of the summed 1,14-diols, defined as *Proboscia* 1,14 diols over the summed C_{30} 1,15- and 1,14-diols (equation 1).

$$DI-1 = \frac{C_{30}1,14 + C_{28}1,14}{C_{30}1,15 + C_{30}1,14 + C_{28}1,14} \quad (1)$$

It was subsequently shown that this ratio followed the same trend as other upwelling related proxies, such as SST reconstructions, organic carbon content, barium/aluminium ratio, and stable isotope composition of specific foraminiferal species in a 90 kyr sediment core offshore Oman (Rampen et al. 2008). Following this, DI-1 was successfully applied to Pliocene sediments from the Benguela upwelling system (Pancost et al. 2009), late Neogene sediments from the Eastern equatorial Pacific (Seki et al. 2012), late Quaternary sediments from southern Australia (Dos Santos et al. 2012) and Holocene sediments from the Mediterranean Sea (Nieto-Moreno et al. 2013) to trace past upwelling.

The 1,14-diols have also been linked to nutrient-rich water in polar areas (Willmott et al. 2010) and, due to the absence of the C_{30} 1,15-diol in polar waters, another diol index (DI-2, equation 2) was proposed:

$$DI-2 = \frac{C_{30}1,14 + C_{28}1,14}{C_{30}1,13 + C_{28}1,13 + C_{30}1,14 + C_{28}1,14} \quad (2)$$

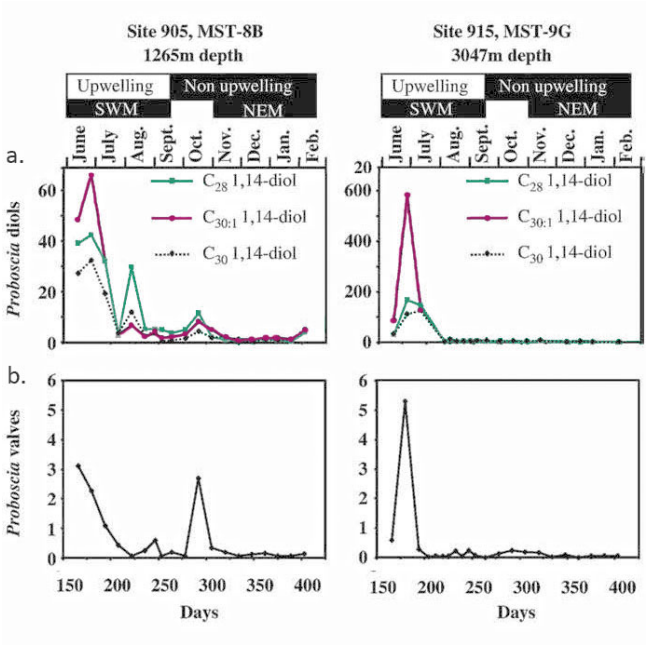

Figure 5: (a) Fluxes of *Proboscia* diols (1,14-diols) and (b) fluxes of *Proboscia* valves in Arabian Sea sediment traps (adapted from Rampen et al. 2008)

This index was used in a study of an 8.5 kyr sediment core from Antarctica to trace the strength of the upwelling of circumpolar waters (Willmott et al. 2010). Contreras et al. (2010) linked the abundance of 1,14-diols to enhanced water column stratification over the Peruvian shelf. In the highly productive Peru upwelling system, *Proboscia* diatoms (producers of 1,14-diols) are blooming after the upwelling period, during water column stratification. The authors later used 1,14-diols abundance in a Holocene sediment core covering the Little Ice Age (LIA) and showed enhanced water stratification during the LIA caused by increased riverine runoff.

Rampen et al. (2014a) subsequently reviewed the use of 1,14-diols as a proxy for specific environmental parameters, such as nutrient availability, upwelling intensity and stratification. They showed that *Proboscia* spp. are blooming under various environmental conditions, not only during upwelling but also during pre-upwelling, in stratified water, in mixed water, and during high nutrient conditions suggesting that 1,14-diols are indicators for the presence of *Proboscia* diatoms as such and not for specific environmental conditions. The DI-1 is negatively correlated with temperature (r^2 = -0.855, $p<0.001$; Rampen et al. 2014b), and positively correlated with nutrient concentrations (nitrate r^2 = 0.579, phosphate r^2 = 0.549, $p<0.001$) indicating that DI-1 proxy is not only reflecting upwelling conditions. DI-1 showed some correlation with stratification (difference in temperature between SST and the sea temperature at 200 m depth; Rampen et al. 2014a) but this was likely due to the strong correlation between stratification and SST and DI-1 and SST. Rampen et al. (2014a) suggested the possibility that organisms other than *Proboscia* diatoms produce 1,14-diols. In contrast to DI-1, DI-2 was not correlated with any environmental parameter but did show elevated values in typical upwelling regions (Rampen et al. 2014a). Thus, DI-2 seems to be an useful indicator for nutrient conditions in the water column although this might depend on local upwelling/nutrient conditions and the presence of other 1,14-diol producers.

4.2 An SST proxy based on 1,13- and 1,15-diols.

Rampen et al. (2012) found a strong correlation between the relative abundances of C_{28} 1,13- and C_{30} 1,13- and C_{30} 1,15-diols with SST in marine surface sediments, i.e. a higher relative abundance of 1,13-diols in cold water and a higher relative abundance of C_{30} 1,15-diol in warm water. The authors developed a new temperature proxy based on these long-chain diols: the Long-chain Diol Index (LDI). The LDI is significantly correlated with annual mean SST based on studies of a series of core-tops (n = 162) distributed worldwide (r^2 = 0.969, $p<0.0014$, Fig.6).

$$LDI = \frac{C_{30}1,15}{C_{30}1,13 + C_{28}1,13 + C_{30}1,15} \quad (3)$$

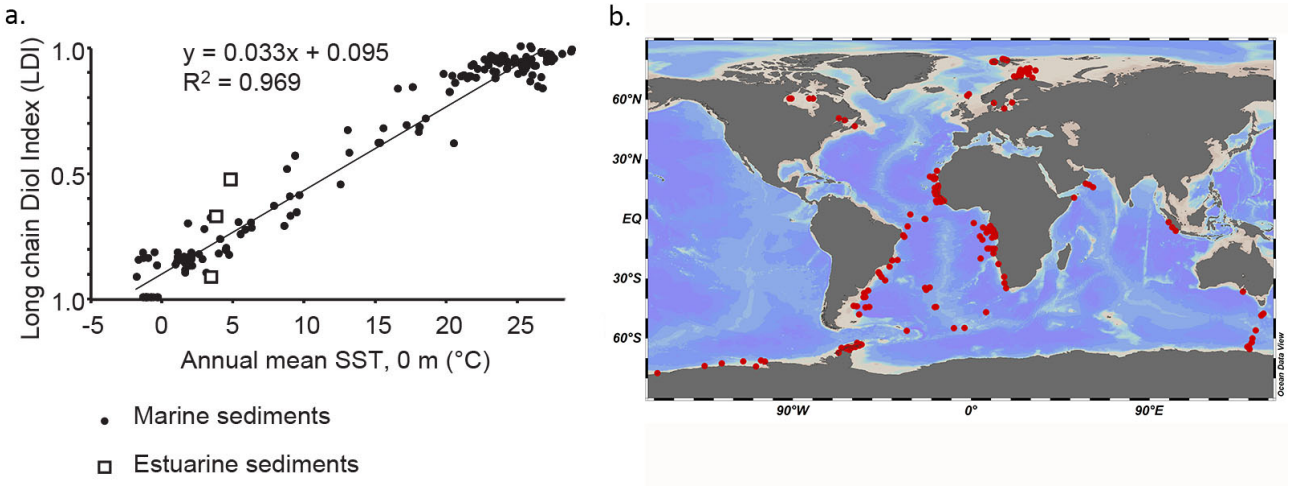

Figure 6: (a) Calibration of the LDI from surface sediments and annual mean sea surface temperature and (b) distribution of the surface sediments used for the calibration (adapted from Rampen et al. 2012)

Several applications of the LDI showed that reconstructing SST using long-chain diols was promising but that seasonality is a parameter which has to be taken into account (Naafs et al. 2012; Dos Santos et al. 2013; Smith et al. 2013; Rodrigo-Gámiz et al. 2014). Due to the lack of knowledge on marine long-chain diol producers and their habitats, the LDI cannot be calibrated using laboratory cultures. Related to this, it is not clear how far back in time the LDI can be applied to reconstruct SST. The oldest SST reconstruction was derived from early Pleistocene sediments (2.49 and 2.41 Ma; Naafs et al. 2012), but this reconstruction was somewhat hampered as the LDI could only be calculated during glacial stages. Furthermore, in some regions the LDI deviates somewhat from the calibration curves (e.g. estuarine surface sediments, Fig. 6) indicating that these regions might be influenced by other environmental parameters or species composition. Finally, Rampen et al. (2014b) also tested the LDI in lake surface sediments from around the globe, but no correlation with lake or air temperatures was observed.

5 Scope and framework of the thesis

As discussed above, marine long-chain diols may have the potential to reconstruct past environmental conditions. However the lack of knowledge regarding their sources and the controls on their distribution in the water column is severely hampering their application as reliable proxies. Therefore, the objective of this thesis is to decipher the controls on long-chain diol production and distribution, to constrain the sources of long-chain diols in both marine and freshwater environments and to investigate the applicability of long-chain diol proxies in environmental and climate reconstructions.

To this end the thesis is divided in two parts: in Part I long-chain diols in modern marine and freshwater environments are investigated to trace their source and distributions and in Part II these diols are applied as indicators of paleoenvironmental and climate changes.

Part I Long-chain diols in modern marine and freshwater environments

In **Chapter 2**, the distribution of long-chain diols present in SPM in the open western equatorial Atlantic, partly seasonally influenced by terrigenous input originating from the Amazon River, were analyzed. The results show that the main long-chain diol is the C_{30} 1,15-diol (>95% of all diols) and that the distribution of the diols is similar for all SPM samples, indicating no major influence of the Amazon plume on the long-chain diol distribution. The abundances of the long-chain diols were higher in the mixed layer when compared to

their abundances in surface water and at the deep chlorophyll maximum. Eustigmatophyte abundances were extremely low suggesting that they cannot be the source of the diols. Furthermore, no correlation was observed between 18S gene copies abundances of eukaryotes and long-chain diol concentrations. However, the absence of correlations might be due to the difference in turnover rates of DNA and lipid, i.e. lipids are much more resistant than DNA so that the diols encountered may be derived predominantly from non-living cells. This severely restricts the possibility to constrain the producers of biomarker lipids by comparison between DNA and lipids concentrations.

The lack of impact of the Amazon River plume on diol distributions was further investigated by studies of four other coastal areas more or less influenced by riverine input: the Gulf of Lion, the Kara Sea, the Amazon shelf and the Berau delta. **Chapter 3** reports on the variations in the long-chain diol distributions in surface sediments of these four coastal areas and in the SPM of the associated rivers (Rhône, Yenisei and Amazon). In all river SPM samples, the major diol was C_{32} 1,15-diol with some C_{30} and C_{28} diols whereas in the shelf seas sediments the prominent diols were either the C_{30} 1,15- or C_{30} 1,13-diols. The C_{32} 1,15-diol was present in minor proportions in the shelf seas and its abundance decreased as the surface sediments are located farther away from the river mouth. This indicates that the C_{32} 1,15-diol originates from the continent, and due to its absence in soils and plants, is probably produced in freshwater bodies (e.g. rivers and lakes). This further suggests that the relative abundance of the C_{32} 1,15-diol in marine settings might be an interesting proxy for river input. Regarding the reconstruction of SST by long-chain diols, it was noteworthy that in the top marine sediments of the Gulf of Lion and the Berau delta, the reconstructed SST was 5 to 10°C lower than the measured SST, while in the Kara Sea the reconstructed SST was 6°C higher close to the river mouths, which corresponds with a higher abundance of the C_{32} 1,15-diol. This indicates that the application of the LDI should be done with care in coastal areas where there is a substantial amount of riverine input.

The distribution and sources of long-chain diols in rivers are further described in **Chapter 4**. The aim was to constrain the controls on their distribution. Three river systems were studied: the Godavari, the Rhine and the Danube, as well as surface sediments from the Black Sea. The distribution of the long-chain diols in the river SPM and sediments was in agreement with previous studies (see Chapter 3), i.e. the C_{32} 1,15-diol was the main diol. In the Godavari and Rhine SPM, the C_{30} 1,15-diol was the second most abundant diol while in the Danube sediments the C_{30} 1,13-diol was the second most abundant diol. There was a clear difference between the diol distribution in the sediments of the Danube and the Black Sea, i.e. the Black Sea sediment contained less than 10% of the C_{32} 1,15-diol, whereas the Danube River contained more than 50% of this diol. A compilation of long-chain diol relative distributions in all riverine SPM and marine sediment samples highlighted the different producers and justify the application of the relative abundance of the C_{32} 1,15-diol as a proxy for river input. The absolute abundance of the diols encountered in freshwater environments are enhanced in stagnant water areas like lakes or shallow ponds. DNA analysis of the Rhine River SPM showed that less than 0.1% of 18S rRNA sequences are related to eustigmatophytes, once again suggesting that they cannot be a source. However, incubation of the Rhine surface water for two days with ^{13}C-labeled bicarbonate showed no label intake in the long-chain diols, indicating that they are not produced in situ but might be produced in quieter habitats of the Rhine. Thus, long-chain diols are mainly produced in stagnant water in lakes and shallow ponds.

Following the conclusion of Chapter 4, two lakes, tropical Lake Chala and temperate Lake Geneva, were studied in more detail. **Chapter 5** describes investigations regarding the origin and distribution of diols in these two lakes. In the sediment traps from Lake Chala, a small crater lake close to the Kilimanjaro, higher concentrations of long-chain diols (mainly the C_{32} 1,15- and C_{30} 1,15-diols) were found during March/April and November each year. This enhancement corresponds to periods of low wind strength and higher precipitation, inducing stratification in the water column. Incubation studies with ^{13}C-labeled bicarbonate were performed in Lake Geneva and the long-chain diols incorporated the label in spring and late summer/autumn, also corresponding with periods of thermal stratification of the lake water. These results indicate that the diols are produced during periods of water column stratification. In Lake Geneva, the distribution of the diols seasonally varies suggesting a change in diol producers between the spring and late autumn blooms. Sequencing of 18S rRNA from the lake water showed that freshwater eustigmatophytes known to produce long-chain diols in cultures were present. Moreover, in Lake Geneva, the number of 18S rRNA gene copies per liter correlates with the summed diol concentration. Together with the results of a previous study (Villanueva et al. 2014) of Lake Chala, it is likely that eustigmatophytes are the long-chain diols producers in lakes.

Part II Paleo application of the long-chain diol proxies

Based on the results presented in Part I the applicability of fractional abundances of the C_{32} 1,15-diol over the C_{30} 1,15-, C_{30} 1,13- and C_{28} 1,13-diols ($F_{C32\ 1,15}$) as a proxy for river input into shelf seas was tested. **Chapter 6** describes the results of diol studies in sediments from the Mozambique Channel and the Mediterranean Sea. Surface sediments from the Mozambique Channel showed that the $F_{C32\ 1,15}$ proxy is higher closer to river mouths and in line with values of the BIT index (Hopmans et al. 2004), a proxy for terrigenous (river and soil) input to marine environments (e.g. Weijers et al. 2009). Application of these proxies in sediment cores from the Mozambique channel and the Mediterranean Sea showed a strong positive correlation between $F_{C32\ 1,15}$ and the BIT index, indicating the potential of the $F_{C32\ 1,15}$ as an indicator of past riverine input. Both proxies are sensitive to sea-level changes, i.e. when the river mouth comes closer to the core site due to a lower sea-level the terrigenous input is higher. Differences between the BIT index and $F_{C32\ 1,15}$ were linked to changes in soil input influencing the BIT index. Thus, the results show that the $F_{C32\ 1,15}$ is a promising proxy to trace past river input in shelf seas.

Chapter 7 describes the results of investigations of long-chain diols in a subpolar semi-enclosed sea, the Sea of Okhotsk. Surface sediments and a sediment core from the center of the Sea of Okhotsk were investigated to test the applicability of the LDI for reconstructing past sea temperatures. First, LDI values in surface sediments were compared with annual or seasonal sea temperature as well as with the temperature at different depths showing that the LDI is significantly correlated with annual and autumn SST (r^2 = 0.93 and r^2 = 0.94, respectively, $p<0.001$, n = 10). The correlation between autumn SST and LDI differs from the global calibration previously published by Rampen et al. (2012). The local core-top calibration was subsequently used to reconstruct past SST from a sediment core spanning the last 180 ka. This showed that LDI-SST was following the general SST variations (like glacial/interglacial changes) as determined by other SST proxies such as the TEX_{86} or the $U^{k'}_{37}$. Although the reconstructed LDI temperature was often lower than the other proxy temperatures it is concluded that the LDI is a promising proxy for reconstructing paleotemperature at high latitude areas.

Chapter 8 describes the LDI record for the past 1.5 Ma of the Sea of Okhotsk. In addition, the DI-2 and $F_{C32\ 1,15}$ were applied to reconstruct productivity and freshwater changes in the central part of the Sea of Okhotsk, respectively. The LDI, as already applied for the last 180 ka (Chapter 7), reflects glacial/interglacial changes and follows the other temperature proxies TEX_{86} or the $U^{k'}_{37}$. However, the reconstructed LDI-SSTs are generally lower than those reconstructed using other proxies. This may be due to an input of 1,14-diols during high diatom productivity periods or to a shift during ice-free interglacials of diol productivity towards colder periods, such as spring or late autumn. The LDI-SST does not reflect a change in Milankovitch cyclicity around the mid-Pleistocene Transition (MPT) as observed for the TEX_{86} sea water temperature record, likely due to the seasonal shift mentioned above. However, the 1,14-diols, which indicate enhanced *Proboscia* productivity during deglaciations, reflect the periodicity change characteristic of the MPT, from 41- to 100-kyr cycle. $F_{C32\ 1,15}$ follows the $\delta\ ^{18}O$ record from the LR04 benthic foraminifera stack record (Lisiecki and Raymo 2005) indicating that the proxy is mainly reflecting sea-level changes, i.e. when the sea-level drops the Amur River mouth gets closer to the core site and brings in more riverine material. This study therefore shows the limitations of the applicability of the LDI as a SST proxy over long periods of time as long-chain diols are strongly impacted by seasonality. However some proxies, such as those based on the 1,14-diols, can be applied over such periods.

All together the results presented in this thesis show that long-chain diols are useful biomarkers as they can be used in marine settings to reconstruct past SST, riverine input and nutrient conditions. Nevertheless, it is necessary to perform checks before applying these proxies. Indeed, before applying the LDI it is necessary to confirm that $F_{C32\ 1,15}$ is low, i.e. low riverine input, but also that the global calibration is suitable for the region or that a regional calibration is needed. Future research should focus on the sources of diols in the oceans, either using high resolution time series data coupled with 18S rRNA analysis, or, even better, exploring the biosynthetic pathway(s) of long-chain diols and the genes responsible for their synthesis. This would allow for special gene targeting, leading to the identification of all possible organisms capable of synthetizing long-chain diols. Subsequent isolation and culturing of the organisms (when possible) should further confirm the presence or absence of long-chain diols in these organisms. The further refinement of these long-chain diol proxies will enable a better understanding of past environmental changes which, in turn, would help to refine and validate climate models and to better understand and predict future climate change.

Part I

Long-chain diols in modern environments

Sunset on the Black Sea, cruise 64PE418, March 2017

Chapter 2

A quest for the biological sources of long chain alkyl diols in the western tropical North Atlantic Ocean

Biogeosciences 15, 5951–5968 (2018)

Sergio Balzano[a,*], Julie Lattaud[a], Laura Villanueva[a], Sebastiaan W. Rampen[a], Corina P. D. Brussaard[a], Judith van Bleijswijk[a], Nicole J. Bale[a], Jaap S. Sinninghe Damsté[a,b], and Stefan Schouten[a,b]

[a] NIOZ, Royal Netherlands Institute for Sea Research, Department of Marine Microbiology and Biogeochemistry (MMB), and Utrecht University, PO Box 59, 1790 AB Den Burg, The Netherlands
[b] Utrecht University, Faculty of Geosciences, Department of Earth Sciences, Princetonlaan 8a, 3584 CD Utrecht, The Netherlands

[*]Corresponding author.
E-mail address: Sergio.balzano@nioz.nl (S. Balzano).
http://dx.doi.org/10.5194/bg-15-5951-2018

Abstract

Long-chain alkyl diols (LCDs) are widespread in the marine water column and sediments but their biological sources are mostly unknown. Here we combine lipid analyses with 18S rRNA gene amplicon sequencing on suspended particulate matter (SPM) collected in the photic zone of the western tropical North Atlantic Ocean at 24 stations to infer relationships between LCDs and potential LCD-producers. The C_{30} 1,15-diol was detected in all SPM samples and accounted for >95% of the total LCDs, while minor proportions of C_{28} and C_{30} 1,13-diols, C_{28} and C_{30} 1,14-diols as well as C_{32} 1,15-diol were found. The concentration of the C_{30} and C_{32} diols was higher in the mixed layer of the water column compared to the deep chlorophyll maximum (DCM), whereas concentrations of C_{28} diols were comparable. Sequencing analyses revealed extremely low contributions ($\approx$ 0.1% of the 18S rRNA gene reads) of known LCD-producers but the contributions from two taxonomic classes to which known producers are affiliated, i.e. Dictyochophyceae and Chrysophyceae, followed a trend similar to that of the concentrations of C_{30} and C_{32} diols. Statistical analyses indicated that the abundance of 4 operational taxonomic units (OTUs) of the Chrysophyceae and Dictyochophyceae, along with 23 OTUs falling in other phylogenetic groups, were weakly ($r \leq 0.6$) but significantly (p-value <0.01) correlated with C_{30} diol concentrations. It is not clear whether some of these OTUs might indeed correspond to C_{28-32} diol-producers or whether these correlations are just indirect and the occurrence of C_{30} diols and specific OTUs in the same samples might be driven by other environmental conditions. Moreover, primer mismatches were unlikely but cannot be excluded and the variable number of rRNA gene copies within eukaryotes, might have affected the analyses leading to LCD-producers being undetected or under sampled. Furthermore, based on the average LCD content measured in cultivated LCD-producing algae, the detected concentrations of LCDs in SPM are too high to be explained by the abundances of the suspected LCD-producing OTUs. This is likely explained by the slower degradation of LCDs compared to DNA in the oxic water column and suggests that some of the LCDs found here were likely to be associated to suspended debris, while the DNA from the related LCD-producers had been already fully degraded. This suggests that care should be taken in constraining biological sources of relatively stable biomarker lipids by quantitative comparisons of DNA and lipid abundances.

Keywords: *Long-chain alkyl diols, HCC, tropical North Atlantic, 18S rRNA gene amplicon sequencing, Eustigmatophyceae, Chrysophyceae, Dictyochophyceae*

1 Introduction

Long chain alkyl diols (LCDs) are lipids that consist of a linear alkyl chain with 22–38 carbons, hydroxylated at both the terminal carbon atom and at an intermediate position, and usually saturated or monounsaturated. LCDs were identified for the first time in Black Sea sediments (de Leeuw et al. 1981) and have subsequently been found with widespread occurrence in both suspended particulate matter (SPM) and sediments from both coastal and off-shore sites throughout the World Ocean (Shanchun et al. 1994; Versteegh et al. 1997; Rampen et al. 2014b). LCDs can be preserved in marine sediments for long periods of time and their distribution can reflect the environmental conditions at the time they were produced.

The most abundant LCDs in seawater are the saturated C_{28} and C_{30} 1,13-diols, C_{28} and C_{30} 1,14-diols, and C_{30} and C_{32} 1,15-diols (Rampen et al. 2014b), which are all likely produced by phytoplankton. However, the marine biological sources of LCDs are still not fully clear because, in contrast with the widespread occurrence of LCDs in the sediment, few marine taxa have been shown to contain these lipids. Eustigmatophyceae contain C_{30} 1,13-, C_{30} 1,15-, and C_{32} 1,15-diols (Volkman et al. 1992; Rampen et al. 2014a) but they comprise mostly freshwater species and only a few rare marine representatives from the genus Nannochloropsis are known (Andersen et al. 1998; Fawley and Fawley 2007). Furthermore, the distribution of LCDs in the marine environment does not match that of LCDs of marine Eustigmatophyceae (Volkman et al. 1992; Rampen et al. 2012). Species of the diatom genera *Proboscia* and the dictyocophycean *Apedinella radians* contain C_{28-32} 1,14-diols (Sinninghe Damsté et al. 2003; Rampen et al. 2009; Rampen et al. 2011), with the former accounting for significant proportions of marine biomass mostly in upwelling regions (Moita et al. 2003; Lassiter et al. 2006), whereas the latter has been occasionally observed in estuarine environments (Seoane et al. 2005; Bergesch

et al. 2008). Few other marine species from classes genetically related to diatoms and Eustigmatophyceae have been recently shown to produce LCDs (Table S1). All the known LCD-producing phytoplankters belong to the eukaryotic supergroup Heterokontophyta, a division which includes, among others, diatoms and brown seaweeds. The widespread occurrence of LCDs in the marine environment, despite the restricted abundance and distribution of marine LCD-producers, suggests that these compounds may be produced by unknown phytoplankton species. In addition LCD in the marine environment might also derive from vegetal debris of terrestrial or riverine origin. For example, C_{30-36} diols functionalised at the 1- and the ω18 or ω20 positions have previously been reported to occur in ferns (Jetter and Riederer 1999; Speelman et al. 2009; Mao et al. 2016) and suggested to be part of the leaf cuticular waxes. Similarly, C_{26-32} diols have been occasionally detected in plants (Buschhaus et al. 2013). This suggests that vegetal debris may in principle also source LCDs in seawater.

Several indices, based on ratios between the different diols, have been proposed for the reconstruction of past environmental conditions. The Diol Index, reflecting the proportion of C_{28} and C_{30} 1,14-diols over the sum of C_{28} and C_{30} 1,14-diols and C_{30} 1,15-diol, has been proposed to track ancient upwelling conditions since the 1,14-diols are believed to be mostly produced by upwelling diatoms of the genus *Proboscia* (Rampen et al. 2008). Another index, the long chain diol index (LDI), which is based on the proportion of the C_{30} 1,15-diol over the C_{28} and C_{30} 1,13-diols, shows a strong correlation with sea surface temperature (SST) and is used to determine past SST (Rampen et al. 2012; Plancq et al. 2014; Rodrigo-Gámiz et al. 2015). In addition, since the C_{32} 1,15-diol is the major component of the LCDs of freshwater Eustigmatophyceae (Volkman et al. 1992; Rampen et al. 2014a), the fractional abundance of C_{32} 1,15-diol has been suggested to be a marker of riverine input in seawater (de Bar et al. 2016;Lattaud et al. 2017a, 2017b). Other markers for riverine inputs in seawater are the C_{30-36} 1,ω20-diols which are produced by the freshwater fern Azolla (Speelman et al. 2009; Mao et al. 2016). However, application of these proxies in the marine realm remains uncertain. For example the growth of *Proboscia* spp. is typically promoted under low concentrations of dissolved silica, whereas other diatoms dominate upwelling area under higher silica concentrations (Koning et al. 2001), making the Diol Index ineffective in predicting upwelling conditions when communities are dominated by other diatoms. In addition, the sources of the major marine C_{30} 1,15-diol are unknown, complicating the application of the LDI as a proxy.

A way of assessing the sources of biomarker lipids is to compare the abundance of lipids in environmental samples with the composition of the microbial community, as determined by genetic methods. For example, Villanueva et al. (2014) analysed both LCDs and eustigmatophycean 18S rRNA gene sequences in a tropical freshwater lake and found five clades of uncultured Eustigmatophyceae in the top 25 m of the water column of the lake, where LCDs were also abundant. Abundance determination by quantitative polymerase chain reaction (qPCR) highlighted that the number of eustigmatophycean 18S rRNA gene copies peaked at the same depth as the LCDs, suggesting that Eustigmatophyceae are a primary source for LCDs in freshwater (Villanueva et al. 2014). However, one of the limitations of this approach is that it relies on specific eustigmatophycean primers designed based on the sequences available in the genetic databases, which could be biased and not target all the existing LCD biological sources. To compensate for this limitation high throughput amplicon sequencing of the 18S rRNA gene allows the exploration of the total marine microbial communities in great detail (Stoeck et al. 2009; Logares et al. 2012; Christaki et al. 2013; Balzano et al. 2015; de Vargas et al. 2015; Massana et al. 2015). The combination of these analyses with lipid composition may potentially assist in identifying the main LCD producers in marine settings.

In the present study, we quantitatively analysed the composition and abundance of LCDs in suspended particulate matter (SPM) collected along the tropical North Atlantic (Fig. 1A) at different depths in the photic zone (surface, deep chlorophyll maximum (DCM) and bottom of the wind mixed layer (BWML); see also Bale et al. (2018). The 18S rRNA gene abundance and composition of the SPM was also analysed by quantitative PCR (qPCR) and high throughput amplicon sequencing to infer the taxonomic composition and to compare the abundance of the different taxa with that of the LCDs, in order to identify the potential marine biological sources of LCDs.

2 Material and methods

2.1 Cruise transect, ancillary data, and SPM collection

Samples were taken during the Heterocystous Cyanobacteria Cruise (HCC) (64PE393), which took place from 24^{th} August to 21^{st} September 2014 along a transect on the tropical North Atlantic Ocean (see Bale et al. 2018

for details). The transect was from Mindelo (Cape Verde) to a location about 500 km from the Amazon River mouth and then westwards along the coast towards Barbados (Fig. 1A). Temperature, salinity and nutrient data have previously been reported in Bale et al. (2018). Seawater was collected from two or three depths at each station to measure the concentration of chlorophyll a (Chl-a) and the abundances of photosynthetic pico and nanoeukaryotes. Seawater was collected during the up cast using Niskin bottles mounted on a CTD frame. The sampling depths were determined based on the evaluation of the vertical profiles of temperature, salinity, and chlorophyll fluorescence after the down cast of the CTD deployment. The depth of the BWML and the DCM were determined based on the lowest position of the mixed layer and the depth at which the highest values of chlorophyll fluorescence were observed. For Chl-a determination seawater was collected from the Niskin bottles and filtered through 0.7 µm pore-size glass-fiber (Whatman GF/F) filters, followed by frozen storage. Chl-a was extracted with methanol buffered with 0.5 M ammonium acetate, homogenized for 15 s and analysed by high performance liquid chromatography.

Photosynthetic pico- and nanoeukaryotes were enumerated by flow cytometry according to the protocol of Marie et al. (2005). In short, 1 mL samples were counted fresh using a Becton-Dickinson FACSCalibur (Erembodegem, Belgium) flow cytometer equipped with an air-cooled Argon laser (488 nm, 15 mW). Phytoplankton were discriminated based on their chlorophyll autofluorescence and scatter signature. Cyanobacteria, i.e. Synechococcus and Prochlorococcus, were not included in the current study. Size fractionation was performed by gravity filtration with >3 µm average cell diameter phytoplankton groups classified as nanoeukaryotic and those <3 µm average cell diameter as picoeukaryotic phytoplankton.

Three McLane in situ pumps (McLane Laboratories Inc., Falmouth) were used to collect SPM from the water column for the analysis of both lipids and microbial communities. As with the collection of seawater with Niskin bottles for Chl-a and flow cytometry analyses, the in situ pumps were deployed at the surface (3 - 5 m depth), the BWML and the DCM (Table S2). Between 100 and 400 L of seawater was pumped and the SPM was collected on pre-combusted 0.7 µm GF/F filters (Pall Corporation, Washington) and immediately frozen at -80°C. For the determination of the organic carbon concentrations, SPM was freeze dried and analysis was carried out using a Flash 2000 series Elemental Analyzer (Thermo Scientific) equipped with a thermal conductivity detector.

2.2 Lipid extraction and analyses of LCDs

Lipids were extracted from the GF/F filters as described previously (Lattaud et al. 2017a). Briefly, a quarter of the filters were dried using a LyoQuest (Telstart, Life Sciences) freeze-dryer and lipids were extracted using base and acid hydrolysis. The base hydrolysis was achieved with 12 mL of a 1 M KOH in methanol solution by refluxing for 1 h. Subsequently, the pH was adjusted to 4 with 2 M HCl:CH_3OH (1:1, v/v) and the extract was transferred into a separatory funnel. The residues were further extracted once with CH_3OH:H_2O (1:1, v/v), twice with CH_3OH, and three times with dichloromethane (DCM). The extracts were combined in the separatory funnel and bidistilled water (6 mL) was added. The combined solutions were mixed, shaken and separated into a CH_3OH:H_2O and a DCM phase, the DCM phase was removed and collected in a centrifuge tube. The aqueous layer was re-extracted twice with 3 mL DCM. The pooled DCM layers were dried over a sodium sulfate column and the DCM was evaporated under a stream of nitrogen. The extract was then acid hydrolyzed with 2 mL of 1.5 M HCl in CH_3OH solution under reflux for 2 h. The pH was adjusted to 4 by adding 2 M KOH:CH_3OH. 2 mL of DCM and 2 mL of bidistilled water were added to the hydrolyzed extract, mixed and shaken and, after phase separation, the DCM layer was transferred into another centrifuge tube. The remaining aqueous layer was washed twice with 2 mL DCM. The combined DCM layers were dried over a sodium sulfate column, the DCM was evaporated under a stream of nitrogen and a C_{22} 7,16-diol was added to the extract as internal standard. The extract was separated on an activated aluminium oxide column into three fractions using the following solvents: hexane:DCM (9:1, v/v), hexane:DCM (1:1, v/v) and DCM:CH_3OH (1:1, v/v). The latter (polar) fraction containing the diols was dried under a gentle nitrogen stream. Diols were derivatized by silylating an aliquot of the polar fraction with 10 µL N,O-bis(trimethylsilyl) trifluoroacetamide (BSTFA) and 10 µL pyridine, heating for 30 min at 60 °C and adding 30 µL of ethyl acetate. The analysis of diols was performed by gas chromatography-mass spectrometry (GC-MS) using an Agilent 7990B GC gas chromatograph, equipped with a fused silica capillary column (25 m x 320 µm) coated with CP Sil-5 (film thickness 0.12 µm), coupled to an Agilent 5977A MSD mass spectrometer. The temperature regime for the oven was the same as that used by Lattaud et al. (2017a): held at 70 °C for 1 min, increased to 130 °C at a rate

of 20 °C min^{-1}, increased to 320 °C at a rate of 4 °C min^{-1}, held at 320 °C for 25 min. The flow was held constant at 2 mL min^{-1}. The MS source temperature was held at 250 °C and the MS quadrupole at 150 °C. The diols were identified and quantified via Single Ion Monitoring (SIM) of the *m/z* = 299.3 (C_{28} 1,14-diol), 313.3 (C_{28} 1,13-diol, C_{30} 1,15-diol), 327.3 (C_{30} 1,14-diol) and 341.3 (C_{30} 1,13-diol, C_{32} 1,15-diol) ions (Versteegh et al. 1997; Rampen et al. 2012). Surface samples, which contained the highest concentrations of LCDs, were also analysed by full scan to evaluate the presence of other eustigmatophycean biomarkers such as long chain alkenols and long chain hydroxy fatty acids. Absolute concentrations were calculated using the peak area of the internal standard as a reference.

2.3 DNA extraction, PCR, qPCR, and 18S rRNA gene sequencing

On ice a small portion of the GF/F filters, corresponding to 1/16 of their initial size, hence containing SPM from ca. 25 L of seawater, was cut into small pieces using sterile scissors and tweezers. Filter pieces were then transferred into 2 mL microtubes and the DNA was extracted using a MOBIO powersoil DNA isolation kit (Qiagen) following manufacturer instructions. We amplified the hypervariable V4 region of the 18S rRNA which is considered the best genetic marker for the identification of microbial eukaryotes (Logares et al. 2012; Massana et al. 2015). The V4 is located in a central region (565-584 bp to 964-981 bp for *Saccharomyces cerevisiae*) of the 18S rRNA and it was amplified from the genomic DNA by PCR using the universal eukaryotic primers TAReuk454FWD1 (5'-CCAGCASCYGCGGTAATTCC-3') and TAReuk454REV3 (5'-ACTTTCGTTCTTGATYRA-3') (Stoeck et al. 2010). Primers were modified for multiplex sequencing on a Roche 454 GS FLX system: a 454-adapter A (CCATCTCATCCCTGCGTGTCTCCGACTCAG), a key (TCAG), and a 10 bp sample-specific Multiple Identifier (MID, Table S3) were bound to the 5' end of the forward primer, whereas a 454-adapter 2 (CCTATCCCCTGTGTGCCTTGGCAGTCTCAG) and a unique MID (CGTGTCA) were bound to the 5' end of the reverse primer for all the samples. The PCR mixture included 25 µL Phusion Flash High-Fidelity PCR Master Mix (ThermoFisher Scientific) 19.1 µL deionised water, 1.5 µL dimethyl sulfoxide, 1.7 µL from each primer and 25 ng genomic DNA and the V4 region was amplified using the same thermal cycling as described by Logares et al. (2012). Amplicons were visualised on a 1% agarose gel and V4 bands were excised and subsequently purified using a QIAquick Gel Extraction Kit (Qiagen) and DNA concentration was measured by Qubit Fluorometric Quantitation (ThermoFisher Scientific). For each sequencing run, 20 samples were pooled in equimolar amount and sequenced using a 454 GS-FLX Plus (Macrogen Korea). Some samples yielded a low number of reads and were re-sequenced; overall 77 samples were sequenced in 5 sequencing runs.

To determine the concentration of total 18S rRNA genes within the seawater sampled we carried out qPCR using the same primers and the same cycling conditions as described above. qPCR analysis was performed on a Biorad CFX96TM Real-Time System/C1000 Thermal cycler equipped with CFX ManagerTM Software. Abundance of 18S rRNA gene sequences was determined with the same primer pair (TAReuk454FWD1/ TAReuk454REV3) used for the 18S rRNA gene diversity analysis. Each reaction contained 12.5 µL MasterMix phusion, 8.25 µL deionised nuclease-free water, 0.75 µL DMSO, 1 µL from each primer and 0.5 µL Sybr green and 1 µL of DNA template. Reactions were performed in iCycler iQTM 96-well plates (Bio-Rad). A mixture of V4 18S rRNA gene amplicons obtained as described above was used to prepare standard solutions. All qPCR reactions were performed in triplicate with standard curves from $6.4x10^3$ to $6.4x10^9$ V4 molecules per microliter. Specificity of the qPCR was verified with melting curve analyses (50 °C to 95 °C).

2.4 Bioinformatic analyses

Bioinformatic analyses were carried out using the python-based bioinformatic pipeline quantitative insight in microbial ecology (QIIME) (Caporaso et al. 2010). Overall, we obtained 372 107 raw sequences; reads with a length comprised between 250 and 500 bp, less than 8 homopolymers, and a phred quality ≥ 25 over 50 bp sliding windows were kept for downstream analyses. Chimeric sequences were then identified by comparison with the Protist Ribosomal Database 2 (PR2) (Guillou et al. 2013) using the Uchime algorithm (Edgar et al. 2011) and removed from the dataset along with singletons (i.e. reads not sharing 100% identity with at least another read).

A total of 238 564 reads remaining after quality filtering were clustered into 2457 Operational Taxonomic Units (OTUs) based on 95% sequence identity using Uclust (Edgar 2010). Samples containing less than 1000

sequencing reads were removed from the dataset. The taxonomic affiliation of the OTUs was then inferred by comparison with the PR2 (Guillou et al. 2013) using BLAST (Altschul et al. 1990) within the QIIME pipeline. Reads from metazoa and multicellular fungi were removed from the dataset which finally contained 1871 OTUs and 184 279 reads. A representative set of sequences from the OTUs used here has been submitted to the GenBank (SUB4388921).The abundance of the different taxa in each sample were estimated by multiplying the percentage of reads with the concentration of V4 copies measured by qPCR. Taxa containing C_{28-32} diol-producers were extracted from the dataset and plotted using Ocean Data View (ODV) (Schlitzer 2002).

2.5 Statistical analyses

Linear regression analyses between the concentrations of the different LCDs were performed to assess whether some of the LCDs were likely to derive from a common source. To investigate relationships between LCDs and environmental conditions we calculated the Spearman rank correlation coefficient (r) using the R package vegan (Dixon 2003). The environmental data used were temperature, salinity, TOC, nutrients (nitrate, nitrite, ammonium, phosphate, and silica), as well the concentration of Chl-a and the abundance of photosynthetic pico and nanoeukaryotes. Samples containing missing data and outliers were removed from the dataset before the calculations. Both correlation coefficients and p-values were calculated and the latter were corrected for False Discovery Rates (Benjamini and Hochberg 1995). Correlations were considered significant for p-values <0.01.

To investigate the relationships between lipids and microbial taxa we also calculated the Spearman's rank correlation coefficient between the LCD concentrations and the abundance of the different taxa at both OTU and class levels. To this end, taxonomic data were normalized based on the number of V4 copies in the different samples measured by qPCR.

Comparisons at class level provide the advantage of pooling distribution data from several closely-related OTUs, thus reducing the number of zeros (samples where a given OTU is absent), which complicates statistical analyses of biological distributions (Legendre and Gallagher 2001). However pooling OTUs at higher taxonomic levels likely leads to combining of species able and unable to produce LCDs falling into the same taxonomic level. We thus removed OTUs that were observed in fewer than 19 samples (25%) and compared the resulting OTU table with the LCD concentrations. These analyses were performed using the qiime script observation_metadata_correlation.py (Caporaso et al. 2010) and the p-values were corrected for false discovery rates (Benjamini and Hochberg 1995).

3 Results

3.1 Ancillary data

The HCC cruise sailed across tropical Atlantic waters (Fig. 1A) in late summer and was targeted at SPM from the photic zone collected at the surface, the BWML and the DCM. The extent of the photic zone as well as the depths of both BWML and DCM at each station were assessed based on the vertical profiles of temperature, salinity and chlorophyll fluorescence. The temperature of photic zone waters ranged from 15 to 29 °C (Fig. 1B, Table S2), the BWML depth was comprised between 9 and 40 m, whereas the depth of the DCM ranged from 45 to 105 m. Temperatures varied at the DCM increasing westwards, whereas they were relatively constant at surface and BWML. Salinity varied between 29 and 36.5 g kg^{-1} (Fig. 1C, Table S2) at the surface, whereas it was fairly constant in the DCM (36 to 37). The concentration of Chl-a varied from 34 to 470 ng L^{-1} (Fig. 1D, Table S2), with the lowest values measured at the surface of the easternmost (1 to 6) and westernmost (21 to 23) stations and the relatively higher concentrations in surface waters of the shallowest stations (11 to 13) located above the continental shelf and about 500 km off the Amazon River mouth (Fig. 1A, Table S2). The POC concentration ranged from 0.6 to 13 mg L^{-1} and also peaked at surface for the shallowest stations (Fig. 1E, Table S2).

Photosynthetic picoeukaryotes, quantified by flow cytometry, were more abundant at the DCM compared to surface and BWML (Fig. 1F). Their abundance peaked at the DCM of Stations 1 and 2 (>1.5x10^7 cell L^{-1}), whereas for surface waters the highest values were measured at Stations 11 to 13. In contrast, photosynthetic nanoeukaryotes did not vary substantially through the water column and their abundance peaked at the surface of Station 17 reaching a density of 1.4x10^5 cell L^{-1} (Fig. 1G).

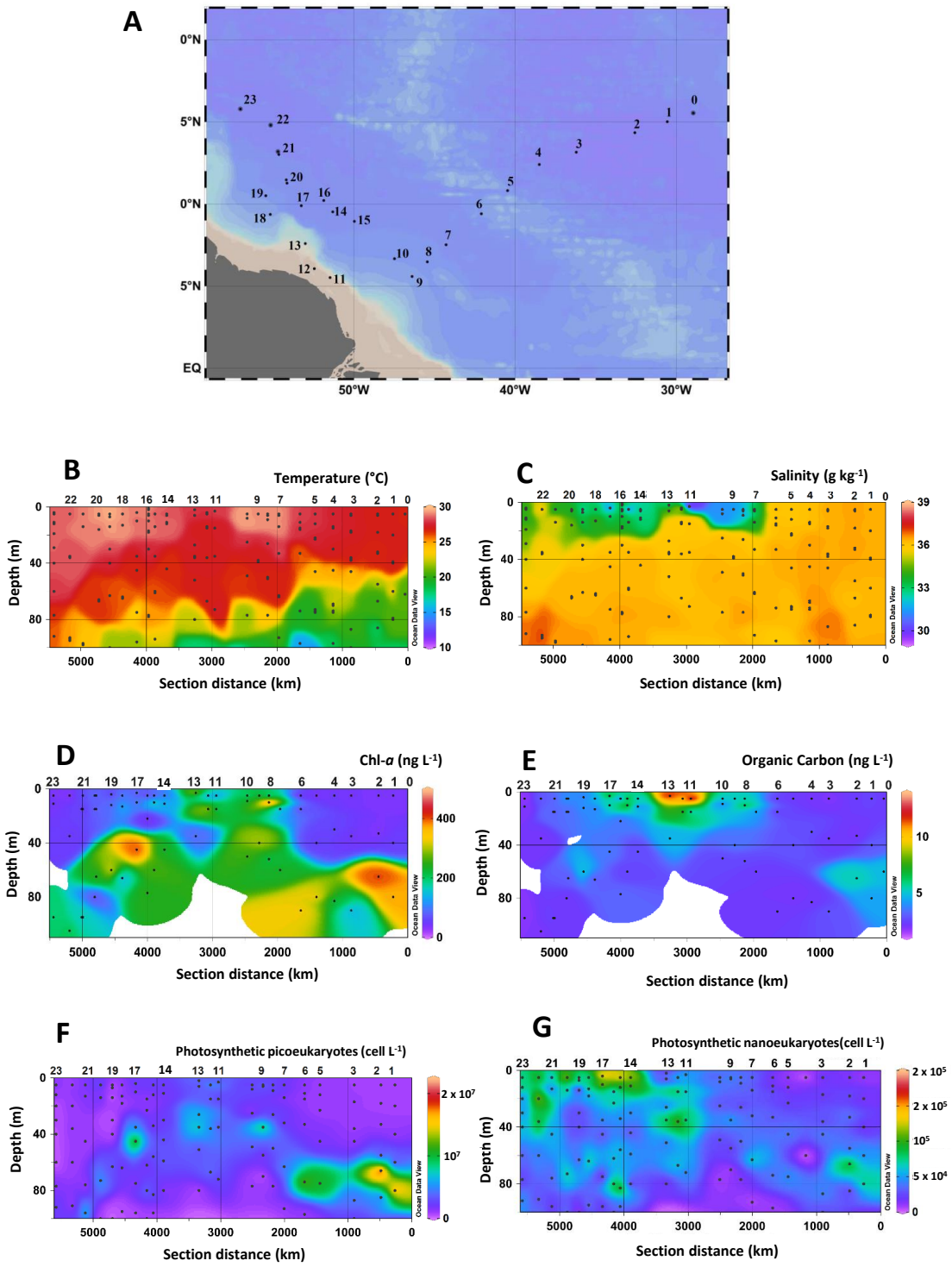

Figure 1: HCC cruise track in the western tropical North Atlantic Ocean, physical seawater properties, and biological parameters. (A) Map of the sampling stations. Spatial distribution of (B) temperature, (C) salinity, the concentration of (D) Chl-a, (E) organic carbon concentrations, and the abundance of photosynthetic (F) picoeukaryotes and (G) nanoeukaryotes. Temperature, salinity as well as the concentrations of Chl-a and organic carbon have been also published by Bale et al. (2018). Data were plotted using ODV software using kriging for interpolation between datapoints (Schlitzer 2002). Dots represent the depth at which SPM was collected.

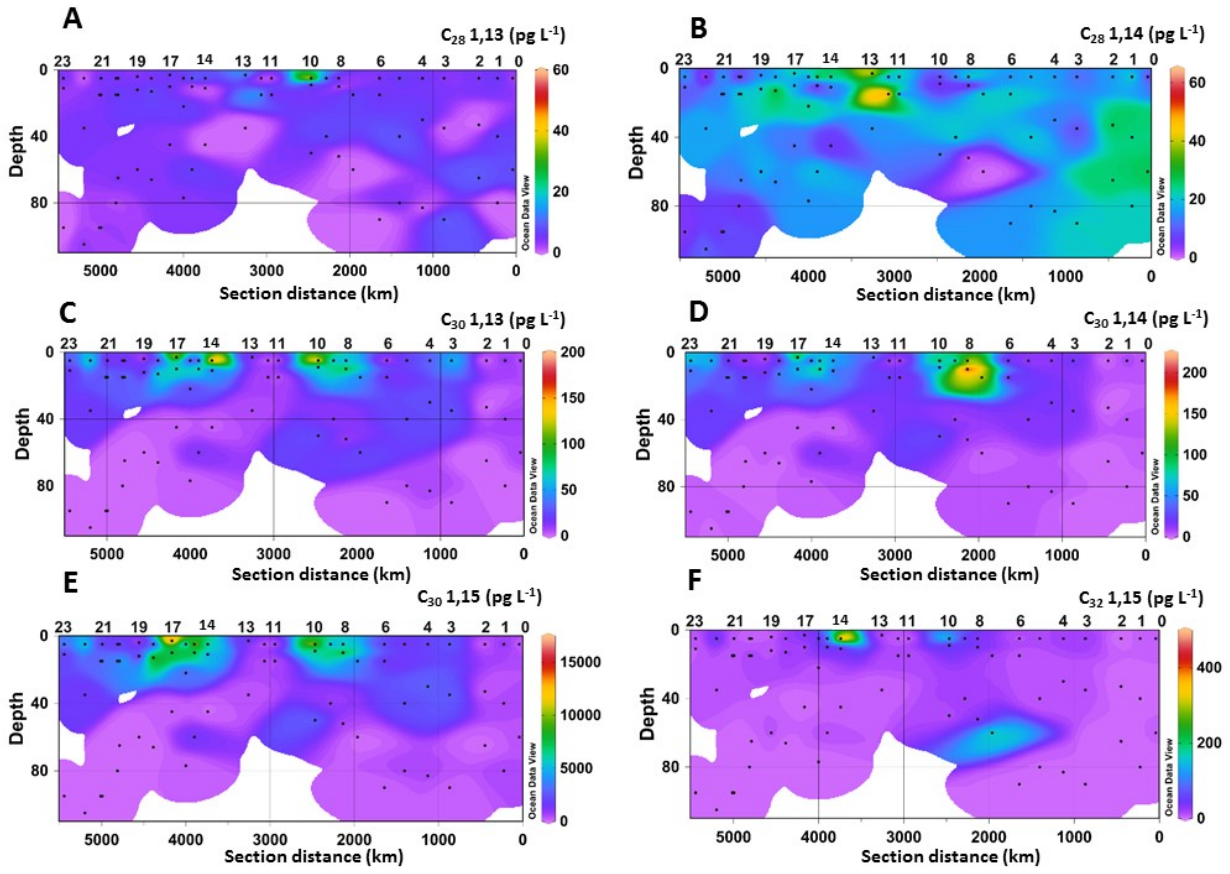

Figure 2: Spatial distribution of the concentration of LCDs: (A) C_{28} 1,13-diol, (B) C_{28} 1,14-diol, (C) C_{30} 1,13-diol, (D) C_{30} 1,14-diol, (E) C_{30} 1,15-diol, and (F) C_{32} 1,15-diol. Data were plotted using ODV software using kriging for interpolation between datapoints (Schlitzer 2002).

3.2 Long chain alkyl diols

Six LCDs were detected, the C_{28} and C_{30} 1,13-diols, C_{28} and C_{30} 1,14-diols and the C_{30} and C_{32} 1,15-diols (Fig. 2, Table S2). The C_{30} 1,15-diol dominated all samples, accounting for >95% of the total LCDs, and its concentration ranged from 100 to 1600 pg L^{-1}. The concentration of the C_{28} 1,13-diol ranged from 0 (i.e. undetectable) to 55 pg L^{-1}, whereas the highest concentration measured for the C_{28} 1,14-diol was 64 pg L^{-1}. The other minor diols were usually more abundant than the C_{28} diols, reaching concentrations up to 190 pg L^{-1} for the C_{30} 1,13-diol, 240 pg L^{-1} for the C_{30} 1,14-diol, and 480 pg L^{-1} for the C_{32} 1,15-diol (Fig. 2). The concentration of the C_{28} 1,13-diol peaked in the surface waters of Station 10, but it was below the detection limit in 19 samples from different depths and stations (Fig. 2A). The C_{28} 1,14-diol reached its highest concentrations at the DCM of Station 12 (64 pg L^{-1}) and at the surface of Station 13 (45 pg L^{-1}) and tended to be more abundant in the waters of the eastern stations (Fig. 2B). The concentrations of both C_{28} 1,13- and C_{28} 1,14-diols did not vary significantly with depth (t-test, p-value >0.1), while those of the C_{30} 1,13-, C_{30} 1,14-, and C_{30} 1,15-diols were higher in the mixed layer (surface and BWML) compared to the DCM (p-value <0.01).

The concentration of the C_{30} 1,13-diol peaked at the surface of Stations 10 and 14 (Fig. 2C), while that of the C_{30} 1,14-diol reached its maximum at the BWML of Stations 7 and 8 (Fig. 2D). The highest concentration of the C_{30} 1,15-diol was measured at the surface of Station 17 (16 ng L^{-1}, Fig. 2E). The concentration of the C_{32} 1,15-diol peaked in the surface waters of Stations 10 and 14 and at the DCM of Station 7 (Fig. 2F) and its concentration did not vary significantly with depth. The concentrations of both the C_{30} and C_{32} diols peaked in the mixed layer of Stations 7-10 and 14-17, which are located in close proximity to the Amazon Shelf (Figs. 2C-F).

3.3 Eukaryotic 18S rRNA gene diversity analysis

Sequencing of the hypervariable V4 region of the 18S rRNA gene of 68 SPM samples resulted in 238 564 reads with an average of 4 987 reads per sample (Table S2). Reads were clustered based on 95% sequence identity and, after removal of reads of Metazoa and multicellular fungi, we obtained 1871 operational taxonomic units (OTUs). Rarefaction analyses indicate that >90% of the genetic diversity was captured (Fig. S1), suggesting that no sample was under sequenced. Most (>90%) reads sequenced here were assigned to Dinophyceae, Syndiniales, Metazoa, Haptophyta, and Radiolaria (Fig. 3). Samples were grouped according to the depth layer (surface, BWML, and DCM) and analysis of similarity (anosim) revealed that the average variance between samples from different groups was higher than the average variance between samples from the same group (p-value $\approx$ 0.001), indicating that the eukaryotic community was mostly influenced by the water depth rather than the geographic location. The proportion of reads from Dinophyceae, Syndiniales, and Haptophyta was slightly higher in the mixed layer compared to the DCM, whereas Radiolaria and Pelagophyceae tended to be slightly more abundant in deeper waters (Fig. 3). All samples except surface waters from Station 12, the BWML from Station 11 and the DCM from Station 22 exhibited high contributions (>50%) from Dinophyceae and Syndiniales (Fig. S2). Radiolaria dominated the DCM at Station 22, diatoms were relatively abundant ($\approx$ 10-20%) at the surface of Stations 12-14 and the BWML of Station 12 while the contribution of diatom reads was <5% for all the other samples.

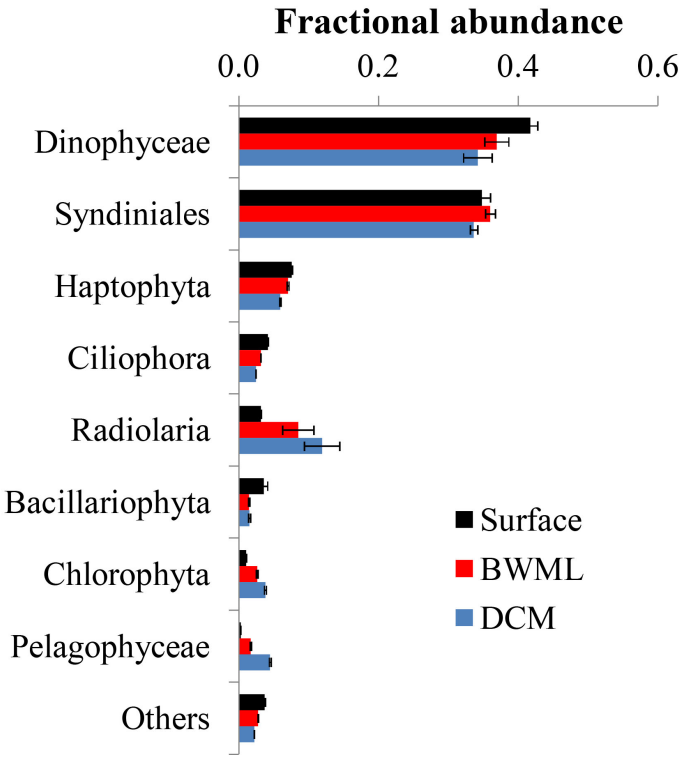

Figure 3: Average fractional abundance of the reads obtained by 18S rRNA gene sequencing of SPM from the western tropical Atlantic Ocean over the various classes of eukaryotes. The V4 fragment of the 18S rRNA gene was sequenced using universal eukaryotic primers. Samples were pooled according to depth and the average contribution from each group at the different depth is shown. Error bars represent the standard deviation in the data from the various stations

18S rRNA gene reads of only four taxa containing known LCD-producers were detected within our dataset: *Proboscia* spp., Florenciellales, *Heterosigma* spp., and Eustigmatophyceae (Table 1). In 33 out of 68 SPM samples we did not detect any 18S rRNA gene read from known LCD-producers, whereas reads from these taxa accounted for <0.1% of the total 18S rRNA reads in 24 samples, 0.1 to 0.5% in 8 samples, 0.5 to 1% in 2 samples and 1.5% in one sample (Station 20, BWML). The 18S rRNA gene reads from putative LCD-producers were mostly recovered from the mixed layer (Table 1). Florenciellales was the most abundant taxon among the known LCD-producers since it exhibited the highest number of reads (99) and was present in 28 out of 68 samples.

The other taxa of putative LCD-producers were detected only in 8 (Eustigmatophyceae) or 2 (*Proboscia* sp. and *Heterosigma akashiwo*) samples (Table 1) accounting from 3 (*Proboscia*) to 45 (Eustigmatophyceae) reads. Eustigmatophyceae (mostly affiliated to *Nannochloropsis oculata*) were found at surface for the Stations 11, 12, and 13, as well as at the DCM of Station 20 (Fig. 4A).

Since species genetically related to cultivated microalgae known to produce LCD may also contain LCDs, we expanded our community composition analyses to groups at a higher taxonomic level and focused on those classes or divisions that contain LCD-producers (Table S1). Specifically we investigated the distribution of Eustigmatophyceae, since they are the most well-known class of LCD-producers, Pelagophyceae and Chrysophyceae, which include the LCD-producers *Sarcinochrysis marin*a and *Chrysosphaera parvula*, respectively (Table S1), Dictyochophyceae, which includes *Apedinella radians* (Rampen et al., 2011), and Raphidophyceae, which include two LCD-producers, *H. akashiw*o and *Haramonas dimorpha*. We did not detect any representative of Pinguiophyceae, a class which include the LCD-producer *Phaeomonas parva* (Table S1). Reads associated to Pelagophyceae, and mostly (97%) affiliated to *Pelagomonas calceolata*, were recovered more frequently as they were present in 55 samples with an average abundance of 85 reads (2% of total reads) per sample and a maximum value of 935 reads (12% of total) in the DCM of Station 23 (Fig. 4B). Pelagophyceae reads were mostly detected in the DCM and were particularly abundant at the 3 westernmost stations investigated, where they comprised 8% of total reads (Fig. 4B).

Chrysophyceae and Dictyochophyceae were also detected in most samples (54 and 57 samples, respectively) and their reads were recovered more frequently at the surface and BWML of the westernmost part of the transect (Stations 20-23) and at the surface of Stations 3-4 (Fig. 4C and D). Their 18S rRNA gene reads reached abundances of up to 55 and 41 reads (0.4 and 0.6% of total, respectively), for Chrysophyceae and Dictyochophyceae respectively, in the BWML of Station 20 (Table S4). Raphidophyceae were present only in three samples from Stations 11, 12, and 13 (Fig. 4F).

4 Discussion

4.1 Comparison of diol distributions

In general, it is thought that 1,13- and 1,15-diols derive from a different source than 1,14- diols in the marine realm (Sinninghe Damsté et al. 2003; Rampen et al. 2007, 2011). Indeed, linear regressions showed that the concentration of C_{30} 1,15-diol is significantly correlated with those of the C_{30} 1,13- and C_{32} 1,15-diols (Figs. 5A-B). We did not observe any significant correlation between the concentrations of the C_{28} 1,13- and the C_{30} 1,13- or C_{30} 1,15-diol (Figs. 5C-D), which might be due to the fact that C_{28} 1,13-diol was below detection limit in 19 out of 71 samples and its distribution could be compared to that of the widespread C_{30-32} diols only for the remaining 52 samples. This low abundance of C_{28} 1,13-diol is consistent with the relatively high temperatures observed for the tropical Atlantic ocean (Fig. 1B), since the LCD core top calibration study has revealed that the fractional abundance of the C_{30} 1,15-diol is high and that of the C_{28} 1,13-diol is low when SST is relatively high (Rampen et al. 2012).

The concentration of the C_{28} 1,14-diol was not correlated with that of the C_{30} 1,14-diol (Fig. 5E), potentially suggesting a different origin for the C_{28} and the C_{30} 1,14-diols. However, the concentration of C_{30} 1,14-diol was significantly correlated with the C_{30} 1,15-diol (Fig. 5F). This is quite surprising as the 1,14-diols in seawater have been suggested to derive from *Proboscia* spp. (Sinninghe Damsté et al. 2003; Rampen et al. 2009), and to a lesser extent from *A. radians* (Rampen et al. 2011), whereas the 1,13- and 1,15-diols are thought to be associated with Eustigmatophyceae (Rampen et al. 2014b and references cited therein). Previous studies highlighted indeed good correlations in the fluxes of C_{28} and C_{30} 1,14-diols in the water column of the Arabian Sea (Rampen et al. 2007) and the northwestern Indian Ocean (Rampen et al. 2008). *Proboscia* spp. contain also unsaturated 1,14-diols which were not found here; specifically the warm water species *Proboscia indica* is dominated by $C_{28:1}$ and $C_{30:1}$ 1,14-diols (Rampen et al. 2007), suggesting that the 1,14-diols found here do not derive from *Proboscia* spp.. This is confirmed by the absence or very low proportions of 18S rRNA gene reads from the major producers of C_{28-30} 1,14-diols, that are *Proboscia* spp. and *A. radians* (Table 1). This suggests different sources for the C_{28} and the C_{30} 1,14-diols. Since the C_{30} 1,15-diol accounted for >95% of the C_{28-32} diols, it is possible that the C_{30} 1,14-diol was biosynthesised in low amounts, along with C_{30} 1,13-diol, by the producers of C_{30} 1,15-diol. This is supported by the fact that Eustigmatophyceae can contain small amounts of 1,14-diols along with large quantities of 1,15-diols (Rampen et al. 2014a); specifically the C_{28} 1,14-diol,

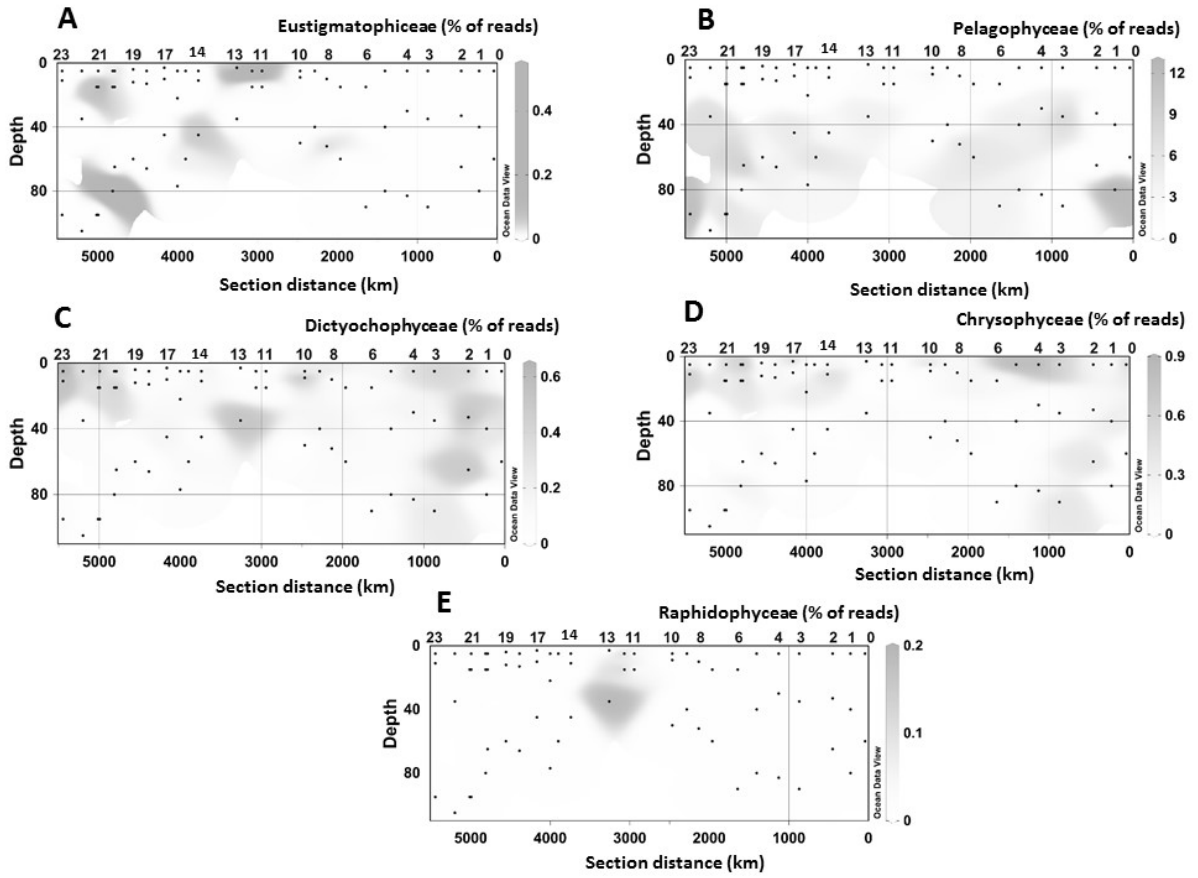

Figure 4: Spatial distribution of the 18S rRNA gene fragments related to taxa containing LCD-producers at different stations and depth. (A) Eustigmatophyceae, (B) Pelagophyceae, (C) Dictyochophyceae, (D) Chrysophyceae, (E) Raphidophyceae. Data were plotted using ODV software using kriging for interpolation between datapoints (Schlitzer 2002).

accounts for up to the 15% of the total LCDs in *Pseudostarastrum enorme*, and lower proportions (1-5%) of C_{30} 1,14-diols were previously found in *Vischeria punctata* and *Eustigmatos vischeri* (Rampen et al. 2014a).

It has been reported that the distributions of LCDs can be affected by riverine input, which is reflected by elevated amounts of the C_{32} 1,15-diol (>10%, de Bar et al. 2016; Lattaud et al. 2017b). However, the fractional abundance of the C_{32} 1,15-diol in the SPM is low (0 to 4%, data not shown), far lower than the values typically measured in river-influenced ecosystems such as the Iberian Atlantic Margin (de Bar et al. 2016), the Kara Sea (Lattaud et al. 2017b) or the Congo River plume (Versteegh et al. 2000). We did not detect other eustigmatophycean biomarkers such as C_{32} alkenols or C_{30-32} hydroxy fatty acids (Volkman et al. 1992; Gelin et al. 1997b), suggesting that riverine or marine Eustigmatophyceae were unlikely to source the C_{28-32} diols found here. The HCC cruise took place in a period of the year (August/September) when the water discharge from the Amazon River is typically low (Molleri et al. 2010), thus leading to low inputs of riverine organic matter into the sea. The distribution of LCDs in the sampled SPM is thus likely not impacted by terrestrial input of LCDs.

Beyond Heterokontophyta, LCDs may also be produced by lower (Speelman et al. 2009) and higher (Wen et al. 2006; Racovita and Jetter 2016) plants. However, only 4 reads from our dataset were associated with a plant species, i.e. *Panax ginseng* (Table S4), which is not known to contain LCDs. The near absence of 18S rRNA gene reads from higher plants confirms the low riverine input of organic matter in the SPM of the tropical North Atlantic waters analysed here. We explored the variations in the concentrations of the LCDs with respect to environmental data. The C_{28} 1,13- and 1,14-diols, both occurring in low abundance, did not exhibit significant correlations with any of the environmental data measured here (Table 2). In contrast the concentrations of C_{30} 1,13-, 1,14- and 1,15-diols exhibited significant but weak positive correlations with temperature and dissolved silica and weak negative correlations with salinity and nitrite. The concentration of the C_{32} 1,15-diol revealed

a correlation with the same environmental variables as the C_{30} diols except for dissolved silica and nitrite and exhibited a weak negative correlation with the concentration of nitrate. The correlations found here are likely simply due to different water masses: the mixed layer, where the highest proportions of LCDs were measured, exhibited indeed higher temperatures and lower salinities compared to the DCM. We repeated the analyses after excluding DCM samples and did not find strong positive or negative correlations between LCDs and environmental variables (data not shown). Thus, there does not seem to be a major control of environmental conditions on the concentrations of LCDs.

4.2 Comparison with eukaryotic abundance and diversity

Although C_{28-32} diols are likely produced by phytoplankton, the variability in LCD abundance is not correlated with that of Chl-a concentration, or photosynthetic pico- and nanoeukaryote abundances (Table 2). This lack of correlation suggests that the LCD-producers accounted for only a small proportion of phytoplankton. The high proportion of Dinophyceae, Syndiniales, and Radiolaria revealed by our genetic libraries agree with previous studies on marine microbial communities based on 18S rRNA gene sequencing in different environments (Comeau et al. 2011; Christaki et al. 2013; de Vargas et al. 2015). However, these taxa do not necessarily dominate marine microbial communities and so our results are likely due to a relatively high number of rRNA gene copies per cell (Zhu et al. 2005). Larger-sized dinoflagellates such as *Prorocentrum minimum* and *Amphidinium carterae* can contain up to 1000 gene copies per cell compared to <10 of rRNA gene copies for smaller sized (<3 µm) species of Chlorophyta, Pelagophyceae, and Haptophyta (Zhu et al. 2005).

LCD-producers

Although the primers used in this study have a perfect match with the 18S rRNA gene sequences of most eukaryotes (including all the classes containing LCD-producers), and the rarefaction curves indicate that we sampled an appropriate (i.e. >90%) proportion of the eukaryotic community, we cannot fully exclude that some species remain undetected because of under sampling, or primer mismatches. Moreover, the large number (100-1000) of rRNA gene copies per cell present within dinoflagellates and Radiolaria might have somehow affected the detection of LCD producers. In particular *Nannochloropsis salina* has been shown to possess only 1-2 copies of 18S rRNA gene (Zhu et al. 2005), and similarly, the other marine *Nannochloropsis* species, which do not differ greatly in size from *N. salina* (Fawley and Fawley 2007), are also likely to have a low number of 18S rRNA gene copies. Known species of LCD-producers were present in only 51% of our SPM samples as revealed by sequencing data (Table 1), whereas the major LCD, the C_{30} 1,15-diol, was present in all samples. This suggests that the LCDs found here were (1) either produced by other species which were not detected using the current methodology, or (2) that the LCD-producers were under sampled because of their low number of rRNA gene copies per cell, or (3) that the DNA of the LCD-producers was no longer present in the SPM at the moment of sampling. Specifically, marine Eustigmatophyceae were represented by only two OTUs (denovo2075, *Nannochloropsis oculata*, and denovo229, uncultured Eustigmatophycea, Table S4) detected in only 8 samples, confirming the hypothesis of Volkman et al. (1992) and Rampen et al. (2012) that they are not the major producers of LCDs in the marine environment. Even if we expand our analyses of LCD-related species to a higher taxonomic level, we do not find large proportions of 18S rRNA reads (generally <0.9% of total reads) except for the class Pelagophyceae, which accounts for up to 12% of total reads (Fig. 2A-E). However, Pelagophyceae are unlikely to be the source of any of the LCDs found here because their vertical distribution (i.e. mostly detected in the DCM, Figs. 3, 4B) does not correspond well to that of LCDs, which were either more abundant in the upper layers (C_{30} 1,13-, 1,14-, and 1,15-diols and C_{32} 1,15-diol) or did not vary greatly with depth (C_{28} diols, Fig. 2). Chrysophyceae and Dictyochophyceae were instead more abundant in the upper layers (Fig. 4B-C) and although none of the three known LCD-producers from these classes produces the most abundant LCD detected in the SPM, i.e. C_{30} 1,15-diol (Table S1), other species within the Chrysophyceae and Dictyochophyceae may possibly be a source for the C_{30} diols.

The C_{28} diols exhibited higher concentrations at the BWML of Station 12 and at surface in Station 13 (Fig. 2A and B), and higher proportions of 18S rRNA gene reads were recovered from Pelagophyceae (2.4%), and Eustigmatophyceae (0.5%), at the surface of Stations 11-12 (Fig. 4D-F). The scattered occurrences of these groups and the mismatches in distributions when compared to the LCDs suggest that the LCDs in the tropical North Atlantic Ocean are unlikely to derive from Pelagophyceae, radial centric diatoms, Raphidophyceae, and/or

Eustigmatophyceae.

Overall the abundance of known LCD producers is low and scattered and does not match the observed abundance patterns observed for the LCDs, suggesting that most of the LCDs measured here were not produced by any of these species.

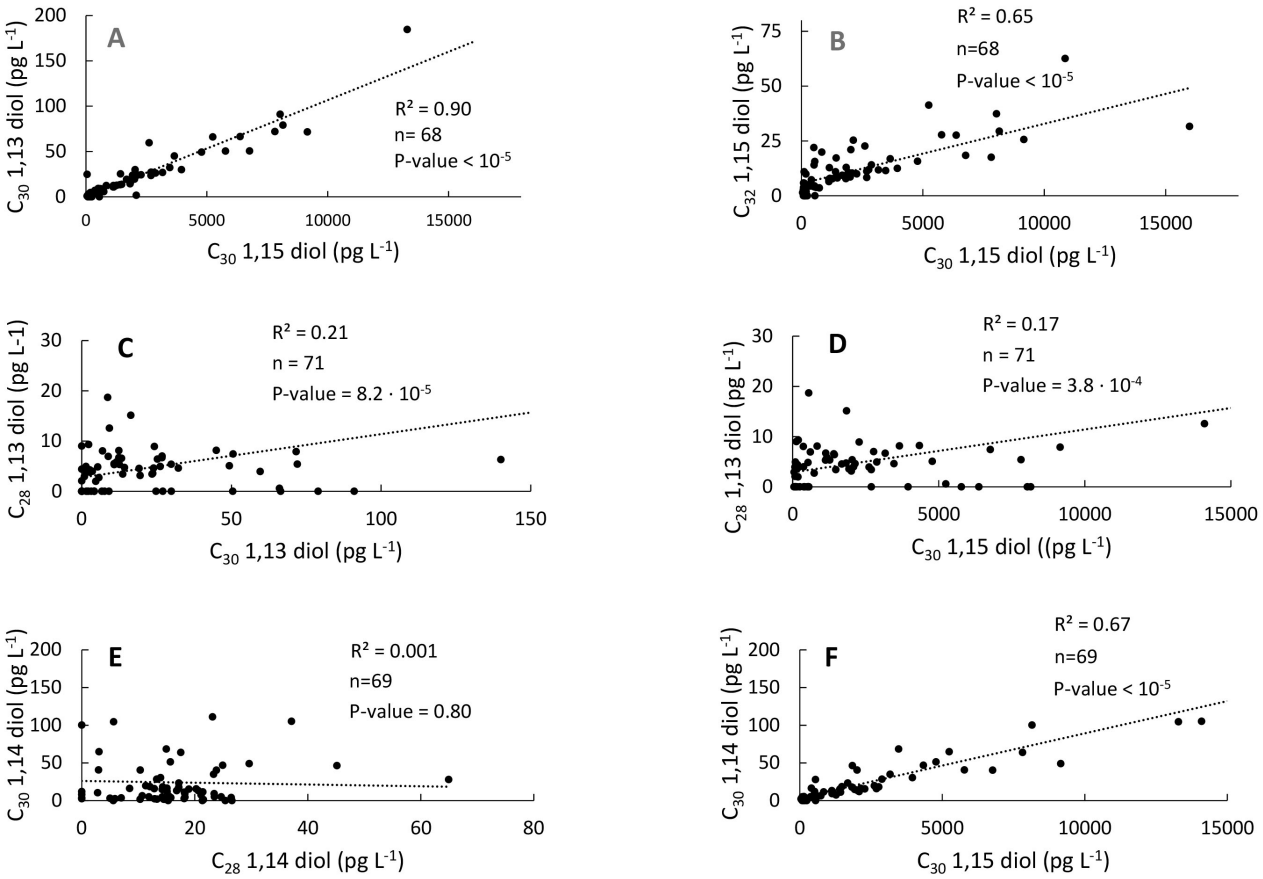

Figure 5: Scatter plots of the concentrations of the different LCDs in the western tropical Atlantic Ocean. (A) C_{30} 1,13-diol vs C_{30} 1,15-diol, (B) C_{32} 1,15-diol vs C_{30} 1,15-diol, (C) C_{28} 1,13-diol vs C_{30} 1,13-diol, (D) C_{28} 1,13-diol vs C_{30} 1,15-diol, (E) C_{30} 1,14-diol vs C_{28} 1,14- diol, (F) C_{30} 1,14-diol vs C_{30} 1,15-diol.

Correlations between the abundance of OTUs and LCD concentration

Since LCDs have been shown to be present within two genetically distant eukaryotic supergroups, the Heterokontophyta and the Archaeplastida, the latter including plants as well as green and red algae, the genetic and enzymatic machinery required for the biosynthesis of LCDs might be present in other genera and classes, including uncultured species. We, therefore, also compared the concentration of LCDs with the composition of the entire eukaryotic microbial community, normalised with respect to the 18S rRNA gene abundance, at both class and OTU levels to identify co-occurrence patterns. No significant correlation was found at class level (data not shown), whereas the correlations at the OTU level were weak ($r \leq 0.60$) but significant (p-value <0.01) for 27 OTUs affiliated to 11 different classes (Table 2). A reason behind the lack of correlation between taxonomic classes and LCDs can be that pooling OTUs at higher taxonomic levels likely leads to combining the LCD-producers with species which are unable to produce LCDs but that are falling in the same taxonomic level. The ability of microorganisms to biosynthesize LCDs can indeed vary, even between genetically related species; some genera include both LCD-producers and species which do not contain LCDs (Table S1).

The C_{30} 1,15-diol exhibited significant correlations (p <0.01) with 23 OTUs and overall, 27 OTUs were significantly correlated with C_{30} or to a lesser extent, C_{32} diols (Table 3). Of the 27 OTUs, 4 OTUs were affiliated to classes containing known LCD-producers (Chrysophyceae and Dictyochophyceae, Table 3). The abundance of the two chrysophycean OTUs (denovo465 and denovo1680, Table 3) exhibited significant correlations with

the concentrations of both C_{30} 1,13- and 1,15-diols and accounted for 52% of the total reads from this class and the only known LCD-producer from this class (*Chrysosphaera parvula*) was found to contain C_{32} 1,15-diol (Rampen, unpublished results). The two OTUs affiliated to Dictyochophyceae (denovo873 and denovo958) and exhibiting positive correlation with $C_{30–32}$ diols, cluster within Pedinellales and Florenciellales families, respectively, and are thus closely related to two known LCD-producers, *Florenciella parvula* and *Apedinella radians*. However, *F. parvula* contains C_{24} 1,13-, C_{24} 1,14-, and C_{24} 1,15-diols (Rampen, unpublished results) and *A. radians* produces C_{28}, C_{30}, and C_{32} 1,14-diols (Rampen et al., 2011), whereas the two dictyochophycean OTUs denovo873 and denovo958 exhibited positive correlation with the C_{30} 1,15-diol (Table 3).

The correlation values found here are nearly all low ($r \approx 0.4$-0.5), raising the question of whether these relationships reflect the ability of these species to produce LCDs or whether they are simply driven by other environmental conditions leading to similar spatial distributions of OTUs and LCDs. Other OTUs showing significant correlations with C_{30} 1,15-diol are rare in the marine environment. For example, species falling in the Centroheliozoa (OTU denovo1066) are mostly known as freshwater predators (Slapeta et al. 2005). In seawater, they have only been sporadically detected in anoxic environments (Stock et al. 2009; Stoeck et al. 2009), suggesting that the centroheliozoan reads found here are unlikely to derive from active microorganisms. In contrast, the other OTUs include marine representatives commonly found in the photic zone of seawater and thus the reads found here might derive from living organisms: Syndiniales are intracellular parasites of other marine protists, and the genetic clades found here (Group I Clade 4, Group II Clades 2, 7, 8, 17, and 23) are commonly detected in the upper 100 m of the water column (Guillou et al. 2008). Spirotrichea include several heterotrophic and mixotrophic marine planktonic ciliates (Agatha et al. 2004; Santoferrara et al. 2017), whereas Phaeocystis is a widespread primary producer. The OTUs of uncultured classes exhibiting significant positive correlations with LCDs (Prasino Clade IX and the HAP-3 clade) are also commonly observed in the photic zone (Shi et al. 2009; Egge et al. 2015; dos Santos et al. 2016). However, cultivated representatives would be required in order to confirm whether species within these clades are capable of LCD synthesis.

4.3 Can 18S rRNA gene-based community composition analysis be used to determine LCD biological sources?

The lack of correlations of C_{28} diols with any OTUs as well as the low degree of correlation between OTUs and $C_{30–32}$ diols and the trace abundance or near absence of known LCD producers suggest that the 18S rRNA genes from the microorganisms sourcing the LCDs were either absent, or present below detection level in the seawater sampled. The fact that we sampled >90% of the OTUs potentially present (Figure S1) and the use of universal eukaryotic primers suggests that LCD-producers have been unlikely to escape detection. However, the relatively low number of rRNA gene copies found for *N. oculata* (Zhu et al. 2005) and likewise also in other smaller-sized marine Eustigmatophyceae, suggest that LCD-producers might have been under sampled with respect to larger-sized species which can contain up to 1000 rRNA copies per cell (Zhu et al. 2005).

It should be considered that both the LCDs and DNA in the SPM might derive not only from active or senescent cells, but also from detritus (Not et al. 2009). In addition, LCDs can persist in seawater for likely much longer periods than the DNA of the related LCD-producers. Although the biological function of LCDs is unclear for most species, they have been shown to be the building blocks of cell wall polymers in Eustigmatophyceae, and likewise they might occur in other biopolymers of marine or terrestrial origin. In *Nannochloropsis* cell wall, LCDs and long chain alkenols are likely to be bound together through ester and ether bonds to form highly refractory polymers known as algaenans (Gelin et al. 1997a; Scholz et al. 2014). These biopolymers are thought to be quite persistent and accumulate in ancient sediments for millions of years (Tegelaar et al. 1989; Derenne and Largeau 2001; de Leeuw et al. 2006). Indeed, LCDs are ubiquitous in recent surface sediments (Rampen et al. 2012) and ancient sediments of up to 65 million years old (Yamamoto et al. 1996) showing their recalcitrant nature.

Recent laboratory experiments highlighted that LCDs from dead biomass of *Nannochloropsis oculata* can persist in seawater for longer than 250 days under both anoxic (Grossi et al. 2001) and oxic conditions (Reiche et al. 2018). In contrast, much shorter turnover times (6 h to 2 months) are typically reported for extracellular DNA in the oxic water column (Nielsen et al. 2007). This suggests that the DNA from LCD-producers likely reflects the living eukaryotic community (recently) present when seawater was sampled, while the LCDs probably represent an accumulation that occurred over longer periods of time (weeks to months or even years).

Because of this large difference in turnover rates between LCDs and the DNA from the LCD-producers,

18S rRNA gene analysis of environmental samples may be unsuccessful for identifying LCD-producers. This is seemingly in contrast to a previous study that showed that the LCD concentration in the upper 25 m of the freshwater lake Chala (Tanzania) was related to the number of eustigmatophycean 18S rRNA gene copies (Villanueva et al. 2014). However, Villanueva et al. (2014) used Eustigmatophyceae-biased primers and since this was a lake system, Eustigmatophyceae are likely to be the major source of LCDs in freshwater ecosystems. Importantly, they found a mismatch for the uppermost part of the water column (0–5 m), where high LCD abundance (38-46 ng L^{-1}) coincided with little or no Eustigmatophyceae 18S rRNA gene copies. This pattern was explained by them to be caused by wind-driven and convective mixing of preserved LCDs, while phytoplankton adjusted its buoyancy at greater depth (Villanueva et al. 2014). The high salinity values ($\geq$ 33 g kg^{-1}) detected in most surface samples, the low proportions of both C_{32} 1,15-diols (2.2% over the total LCDs) and 18S rRNA gene reads associated with plants (4 out of 238 564), as well as the low input of freshwater from the Amazon River to the stations analysed here during the sampling period (Molleri et al. 2010) suggest that the LCDs found here are unlikely to have a freshwater origin.

Laboratory experiments carried out under different conditions of temperature, light irradiance, salinity and nitrate concentrations revealed average cellular LCD content of about 23 fg $cell^{-1}$ (Balzano et al. 2017) for *Nannochloropsis oceanica*. The average LCD concentration in the SPM investigated was ca. 2.6 ng L^{-1}, which would correspond to ca. 1.1 x 10^6 pico/nano algal cells L^{-1}. We detected average phytoplankton abundances of 3.3 x 10^6 cell L^{-1} for picoeukaryotes and 3.6 x 10^4 cell L^{-1} for nanoeukaryotes. Although nanoplanktonic Eustigmatophyceae might produce larger amounts of LCDs than those measured in our previous study (Balzano et al. 2017), because of their larger cell size, the nanoplankton abundances measured here are two orders of magnitude lower than the densities required to source the LCDs (1.1 x 10^6 cell L^{-1}). Therefore, if the LCDs measured here were biosynthesised by intact microorganisms in the water column, nanoplankton alone would not be able to source all the LCDs measured, and therefore in addition at least one-third of the picophytoplankton should be able to produce LCDs, which is unrealistic. This supports the idea that most of the LCDs detected here are of fossil nature and not contained in living cells. The higher concentrations of LCDs found in the SPM from the mixed layer compared to the DCM suggest that LCDs were originally produced at a higher frequency in the mixed layer. Moreover, their possible fossil nature indicates that LCDs were likely to persist in the mixed layer for long periods, eventually associated with suspended particulate matter.

The combination of lipid and DNA analyses is often complicated by different turnover rates, especially for refractory compounds such as LCDs. Studies focused on more labile biomarker lipids such as fatty acids or intact polar lipids can be more successful, e.g. with short branched fatty acids (Balzano et al. 2011), cyanobacterial glycolipids (Bale et al. 2018), or archaeal phospholipids (Pitcher et al. 2011; Buckles et al. 2013). Therefore, care has to be taken in inferring sources of biomarker lipids by the quantitative comparison of DNA abundance with biomarker lipid concentrations. Analysis of intact polar lipids, rather than total lipids, might have facilitated the identification of diol producers.

5 Conclusion

The combination of lipid analyses and 18S rRNA gene amplicon sequencing revealed some weak correlations between the abundances of 27 OTUs and the concentration of C_{30} diols. Four of these OTUs are affiliated to classes that include few LCD-producing species (i.e. Chrysophyceae and Dictyochophyceae), whereas the remaining 23 OTUs belong to taxa in which the presence of LCDs has never been assessed. In both cases it remains unclear whether the correlation between these 27 OTUs and the C_{30} diols reflects novel LCD-producers or is driven by other environmental conditions.

The abundances of photosynthetic pico and nanoeukaryotes measured here suggest that these microbial populations are highly unlikely to source all the LCDs found. Some of the LCDs found here might be associated with suspended debris rather than intact cells, with the DNA from their producers being already degraded at the time of sampling. DNA degradation rates in the oxygenated water column are indeed faster than those of most lipids, including LCDs. The freshness of the organic matter and the turnover rates of both lipids and DNA in a given environment should thus be considered when identifying the biological sources of a specific class of lipids through DNA sequencing. In addition, the extraction methods applied in our study did not discriminate between free and bound lipids and we thus do not know if the compounds found here were originally present in seawater as free or ester-bound diols. Finally, the 18S rRNA gene amplicon sequencing can be suitable to track

LCD sources (1) for simple ecosystems or laboratory/in situ mesocosms with high proportions of fresh organic matter and (2) for low oxygen/anoxic environments where extracellular DNA can persist for longer periods.

Tables

Table 1: Distribution of the18S rRNA gene reads associated with known LCD-producers

Taxon	Florenciellales	*Heterosigma*	Eustigmatophyceae	*Proboscia*	Total
No of samples[a]	28	2	8	2	35
Surface	12	1	2	0	12
BWML[b]	11	0	2	2	13
DCM[c]	5	1	4	0	10
No of reads[d]	99	10	45	3	157
% total	0.04	0.004	0.02	0.001	0.06
Surface	48	4	25	0	77
BWML	41	0	9	3	53
DCMl	10	6	11	0	27

[a] Number of samples where 18S rRNA gene reads from C_{28-32} diol-producers were found Overall 68 samples were screened for the presence of 18S rRNA genes affiliated to LCD-producers.
[b] Bottom wind mixed layer
[c] Deep chlorophyll maximum
[d] Number or proportion of 18S rRNA gene reads associated with C_{28-32} diol-producers.

Table 2: Spearman rank correlation coefficients between LCD and environmental variables[a]

	C_{28} 1,13	C_{28} 1,14	C_{30} 1,13	C_{30} 1,14	C_{30} 1,15	C_{32} 1,15
Organic carbon	0.3	0.2	0.2	0.3	0.3	0.3
Salinity	-0.2	0.0	**-0.5**	**-0.7**	**-0.6**	**-0.6**
Temperature	0.2	-0.1	**0.5**	**0.5**	**0.5**	**0.5**
Phosphate	0.0	0.2	-0.3	-0.2	-0.3	-0.2
Ammonium	0.0	0.1	-0.3	-0.4	-0.4	-0.2
Nitrite	-0.2	0.0	**-0.6**	**-0.5**	**-0.6**	-0.4
Nitrate	0.0	0.2	-0.4	-0.3	-0.3	**-0.5**
Silica	0.1	0.0	0.4	**0.5**	**0.5**	0.4
Chl-a	-0.1	0.0	-0.2	-0.2	-0.3	-0.1
Picoeukaryotes	-0.1	-0.1	-0.4	-0.3	-0.4	-0.2
Nanoeukaryotes	0.0	-0.1	0.1	0.2	0.2	0.2

[a] Significant (p-value < 0.01) correlation values are in bold.

Table 3. Correlation coefficient r for the Operational Taxonomic Units (OTUs), representing 95 % of sequence identity, whose abundance was correlateda with the concentration of LCDs in SPM samples obtained in the HCC cruise. a Only significant (p-value < 0.01 after FDR correction) correlations are shown. b OTUs closely related to known LCD-producers are in bold.

OTU ID[b]	Taxon	Class	C_{30} 1,13	C_{30} 1,14	C_{30} 1,15	C_{32} 1,15	Total 1,13	Total 1,14	Total 1,15
denovo2033	Choreotrichia	Spirotrichea							0.4
denovo2137	*Climacocylis scalaria*		0.45		0.49		0.45		0.49
denovo940	*Laboea strobila*		0.53	0.46	0.6		0.56	0.45	0.59
denovo685	Oligotrichia				0.41				0.4
denovo1804	*Pseudotontonia*		0.56	0.47	0.56	0.47	0.53	0.41	0.57
denovo492	*Blastodinium spinulosum*	Dinophyceae	0.43	0.44	0.46				0.45
denovo720	*Ceratocorys horrida*				0.46		0.44		0.45
denovo1682	*Neoceratium fusus*							0.47	
denovo526	*Protodinium simplex*			0.43	0.44			0.48	0.43
denovo267	*Pyrophacus_steinii*				0.43				0.42
denovo732	Dino Group I Clade 4	Syndiniales			0.4		0.46		0.41
denovo555	Dino Group II Clade 2				0.49		0.41		0.48
denovo1077	Dino Group II Clade 7				0.44		0.42		0.43
denovo1834	Dino Group II Clade 8				0.44		0.45		0.45
denovo1145	Dino Group II Clade 17		0.5		0.49		0.53	0.42	0.48
denovo2080	Dino Group II Clade 23				0.4		0.43		0.4
denovo725	Prasino Clade 9B	Prasino Clade IX			0.42		0.41		0.41
denovo1066	Pterocystida	Centroheliozoa			0.46				0.46
denovo400	HAP3	Haptophyta		0.47	0.49			0.47	0.48
denovo2132	*Phaeocystis*						0.46		
denovo972	*Haptolina*						0.44		
denovo465	**Chrysophyceae Clade G**	Chrysophyceae	0.44		0.43		0.45		0.42
denovo1680	**Chrysophyceae Clade H**		0.44		0.42		0.48		0.42
denovo1988	Raphid pennate	diatoms			0.41				0.41
denovo873	**Pedinellales**	Dictyochophyceae	0.56	0.45	0.55	0.52	0.55		0.56
denovo958	**Florenciellales**	Dictyochophyceae			0.43		0.45		0.44
denovo2433	Unidentified picozoan	Picozoa	0.49	0.5	0.55		0.47	0.46	0.55

Acknowledgments

We thank the captains and the crew of the R/V Pelagia for their support during the cruise. We thank Denise Dorhout for sample collection, Sharyn Ossebaar for nutrient analysis, H. Witte, E. Panoto, and S. Vreugdenhil for support in molecular biology, H. Malschaert for the bioinformatics and M. Besseling for helpful discussions. John Volkman and two anonymous referees provided helpful comments on an earlier version of this paper. This research was funded by the European Research Council (ERC) under the European Union's Seventh Framework Program (FP7/2007-2013) ERC grant agreement [339206]. S.S. and J.S.S.D. receive financial support from the Netherlands Earth System Science Centre (NESSC) though a gravitation grant (NWO 024.002.001) from the Dutch Ministry for Education, Culture and Science

Supplement

The Supplement related to this article is available online at https://doi.org/10.5194/bg-15-5951-2018-supplement.

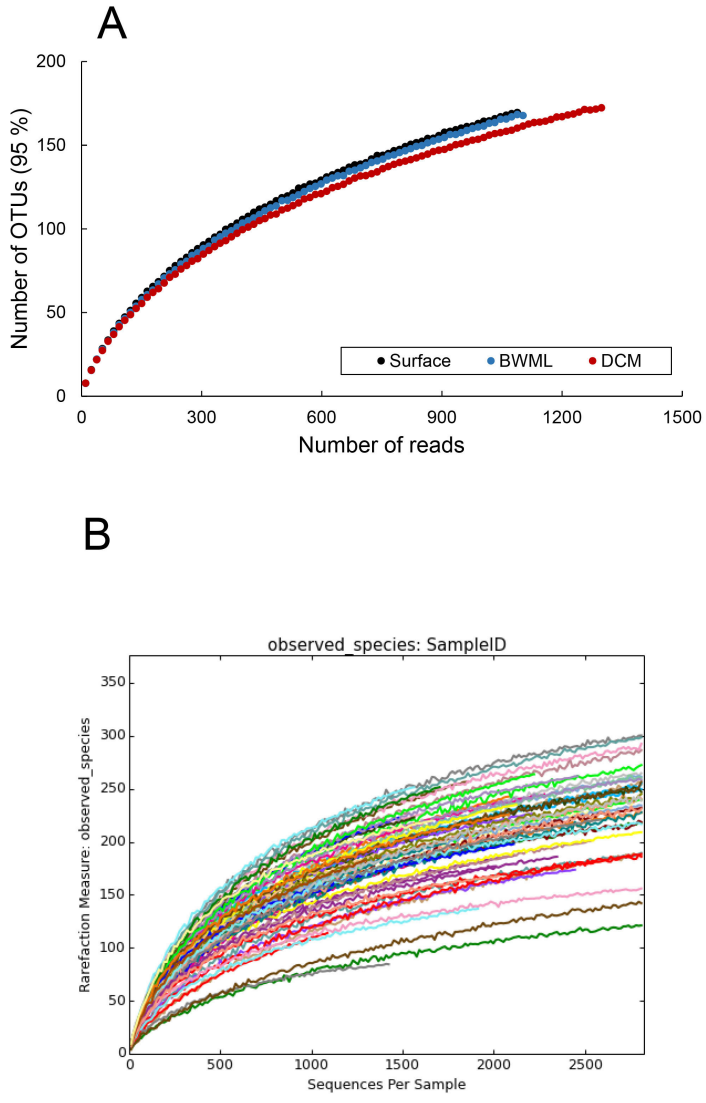

Figure 1: Accumulation vurves of the operational taxonomy units (OTUs) representing sequences clustered at 95% identity. The curves shows for (A) samples pooled by their depth features or for (B) individual samples

Supplementary Figure S2

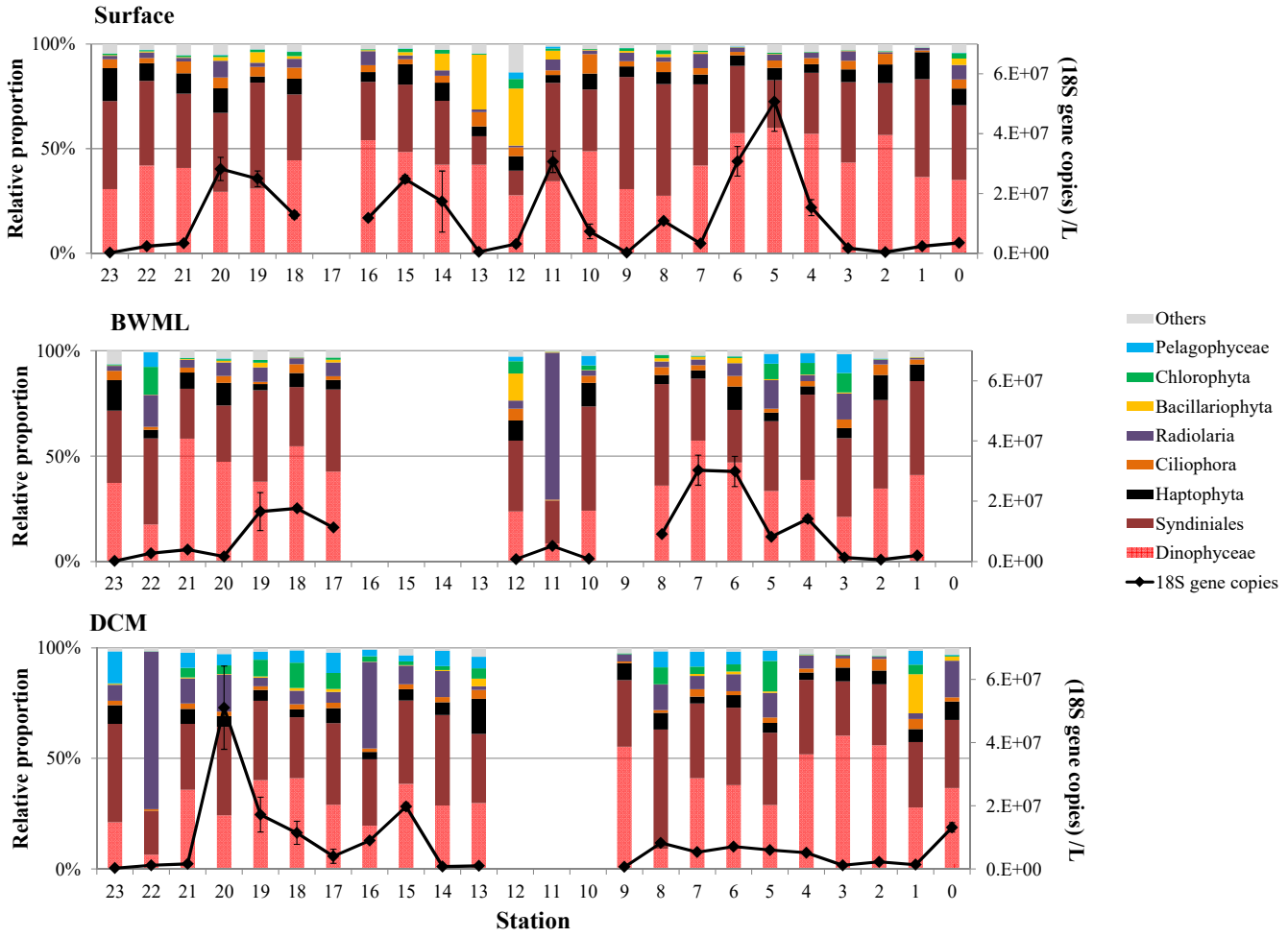

Fig. S2. Relative abundance (left axis) of the different protistan taxa and number of the 18S rRNA gene copies (right axis) in the SPM collected during the HCC cruise. Relative abundance data were inferred by high throughout sequencing of the conserved V4 region of the 18S rRNA gene, whereas the number of 18S rRNA gene copies was inferred by quantitative PCR.

Multicore from the Black Sea, credit @Rose Leahy

Chapter 3

The C_{32} alkane-1,15-diol as a tracer for riverine input in coastal seas

Geochimica et Cosmochimica Acta 202 (2017) 146–158

Julie Lattaud [a,*], Jung-Hyun Kim [a,1], Cindy De Jonge [a,2], Claudia Zell [a,3], Jaap S. Sinninghe Damsté [a,b], Stefan Schouten [a,b]

[a] NIOZ, Royal Netherlands Institute for Sea Research, Department of Marine Microbiology and Biogeochemistry (MMB), and Utrecht University, PO Box 59, 1790 AB Den Burg, The Netherlands
[b] Utrecht University, Faculty of Geosciences, Department of Earth Sciences, Princetonlaan 8a, 3584 CD Utrecht, The Netherlands

*Corresponding author.
E-mail address: Julie.lattaud@nioz.nl (J. Lattaud).
[1] Current address: Korea Polar Research Institute, 26 Songdomirae-ro, Yeonsu-gu, Incheon 21990, South Korea.
[2] Current address: Department of Biology, Antwerpen University,Campus Drie Eiken, Universiteitsplein 1, 2610 Wilrijk, Belgium.
[3] Current address: Département Biogéochimie, Pierre and Marie Curie University, UMR 7619 METIS, 4 Place Jussieu, 75252 Paris, France.
http://dx.doi.org/10.1016/j.gca.2016.12.030

Abstract

Long chain alkyl diols are lipids that occur ubiquitously in marine sediments and are used as a proxy for sea surface temperature (SST), using the Long chain Diol Index (LDI), and for upwelling intensity/high nutrient conditions. The distribution of 1,13- and 1,15-diols has been documented in open marine and lacustrine sediments and suspended particulate matter, but rarely in coastal seas receiving a significant riverine, and thus continental organic matter, input. Here we studied the distribution of diols in four shelf seas with major river outflows: the Gulf of Lion, the Kara Sea, the Amazon shelf and the Berau delta, covering a wide range of climate conditions. The relative abundance of the C_{32} 1,15-diol is consistently higher close to the river mouth and particularly in the suspended particulate matter of the rivers suggesting a terrigenous source. This is supported by statistical analysis which points out a significant positive correlation between the C_{32} 1,15-diol and the Branched and Isoprenoid Tetraether index, a proxy reflecting soil and riverine input in marine environments. However, the C_{32} 1,15-diol was not detected in soils and is unlikely to be derived from vegetation, suggesting that the C_{32} 1,15-diol is mainly produced in rivers. This agrees with the observation that it is a dominant diol in most cultivated freshwater eustigmatophyte algae. We, therefore, suggest that the relative abundance of the C_{32} 1,15-diol can potentially be used as a proxy for riverine organic matter input in shelf seas. Our results also show that long chain alkyl diols delivered by rivers can substantially affect LDI-reconstructed SSTs in coastal regions close to river mouths.

Keywords: *Long-chain diols; Long-chain Diol Index; 1,13-,1,14- and 1,15-diols; C_{32} 1,15-diol; River outflow; Terrigenous output; Sea Surface Temperature*

1 Introduction

Long-chain alkyl diols (LCD) are molecules composed of a long alkyl chain (number of C atoms >28) containing alcohol groups at C_1 and at a mid-chain position (e.g. carbon number 12, 13, 14, 15), which have been reported in a wide range of environments (de Leeuw et al. 1981; Versteegh et al. 1997, 2000; Gogou and Stephanou 2004; Schmidt et al. 2010; Rampen et al. 2012, 2014b; Romero-Viana et al. 2012; Plancq et al. 2015; Zhang et al. 2011 and references therein). In marine environments, the major LCDs are typically C_{28} and C_{30} 1,13-diols, C_{28} and C_{30} 1,14-diols, and C_{30} and C_{32} 1,15-diols (Rampen et al., 2014a). C_{28} and C_{30} 1,14-diols are biosynthesized by the diatom genus *Proboscia* (Sinninghe Damsté et al. 2003; Rampen et al. 2007) and the marine algae *Apedinella radians* (Rampen et al. 2011), while C_{28} and C_{30} 1,13-diols and C_{30} and C_{32} 1,15-diols have been reported in eustigmatophyte algae (Volkman et al. 1992, 1999; Gelin et al. 1997a; Méjanelle et al. 2003). However, eustigmatophyte algae are rarely reported in the marine environment and the distribution of diols present in marine eustigmatophyte algae (genus *Nannochloropsis*) does not match with the diol distribution in marine environments (Volkman et al. 1992, Versteegh et al. 1997; Rampen et al. 2014a).

Multiples indices using LCDs have been developed that reflect different environmental parameters in the marine environment. One such index is the LDI (Long-chain Diol Index, equation 1, $[C_{30}1,15]$ stands for fractional abundance of the diol), which is used as a proxy for Sea Surface Temperature (SST; Rampen et al. 2012):

$$LDI = \frac{[C_{30}1,15]}{[C_{30}1,15] + [C_{30}1,13] + [C_{28}1,13]} \quad (1)$$

The LDI of marine surface sediments shows a strong correlation ($r^2 = 0.97$) with SST (between -3°C and 27°C). Another index is DI-1 (equation 2) which has been developed by Rampen et al. (2008) to trace upwelling conditions.

$$DI-1 = \frac{[C_{30}1,14] + [C_{28}1,14]}{[C_{30}1,14] + [C_{28}1,14] + [C_{30}1,15]} \quad (2)$$

This index is based on the fractional abundance of C_{30} 1,14- and C_{28} 1,14- diols, produced primarily by *Proboscia* diatoms. As *Proboscia* diatoms thrive in upwelled, nutrient-rich water they are a good indicator

of upwelling conditions. This upwelling index has been applied for the upwelling region of the Arabian Sea (Somalian upwelling; Rampen et al. 2008). Willmott et al. (2010) constructed another diol index (DI-2, equation 3) as a proxy for paleo productivity of *Proboscia* diatoms and upwelling intensity at high latitudes (around the Antarctic peninsula).

$$DI-2 = \frac{[C_{30}1,14] + [C_{28}1,14]}{[C_{30}1,14] + [C_{28}1,14] + [C_{30}1,13] + [C_{28}1,13]} \quad (3)$$

Rampen et al. (2014a) studied these two indices in globaly distributed marine sediments and showed that the DI-1 is likely impacted, besides by upwelling and high nutrients, by SST, while the DI-2 is more widely applicable as an indicator of upwelling conditions. Another diol index (DI-3, equation 4) has been created for the Congo River fan by Versteegh et al. (1997), (2000) to assess relative changes in salinity.

$$DI-3 = \frac{[C_{30}1,15]}{[C_{30}1,15] + [C_{32}1,15]} \quad (4)$$

However, Rampen et al. (2012) showed that, on a global scale, this diol index only had a weak correlation with salinity (Pearson correlation r<0.3).

With respect to freshwater environments, Rampen et al. (2014b) showed that the LDI in surface sediments of lakes only correlated weakly with mean annual air temperature (a proxy for lake surface temperature) and that the distributions of LCDs differ from those in marine sediments. This indicates that the producers and environmental controls on diols in lakes are different compared to those in marine environments. Interestingly, only a few studies have investigated the diol distributions in marine environments affected by continental input, i.e near large river outflows. A recent study by de Bar et al. (2016) on long chain diol distributions of the Portugese margin suggested that some diols, in particular the C_{32} 1,15-diol, may be partially derived from a continental source. Indeed, Rampen et al. (2014a) also reported relatively high amounts of the C_{32} 1,15-diol in several estuarine sediments and Versteegh et al. (1997) showed that this diol was relatively more abundant close to the river mouth of the Congo River, suggesting also a partial source from the continent. However, it is unclear if the C_{32} 1,15-diol is consistently derived from continental sources in coastal seas and from which sources on the continent the C_{32} 1,15-diol is derived.

To constrain the distribution and origin of the C_{32} 1,15-diol in coastal marine environments, we studied four coastal seas with a substantial river input and from different climate zones: The Gulf of Lion and the Rhône River (Mediterrannean Sea) with a temperate climate, the Amazon shelf and the Amazon River (Atlantic Ocean) and Berau delta region (Pacific Ocean) with a tropical climate, and the Yenisei River and Kara Sea (Arctic Ocean) with a (sub)polar climate (Fig. 1). Our results shed light on the origin of the C_{32} 1,15-diol in coastal seas and suggest its potential as a proxy for the input of riverine organic matter (OM).

2 Material and methods

2.1 Study sites and sampling

Gulf of Lion

The Gulf of Lion is located in the northwestern part of the Mediterranean Sea (42°N 3°E and 44°N 6°E; Fig. 1) with a fairly broad and crescent shaped continental shelf and is under the strong influence of rivers. The major river discharging into the Gulf of Lion is the Rhône River, with a catchment area of 98 000 km^2 and a length of 813 km. Its source is the Rhône glacier in the Swiss Alps. The river is subsequently discharged through the Lake Geneva and southern France into the Gulf of Lion (Mediterranean Sea). The average water discharge is ca. 1.7 x 103 m^3/s (Thill et al. 2001), and a mean sediment discharge of 7-10 x 10^6 tons/yr represents 80 % of the inflow into the Gulf of Lion (de Madron et al. 2000; Sabatier et al. 2006). Other rivers besides the Rhône River which discharge into the Gulf of Lion are the Vidourle, Herault, Orb, Aude, Agly, Têt and Tech rivers in France and the Riu Ter, Fluvia and Tordera rivers in Spain. These rivers have more episodic discharges corresponding with major rainfalls associated with storms. The major current in the Gulf of Lion is the Liguro-Provencal going from East to West. The Mediterranean climate is characterized by warm, dry summers and mild to cool, wet winters. The mean annual sea surface temperature (SST) is ranging from 16°C to 19°C (Kim et al. 2015). The mean annual air temperature (MAAT) in the Rhone catchment is 9°C (Olivier et al. 2009).

The Gulf of Lion sample set consisted of 50 surface (0-0.5 or 0-1 cm) sediments and one sample of suspended particulate matter (SPM) of the Rhône river. The samples were previously studied for Glycerol Dialkyl Glycerol Tetraether (GDGT) lipids and bulk parameters by Kim et al. (2006), (2007), (2010), (2014), (2015). The surface samples have been collected during several French research programs (River-Dominated Ocean Margins, Climate and Human-Induced Alterations in Carbon Cycling at the River–Sea Connection) and research programs funded by the European Union (Hotspot Ecosystem Research on the Margins of European Seas, European Margin Strata Formation). The SPM was collected close to the water surface in the Rhône River: 5 l of water were filtered through pre-ashed glass fiber filters (Whatman GF-F, 0.7 µm, 142 mm diameter) with an in-situ pump system (WTS, McLane Labs, Falmouth, MA). All samples were kept frozen at -20°C and freeze dried before analysis.

Amazon shelf

The Amazon River is the largest drainage system in the world (6.1 x 10^6 km^2) in term of fresh-water discharge (Milliman and Meade 1983) and catchment area (Goulding et al. 2003). Both its main (the Madeira River) and secondary (the Solimoes River) tributaries originate in the Bolivian Andes. Due to the equatorial position, the temperature in the drainage basin is relatively constant year-round with a MAAT of 26°C (New et al. 2002). The coldest temperature is in the Andes Mountains due to the high elevation. The mean annual water discharge is 2 x 10^5 m^3/s at Óbidos (Callede et al. 2000) and the mean annual sediment discharge is 8-12 x 10^{11} kg/yr (Dunne et al. 1998). The mean annual SST for the Atlantic Ocean offshore the Amazon River mouth is 28°C (Zell et al. 2014).The major current on the Amazon shelf is the North Brazilian Current, transporting riverine suspended matter to the northwest, along the North Brazilian coast.

From the Amazon region, 14 marine surface sediments and 36 samples of riverine SPM (Fig. 1) were collected as described by Zell et al. (2014). These samples have been previously studied for GDGTs by Kim et al. (2012), Zell et al. (2013a), (2013b), (2014) and for long chain glycolipids by Bale et al. (2015). Surface sediments of the Amazon shelf and slope were collected on board of the R/V Knorr, cruise 197-4 between February and March 2010. All sediment samples were freeze dried prior to analyses. SPM was collected along the Amazon River main stem, in four tributaries (Solimones, Negro, Madeira, and Tapajos), and in five varzeas (Cabaliana, Janauaca, Marituba, Canacari, and Curuai). All SPM samples were kept frozen at -20°C and freeze dried before analysis.

Yenisei River and Kara Sea

The Yenisei River is the ninth largest river in the world in terms of discharge (Telang et al. 1991), and it crosses Mongolia and Siberian Russia in a south to north direction covering different climate zones. Thus, the Yenisei river watershed is characterized by large differences in MAAT, i.e. -6°C in the southern part of the catchment dropping to -11.4°C in the most northern parts (Jonge et al. 2014b). The mean annual discharge is estimated at 2 x 10^4 m^3/s. The Yenisei River catchment area is approximately 2.6 x 10^6 km^2. It discharges into the Kara Sea, which is the second largest shelf area of the Arctic Ocean. A fifth of the continental run-off of the Eurasian continent drains into the Kara Sea (Lammers and Shiklomanov 2000), where the Ob and Yenisei rivers provide the largest part of the water discharge. The two rivers are separated by the Gydan peninsula. The Yenisei discharge and Kara Sea circulation are characterized by a strong seasonality. During the summer months, the surface currents in the Kara Sea follow a cyclonic circulation. From mid-October to mid-May the Kara Sea and Yenisei River estuary are almost entirely ice-covered. The mean annual SST for the Kara Sea is -1°C (Boyer et al. 2013).

SPM from the Yenisei river water (16 river SPM) and the Kara Sea (21 surface sediments, Fig. 1) were obtained as described by Jonge et al. (2014b) by filtrating water through a GF/F glass fiber filter (0.7 µm pore size) using a McLane in-situ pump. For some sites in the Kara Sea, surface sediments were obtained via box coring on the R/V Akademik Mstislav Keldysh. These samples have been previously studied for GDGTs and bulk parameters by Jonge et al. (2014b), (2015a), (2015b).

Berau delta

The Berau delta is situated along the east coast of Kalimantan (Indonesia) and is a coastal and shallow embayment. It is situated north of the Makassar Trait, which is one of the main passages between the Indian

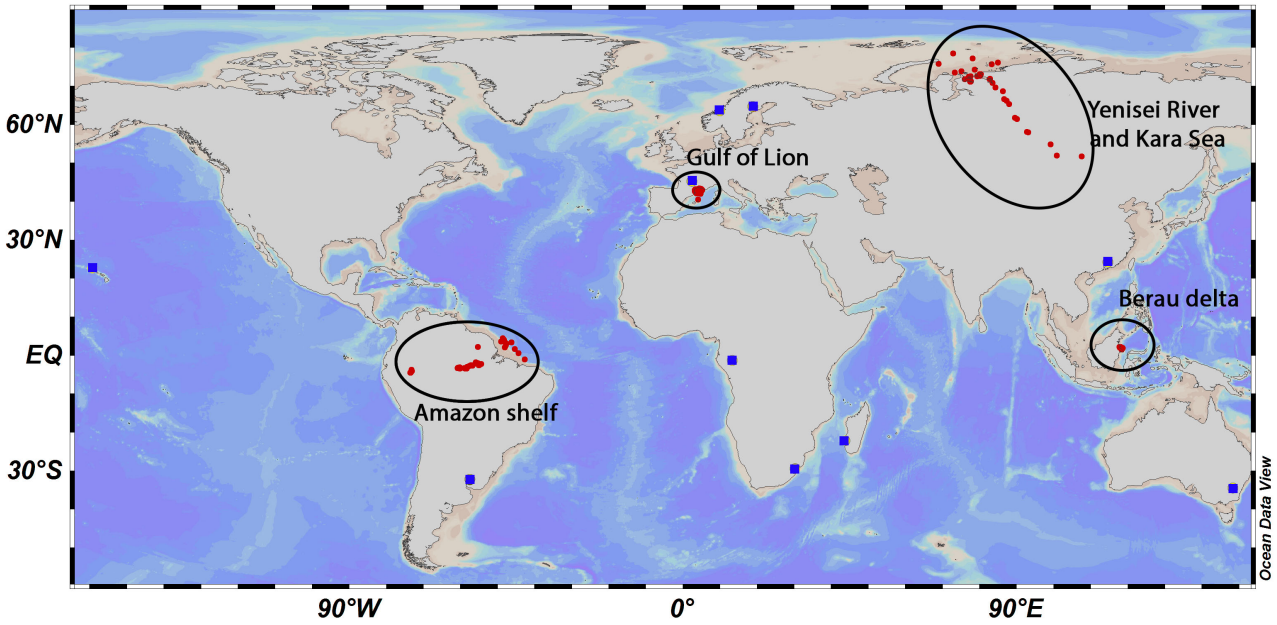

Figure 1: Location of the study sites. Surface sediments and suspended particulate matter are represented by red circles, soil samples are represented by blue squares.

Ocean and Pacific Ocean. The catchment area of the Berau River, which accounts for most of the freshwater input, is estimated at 1x10^4 km^2 (Booij et al. 2012) and the area of the delta is about 800 km^2 (Sinninghe Damsté 2016). Kalimantan has a tropical climate with a dry season from May to October and two rainfall seasons: December to January and April to May. The surface water temperature in the Berau delta is relatively constant around 30°C (Arifin and Koesmawati 2007) and the MAAT in the catchment is around 28°C (Harger 1995).

A total of 37 surface sediments of the Berau delta were obtained. Samples from transects in the delta were retrieved during a cruise of the R/V Geomarin I in July 2003 and surface sediments (0-5 cm) from stations closer to the river mouth were collected in April 2007 using a Smith-McIntyre grab sampler as described by Booij et al. (2012) and were frozen at -20°C on board (Fig. 1). These samples have been studied previously for polycyclic aromatic hydrocarbons (Booij et al. 2012) and for GDGTs and bulk isotopes (Sinninghe Damsté 2016).

Soils

Ten soil samples from ten different countries (South Africa, Uruguay, Hawai, Norway, Honduras, Gabon, France, China, Brazil and Australia, fig.1) covering a large range of climate zones, were analyzed for long chain diols. These samples are part of the original set of soils used for branched GDGT analysis reported in Weijers et al. (2007); Peterse et al. (2009), (2011) and Jonge et al. (2014a).

2.2 Diol analysis

The surface sediments of the Gulf of Lion have been previously extracted as described in Kim et al. (2006). Briefly, the samples were extracted with an Accelerated Solvent Extractor (DIONEX ASE 200) using a mixture of DCM : MeOH (9 : 1 v/v), and the extracts were separated over an activated aluminium oxide column into three fractions (apolar, ketone and polar). The sediments from the Berau delta were extracted and fractionated in a similar way (see Sinninghe Damsté 2016). The surface sediments and SPM of the Yenisei basin and Amazon basin have been extracted previously as described in Jonge et al. (2014b) and Zell et al. (2014), respectively. Briefly, the freeze-dried filters and sediments were extracted using a modified Bligh and Dyer method and separated into core GDGT lipids and intact polar lipids over a silica column.

The total lipid extracts of 10 soils were base hydrolyzed in 2 mL of 1 N KOH in 96% methanol and refluxed for 1h. After cooling the mixture was centrifuged, and acidified by adding 1mL of 2 N HCl in a H_2O/MeOH

mixture. 2 mL of DCM was added followed by centrifugation, and the organic phase was collected. This procedure was repeated 3 times. This extract was separated on an activated aluminum oxide column into three fractions using the following solvents: Hexane : DCM (9 : 1, v/v), Hexane : DCM (1 : 1, v/v) and DCM : MeOH (1 : 1, v/v). The latter (polar) fraction containing the diols was dried under a gentle nitrogen stream.

Diols were derivatized by silylating an aliquot of the polar fraction with 10 µL N,O-Bis(trimethylsilyl) trifluoro-acetamide (BSTFA) and 10 µL pyridine, heated for 30 min at 60°C and adding 30 µL of ethyl acetate. The analysis of diols was performed by gas chromatography-mass spectrometry (GC-MS) using an Agilent 7990B GC gas chromatograph, equipped with a fused silica capillary column (25m x 320 µm) coated with CP Sil-5 (film thickness 0.12 µm), coupled to an Agilent 5977A MSD mass spectrometer. The temperature regime for the oven was as follows : 70 °C for 1 min, increased to 130 °C at 20 °C/min, increased to 320 °C at 4 °C/min, held at 320 °C during 25 min. The gas flow was held constant at 2 mL/min. The MS source temperature was held at 250 °C and the MS quadrupole at 150 °C. The electron impact ionization energy of the source was 70 eV. The diols were quantified using Single Ion Monitoring (SIM) of the *m/z* 299.3 (C_{28} 1,14), 313.3 (C_{28} 1,13, C_{30} 1,15), 327.3 (C_{30} 1,14) and 341.3 (C_{30} 1,13, C_{32} 1,15) ions (Versteegh et al. 1997; Rampen et al. 2012). The fractional abundance of the diols is expressed as a percentage of the five diols quantified:

$$\%Diol_x = \frac{ADiol_x}{AC_{32}1,15 + AC_{30}1,15 + AC_{28}1,13 + AC_{30}1,13 + AC_{30}1,14 + AC_{28}1,14} \times 100 \quad (5)$$

Where A is the peak area of diol and x the diol quantified
We calculated the LDI (equation 5) and used the global calibration to obtain the SST as followed (equation 6, Rampen et al. 2012):

$$SST = \frac{LDI - 0.095}{0.033} \quad (6)$$

2.3 Statistical analyses

The data were processed through statistical analysis with the software XLStat 2016. A Principal Component Analysis (PCA) was performed on the fractional abundances of the diol isomers to provide a general view of the variability within the distribution of the diols. Correlations have been evaluated with Pearson r values and considered significant if p values were smaller than 0.005. The average data are reported with their corresponding standard deviation.

3 Results

Sediments from the Gulf of Lion and river SPM from the Rhône River all contained diols with variable distributions (Fig. 2; see Appendix A for values). The C_{30} 1,15-diol was the major diol with 50% of total diols in the SPM, with the C_{32} 1,15-diol as second most abundant diol (18%). For most of the marine surface sediments, the C_{30} 1,15-diol was also the dominant diol (average 55 ± 15% of all diols) followed by the C_{30} 1,14-, C_{32} 1,15- and C_{30} 1,13-diols. The C_{30} 1,15-diol is more abundant in the open marine sediments compared to coastal sediments, which is also the case for the C_{28} 1,13- and C_{28} 1,14-diols (Fig. 3). The C_{32} 1,15-diol comprises 0 to 45% of diols with a trend towards a higher fractional abundance closer to the coast.

In the Amazon basin the C_{30} 1,15-diol was the dominant diol in marine surface sediments (55 to 90%), followed by the C_{30} 1,14 (average of 7 ± 3%, Fig. 2). In the river SPM the C_{32} 1,15-diol (average of 30 ± 22% reaching up to 76%) and C_{30} 1,15-diol (average of 20 ± 7% and reaching up to 47%) are relatively dominant, while the fractional abundance of C_{32} 1,15-diol in the marine sediments is relatively low (average of 2 ± 1 %, Fig. 4).

The C_{32} 1,15-diol (41 ± 18% with values up to 76%) and C_{30} 1,15-diol (average of 19 ± 16% and up to 64% of total diols) are generally the dominant diols in SPM of the Yenisei River and the marine sediments of the Yenisei estuary and Kara Sea (Figs. 2 and 5). The C_{30} 1,13- and C_{28} 1,13-diols were relatively abundant in these samples with a combined average of 26 ± 20%.

The surface sediments from the Berau delta all contained diols with the C_{30} 1,15-diol being the dominant diol in the sediments further away from the river mouth (average of 68 ± 20%), while those close to the mouth of the Berau River contained much lower amounts (average of 27 ± 11%) and relatively high fractional abundances

of the C_{32} 1,15- and C_{30} 1,14-diol (average of 18 ± 4% and 19 ± 10 %, respectively) (Fig. 1). The sediments further away from the coast also have a lower abundance (average of 10 ± 4%) of the C_{32} 1,15-diol compared to those close to the river mouth (Fig. 6).

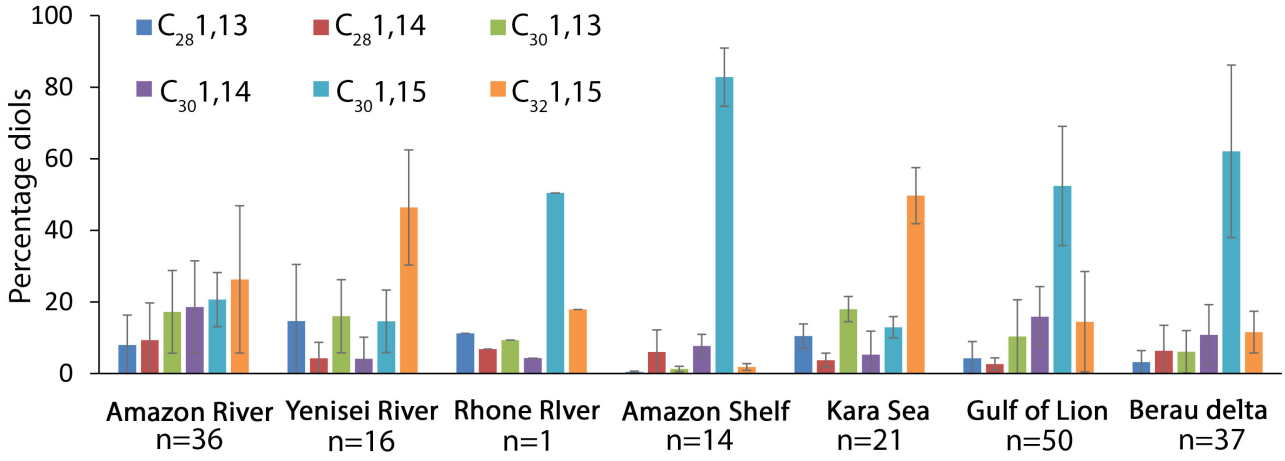

Figure 2: Average diol (C_{28} 1,13, C_{28} 1,14, C_{32} 1,15, C_{30} 1,13, C_{30} 1,14 and C_{30} 1,15-diols) distributions for the four coastal areas studied. Distributions for both surface sediments and riverine suspended particulate matter (when available) are given. Error bars indicate the standard deviations and n is the number of samples for each location.

4 Discussion

4.1 Distribution of diols in coastal sediments and river SPM

Our study shows that the diol distribution varies substantially within and between the different regions. The Gulf of Lion, Berau delta and Amazon marine surface sediments contain the C_{30} 1,15-diol as the major diol, whereas for the marine surface sediments of the Kara Sea and the Amazon Shelf the C_{32} 1,15-diol is the major diol (Fig. 2). Another interesting feature concerns a latitudinal trend in the proportion of 1,13-diols in marine surface sediments (Fig. 2). The most abundant 1,13-diols are found in surface sediments of the Kara Sea (>30 %), followed by the Gulf of Lion and the Berau delta (between 5-20 %) and the Amazon basin (<3%), i.e. the colder the SST of the shelf sea, the higher the fractional abundance of the 1,13-diols is found. This is in good agreement with the observations made by Rampen et al. (2012), (2014a), who reported higher relative abundances of 1,13-diols in marine sediments with decreasing sea surface temperatures. The fractional abundance of the C_{32} 1,15-diol is generally higher close to the mouth of the river in all four areas investigated (Figs. 3-6) and generally the highest in riverine SPM (Fig. 2). For example, for the Amazon shelf, the surface sediments only have a fractional abundance of 2 ± 1% for the C_{32} 1,15-diol, while in the SPM of the Amazon it amounts 29 ± 22 %.

To confirm the different behavior of the different diols we performed a Principal Component Analysis (PCA, Fig. 7). The first two principal components combined explain 93 and 76 % of the total variance in the distribution of the LCDs for the surface sediments and SPM, respectively. The PCA for the surface sediments shows that for PC1 the C_{30} 1,15-diol is loaded opposite to the C_{28} and C_{30} 1,13-diols which aggregate closely together. This opposite loading is consistent with the behavior of these diols with respect to variations in temperature (cf. Rampen et al. 2012). PC2 of the PCA of the surface sediments separates the 1,14-diols from the other diols, confirming that they are derived from a different source, i.e. *Proboscia* diatoms (Sinninghe Damsté et al. 2003; Rampen et al. 2007). Interestingly, the C_{32} 1,15 diol scores opposite to the C_{30} 1,15-diol on PC1, suggesting a different behavior compared to the C_{30} 1,15 diol. This is even more evident for the PCA of LCD distribution of the riverine SPM where the C_{32} 1,15-diol loads opposite all other diols on PC1. This suggests that the C_{32} 1,15-diol does not have the same source and/or environmental controls as the other diols.

To further investigate the controls on the fractional abundance of the C_{32} 1,15-diol, we investigated the

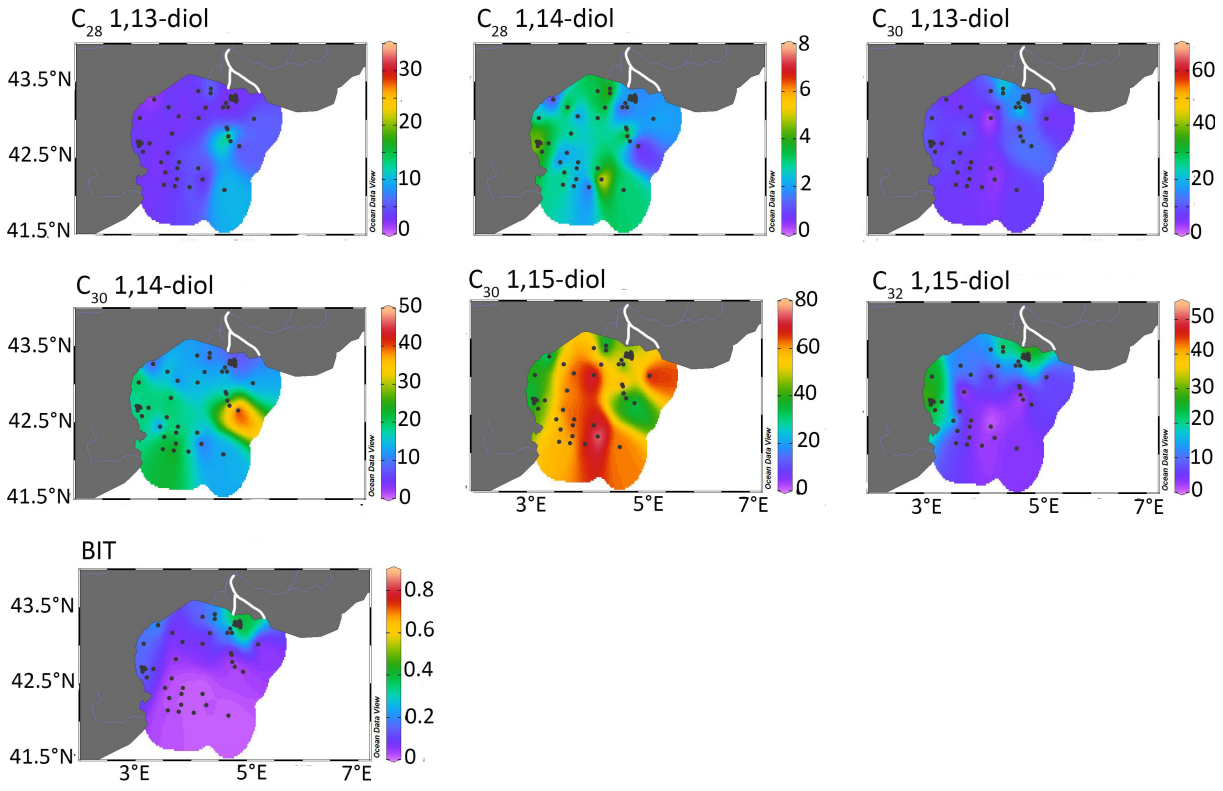

Figure 3: Spatial distribution of the relative abundance of the six diols studied (C_{28} 1,13, C_{28} 1,14, C_{32} 1,15, C_{30} 1,13, C_{30} 1,14 and C_{30} 1,15-diols) and, for comparison, the BIT index (from Kim et al. 2006, 2015) in the surface sediments of the Gulf of Lion (the southernmost site has been excluded). The map was made by Ocean Data View software, using DIVA gridding.

relationships between the fractional abundance of the C_{32} 1,15-diol, annual mean SST, TOC, $\delta^{13}C$ of bulk OM ($\delta^{13}C_{OM}$), BIT index and distance to the river mouth. The $\delta^{13}C_{OM}$ is a proxy for bulk terrigenous versus marine OM (Meyers 1994) and the BIT index is a proxy for input from continental (riverine and soil) OM into the marine realm (Hopmans et al. 2004; Walsh et al. 2008; Zell et al. 2014 and Jonge et al. 2015a). For this comparison we excluded the 1,14-diols from the data set as the 1,14 diols are known to be produced by another group of organisms (*Proboscia* diatoms; Sinninghe Damsté et al. 2003; Rampen et al. 2007) than the 1,13- and 1,15-diols. Thus, the abundance of C_{32} 1,15-diol was normalized on the sum of all 1,13 and 1,15-diols (equation 7):

$$\%C_{32}1,15 = \frac{AC_{32}1,15}{AC_{32}1,15 + AC_{30}1,15 + AC_{28}1,13 + AC_{30}1,13} \times 100 \quad (7)$$

The results for the combined dataset show no relationship between the percentage of C_{32} 1,15-diol and SST (r = 0.001, p value = 0.99; Table 1) agreeing with the conclusion of Rampen et al. (2012). To the contrary, there is a significant positive correlation between C_{32} 1,15-diol and BIT index (r = 0.3, p<0.005, Table 1) and a significant negative correlation with $\delta^{13}C_{OM}$ (r = -0.6, p<0.005, Table 1).

On a regional level, the correlation between C_{32} 1,15-diol and BIT index is also observed in the Gulf of Lion and the Berau delta (r = 0.73, p value <0.005 and r = 0.80 p<0.005, respectively) but not for the Kara Sea and Amazon shelf. In the Kara Sea, the BIT index is high in all surface sediments (>0.4), except for the most northern sediments, indicating long-distance transport of soil- and riverine derived OM (Jonge et al. 2015b). The $\%C_{32}$ 1,15 is showing the same pattern as the BIT, also indicating long-distance transport of material into the Kara Sea (Fig. 5). However, because of soil input from cliffs in the Kara Sea (Jonge et al. 2015b), the BIT index is also high close to the coast despite a lack of riverine input, while $\%C_{32}$ 1,15-diol is low. Therefore, no significant correlation between BIT index and $\%C_{32}$ 1,15-diol is observed. For the Amazon shelf, the BIT index is low (mostly <0.1) and $\delta^{13}C_{OM}$ values are relatively positive (between -22 and -19‰), suggesting no substantial continental input in these marine sediments. This coincides with a low percentage of C_{32} 1,15-diol

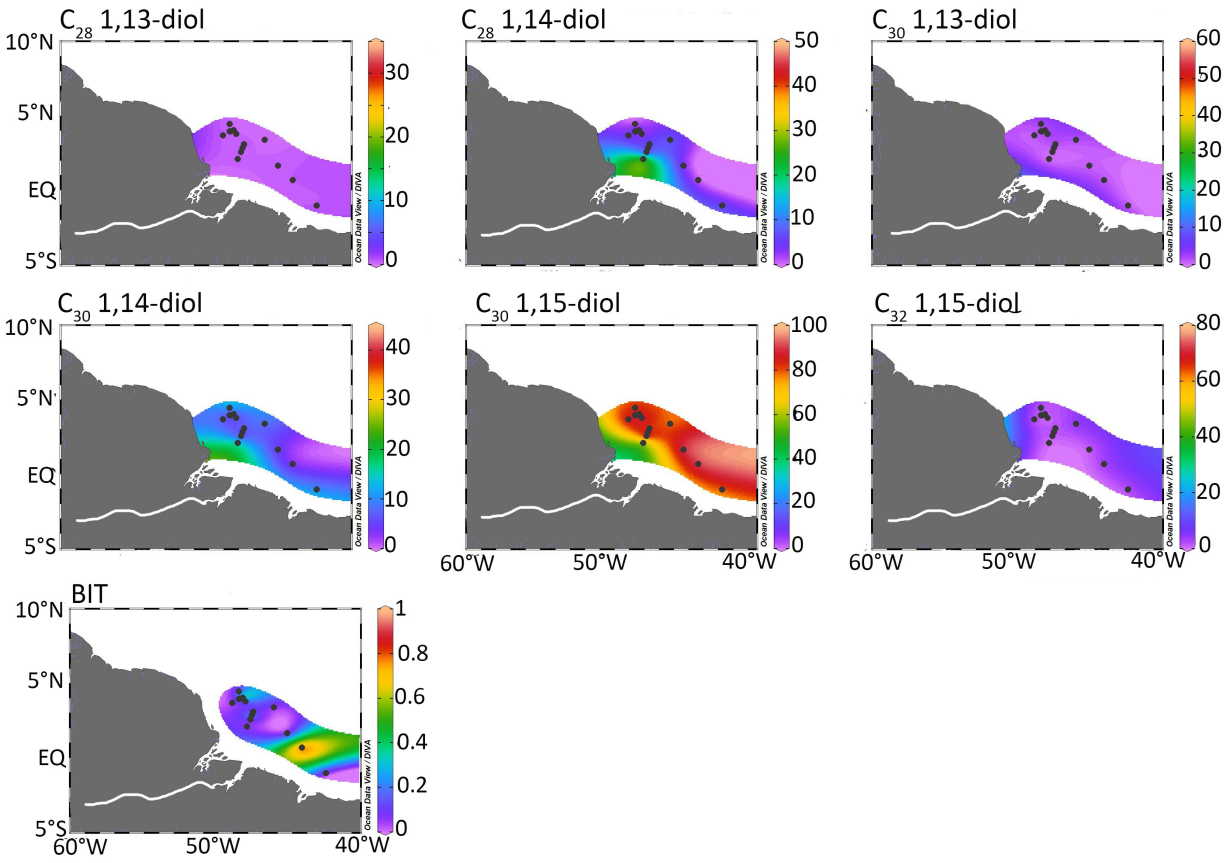

Figure 4: Spatial distribution of the relative abundance of the six diols studied (C_{28} 1,13, C_{28} 1,14, C_{32} 1,15, C_{30} 1,13, C_{30} 1,14 and C_{30} 1,15-diols) and, for comparison, the BIT index (from Kim et al. 2012; Zell et al. 2013a, 2013b) in the surface sediments of the Amazon shelf. The map was made by Ocean Data View software, using DIVA gridding.

(<6 %), i.e. much lower than in the other coastal marine sediments and riverine SPM (Fig. 2) and similar to those of open marine sediments (Rampen et al. 2012)

Table 1: Pearson correlation table between the C_{32} 1,15-diol and environmental parameters for all the areas combined. SSTs are from observational data. Values in bold are significant values (p<0.005)

	TOC	δ^{13}C	SST	BIT Index	Distance	C_{32} 1,15-diol
TOC						
δ^{13}C	**-0.758**					
SST	-0.132	**-0.305**				
BIT index	**0.591**	**-0.645**	-0.123			
Distance	-0.135	**0.517**	**-0.855**	-0.027		
C_{32} 1,15-diol	**0.608**	**-0.617**	0.001	**0.341**	-0.219	

Thus, in general the $\%C_{32}$ 1,15 is higher close to river mouths, i.e. in sediments with high BIT indices and low $\delta^{13}C_{OM}$ values and, thus, containing a relatively high contribution of terrigenous OM. In contrast, $\%C_{32}$ 1,15 is low (<10%) in open marine sediments not containing a substantial terrigenous contribution as evidenced by low BIT index and high $\delta^{13}C_{OM}$ values. Together with the substantially elevated amounts of C_{32} 1,15-diol in riverine SPM versus the low amount in nearby marine sediments (Fig. 2), this collectively suggests that the C_{32} 1,15-diol derives, at least in part, from the continent. These results thus confirm the initial observations of De Bar et al. (2016) for surface sediments of the Portuguese margin that $\%C_{32}$ 1,15 is higher close to river mouth due to an input from the continent.

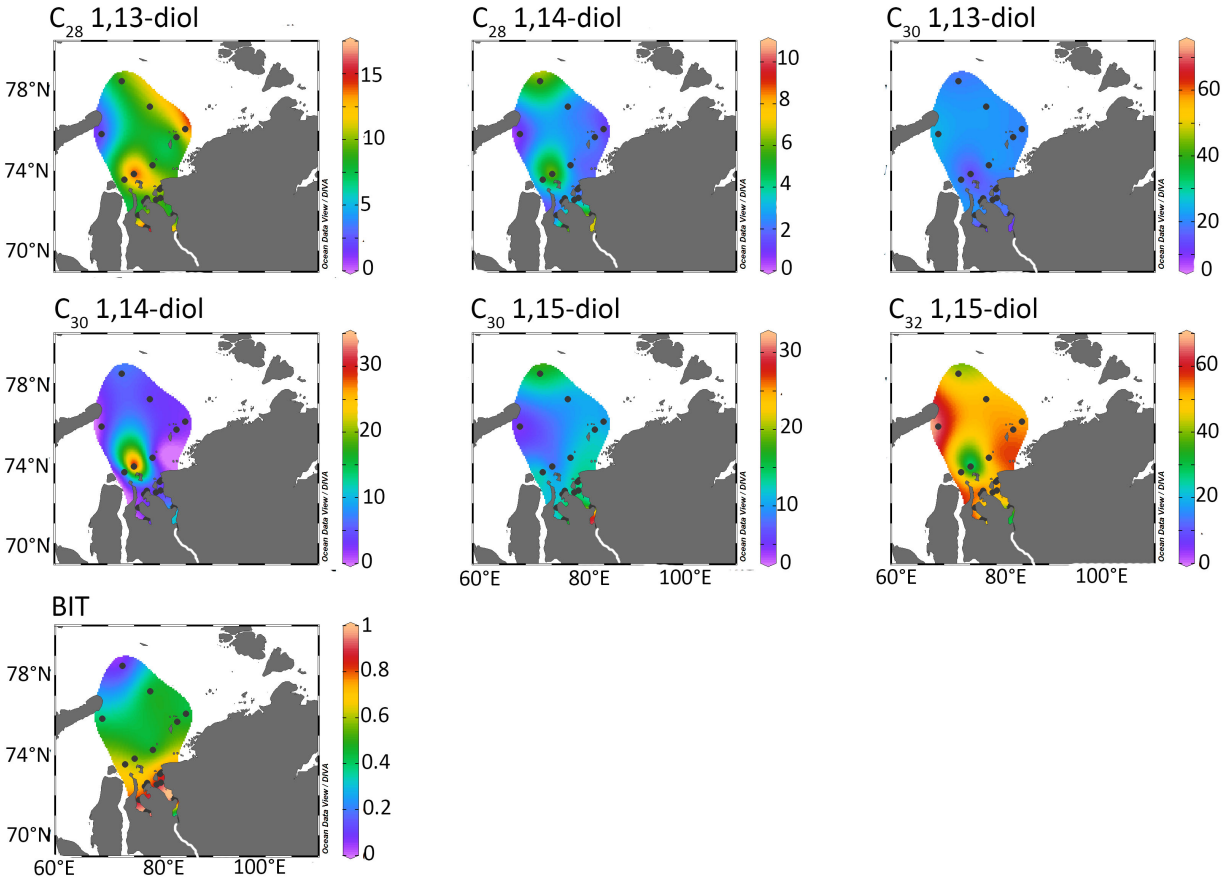

Figure 5: Spatial distribution of the relative abundance of the six diols studied (C_{28} 1,13, C_{28} 1,14, C_{32} 1,15, C_{30} 1,13, C_{30} 1,14 and C_{30} 1,15-diols) and, for comparison, the BIT index (from Jonge et al. 2014b, 2015b) in the surface sediments of the Kara Sea. The map was made by Ocean Data View software, using DIVA gridding.

4.2 Riverine production of the C_{32} 1,15-diol

To assess if the C_{32} 1,15-diol is derived from riverine production, or transported by rivers from soil or vegetation, we analyzed ten soils from diverse areas for the presence of diols. No 1,13-, 1,14- or 1,15-diols were detected in the examined soils, which implies that, most likely, the presence of C_{32} 1,15-diol in riverine SPM does not originate from soil erosion transporting material originally produced in soil to the river. This is in agreement with Shimokawara et al. (2010) who reported traces of some LCDs (C_{32} 1,17- and C_{34} 1,15-diols) in the surrounding soils of lake Baikal (slopes of the lake) but not the C_{32} 1,15-diol. Furthermore, de Bar et al. (2016) could not detect the C_{32} 1,15-diol in Portuguese soils. Alternatively, the C_{32} 1,15-diol could come from vegetation, as some mid-chain diols (C_{30} to C_{36} 1,ω20-diols) have been reported in land plants and a freshwater fern (Jetter et al. 1996; Jetter and Riederer 1999; Jetter 2000; Speelman et al. 2009). However, to the best of our knowledge the C_{32} 1,15-diol has not been reported in higher plants. Thus, by elimination, it seems likely that the C_{32} 1,15-diol is produced in the rivers themselves and subsequently transported to the marine environment.

Freshwater eustigmatophyte algae are known to produce the C_{32} 1,15-diol (Volkman et al. 1992, 1999; Rampen et al. 2014b). Within the order Eustigmatophyteae, species of the families Monodopsidaceae and Goniochloridaceae all produce the C_{32} 1,15-diol as a major diol, i.e. with a fractional abundance of 40 - 60 % for the Goniochloridaceae and 40 - 80 % for the Monodopsidaceae (Rampen et al. 2014b). Furthermore, the C_{32} 1,15 diol was found in 90 % of the 62 lakes used in the global study of Rampen et al. (2014b) with 75 % of the South American lakes and 30 % of the European lake having the C_{32} 1,15 diol as the major diol in the sediments. Also, Castaneda et al. (2011) found that the C_{32} 1,15-diol was the major diol in lake Malawi. In contrast, in open marine environments, the C_{32} 1,15-diol is generally <20 % of the total LCDs (Rampen et al. 2014b; this study). The regions where the C_{32} 1,15-diol represents more than 20 % of the total LCDs are areas under strong riverine influence like the Hudson Bay (Rampen et al. 2014b). This suggests that riverine/freshwater eustigmatophytes

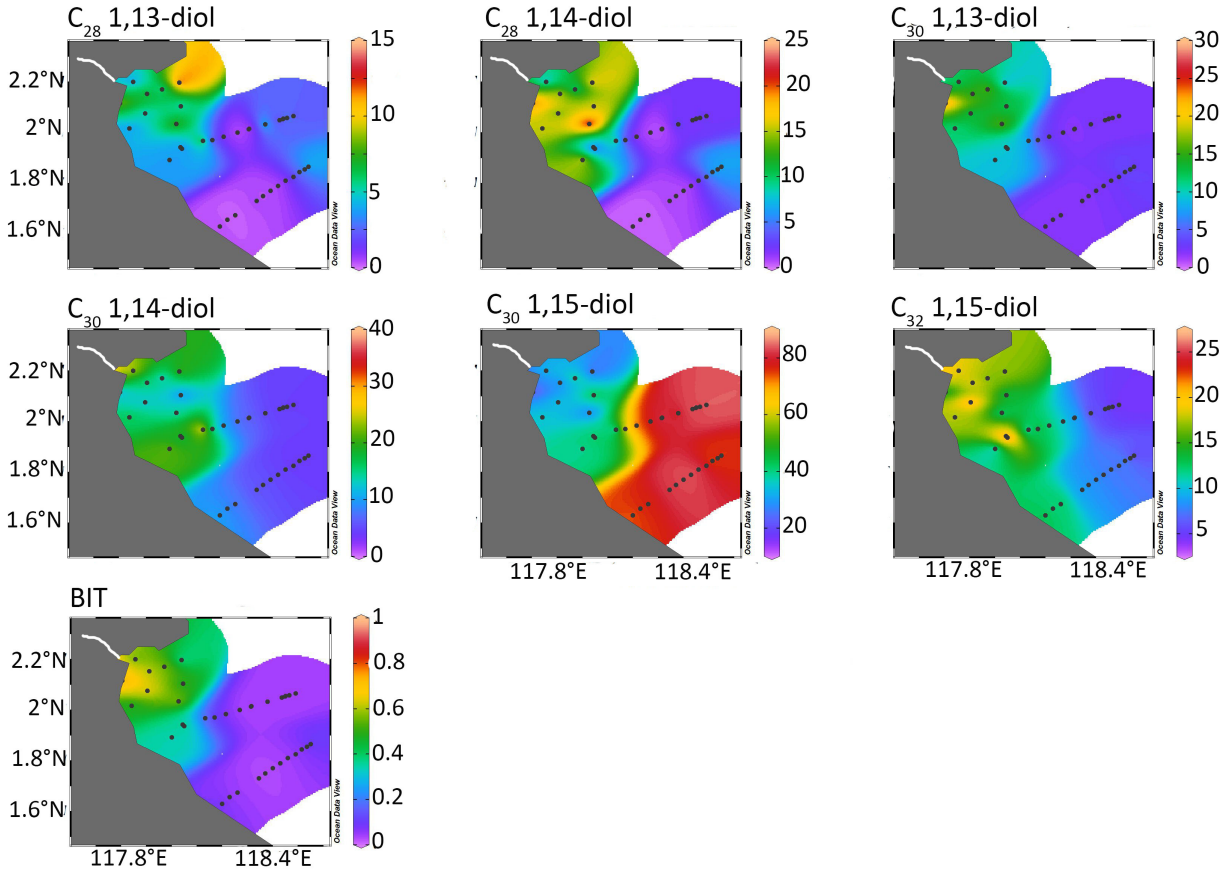

Figure 6: Spatial distribution of the relative abundance of the six diols studied (C_{28} 1,13, C_{28} 1,14, C_{32} 1,15, C_{30} 1,13, C_{30} 1,14 and C_{30} 1,15) and, for comparison, the BIT index (from Sinninghe Damsté 2016) in the surface sediments of the Berau delta. The map was made by Ocean Data View software, using DIVA gridding.

produce the C_{32} 1,15-diol in much higher fractional abundances than the marine producers of LCDs.

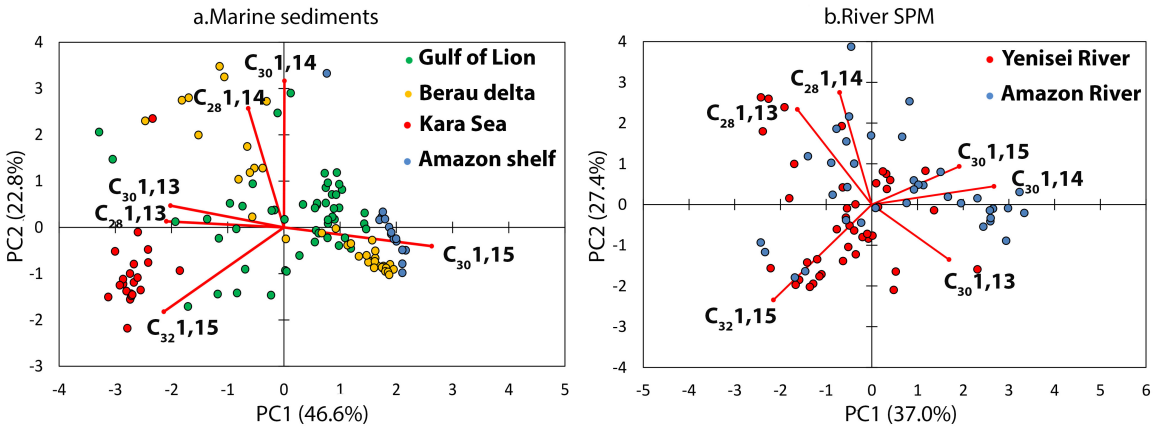

Figure 7: PCA on the relative abundances of C_{28} 1,13, C_{28} 1,14, C_{30} 1,13, C_{30} 1,14, C_{30} 1,15 and C_{32} 1,15-diols for four coastal regions (Gulf of Lion, Amazon shelf, Kara Sea and Berau delta) for (a) surface sediments and (b) riverine suspended particulate matter.

Although further research should confirm this hypothesis, our results suggest that the C_{32} 1,15-diol is predominantly produced in rivers and may therefore potentially serve as a proxy for riverine OM input in marine environments. Currently, there is no organic proxy which solely reflects riverine OM input. For example, the

BIT index contains both a soil and riverine production component (Weijers et al. 2007; Zell et al. 2014; Jonge et al. 2015a). Long chain n-alkanes are related to vegetation and soils (Eglinton and Hamilton 1963), while the δ^{13}C and C/N ratio of bulk OM are also reflecting vegetation, soil and to some extent riverine OM (Hedges et al. 1997). The different influences on the terrigenous proxies is illustrated in our regional datasets where sometimes significant correlations between the fraction of C_{32} 1,15-diol and the BIT index or $\delta^{13}C_{OM}$ is observed (Gulf of Lion, Berau delta), but sometimes not (Kara Sea). The study of proxies reflecting different parts of terrigenous OM could potentially disentangle the input of riverine, soil and vegetation OM in the marine realm.

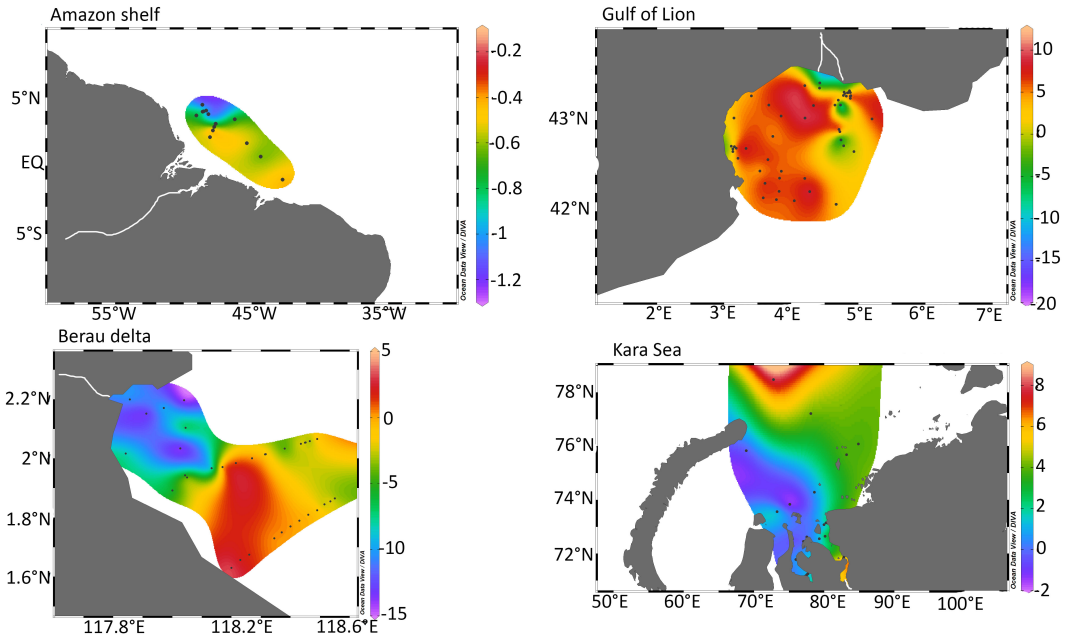

Figure 8: Difference between satellite-derived SST and SST estimated from the LDI for the Gulf of Lion, Berau delta, Amazon shelf and Kara Sea. The map was made by Ocean Data View software, using DIVA gridding.

4.3 Effect of riverine input on LDI

Our results indicate that the C_{32} 1,15 diol is produced in rivers and subsequently transported to coastal marine environment. This may have an impact on diol distributions in coastal marine sediments, specifically on SST determination using the LDI, since the eustigmatophytes in rivers most likely also produce LCDs other than the C_{32} 1,15 diol. We investigated this by calculating SST from the LDI using the calibration of Rampen et al. (2012) and comparing the values obtained with the satellite-derived annual mean SST (for the Gulf of Lion and Berau Delta) or annual mean SST obtained from the World Ocean Database (for the Kara Sea and Amazon shelf). Figure 8 shows the geographical distribution of this temperature difference for the different areas studied. The LDI-estimated SSTs for the Amazon shelf do not show any substantial difference with the satellite-derived SSTs, which agrees with the idea that their surface sediments are unlikely to be affected by a substantial input from the Amazon River (see the discussion above). In contrast, the LDI-SST values for the Kara Sea are much higher than observed annual mean SST (+0 to +11°C), with a higher difference close to the Yenisei river mouth. This may derive from a seasonal bias, i.e. the diols can be produced during a specific season and not reflect annual mean SSTs. For the subpolar Kara Sea, the diols may be more likely produced during summer time rather than winter time when the sea is frozen and light penetration for photosynthesis is limited. Indeed, when we compared the LDI-SST with summer SST, the values are much closer, between +0 to +7°C (Fig. 8) with the highest difference found close to the river mouth and in the northern surface sediments. The higher values close to the river mouth may relate to the input of diols from the river. Indeed, there is more C_{30} 1,15-diol than 1,13-diols in the Yenisei River SPM (Fig. 2), which results in higher LDI values and, consequently, higher LDI-SST.

For the Berau delta, the LDI-SST underestimates SST close to the Berau River mouth (Fig. 8, up to -10°C)

but is similar to the satellite-derived SST further away from the river mouth and within the ± 2°C error range of the LDI-SST calibration (Rampen et al. 2012). This is also the case for the Gulf of Lion, where the LDI-SST is lower than the satellite-derived SST close to the Rhône mouth (Fig. 8 up to -5°C). These trends are similar to what De Bar et al. (2016) found in the Portugal margin where the SST-LDI gave colder SST-LDI values closer to the river mouth. De Bar et al. (2016) suggested that this could come from the presence of different diol producer communities in the delta region, leading to a production of diols in different proportions than those of the open marine communities. Regardless of the exact causes, our results suggest that the LDI should be used with caution in coastal, river influenced areas.

Conclusion

The diol distribution in surface sediments from four shelf seas from different climate regions shows that the C_{32} 1,15-diol is more abundant close to the coast and even more in rivers sediments and SPM. The relative abundance of the C_{32} 1,15-diol is also strongly positively correlated to the BIT index, a proxy for soil and riverine OM input. Together with the absence of the C_{32} 1,15-diol in soils and vegetation, this indicates that the C_{32} 1,15-diol in rivers is predominantly derived from riverine in-situ production, most likely by freshwater eustigmatophyte algae. This makes the relative abundance of the C_{32} 1,15-diol a potential proxy for tracing riverine input, both in present day environments such as river mouths as well as in marine sedimentary records of river outflows. Our study shows that riverine diols affect LDI-reconstructed SSTs in coastal seas under riverine influence.

Acknowledgments

We thanks Jort Ossebaar, Anchelique Mets and Denise Dorhout for analytical support, Dr. Sebastiaan Rampen for helpful discussions and Ivan Tomberg, Dr. Roselyne Buscail, Dr. Alina Stadnitskaia, Dr. Georgy Cherkashov, Dr. David Hollander, Dr. Kees Booij and Wim Boer for access to samples. We thanks three anonymous reviewers for their thoughtful comments that improved the manuscript. This research has been funded by the European Research Council (ERC) under the European Union's Seventh Framework Program (FP7/2007-2013) ERC grant agreement [339206] to SS. JSSD and SS receive funding from the Netherlands Earth System Science Center (NESSC) though a gravitation grant from the Dutch ministry for Education, Culture and Science

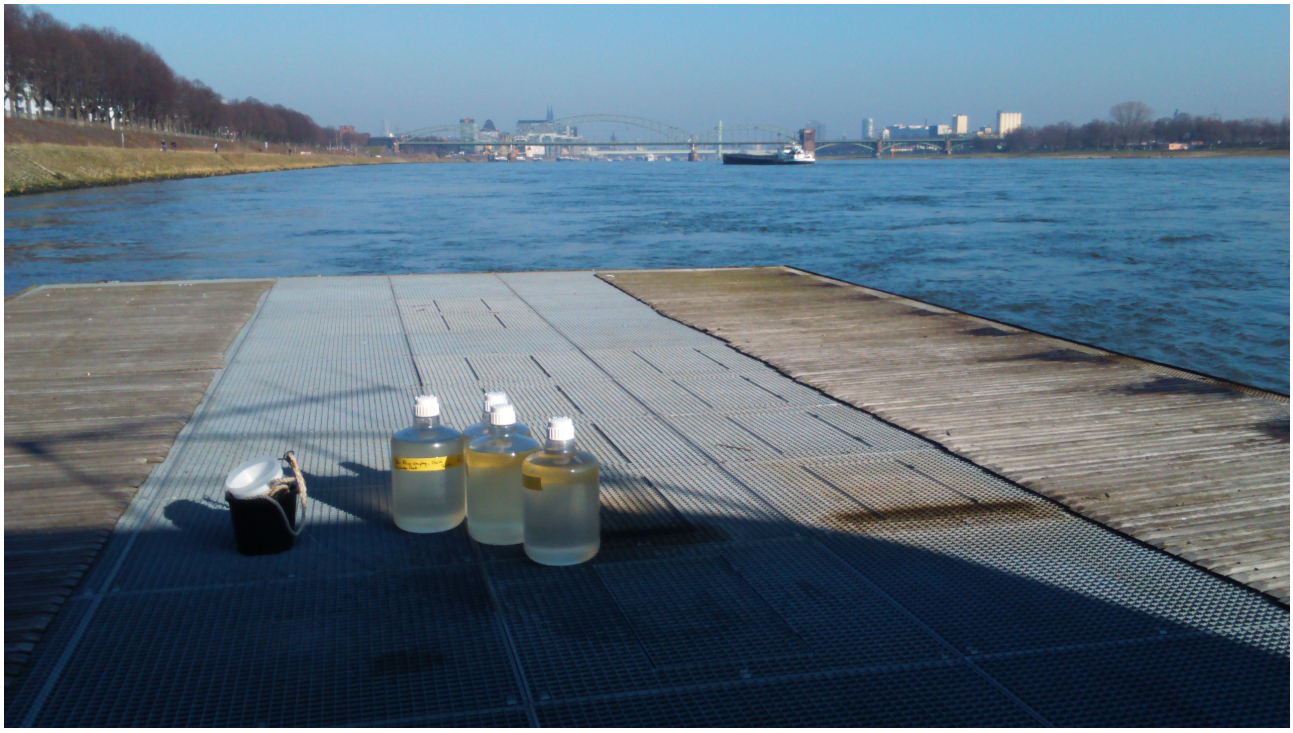

Sampling in the Rhine, Cologne 2017

Chapter 4

Long-chain diols in rivers: distribution and potential biological sources

Biogeosciences 15, 4147-4161 (2018)

Julie Lattaud [a,*], Frederique Kirkels[b], Francien Peterse[b], Chantal V. Freymond[c], Timothy I. Eglinton[c], Jens Hefter [d], Gesine Mollenhauer [d], Sergio Balzano [a], Laura Villanueva [a], Marcel T. J. van der Meer[a], Ellen C. Hopmans [a], Jaap S. Sinninghe Damsté[a,b], Stefan Schouten[a,b]

[a] NIOZ, Royal Netherlands Institute for Sea Research, Department of Marine Microbiology and Biogeochemistry (MMB), and Utrecht University, PO Box 59, 1790 AB Den Burg, The Netherlands
[b] Utrecht University, Department of Earth Sciences, Faculty of Geosciences, Princetonlaan 8a, 3584 CD Utrecht, The Netherlands.
[c] Geological Institute, ETH Zürich, Sonneggstrasse 5, 8092 Zürich, Switzerland.
[d] Alfred Wegener Institute, Department of Geosciences, Marine Geochemistry, Am Handelshafen 12, Bremerhaven, Germany.

[*] Corresponding author.
E-mail address: Julie.lattaud@nioz.nl (J. Lattaud).
https://doi.org/10.5194/bg-15-4147-2018

Abstract

Long chain diols (LCDs) occur widespread in marine environments and also in lakes and rivers. Transport of LCDs from rivers may impact the distribution of LCDs in coastal environments, however relatively little is known about the distribution and biological sources of LCDs in river systems. In this study, we investigated the distribution of LCDs in suspended particulate matter (SPM) of three river systems (Godavari, Danube, and Rhine) in relation with precipitation, temperature, and source catchments. The dominant long-chain diol is the C_{32} 1,15-diol followed by the C_{30} 1,15-diol in all studied river systems. In regions influenced by marine waters, such as delta systems, the fractional abundance of the C_{30} 1,15-diol is substantially higher than in the river itself, suggesting different LCD producers in marine and freshwater environments. A change in the LCD distribution along the downstream transects of the rivers studied was not observed. However, an effect of river flow is observed, i.e. the concentration of the C_{32} 1,15-diol is higher in stagnant waters, such as reservoirs and during seasons with river low stands. A seasonal change in the LCD distribution was observed in the Rhine, likely due to a change in the producers. Eukaryotic diversity analysis by 18S rRNA gene sequencing of SPM from the Rhine showed extremely low abundances of sequences (i.e. <0.32% of total reads) related to known algal LCD producers. Furthermore, incubation of the river water with ^{13}C-labelled bicarbonate did not result in ^{13}C incorporation into LCDs. This indicates that the LCDs present are mainly of fossil origin in the fast flowing part of the Rhine. Overall, our results suggest that the LCD-producers in rivers predominantly reside in lakes or side ponds that are part of the river system.

Keywords: *Long-chain diols; C_{32} 1,15-diol; eustigmatophyte, Godavari River, Danube River, Rhine River*

1 Introduction

Long-chain diols (LCDs) occur widespread in marine environments and have been shown to mainly consist of C_{28} and C_{30} 1,13-diols, C_{30} and C_{32} 1,15-diols (Versteegh et al. 1997, 2000; Gogou and Stephanou 2004; Smith et al. 2013; Schmidt et al. 2010; Rampen et al. 2012, 2014b) and C_{28} and C_{30} 1,14-diols (Sinninghe Damsté et al. 2003; Rampen et al. 2011, 2014b). Culture studies showed that eustigmatophyte algae (isolated from snow, soil, marine and freshwater environments) produce 1,13- and 1,15-diols (Volkman et al. 1999; Rampen et al. 2007, 2014a), but with a distribution different than encountered in marine sediments, i.e. cultures of eustigmatophytes produce mainly the C_{32} 1,15-diol, while in marine sediments the C_{30} 1,15-diol is generally dominant. Furthermore, eustigmatophyte algae are rarely reported in marine environments, indicating that the cultivated marine eustigmatophytes are likely not the main producers of 1,13- and 1,15-diols in marine environments (Volkman et al. 1999). Culture studies of *Proboscia* diatoms show that they produce mainly 1,14-diols and minor amounts of 1,13-diols (Sinninghe Damsté et al. 2003; Rampen et al. 2007), while the marine dictyochophycean alga *Apedinella radians* (Rampen et al. 2011) also produces 1,14-diols. *Proboscia* diatoms are mainly present in upwelling areas and are likely the main source of 1,14-diols in nutrient-rich marine environments (Rampen et al. 2008; Willmott et al. 2010; Gal et al. 2018).

LCDs also occur in freshwater environments, i.e. in lakes (Shimokawara et al. 2010; Castaneda et al. 2011; Zhang et al. 2011; Romero-Viana et al. 2012; Rampen et al. 2014a; Villanueva et al. 2014) and in rivers (de Bar et al. 2016; Lattaud et al. 2017b). Shimokawara et al. (2010) showed that the LCD distribution in Lake Baikal was similar to that of cultivated freshwater eustigmatophytes, indicating that they may be a source of LCDs in freshwater environments. In addition, Villanueva et al. (2014) observed a correlation between the LCD concentration in the water column of Lake Chala and the abundance of 18S rRNA gene copies of uncultivated eustigmatophytes. Rampen et al. (2014a) studied the LCD distribution of several freshwater eustigmatophyte cultures, showing that for the Goniochloridaceae and Monodopsidaceae families the main LCD is the C_{32} 1,15-diol, while the LCDs of members of the Eustigmataceae family are dominated by a mix of C_{28} 1,13-, C_{30} 1,15- and C_{32} 1,15-diols. Interestingly, an increase in the temperature at which these algae were cultivated resulted in an increase of the fractional abundance of the C_{32} 1,15-diol (Rampen et al. 2014a). Apart from lakes, LCDs have recently also been reported to occur also in rivers (de Bar et al. 2016; Lattaud et al. 2017b) with the C_{32}

1,15-diol and, to a lesser extent, the C_{30} 1,15-diol as the most abundant LCDs. In contrast to marine and lake systems, however, the spatial occurrence and sources of LCDs in river systems have not been studied in detail.

In this study we investigated three river systems, i.e. the Rhine, Godavari, and Danube rivers, to constrain the impact of river characteristics on the distribution of LCDs. Furthermore, we analyzed the algal community composition using 18S rRNA gene sequencing and quantitative PCR (qPCR) analysis and performed labelling studies in the Rhine to constrain potential biological sources of LCDs.

2 Material and methods

2.1 Material

Godavari

The Godavari is the largest river of India not draining the Himalayas with a catchment area of 310x10^3 km^2 (Balakrishna and Probst 2007) and a length (of the main river) of 1465 km (Ramasubramanian et al. 2006). The principal tributaries of the river are the Pranhita, Waiganga and Wardha forming a subcatchment (called Pranhita) in the North and the Indravati and Sabari draining the Eastern Ghats (called Indravati). In addition to these subcatchments, the main stem of the Godavari River can be divided into the Upper Godavari (from the source to Sironcha), the Middle Godavari (from Sironcha to the Dowleswaram reservoir) and the lower Godavari (downstream of the reservoir). The climate over the basin is semi-arid to monsoonal (10 to 45°C, Biksham and Subramanian 1988) and rainfall increases along a west-east gradient. Maximal rainfall is experienced during the Southwest monsoon over India (annual rainfall is 1185 mm with 84% falling during monsoonal months, June to September, Biksham and Subramanian 1988; Pradhan et al. 2014). Ca. 98% of the total suspended sediment load of the Godavari River is transported during the monsoon period (Rao et al. 2015).

A total of 62 (20 in dry and 42 in wet season) SPM and 65 (34 in dry and 30 in wet season) riverbed sediments were collected as described by Usman et al. (2018) during the dry (February/March) and the wet (July/August) seasons in 2015 (Fig. 1). The SPM was generally sampled at the surface of the river except for two location where multiple depth profiles (0, 4 and 8 m deep) were obtained during the wet and dry seasons. For SPM sampling, 5-50 L of river water was filtered over a pre-ashed glass fiber filter (Whatman GF-F, 0.7 µm, 142 mm diameter). Riverbed sediments were collected from the middle of the stream from bridges, using a van Veen grab sampler.

Danube and Black Sea

The Danube is the second largest river of Europe with a catchment area of 800x10^3 km^2 and a length of 2850 km (Freymond et al. 2017). Its catchment can be divided into four sub-regions: the upper Danube (from the source to the Gate of Devin), the Middle Danube (from the Gate of Devin to the Iron Gates reservoir) and the lower Danube (downstream of the Iron Gates reservoir to the delta) and the delta. The Danube flows directly into the Black Sea through three main branches of its delta: Chilia, Sulina, and Sf. Gheorghe. In the Black Sea, south of the Crimea peninsula, surface water flows westward onto the northwestern shelf. On the shelf, the surface current turns southward along the coast (Tolmazin 1985). The climate in the Danube catchment is diverse, with an oceanic influence on the western part of the upper basin, a Mediterranean influence in the south and central part of the middle basin and a continental climate influence in the other parts. The annual precipitation varies from 2000 mm.y-1 in the mountain area to 500 $mm.y^{-1}$ in the plains (Rîmbu et al. 2002).

46 riverbed sediments (main river and tributaries, Fig.3) were collected as described by Freymond et al. (2018) in spring 2013 and 2014. The riverbed sediments were wet sieved with milliQ water over a 63 µm sieve on a shaking table and the fine fraction (<63 µm) was studied. In total 14 surface sediments from the Black Sea were included in this study. Of these, 10 surface sediments (Fig. 3) were obtained as described by Kusch et al. (2010), (2016); called the Meteor/Poseidon surface sediments), one was collected in 2016 by the R/V Pelagia during the cruise 64PE408, and three were collected in 2017 with the R/V Pelagia during the cruise 64PE418 (collectively called the Pelagia surface sediments).

Rhine

The Rhine is the third largest river of Europe with a catchment area of 185x10^3 km^2 and a length of 1320 km (Hoffmann et al. 2009). It can be divided into three hydrological areas: the upper Rhine (the Alpine region), the Middle Rhine (German and French Rhine) and the lower Rhine (the delta region). The upper Rhine receives up to 2000 mm of precipitation per year, the middle Rhine is characterized by a temperate oceanic climate, with annual rainfall ranging from 570 to 1100 mm and the lower Rhine receives an average of 800 mm of rain per year and has a temperate oceanic climate influenced by the North Sea and the Atlantic Ocean (Pfister et al. 2004).

Five sites along the middle Rhine were sampled (Fig. 2): Karlsruhe (station of the Landesanstalt für Umwelt, Messungen und Naturschutz Baden-Württemberg), Mainz (station of the Landesamt für Umwelt, Wasserwirtschaft und Gewerbeaufsicht), Koblenz (station of Landesamt für Umwelt Rheinland-Pfalz), Cologne (Ecological Rhine-Station of the University of Cologne) and Kleve-Bimmen (International monitoring station). 62 L of river water was collected manually with a bucket at the side of the river at each station in March and September 2016. Of this 20 L was used for LCD analysis, 1 L for DNA analysis and 500 mL for chlorophyll analysis and 40 L was used for stable carbon isotope incubations.

2.2 Methods

^{13}C-labelling study

For the incubation experiments, two 20 L Nalgene bottles were filled with Rhine water and incubated in presence of light at ambient air temperature during 52 h (day/night cycle) with 100 mg ^{13}C-labelled bicarbonate (Cambridge Isotope Laboratories, Inc., USA). The bottles were shaken at the start of the incubation, then once a day to avoid particles sinking to the bottom of the bottle. The bottles were not sealed so gas exchange with the atmosphere was possible. The water was filtered using pre-ashed glass fiber filters (Whatman GF-F, 0.7 µm, 142 mm diameter) using a peristaltic pump (WTS, McLane Labs, Falmouth, MA). All samples were kept frozen at -20°C.

Lipid extraction

Filters of the Rhine and the incubation experiment were base hydrolyzed with 12 mL of 1 N KOH in methanol (MeOH) solution by refluxing for 1 h. Afterwards the pH was adjusted to 4 with 2 N HCl : MeOH (1 : 1, v/v) and the extract was transferred into a separatory funnel. The residues were further extracted once with MeOH : H_2O (1 : 1, v/v), twice with MeOH, and three times with dichloromethane (DCM). The extracts were combined in the separatory funnel and bidistilled water (6 mL) was added. The combined solutions were mixed, shaken and separated into a MeOH : H_2O and a DCM phase, after which the DCM phase was removed and collected into a centrifuge tube. The MeOH : H_2O layer was re-extracted twice with 3 mL DCM. The pooled DCM layers were dried over a Na_2SO_4 column and the DCM was evaporated under a stream of nitrogen. The extract was then acid hydrolyzed with 2 mL of 1.5 N HCl in MeOH solution under reflux for 2 h. The pH was adjusted to 4 by adding 2 N KOH : MeOH. 2 mL of DCM and 2 mL of bidistilled water were added to the hydrolyzed extract, mixed and shaken and, after phase separation, the DCM layer was transferred into another centrifuge tube. The remaining aqueous layer was washed twice with 2 mL DCM. The combined DCM layers were dried over a Na_2SO_4 column and the DCM was evaporated under a stream of nitrogen.

The SPM filters and riverbed sediments from the Godavari were freeze-dried, and river sediments were homogenized by milling. Both filters and riverbed sediments were extracted as described by Usman et al. (2018). Briefly, extraction was performed (3x) using an Accelerated Solvent Extractor (ASE 350, Dionex, Thermo-Scientific, Sunnyvale, CA, USA) with 9 : 1 (v/v) DCM : MeOH at 100°C and 7.6 × 106 Pa. The extracts were dried under N_2 and an 80 % aliquot was further processed for analysis. The samples from the Danube were extracted as described by Freymond et al. (2018) using microwave–extraction (MARS) with 9 : 1 DCM : MeOH (v/v, 25 min at 100°C). The Meteor/Poseidon Black Sea surface sediments were extracted three times ultrasonically with a 9 : 1 DCM : MeOH (v/v) solvent mixture after addition of 1.96 µg of C_{22} 7,16-diol as internal standard. The four Pelagia Black Sea surface sediments were extracted using an ASE with a DCM : MeOH mixture 9 : 1 (v/v) and a pressure of 7.6 × 10^6 Pa at 100°C.

Separation of the lipid extract

To the total lipid extracts of the Rhine SPM, the incubation experiment and the Pelagia Black Sea surface sediments an internal standard was added (C_{22} 7,16-diol). They were subsequently separated into 3 fractions on an Al_2O_3 (activated for 3 h at 150 °C) column. The apolar fraction was eluted with 4 column volumes of 9 : 1 (v/v) hexane (hex) : DCM, the ketone fraction with 3 column volumes of 1 : 1 (v/v) hex : DCM and the polar fraction (containing the diols) with 3 column volumes of 1 : 1 (v/v) DCM : MeOH.

For all other samples, the C_{46} glycerol trialkyl glycerol tetraether (GDGT, Huguet et al. 2006) was added as an internal standard.

The Godavari SPM from the wet season and Danube total extracts were saponified with KOH in MeOH (0.5 M, 2 h at 70°C). 5 mL of MilliQ water with NaCl was added and the neutral phase was back extracted with hexane and further separated into an apolar and polar fractions on a SiO_2 column with hex : DCM (9 : 1, v/v) and DCM : MeOH (1 : 1, v/v), respectively. For the Godavari river sediments and SPM from the dry season, the total extracts were saponified with KOH in MeOH (0.5 M, 2 h at 70°C) and subsequently separated on a SiO_2 column with hex : DCM (9 : 1, v/v) and DCM : MeOH (1 : 1, v/v), respectively. The Meteor/Poseidon surface sediments total extracts were saponified with KOH in MeOH at 80°C for 2 hours. The neutral fraction was recovered in hexane and separated into an apolar and a polar fraction by silica gel column chromatography using DCM : hex (2 : 1, v/v) for the apolar and DCM : MeOH (1 : 1, v/v) for the polar fraction.

Diol analysis

The polar fractions were transferred into GC vials and silylated with N,O-Bis(trimethylsilyl)trifluoro¬acetamide (BSTFA) and pyridine (10 µL each) and heated at 60°C for 30 min, after which ethyl acetate was added. All diols except the Meteor/Poseidon Black Sea surface sediments were analyzed by gas chromatography (Agilent 7990B GC) coupled to mass spectrometry (Agilent 5977A MSD) (GC-MS) equipped with a fused silica capillary column (Agilent CP Sil-5, length 25 m; diameter 320 µm; film thickness 0.12 µm). The temperature program for the oven was as follows: starting at 70°C, increased to 130°C at 20°C/min, increased to 320°C at 4°C/min, held at 320°C during 25 min. Flow was held constant at 2 mL/min. The MS source is held at 250°C and the quadrupole at 150°C. The electron impact ionization energy of the source was 70 eV. The diols of the Meteor/Poseidon Black Sea surface sediment were analyzed by GC-MS using an Agilent 6850 GC coupled to an Agilent 5975C MSD equipped with a fused silica capillary column (Restek Rxi-1ms, length 30 m; diameter 250 μm; film thickness 0.25 µm). The temperature program for the oven was as follows: held at 60°C for 3 min, increased to 150°C at 20°C/min, increased to 320°C at 4°C/min, held at 320°C during 15 min. Flow was held constant at 1.2 mL/min. The MS source is held at 230°C and the quadrupole at 150°C. The electron impact ionization energy of the source was 70 eV.

The diols were identified and quantified via SIM (Single Ion Monitoring) of the m/z = 299.3 (C_{28} 1,14-diol), 313.3 (C_{28} 1,13-diol, C_{30} 1,15-diol), 327.3 (C_{30} 1,14-diol) and 341.3 (C_{30} 1,13-diol, C_{32} 1,15-diol) ions (Versteegh et al. 1997; Rampen et al. 2012).

Absolute concentrations were calculated using the C_{22} 7,16-diol as internal standard for the Rhine SPM, Meteor/Poseidon and Pelagia surface sediments and the C_{46} GTGT as internal standard for the Godavari sediments and SPM and Danube SPM.

^{13}C analysis of LCDs

LCDs in the polar fractions of the extracts of the SPM of the ^{13}C incubation experiments were isolated using semi-preparative normal phase HPLC. Prior to injection the polar fraction was dissolved in 750 µL hex : isopropanol (99 : 1, v/v) and filtered over a polytetrafluoroethylene (PTFE) filter (0.45 µm pore size). 3x 250 µL was injected on an 1260 infinity LC system (Hewlett Packard, Palo Alto, CA, USA) equipped with a thermostated autoinjector, column oven, and a Foxy R1 fraction collector (Teledyne Isco, Lincoln, NE, USA) as described in De Bar et al. (2016). Briefly, the different diol isomers were separated over a normal phase semi preparative Alltech Econosphere silica column (250 mm x 10 mm; 10 µm) at room temperature. After 35 min at 14 % A (hex :isopropanol, 9 : 1, v/v) and 86 % B (hexane) the mobile phase was adjusted to 100 % A in 1 min. It was then held at 100 % A between 35 and 55 min. Finally, the column was reconditioned with 14 % A in hex at 3 mL/min. The fractions were collected from 15 to 40 min every 30 s and analyzed by GC-MS as described above. The LCDs of interest eluted between 22.5 and 27.5 min and were collected in 3 pools. Pool 1 from 22.5 to

24.5 min (containing 100 % C_{32} 1,15-diol, 95 % C_{30} 1,15-diol), pool 2 from 25 to 26 min (containing 83 % C_{28} 1,14-diol and 5 % C_{30}1,15-diol) and pool 3 from 26.5 to 27.5 min (containing 100 % C_{28} 1,13-diol, 17 % C_{28} 1,14-diol and 100 % C_{30} 1,13-diol). These pools were analyzed using gas chromatography–isotope ratio mass spectrometry (GC irMS, ThermoFinningan DeltaPLUS isotope ratio monitoring mass spectrometer coupled to an Agilent 6890 GC via a Combustion III interface). The gas chromatograph was equipped with a fused silica capillary column (25 m x 320 µm) coated with CP Sil-5 (film thickness = 0.12 µm) with helium as carrier gas (2 mL/min). The LCDs were silylated as described above using BSTFA with a known δ^{13}C value of -32.2 ± 0.5‰. Subsequently, the LCDs were injected splitless at an oven temperature of 70°C (injector temperature was 250°C), then the oven was programmed to 130°C at 20°C/min, and then at 20°C/min to 320°C/min at which it was held for isothermal (10 min). The δ^{13}C values were calculated by integrating the masses 44, 45, and 46 ion currents of the peaks produced by combustion of the chromatographically separated compounds and that of CO_2-peaks produced by the CO_2 reference gas with a known ^{13}C-content at the beginning and end of the analytical run. All samples were analyzed in triplicate and the average is reported.

Glycerol Dialkyl Glycerol Tetraether (GDGT) analysis

GDGTs were analyzed from the polar fractions of the Rhine and Pelagia Black Sea surface sediments. Prior to GDGT analysis an aliquot of the polar fractions was filtered through a 0.45 µm PTFE membrane filter using hex : isopropanol (99 : 1, v/v). Analysis were performed using Agilent 1260 UHPLC coupled to a 6130 quadrupole MSD in selected ion monitoring mode following the method described by Hopmans et al. (2016). The Branched versus Isoprenoid Tetraether (BIT) index was calculated according to Hopmans et al. (2004). This proxy reflects soil and river input into marine environments but is also affected by in-situ marine production of brGDGT (Jonge et al. 2014b; Sinninghe Damsté 2016).

18S rRNA gene sequencing analysis

18S rRNA gene sequencing analysis was performed exclusively on DNA extracted from the Rhine water. To this end, 1/8 of the "DNA" filter was extracted using the PowerSoil kit (QIAGEN, Valencia, CA) following manufacturer's instructions. To amplify the eukaryotic V4 region of the 18S rRNA gene, we used the universal forward primer TAReuk454FWD1, V4F (5'-CCA GCA SCY GCG GTA ATT CC-3', *S. cerevisiae* position 565-584) and a reverse primer TAReuk454REV3, V4R (5'-ACTTTCGTTCTTGAT(C/T)(A/G)A-3', *S. cerevisiae* position 964-981) from Stoeck et al. (2010). PCR reactions were performed on 5 replicates for each sample and each reaction included about 6 ng DNA template, 1.75 µL of each primer, 25 µL MasterMix phusion, 1.5 µL of DMSO and 19.25 µL deionised nuclease-free water for a total volume of 50 µL. Specifically, PCR consisted of an initial denaturation at 98°C for 30 s, 11 x [98°C for 10 s, 53°C for 30 s, 72°C for 30 s]; 17 x [98°C for 10 s, 48°C for 30 s, 7°C for 30 s] as described in Logares et al. (2012). The PCR products were stained with SYBR® Safe (Life Technologies, the Netherlands) and visualised on a 1% agarose gel. Bands were excised with a sterile scalpel and purified with Qiaquick Gel Extraction Kit (QIAGEN, Valencia, CA) following the manufacturer's instructions. Equimolar concentrations of the barcoded PCR products were pooled and sequenced on GS FLX Titanium platform (454 Life Sciences) by Macrogen Inc., South Korea.

To estimate the concentration of total 18S rRNA genes of the Rhine SPM we carried out quantitative PCR (qPCR) using the same primers and the same cycling conditions as described above. qPCR analysis was performed on a Biorad CFX96TM Real-Time System/C1000 Thermal cycler equipped with CFX ManagerTM Software. Each reaction contained 12.5 µL MasterMix phusion, 8.25 µL deionised nuclease-free water, 0.75 µL DMSO, 1 µL from each primer and 0.5 µL Sybr green and 1 µL of DNA template. Reactions were performed on an iCycler iQTM 96-well plates (Bio-Rad). A mixture of V4 18S rRNA gene amplicons obtained as described above was used to prepare standard solutions. All qPCR reactions were performed in triplicate with standard curves from 640 to 6.4 x 10^8 V4 18S rRNA molecules per microliter. Specificity of the qPCR was verified with melting curve analyses (50°C to 95°C).

Bioinformatic analyses

Bioinformatic analyses of the sequencing results were carried out using the bioinformatic pipeline Quantitative Insight Into Microbial Ecology (QIIME) (Caporaso et al. 2010). 121 232 raw sequencing reads were cleaned and

demultiplexed, then chimeras and singletons were removed as described previously (Balzano et al. 2015) for a final dataset consisting of 58 480 good quality reads. Sequences were clustered into operational taxonomic units (OTUs) based on 97 % sequence identity. The dataset was then normalized by multiplying the percentage of reads with the concentration of V4 copies measured by qPCR. Relationships between LCDs and microbial eukaryotes were inferred by Spearman correlation analyses using the QIIME script observation-metadata-correlation.py and p-values were corrected for false discovery rate (Benjamini and Hochberg 1995).

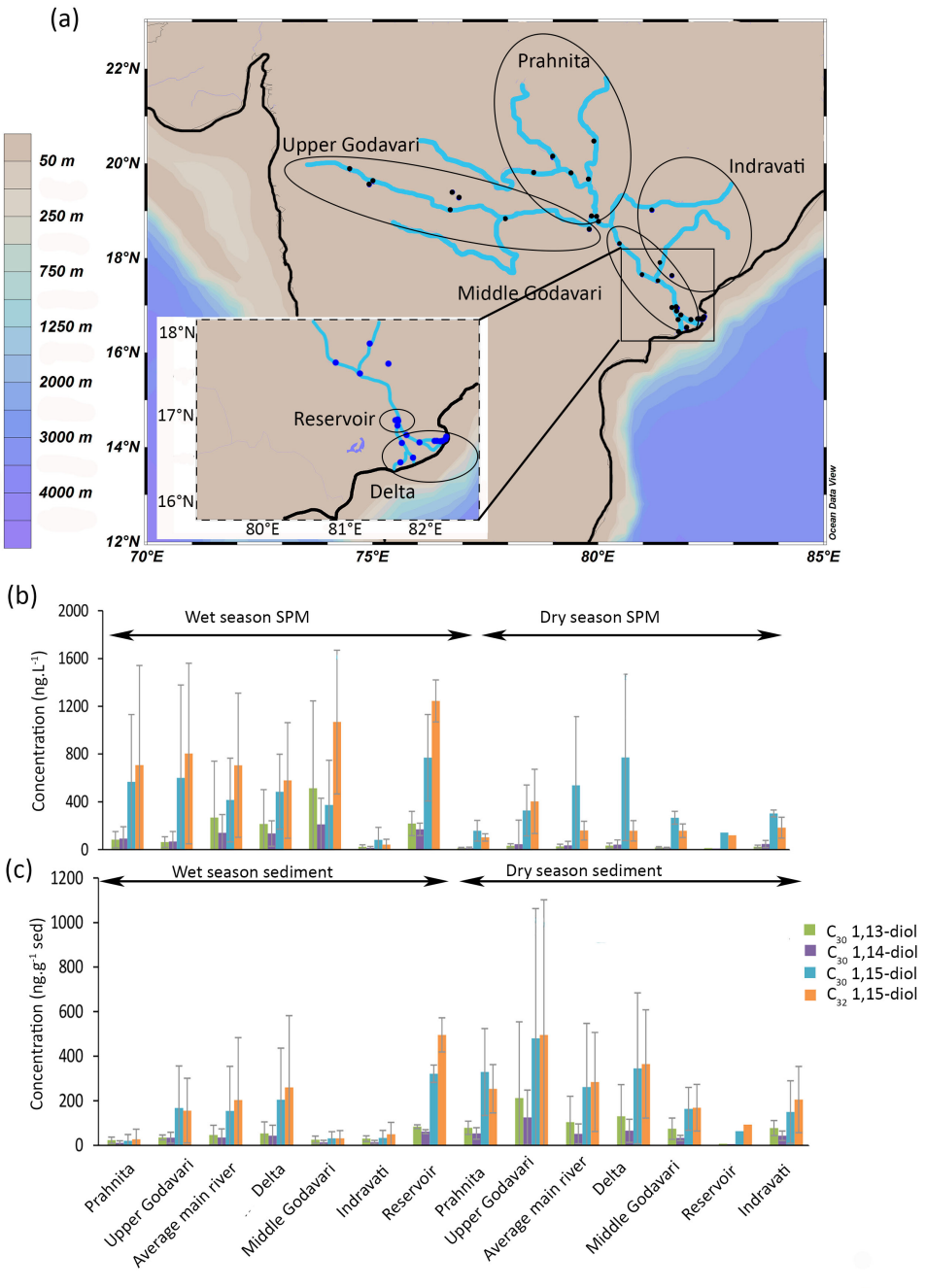

Figure 1: a. Location of the Godavari samples (Usman et al. 2018) with enhanced view of the delta region, b. concentrations of LCDs in SPM (collected during wet and dry seasons) and c. concentrations of LCDs in sediments (collected during wet and dry seasons). Grey bars indicate standard deviation for each area.

Chlorophyll analysis

Rhine River water filters for pigment analysis were extracted following Holm-Hansen et al. (1965) and Arar and Collins (1997). Briefly, 20 mL cold acetone was added to the filters and stored in the fridge overnight. Subse-

quently, they were sonicated for 2 min in an ice bath to avoid chlorophyll degradation and 10 mL was transferred into a centrifuge tube and centrifuged for 10 min at 4000 rpm. 3 mL of the extract was then transferred into the observatory cuvette. The chlorophyll measurement was realized using a Fluorescence Spectrophotometer (Hitachi f-2500) calibrated with two standards containing 50 µg/L and 100 µg/L of chlorophyll a in acetone. Samples were measured one time to obtain Rb (fluorescence before acidification) and another time when 2 drops of a solution of 10 % hydrochloric acid was added to obtain Ra (fluorescence after acidification). Chlorophyll concentration was then calculated as followed:

$$Chl - a = \frac{(Rb - Ra) \times \frac{A}{B} \times V_{extracted}}{V_{filtrated}} \quad (1)$$

Where Chl-a is the chlorophyll a concentration, A and B are constants obtained by measuring the standards (A = Chl-$a_{standard}/Rb_{standard}$ and B = $1 - Ra_{standard}/Rb_{standard}$).

3 Results

3.1 LCDs in the Godavari

The most abundant LCD in the SPM collected during the dry season is the C_{30} 1,15-diol (average 500 ± 520 ng L^{-1}, n = 18) followed by the C_{32} 1,15-diol (200 ± 170 ng L^{-1}, Fig. 1b). The C_{30} 1,13- and C_{30} 1,14-diols occur in substantially lower concentrations (30 ± 30 ng L-1 and 30 ± 20 ng L^{-1}, respectively), whilst the C_{28} 1,13 and C_{28} 1,14-diols only occur in even lower concentrations (4 ± 5 ng L^{-1} and 4 ± 6 ng L^{-1} respectively, Fig. 1). In the SPM collected during the wet season, the concentration of total LCDs is significantly higher than during the dry season (t-test, p<0.05). The C_{32} 1,15-diol is the most abundant of the LCDs in the wet season SPM (Fig. 1, 740±710 ng L^{-1}, n = 41), followed by the C_{30} 1,15-diol (500 ± 530 ngL^{-1}), with much lower concentrations of C_{30} 1,13- and C_{30} 1,14-diol (20 ± 10 and 30 ± 20 ng L^{-1}, respectively).

In the Godavari riverbed sediments, the C_{32} 1,15-diol and C_{30} 1,15-diol are the most abundant LCDs. The C_{32} 1,15-diol is higher in abundance in the sediments collected during the dry season than in the wet season sediments (330 ± 370 ng g^{-1}, n = 30; 160 ± 240 ng g^{-1}, n = 34, respectively; Fig. 1) except for the wet season sediments from the Dowleswaram reservoir where highest abundances are found (500 ± 80 ng g^{-1}, n = 2).

3.2 LCDs in the Danube and Black Sea

In the Danube sediments the main LCD is also the C_{32} 1,15-diol (3600 ± 1300 ng g^{-1}, n = 51), followed by the C_{30} 1,15-diol and the C_{30} 1,13-diol (1500 ± 1000 ng g^{-1} and 500 ± 100 ng g^{-1} respectively). Furthermore, sediment from the Iron Gates reservoir shows the highest concentration (t-test, p<0.001) of C_{32} 1,15-diol (5400 ng g^{-1}, n = 1, Fig 2b) in comparison with any of the other parts of the Danube River system (1500 ± 3200 ng g^{-1}, n = 22 in the Upper Danube; 3800 ± 2400 ng g^{-1}, n = 14 in the Middle Danube; 4400 ± 3400 ng g^{-1}, n = 10 in the Lower Danube; and 3000 ± 1400 ng g^{-1}, n = 4 in the delta).

For the Black Sea sediments (n = 14) the C_{30} 1,15-diol is the main LCD, with the two sediments from sites located closest to the river mouth (P128 and P177, Fig. 3) having a lower fractional abundance of this diol (0.57) than all other sediments (0.80 of all LCDs). In the Black sea sediments the main LCDs were the C_{30} 1,15-diol (6500 ± 9000 ng g^{-1}) followed by the C_{30} 1,14-diol (1100 ± 1600 ng g^{-1}).

3.3 LCDs in the Rhine

The main LCD in the SPM (n = 5 in March; n = 5 in September) of the Rhine is the C_{32} 1,15-diol (2.7 ± 1.2 ng L^{-1} in March; 4.6 ± 2.5 ng L^{-1} in September) followed by the C_{30} 1,15-diol (0.7 ± 0.2 ng L^{-1} in March; 2.5 ± 0.9 ng L^{-1} in September). The C_{30} 1,13-diol (0.5 ± 0.2 ng L^{-1} in March; 0.6 ± 0.2 ng L^{-1} in September) and C_{28} 1,13-diol (0.3 ± 0.1 ng L^{-1} in March; 1.2 ± 0.3 ng L^{-1} in September) are also present, while the C_{30} 1,14-diol (0.1 ± 0 ng L^{-1} in March; 0.4 ± 0.2 ng L^{-1} in September) and C_{28}1,14-diol (0.1 ± 0 ng L^{-1} in March and 0.2 ± 0.1 ng L^{-1} in September) are only minor compounds. The concentrations of the C_{32} 1,15-diol was the highest at the sampling location in Karlsruhe in September with 9.1 ng L-1 (see Fig. 2) and varies from 1.6 - 9.1 ng L^{-1} for all sites, while the C_{30} 1,15-diol varies from 1.0 - 7.6 ng L^{-1}. The LCD concentration is significantly higher in September than in March (sum of all diols is 9.4 ± 3.8 ng L^{-1} and 4.3 ± 1.5 ng L^{-1}, respectively, p<0.001).

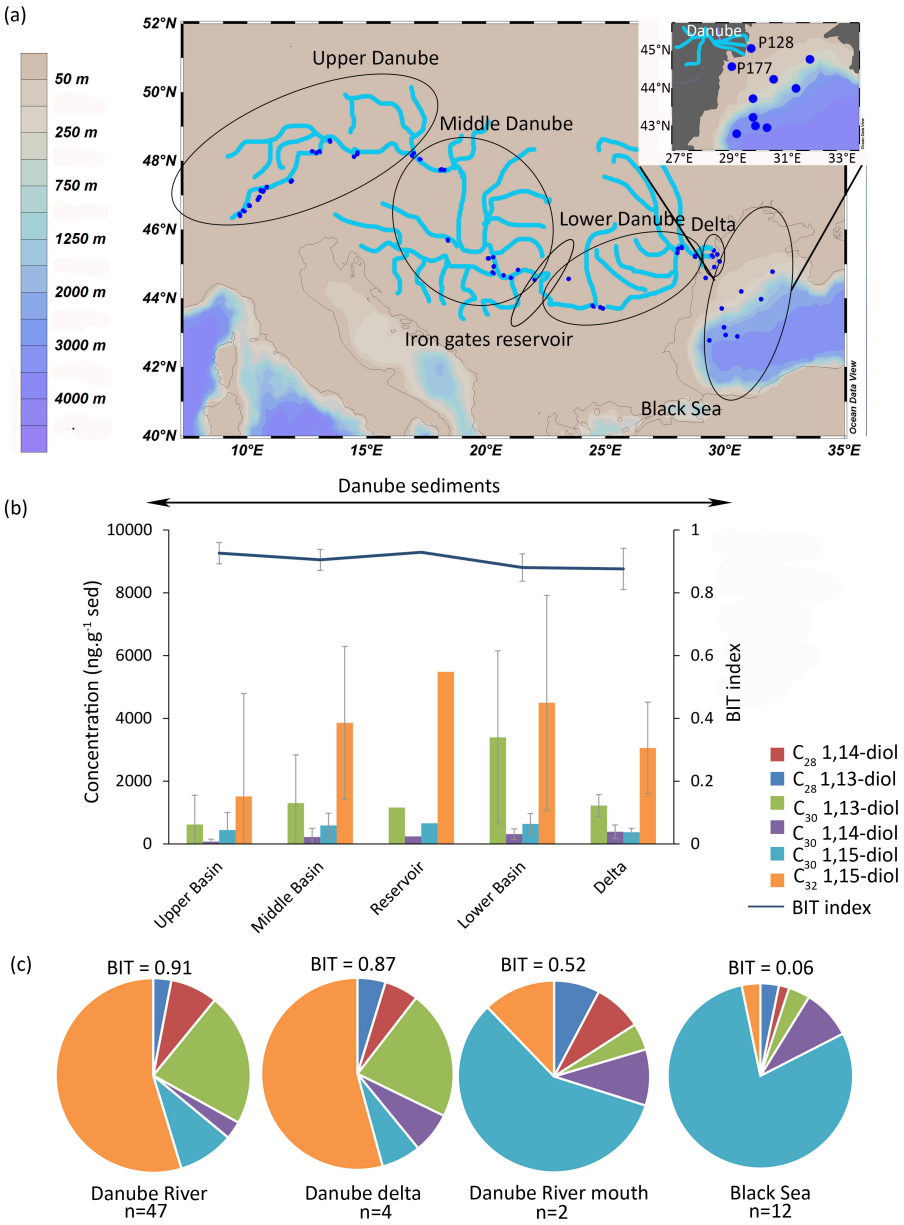

Figure 2: a. Location of the Danube samples with enhanced view of the Danube river mouth samples, b. concentration of LCDs (this study) and BIT values (from Freymond et al. 2017) in the Danube sediments (n = 1 for the reservoir) and c. fractional abundance of the LCDs in the Danube (average of the Upper, Middle and Lower Danube), Danube delta, Danube river mouth (stations P128 and P177) and Black Sea (12 stations). Grey bars indicate standard deviation for each area.

The BIT index varies from 0.64 to 0.93 (Fig. 2), and is higher in September than in March (average 0.92 ± 0.01 and 0.79 ± 0.02, respectively). In March there is an increase of the BIT index downstream (0.64 in Karlsruhe to 0.86 in Kleve) but it remains constant in September. The chlorophyll concentrations vary from 1 to 6 µg L^{-1} and peak in September at most locations (4 ± 2 and 3 ± 1 µg L^{-1} in September and March, respectively) indicating a small seasonal trend.

We sequenced the 18S rRNA gene from the Rhine SPM using universal eukaryote primers. Overall the libraries were dominated by reads affiliated to Opisthokonta (31 %), Stramenopiles (28 %), Hacrobia (24 %) and Alveolata (10 %) (see supplemental Figure 3). All the LCD-producing phytoplankton known to date (Eustigmatophyceae, *Proboscia* spp., and *Apedinella radians*) are affiliated to the Stramenopile supergroup, and the Stramenopiles found here mostly include diatoms and Chrysophyceae. However the diatom operational taxonomic units (OTUs) most closely related to *Proboscia* belong to the genera *Melosira*, *Aulacoseira*, and *Actinocyclus* which have never been reported to contain LCDs. The presence of LCDs within Chrysophyceae

has also never been determined.

One eustigmatophyceaen OTU (denovo161 *Monodus guttula*, Supplement 3) represented by two reads (one in Koblenz and one in Kleve in September) and five 18S rRNA gene reads (one in Cologne in March, three in Mainz, one in Koblenz and two in Kleve in September) associated with two OTUs from Pedinellales (denovo18 unidentified Pedinellales and denovo338 *Pseudopedinella* sp., Supplement 3) were found in the Rhine SPM. The concentration of 18S rRNA genes varied between $2.7 \pm 0.1 \times 10^7$ and $1.0 \pm 0.1 \times 10^8$ copies L^{-1} in March and $1.6 \pm 0.1 \times 10^7$ and $4.7 \pm 0.7 \times 10^7$copies L^{-1} in September (Fig. 5c and supplement 1). Spearman rank correlation analyses performed using QIIME indicate that none of the OTU found here exhibit significant correlation with LCDs (data not shown).

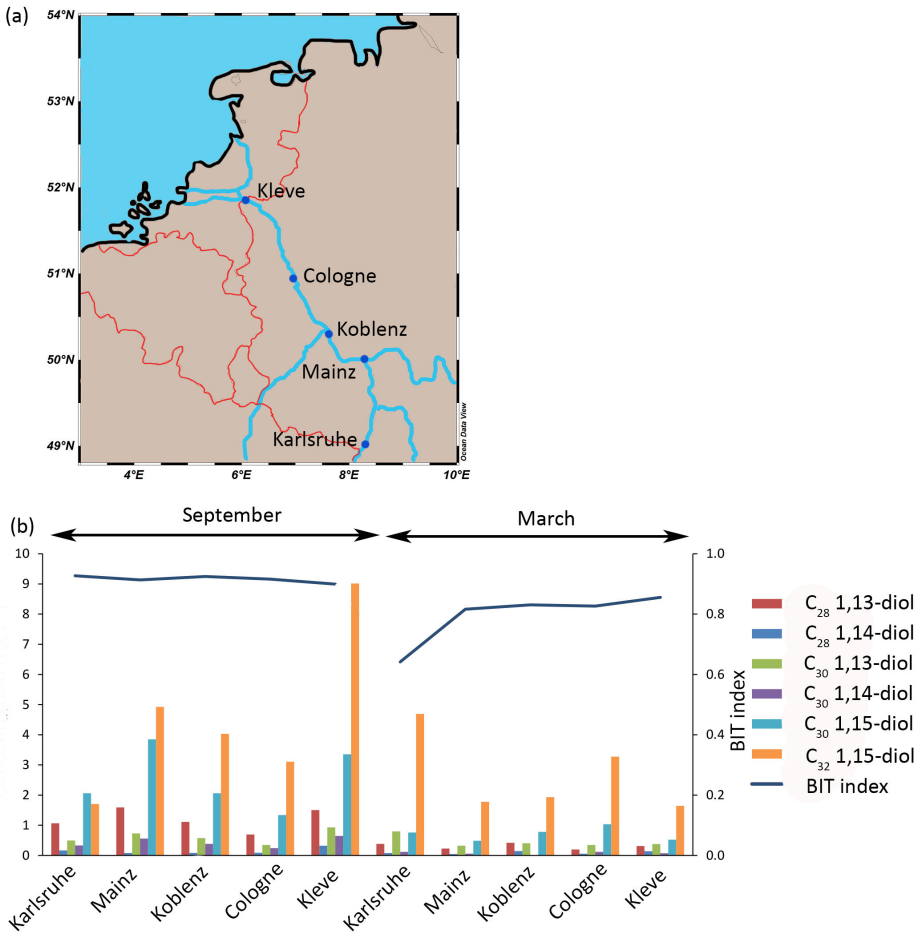

Figure 3: a. Location of the Rhine samples (n = 1 per site) and b. concentration of LCDs and BIT values (September and March) in the Rhine SPM.

4 Discussion

4.1 Where are LCDs produced in rivers?

For the different river systems a link between water conditions and LCD concentrations can often be observed. In particular, for the Godavari SPM there is a higher concentration of LCDs in the SPM from the wet season compared to that of the dry season (1900 ± 1000 ng L^{-1} vs. 570 ± 260 ng L^{-1}, respectively). The Godavari sediments collected during the dry season have higher concentration in LCDs (t-test, $p < 0.05$) than the riverbed sediments from the wet season, opposite to what is observed in the SPM. During the wet season, the Godavari is more turbid and has a higher flow velocity. This high turbidity of the river water (Balakrishna and Probst 2007; Syvitski and Saito 2007) may reduce LCD production as this limits light availability and, therefore, algal productivity. However, the higher concentration of LCDs observed in the SPM during the wet season

indicates that this explanation is likely not valid. Alternatively, the low concentration of LCDs in the wet season sediments could be due to the high flow velocity of the river water that prevents the LCDs formed in the rivers to be deposited in the river bed sediments.

During the wet season, the C_{32} 1,15-diol is present in significantly (t-test, $p<0.001$) higher quantities in the sediments of the Dowleswaram reservoir (500 ± 80 ng g^{-1}) compared to other parts of the river system, indicating that either the C_{32} 1,15-diol production is enhanced in the reservoir or that the C_{32} 1,15-diol is transported from upstream and accumulates within the reservoir. In the reservoir, both SPM and sediments have a higher organic carbon content compared to the rest of the river, whereas the suspended particle load is only slightly lower (Usman et al. 2018), which could be explained by contribution of primary produced organic carbon. This suggests that increased production of the C_{32} 1,15-diol is facilitated by the calm stagnant conditions in the reservoir. Similarly, in the Danube system the highest concentration of the C_{32} 1,15-diol is also found in a calm and stagnant water area: the Iron Gates reservoir (5500 ng g^{-1} vs. 3200 ± 1100 ng g^{-1} on average for the rest of the catchment, Fig. 3).

Pradhan et al. (2014) reported a major input (i.e. 40-45 %) of OM from freshwater algae in sediments from the Upper Godavari, based on the C/N ratio and $\delta^{13}C$ values of the sedimentary organic carbon, suggesting optimal conditions for aquatic production in impoundments in this driest part of the river basin. Indeed, significantly (t-test, $p<0.05$) higher concentrations of the C_{32} 1,15-diol are found in the Upper Godavari sediments collected during the dry season compared to the rest of the catchment, indicating that low flow, calm and stagnant water conditions are optimal for C_{32} 1,15-diol production.

Collectively, our results suggests that LCDs and especially the C_{32} 1,15-diol are preferentially produced in relatively calm and stagnant areas of river systems.

4.2 River versus marine LCDs

During the dry season, the SPM in the delta of the Godavari exhibits a LCD distribution significantly (t-test, $p<0.05$) deviating from the general distribution in river SPM and sediments, i.e. the LCDs are dominated by the C_{30} 1,15-diol (fractional abundance of 0.74 ± 0.14 for the delta vs. 0.47 ± 0.16 for the rest of the river in the dry season) rather than the C_{32} 1,15-diol. This dominance of the C_{30} 1,15-diol is different from LCD distributions usually found in rivers (de Bar et al. 2016; Lattaud et al. 2017b; this study), but similar to that observed in tropical marine sediments (Rampen et al. 2014b; Lattaud et al. 2017b). This suggests a marine influence on the LCDs in the delta during the dry season. Indeed, the electrical conductivity of the delta river water in this season is typical for brackish water (Gupta et al. 1997; Sarma et al. 2009, 2010). The electrical conductivity decreases land inwards, indicating that the influence of marine waters is substantially reduced upstream.

The LCD distributions in the Black Sea sediments are also dominated by the C_{30} 1,15-diol (fractional abundance >0.9, Fig. 3), whereas the C_{32} 1,15-diol is the most abundant diol in the sediments of the Danube. The fractional abundance of the C_{32} 1,15-diol decreases with increasing distance from the river mouth as do the values for the BIT index (Fig. 3). This decrease in C_{32} 1,15-diol abundance is similar to that observed in the delta of the Godavari River during the dry season, but can now be followed along a much larger gradient; the Black Sea sediment has a clear marine signal (BIT = 0.06 ± 0.03, n = 12, this study; Kusch et al. 2016) with a dominant C_{30} 1,15-diol, whereas the Danube River is dominated by the C_{32} 1,15-diol and has an average BIT index value of 0.91 ± 0.04 (n = 43, Freymond et al. 2017).

To visualize the differences between marine and river LCD distributions, a ternary plot was generated with the poles representing the different fractional abundances of the LCDs: C_{30} 1,15-diol, C_{32} 1,15-diol and the sum of C_{30} 1,13 and C_{28} 1,13-diols (Fig. 4). The 1,14-diols were excluded from this plot as they likely have a different biological source (Sinninghe Damsté et al. 2003; Rampen et al. 2011, 2014a). Data from the river SPM from this study have been included as well as river SPM and sediments from Lattaud et al. (2017b) and lake sediments from Rampen et al. (2014a). For the marine dataset, the marine sediments from the studies of Lattaud et al. (2017a), Rampen et al. (2012) and de Bar et al. (2016) were used. This ternary diagram shows that river SPM and sediments, as well as the lake sediments contain a higher proportion of C_{32} 1,15-diol than open marine surface sediments, where their fractional abundance nearly always is <10 %. This major difference in the distribution of LCDs in marine and freshwater environments suggests that LCDs are likely produced by different organisms in freshwater and marine systems (cf. Lattaud et al. 2017b). This difference is useful to differentiate river influenced sediments and marine sediment (cf. Lattaud et al. 2017a).

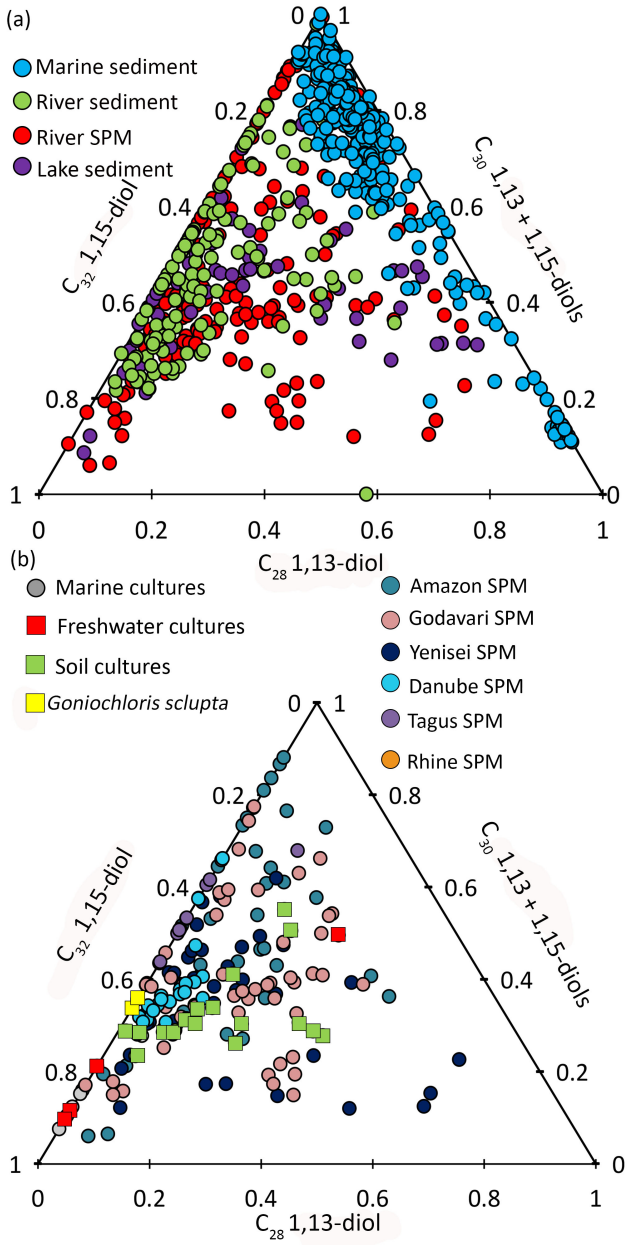

Figure 4: Ternary plot (C_{28} 1,13-diol; C_{30} 1,13- and C_{30} 1,15-diols; C_{32} 1,15-diol) of a. marine sediments (from Rampen et al. 2012; de Bar et al. 2016; Lattaud et al. 2017a), river sediments (this study; Lattaud et al. 2017b), lake sediment (from Rampen et al. 2014a) and river SPM (this study; Lattaud et al. 2017b) and b. cultivated algae (Rampen et al. 2014a) and river SPM (this study; Lattaud et al. 2017b).

4.3 Who is producing LCDs in river systems?

Comparison with culture data

In all of the three river systems investigated here the C_{32} 1,15-diol is the major diol (average fractional abundance of 0.47 ± 0.17 for Danube, Rhine, and Godavari), followed by the C_{30} 1,15-diol (0.31 ± 0.21) (Fig. 1-2). To constrain potential biological producers of the LCDs, the LCD distributions in river SPM from this study and those of Lattaud et al. (2017b) and de Bar et al. (2016) were plotted in another ternary diagram (Fig. 4), along with the LCD distribution of cultured eustigmatophyte algae (data from Rampen et al. 2014a). This diagram uses the fractional abundances of the C_{28} 1,13-diol, C_{32} 1,15-diol and the sum of the C_{30} 1,13- and C_{30} 1,15-diols. SPM from delta regions with a clear marine contribution were excluded, i.e. SPM with low BIT values (BIT<0.3).

Most of the river LCD distributions are similar to the LCD distribution of *Goniochloris sculpta* from the

Goniochloridaceae family, especially for the Rhine (this study), Danube (this study) and Tagus (data from de Bar et al. 2016). However, LCD distributions in rivers from a tropical region such as the Godavari and Amazon do not plot close to this species (Rampen et al. 2014a). This observation may point at a role of temperature in the distribution of LCDs, or at different producers in tropical freshwater systems. However, there is no significant correlation between the fractional abundance (excluding 1,14-diols) of the C_{32}1,15-diol, or other diols, in rivers and mean annual air temperature of the river catchment (r^2 = 0.002, p = 0.6). This is in contrast to the study of Rampen et al. (2014a), where a positive relation between the growth temperature of cultures of eustigmatophyte families and the fractional abundance of C_{32} 1,15-diol was observed. Potentially, this difference could be due to the fact that we are using mean annual air temperature and not in situ river temperatures.

Villanueva et al. (2014) determined the diversity and abundance of specific eustigmatophyte algae using 18S rRNA gene sequences of the SPM at different water depths in Lake Chala, tropical East Africa. Villanueva et al. (2014) found 214 eustigmatophycean sequences affiliated to 5 distinct phylogenetic clades one of which affiliated to the Goniochloridaceae family, and four novel groups, two of which closely related to the Monodopsidaceae and Eustigmatophyceae families. This suggests a role of novel uncultured Eustigmatophyceae in LCD production in riverine ecosystems. Furthermore, they quantified LCDs in monthly sediment trap material from the middle of the lake and observed that LCD distributions varied on a seasonal basis. The proportion of C_{32} 1,15-diol was highest in February and June, while the C_{30} 1,15-diol dominated in April, indicating separate blooms of different LCD producers. Our results suggest that there are potentially unknown eustigmatophycean LCD producers in river systems or that there may be multiple LCD producers, depending on the season and the location.

18S rRNA gene sequencing analysis of SPM in the Rhine

An alternative approach to comparing culture data to lipid distribution for identifying producers of LCDs is to analyze the DNA composition of river water in which LCDs are detected (cf. Villanueva et al. 2014). To characterize the producers of the 1,13- and 1,15-diols, we sequenced V4 region of the 18S RNA gene in the SPM from the Rhine using 454 sequencing. This sequencing effort yielded ca. 60 000 reads for the pooled samples (see Supplement 3) but we only detected 3 OTUs and 9 reads associated with potential LCD producers. Indeed, the near absence of eustigmatophyte reads in the Rhine SPM (Fig. 5) suggests that they are not the major producers of LCDs. Also dichtyochophytes were not detected in all the SPM in contrast to LCDs. There is no correlation between the OTUs found in the Rhine River and the concentration of 1,13- and 1,15-diols.

To pinpoint the producers of the 1,14-diols, we investigated the diatom distribution in the Rhine water. *Proboscia*, the only currently known diatom genus producing 1,14-diols (Sinninghe Damsté et al. 2003; Rampen et al. 2014a), contains marine species (Moita et al. 2003; Lassiter et al. 2006; Takahashi et al. 1994) and, consistently, was not detected in our libraries. Other genera from the same group as *Proboscia* (radial centric diatoms) were found at all sites in March, and are also found in Karlsruhe and Mainz in September (Fig. 5). To establish whether these diatoms represent a potential source of 1,14-diols, we estimated their abundance by quantifying the concentration of total 18S rRNA gene copies multiplied with the percentage of each OTU of the total reads. However, there is no correlation between the concentration of 1,14-diols and the number of gene copies per liter of radial centric diatoms (r^2 = 0.08; p value = 0.4).

Are LCDs coming from dead OM or in situ living organisms?

Interestingly, there is no significant correlation (r^2 = 0.2, p = 0.2) between the concentration of chlorophyll a (Fig. 5) and the concentration of total LCDs, 1,14-diols , or 1,13- plus 1,15-diols (Fig. 5), i.e. there is no apparent link between primary production and LCD production. The lack of correlation between LCDs and both OTUs and Chl-a suggests that the LCDs in the Rhine are either not produced in situ or are derived from unknown organisms (Villanueva et al. 2014).

To distinguish if the LCDs are a part of dead organic matter, we performed an incubation experiment using ^{13}C-labelled bicarbonate. After 52 h, ^{13}C incorporation was detected in lipids such as β-sitosterol ($\Delta\delta$ = +120‰) indicating uptake by phytoplankton. However, at the same time, we did not detect any incorporation of ^{13}C in LCDs, suggesting that the incubation time may be too short for LCD producers to take up the ^{13}C or that the LCDs are not synthesized in situ during the time of sampling. If LCD producers are photosynthetic eukaryotes as indicated by culture studies (Volkman et al. 1999; Rampen et al. 2007, 2014a) then the incubation time used

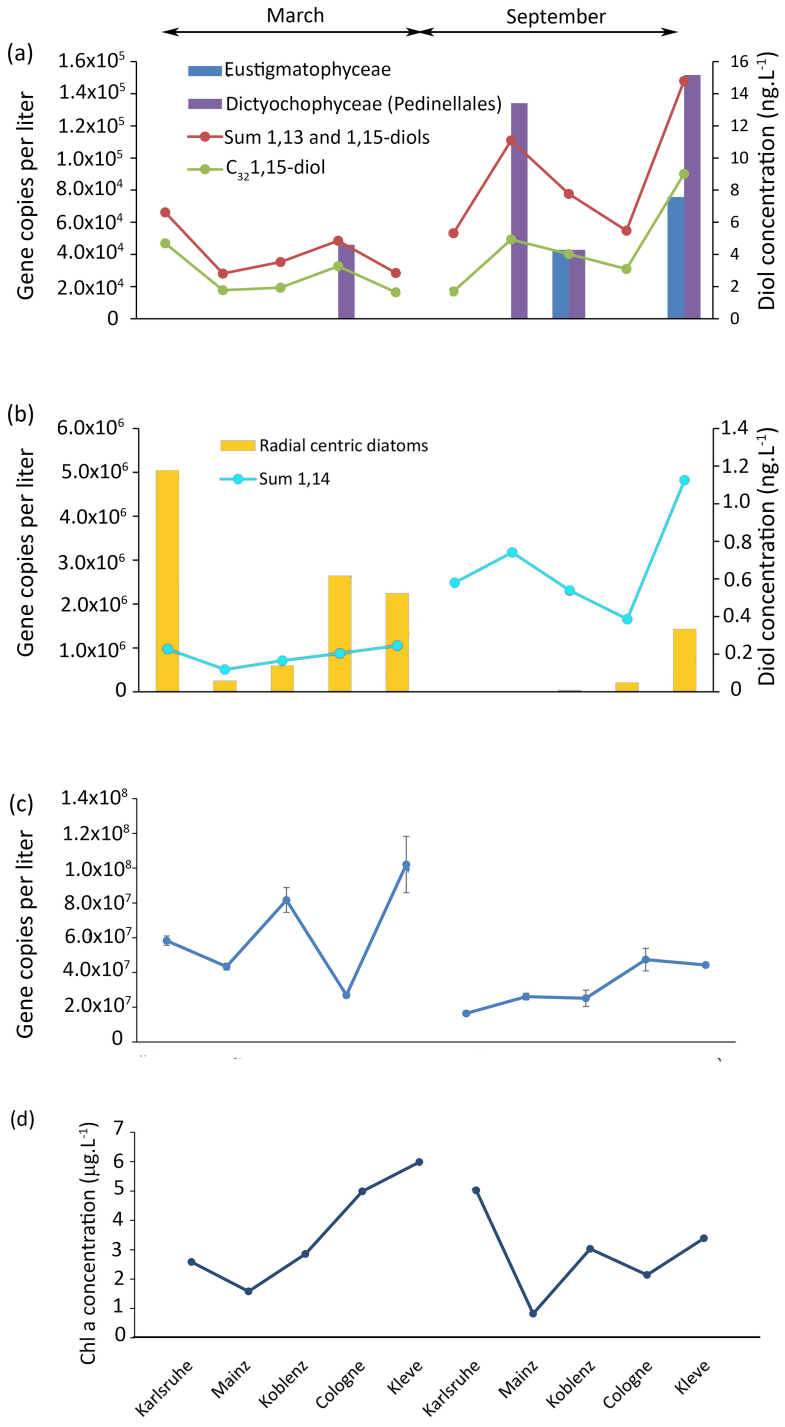

Figure 5: Results of the 18S rRNA analysis of the Rhine water, a. gene copy per liter of eustigmatophytes and dictyochophytes and concentration of 1,13- and 1,15-diols as well as concentration of the C_{32} 1,15-diol, b. gene copy number per liter of radial centric diatoms and concentration of 1,14-diols, c. total gene copy per liter and d. chlorophyll a concentration.

in the experiment should be sufficient for them to take up the ^{13}C-bicarbonate dissolved in the water. This suggests that LCDs are likely not synthesized at any of the sampling locations of the Rhine.

The absence of in situ LCD production could be due to the high flow velocity at these sampling sites. As also observed in the Godavari and Danube, the high flow velocity flow areas show a lower abundance of LCDs, while low flow areas show a higher abundance of LCDs. It is likely that LCDs in the Rhine would be produced in more stagnant waters like in lakes, or dead river branches, and that they would be more abundant in these areas. Thus, LCDs, which are likely degraded more slowly than DNA, reflect a fossil signal, while the DNA

reflects an in situ signal. Similarly, Villanueva et al. (2014) showed that, while LCDs were abundantly present in the surface water of Lake Chala, the DNA of eustigmatophytes could not be detected.

Conclusion

We studied three river systems to determine where LCDs are produced in rivers, if their distribution is different from that of marine LCDs, and to constrain their producers. Confirming previous results, riverine LCDs show a striking difference in distribution from marine LCDs as they are characterized by a high fractional abundance of the C_{32} 1,15-diol (>40 %), while marine LCDs have generally more of the C_{30} 1,15-diol (>50 %). The C_{32} 1,15-diol is more abundant in calm stagnant waters than in fast flowing parts of the rivers, indicating that they are likely produced in calmer water. Comparison of LCD distributions of Eustigmatophyceae cultures with those in rivers indicate that Goniochloris species might be an important 1,13- and 1,15-diols producer in some river systems. 18S rRNA gene analysis of one of these rivers, the Rhine, did, however, not lead to any identification of this species, nor did a labelling study using bicarbonate lead to labelling of LCDs. This might indicate that LCDs in fast flowing parts of rivers are not derived from in situ living plankton but from plankton residing in stagnant waters of these river systems such as lakes or side ponds.

Competing interests

The authors declare that they have no conflict of interest.

Acknowledgements

An anonymous reviewer and Dr. J. Planq are thanked for their comments which improved the manuscript. We thank Gabriella Weiss, Anchelique Mets, Kirsten Kooijman and Jort Ossebaar for analytical help. Heike Robakowski and the LUBW Landesanstalt für Umwelt, Messungen und Naturschutz Baden-Württemberg, Dr. Peter Diehl and the LUWG, Dr. Helmut Fisher and the Landesamt für Umwelt Rheinland-Pfalz, Dr. Georg Becker and the University of Cologne, Jochen Lacombe and the Internationale Messstation Bimmen-Lobith and Sophie Reiche for providing help with the sampling. Huub Zwart, Chris Martes (UU), Muhammed Usman (ETH), and Sayak Basu (IISER Kolkata) are thanked for help in the field during Godavari fieldwork, we thank the captain and crew of the R/V Pelagia of cruise 64PE408 and 64PE418.

This research has been funded by the European Research Council (ERC) under the European Union's Seventh Framework Program (FP7/2007-2013) ERC grant agreement [339206] to S.S. The work was further supported by funding from the Netherlands Earth System Science Center (NESSC) through a gravitation grant (NWO 024.002.001) from the Dutch Ministry for Education, Culture and Science to J.S.S.D., E.C.H., and S.S. The Godavari River project was funded by NWO-Veni grant #863.13.016 to F.P. The Danube River project (CAPS-LOCK and CAPS-LOCK2; #200021-140850) was supported by the Swiss National Science Foundation SNF by a grant to T.E.

Supplements

Table 1: Rhine River 18S rRNA sequencing of potential LCDs producers

Location	Number of sequence	STD	Gene copy per liter	STD	Eustigmatophycea	Dictyochophyceae	Radial centric diatioms	Chlorophyll (µ/L)
Karlsruhe	7.3E+6	3.4E+5	5.8E+7	2.7E+6	0	0	59	2.58
Mainz	5.4E+6	2.4E+5	4.3E+7	1.9E+6	0	0	4	1.58
Koblenz	1.0E+7	8.9E+5	8.2E+7	7.1E+6	0	0	5	2.85
Cologne	3.4E+6	1.7E+5	2.7E+7	1.4E+6	0	1	67	4.99
Kleve	1.3E+7	2.0E+6	1.0E+8	1.6E+7	0	0	15	5.99
Karsruhe	2.1E+6	1.2E+5	1.6E+7	9.6E+5	0	0	0	5.02
Mainz	3.3E+6	2.3E+5	2.6E+7	1.9E+6	0	3	0	0.82
Koblenz	3.1E+6	5.9E+5	2.5E+7	4.7E+6	1	1	1	3.03
Cologne	5.9E+6	8.1E+5	4.7E+7	2.6E+6	0	0	3	2.14
Kleve	5.5E+6	3.0E+4	4.4E+7	2.4E+5	1	2	22	3.39

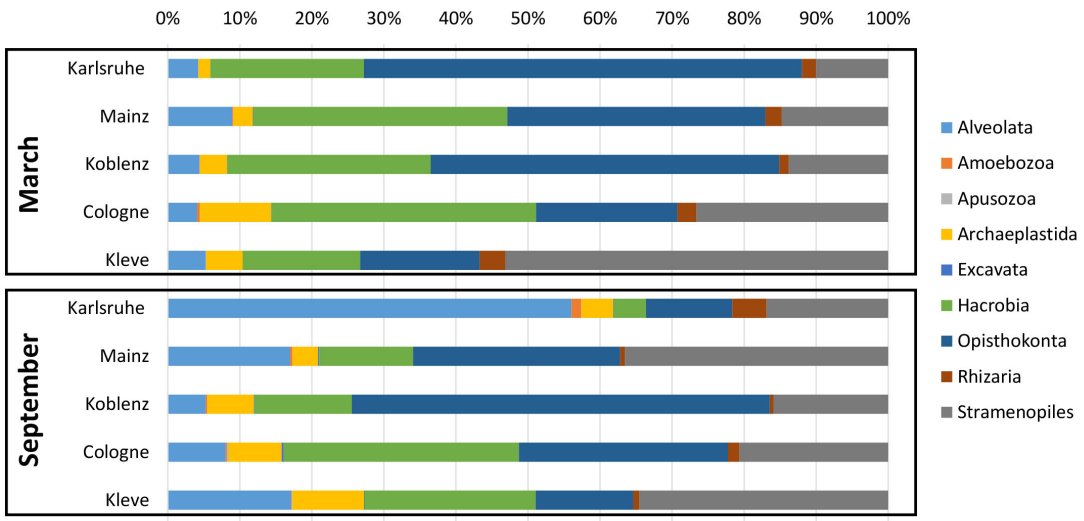

Figure 1: Results of the 18S rRNA sequncing

Chapter 5

Sources and seasonality of long-chain diols in a temperate and a tropical lake

In preparation for biogeosciences

Julie Lattaud [a,*], Loes G. J. van Bree[b], Francien Peterse[b], Sergio Balzano[a], Laura Villanueva[a], Ellen C. Hopmans [a], Marcel T. J. van der Meeer [a], Jaap S. Sinninghe Damsté[a,b], Stefan Schouten[a,b]

[a]NIOZ, Royal Netherlands Institute for Sea Research, Department of Marine Microbiology and Biogeochemistry (MMB), and Utrecht University, PO Box 59, 1790 AB Den Burg, The Netherlands
[b]Utrecht University, Department of Earth Sciences, Faculty of Geosciences, Department of Earth Sciences, Princetonlaan 8A, 3584 CB Utrecht, The Netherlands

[*]Corresponding author.
E-mail address: Julie.lattaud@nioz.nl (J. Lattaud).

Abstract

Long-chain diols are common lipids in freshwater environments and are composed of a long carbon chain (≥ 28 carbon atoms) with two alcohol groups, one on C_1 and one on a middle position (C_{12} to C_{16}). Previous studies showed that they are likely produced in lakes and low water-flow regions of rivers, but their sources and controls on their abundances are poorly constrained. Here we performed a seasonal study of suspended particulate matter in Lake Geneva, a temperate European lake, and of settling particles in Lake Chala, a lake in equatorial East Africa, to assess the production of long-chain diols in lakes. In Lake Chala, elevated fluxes of long-chain diols are observed during periods with stratified water column conditions caused by low wind strength and high rainfall, indicating that long-chain diols are likely produced during water column stratification, in agreement with a previous study on suspended particulate matter of this lake. In Lake Geneva, long-chain diols are more abundant from late spring to early autumn, also during thermal stratification of the water column. Incubation of Lake Geneva water with ^{13}C-labelled bicarbonate only showed uptake of inorganic carbon in long-chain diols from spring to early autumn. Interestingly, diol isomers were produced at different rates throughout the year, which points towards multiple producers. A subsequent 18S rRNA gene amplicon analysis revealed that eustigmatophytes known to produce long-chain diols are present in Lake Geneva and show the same seasonal trend in abundance as the long-chain diols. Together with the previously shown link between eustigmatophyte gene counts and diol concentrations in Lake Chala, our results demonstrate that eustigmatophytes are likely the most important producers of long-chain diols in lakes.

Keywords: *Long-chain diols; 18S rRNA; Eustigmatophytes, ^{13}C incubation*

1 Introduction

Long-chain diols (LCDs) are lipids commonly found in marine environments (e.g. Versteegh et al. 1997, 2000; Schmidt et al. 2010; Rampen et al. 2012, 2014a; de Bar et al. 2016, 2018; Lattaud et al. 2017b; Ruan et al. 2017; Balzano et al. 2018; Gal et al. 2018; Zhu et al. 2018). They are composed of a long alkyl chain (number of C atoms ≥ 28) containing one alcohol group at C_1 and one at a mid-chain position (e.g. carbon number 12, 13, 14, 15, 16). Previous findings have shown that LCDs preserved in marine sedimentary environments can be used to reconstruct past sea surface temperatures via the Long-chain Diol Index (LDI, Rampen et al. 2012), a proxy which has now been applied in several regions worldwide (Pancost et al. 2009; Naafs et al. 2012; dos Santos et al. 2013; Smith et al. 2013; Rodrigo-Gámiz et al. 2014; Becker et al. 2015; Plancq et al. 2015; de Bar et al. 2018; Jonas et al. 2017; Kotthoff et al. 2017; Warnock et al. 2017; Lattaud et al. 2018b). However, in coastal regions like the Kara Sea (Lattaud et al. 2017b) or the Portuguese margin (de Bar et al. 2016), LDI-temperatures in surface sediments did not match measured temperatures. Furthermore, Versteegh et al. (1997) and Rampen et al. (2012) observed that close to estuaries and river deltas, the distribution of marine LCDs is changing towards a dominance of the C_{32} 1,15-diol instead of the C_{30} 1,15- or 1,13-diol, indicating an influence of the nearby river environment on LCD distributions. Indeed, LCDs are also common in rivers (de Bar et al. 2016; Lattaud et al. 2017b, 2018a) as well as in lakes (Cranwell et al. 1987; Robinson et al. 1989; Xu and Jaffé 2009; Shimokawara et al. 2010; Castaneda et al. 2011; Zhang et al. 2011; Romero-Viana et al. 2012; Atwood et al. 2014; Rampen et al. 2014a; Villanueva et al. 2014; van Bree et al. 2018).

The main LCDs encountered in freshwater environments are the C_{32} 1,15 and C_{30} 1,15-diols (Rampen et al. 2014a; Lattaud et al. 2017b, 2018a). Lattaud et al. (2017b) used this observation to propose a new riverine input proxy based on the fractional abundance of the C_{32} 1,15-diol ($F_{C32\ 1,15}$), which increases with increased influence of the river. Lattaud et al. (2018a) showed that LCDs are likely produced in stable, low flow freshwater areas such as alluvial lakes and ponds and not within flowing rivers or floodplain soils. The most likely producers of 1,13- and 1,15-diols in freshwater environments are eukaryotic algae belonging to the Eustigmatophyceae (eustigmatophytes), because the LCD distributions in suspended particulate matter (SPM) collected from rivers, lakes and riverbed sediments fit with those of eustigmatophyte cultures, that have a prevalence of the C_{32} 1,15-diol (Rampen et al. 2014a). Furthermore, in the water column of the East African Lake Chala, the distribution of eustigmatophyte 18S rRNA gene copies matched those of LCD concentrations, i.e. a maximum in abundance

occurred at 9 m depth for both (Villanueva et al. 2014). A seasonal study of SPM from Lake Chala showed that LCDs were mainly abundant during periods with a stratified water column (van Bree et al. 2018), although no link could be made with microscopic algal cell counts, likely because of the small size of eustigmatophyte algae (<3 µm). Hence, it is unclear if eustigmatophytes are a common source of LCDs in lakes, nor is known what controls LCD abundances. For example, 1,14-diols are frequently encountered in some freshwater systems (Lattaud et al. 2017b; 2018a), but the sources of these LCDs in freshwater systems are unclear, although a species belonging to the eustigmatophyte family Goniochloridaceae, *Pseudostaurastrum enorme* (Fawley et al. 2014), is known to produce C_{28} 1,14- and C_{30} 1,14-diols in culture (Rampen et al. 2014a). In contrast, their producers in marine environments are well known, i.e. the diatom *Proboscia* (Bacillariophyceae) and *Apedinella radians* of the Dictyochophyceae (Sinninghe Damsté et al. 2003, Rampen et al. 2007).

In this study, we investigated the seasonal distribution of LCDs in two seasonally stratified lakes from different climate zones, the temperate Lake Geneva in Switzerland/France and the tropical Lake Chala in Kenya/Tanzania, to constrain the environmental control(s) on the production of LCDs. Furthermore, we analyzed the algal community composition and abundance in Lake Geneva using 18S rRNA gene amplicon sequencing and quantitative PCR (qPCR) in order to constrain the biological sources of LCDs.

2 Material and Methods

2.1 Study sites

Lake Geneva is a large sub-alpine lake located at an altitude of 372 m on the border between France and Switzerland. It is the largest lake of Western Europe with a surface area of 580.1 km^2, a volume of 89 km^3, and a maximum depth of 310 m (Fig. 1a). The lake is meso-oligotrophic and monomictic with its principal mixing period from late fall to early spring, which can be complete (the whole water column) or partial (the upper 100 m only) (Rimet et al. 2015). The last complete mixing of the lake water column occurred in winter 2012 (Rapport CIPEL, 2017). The Rhône River discharges water to the eastern tip of the lake and flows southwestwards (Oesch et al. 2005). Winter (December to February) in Lake Geneva is characterized by low water temperatures (5-7 °C), high nutrient availability and low zoo- and phytoplankton biomass with mainly diatoms present, such as Stephanodiscus neoastrae (Anneville et al. 2002). Spring blooms typically occur between March and June, after the onset of thermal stratification, leading to a decrease in water transparency (Anneville et al. 2002). These spring blooms mainly consist of unicellular phytoplankton with indicator species belonging to Bacillariophyceae (diatoms) and Cryptophyceae (Anneville et al. 2002). In June, a characteristic clear-water phase occurs as a result of zooplankton grazing of phytoplankton and depletion of dissolved silica (Si) by diatoms in the upper water column. Upon a further increase of the surface water temperature, an early summer phytoplankton bloom develops and a shift to microplankton grazers occurs. Once the stratified upper water column becomes nutrient depleted, a late summer phytoplankton community develops, characterized by the dinoflagellate *Ceratium hirundinella* and the diatom *Fragilaria crotonensis*, which do well under nutrient limited conditions (Anneville et al. 2002). Once the onset of mixing ends the stratified conditions, an autumn phytoplankton community arises with indicator species like the diatom *Stephanodiscus binderanus* or the cyanobacteria *Planktothrix rubescens*, which tolerate water column mixing and lower temperatures to benefit from renewed nutrient upwelling and low insolation of the surface water (Anneville et al. 2002).

Lake Chala is located at an altitude of 880 m in a volcanic caldera close to Mount Kilimanjaro in equatorial East Africa, on the border between Tanzania and Kenya (Fig. 1b). It has a small catchment area (1.38 km^2) and 80% of its water input is subsurface inflow of groundwater originating from the rainfall over the wet montane forest of Mt Kilimanjaro (Payne 1970; Verschuren et al. 2009). Lake Chala is a permanently stratified (meromictic) lake with daily wind-driven mixing to 15-20 m depth (shallow mixing) and deep (45-60 m) seasonal mixing during dry seasons, particularly between July and September when the surface water temperature drops to 23 °C (Buckles et al. 2014). The temperature of surface water typically peaks at about 28 °C in April. The lake receives high precipitation twice a year due to biannual passage across the equator of the tropical rain belt associated with the Intertropical Convergence Zone (ITCZ). This results in a long rain season from March to mid-May and a shorter rain season from late October to December (Hemp 2006; Sinninghe Damsté et al. 2009). Phytoplankton succession in Lake Chala is driven by changes in stratification and nutrient levels (van Bree et al. 2018) and changes strongly from year to year. In 2014, there was a long chlorophyte bloom (mainly *Tetraedron minimum*) during the deep mixing period (June to September) followed by a diatom bloom (mainly

Afrocymbella barkeri and *Ulnaria/Fragilaria* spp.) at the end of the deep mixing period (July to October). Cyanobacteria were mainly abundant during periods of deep and shallow mixing (June to August and December to January) (van Bree et al. 2018).

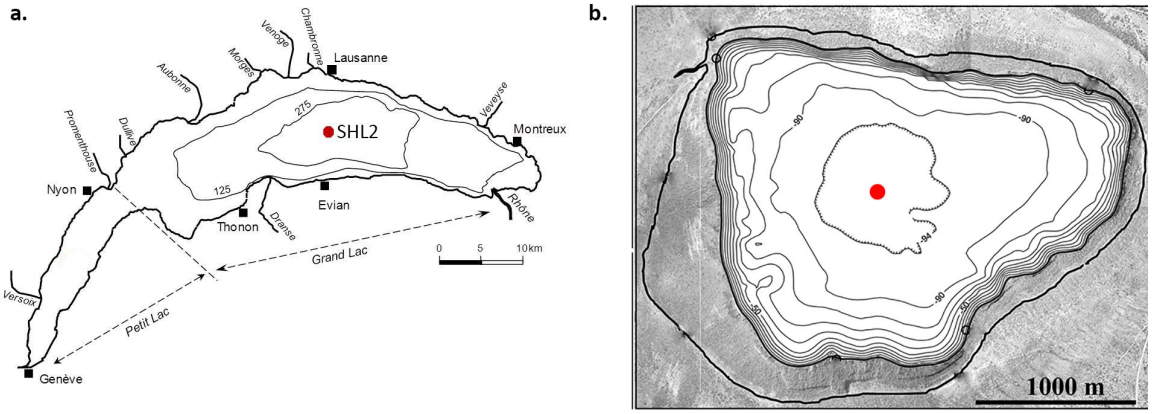

Figure 2: (a) Map showing the location of the sampling site (SHL 2) in Lake Geneva and (b) map showing the location of the Lake Chala's sediment trap (adapted from Moernaut et al. 2010 and van Bree et al. 2018).

2.2 Methods

Lake Geneva sampling

On five dates between August 2017 and June 2018, about 60 L of surface water was collected with a bucket at the Observatoire des lac alpins (UMR CARTEL) sampling station SHL2 at the deepest part of the lake (Fig. 1a). Each time ca. 20 L of the water was used to study long-chain diol distributions and 40 L was used for labeling experiments. For these labeling experiments, two 20 L Nalgene bottles were filled with lake water and incubated for 52 h (normal day/night cycle) with 100 mg ^{13}C-labelled bicarbonate (Cambridge Isotope Laboratories, Inc., USA) as described in Lattaud et al. (2018a). The bottles were shaken at the start of the incubation, then once a day to avoid particles sinking to the bottom of the bottle. The bottles were not sealed so gas exchange with the atmosphere was possible.

SPM from both the time series as well as the labeling experiments was filtered from the water using pre-ashed glass fiber filters (Whatman GF-F, 0.7 µm, 142 mm diameter) and a peristaltic pump (WTS, McLane Labs, Falmouth, MA). Half of the filter was used for lipid analysis and 1/8th of the filter was used for DNA extraction. All filters were kept frozen at -10 °C for 3 days and then kept at -80 °C until extraction.

Lake Chala sampling

A sediment trap (UWITEC, double-funnelled, 86 mm diameter) suspended at 35 m water depth at a mid-lake position (Fig. 1b) was installed in November 2006, after which it was emptied and redeployed at about monthly intervals. Collected material was allowed to settle for 2 days, and stored frozen after decantation of excess water. Prior to analysis, the samples were thawed, filtered over pre-weighed and pre-combusted (400ºC, 5 h) glass fiber GF/F filters (Whatman GF-F, 0.7 µm, 110 mm diameter), frozen and freeze-dried. This study focuses on the settling particles collected between August 2011 and January 2015.

Lipid analysis

Filters from the time series and the incubation experiments from Lake Geneva were extracted as described in Lattaud et al. (2018a). In short, the filters were base hydrolyzed using 1N KOH/methanol (MeOH), then acid hydrolyzed using 1.5 N HCl/MeOH after which an internal standard was added (C_{22} 7,16-diol). The hydrolyzed extracts were subsequently separated intothree fractions: apolar, ketone and polar fractions (containing the LCDs) using Hexane : Dichloromethane (DCM) (9 : 1, v/v), Hexane : DCM (1 : 1, v/v) and DCM : MeOH (1 : 1, v/v), respectively.

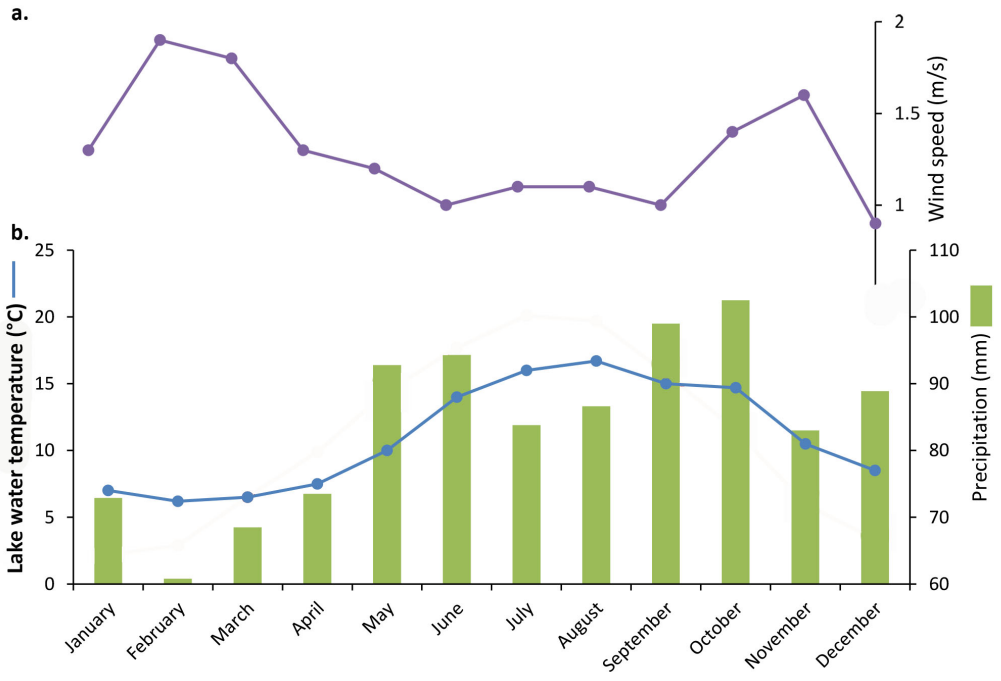

Figure 3: Climate conditions in Thonon-les-Bains (next to Lake Geneva) representing the average of the last 40 years (CIPEL report, 2017) (a) wind speed, (b) precipitation and lake temperature.

The freeze-dried filters with sediment-trap material of Lake Chala were cut in small pieces and extracted directly by acid hydrolysis with 1.5N hydrochloric acid (HCl) in MeOH. After 2 h reflux at 80ºC, the pH was adjusted to 4-5 with KOH/MeOH, and washed three times with DCM. The combined supernatant was dried over a Na_2SO_4 column and dried under N_2. This total lipid extract was separated on an activated Al_2O_3 column into an apolar, neutral and polar fraction, using hexane : DCM (9 : 1, v/v), DCM, and DCM : MeOH (2 : 1, v/v) as eluents, respectively. The latter fraction (containing the LCDs) was filtered using a polytetrafluoroethylene (PTFE) 0.45 µm filter and the C_{22} 7,16-diol (internal standard) was added.

Diol analysis

For detection and quantification of the LCDs, the polar fractions were analyzed as described in Lattaud et al. (2018a). Briefly, the fraction was silylated using N,O-Bis(trimethylsilyl)trifluoroacetamide (BSTFA) and pyridine (10 µL each) and the LCDs were identified and quantified via Single Ion Monitoring (SIM) of the *m/z* = 299.3 (C_{28} 1,14-diol, C_{30} 1,16-diol), 313.3 (C_{28} 1,13-diol, C_{30} 1,15-diol), 327.3 (C_{30} 1,14-diol), 339.3 ($C_{32:1}$ 1,15-diol) and 341.3 (C_{30} 1,13-diol, C_{32} 1,15-diol, C_{34} 1,17-diol) ions (Versteegh et al. 1997; Rampen et al. 2012). Absolute concentrations were calculated using the C_{22} 7,16-diol as internal standard (*m/z* = 187.2).

The fractional abundance of each LCD was calculated as follows, where x represents a LCD isomer:

$$F_{Diolx} = \frac{Diolx}{\sum alldiols} \quad (1)$$

The LCD fluxes in Lake Chala were calculated as follows:

$$Flux_{Diolx} = \frac{C_{diolx}}{Bulkflux} \quad (2)$$

Where $C_{diol\ x}$ is the concentration of LCD x in ng g^{-1} sediment and bulk flux is the particle flux in ng m^{-2} d^{-1}.

Isotope analysis of LCDs from the ^{13}C incubation experiment

Before stable carbon isotope analysis, the different LCD isomers were isolated from the polar fraction of the incubation experiments using semi-preparative normal phase High Performance Liquid Chromatography (HPLC) following the method of de Bar et al. (2016). For this, the polar fraction was dissolved in 150 µL hexane : isopropanol (99 : 1, v/v) and filtered over a PTFE filter (0.45 µm pore size) prior to injection on an 1260 infinity Liquid Chromatography (LC) system (Agilent) equipped with a thermostated autoinjector, and a Foxy R1 fraction collector (Teledyne Isco, Lincoln, NE, USA). The different diol isomers were separated over a Sunfire silica column (Waters, 250 mm x 10 mm; 5 µm) at room temperature. After 35 min at 18 % A (hexane : isopropanol, 9 : 1, v/v) and 82 % B (hexane) the mobile phase was adjusted to 100 % A in 1 min and then held at 100 % A from 35 to 61 min. Finally, the column was reconditioned with 18 % A and 82 % B at 3 mL min^{-1}. Fractions were collected every 30 s from 30 to 44 min and analyzed by GC-MS as described above. The LCDs of interest eluted between 33.5 and 37.5 min and were collected in three pools. Pool 1 from 33.5 to 35 min (containing 100 % of the C_{32} 1,15-diol originally present), pool 2 from 35.5 to 36 min (containing 80 % of the C_{30} 1,15-diol originally present) and pool 3 from 36.5 to 37.5 min (containing 100 % of the C_{30} 1,13- and C_{28} 1,13-diols). de Bar et al. (2016) showed that if more than 80 % of the compound was retrieved, carbon isotopic fractionation due to semi-preparative HPLC is < 0.5 ‰, i.e. within the analytical error of a typical gas chromatography–isotope ratio mass spectrometry (GC–irMS) analysis. The pooled fractions were analyzed on a GC-irMS using a ThermoFinningan DeltaPLUS isotope ratio monitoring mass spectrometer coupled to an Agilent 6890 GC via a Combustion III interface. The gas chromatograph was equipped with a fused silica capillary column (25 m x 320 µm) coated with CP Sil-5 (film thickness = 0.12 µm) with helium as carrier gas (2 mL min^{-1}). The LCDs for isotope analysis were silylated as described above using BSTFA with a known δ^{13}C value of -32.2 ± 0.5‰. Subsequently, the LCDs were injected splitless at an oven temperature of 70 °C (injector temperature was 250 °C), then the oven was programmed to 130 °C at 20 °C min^{-1}, and then at 20 °C min^{-1} to 320 °C min^{-1} at which it was held for isothermal (10 min). The isotopic values were calculated by integrating the masses 44, 45, and 46 ion currents of the peaks produced by combustion of the chromatographically separated compounds and compared with the CO_2 reference gas peaks with a known ^{13}C-content at the beginning and end of each analytical run. Duplicates were measured when possible. The labelled samples were compared to natural abundance isotope values of diols from SPM collected in August 2017.

The δ ^{13}C value of the LCDs have been corrected for BSTFA addition as follows:

$$\delta^{13}C_{LCD} = \frac{(nC_{LCD} + 2 \times nC_{BSTFA}) \times \delta^{13}C_{LCDmeas} - 2 \times nC_{BSTFA} \times \delta^{13}C_{BSTFA}}{nC_{LCD}} \quad (3)$$

With nC_{LCD} = number of carbon atoms of LCD, nC_{BSTFA} = 3 and δ $^{13}C_{BSTFA}$ = -32.2 ± 0.5‰. This correction leads to an additional uncertainty of ca. ± 0.2‰.

DNA extraction, PCR, and 18S rRNA gene amplicon sequencing

DNA was extracted from a $1/8^{th}$ portion of the GF/F filters using the PowerSoil kit (QIAGEN, Valencia, CA) following manufacturer's instructions. We amplified a region of the 18S rRNA gene approximately corresponding to the initial 450 base pairs (bp), using the primers SSU_F04 (5'-GCTTGTCTCAAAGATTAAGCC-3) and SSU_R22mod (5'-CCTGCTGCCTTCCTTRGA-3') as described previously (Sinniger et al. 2016). PCR reactions were performed on three replicates of each sample and each reaction included about 5 µL DNA template, 3 µL of each primer (10 µM), 10 µL of Phusion High-Fidelity PCR buffer (Thermo Scientific), 4 µL dNTP at 2.5 mM, 2 µL of BSA at 20 mg mL^{-1}, 0.5 µL of Phusion High-Fidelity DNA Polymerase (Thermo Scientific) and 22.5 µL deionized nuclease-free water for a total volume of 50 µL. Specifically, the PCR consisted of an initial denaturation at 98 °C for 30 s, 27 x [98 °C for 10 s, 60 °C for 20 s, 72 °C for 30 s] and 5 min at 72 °C. The PCR products were stained with SYBR® Safe (Life Technologies, the Netherlands) and visualized by electrophoresis on a 1 % agarose gel at 75 V during 50 min. Bands were excised with a sterile scalpel and purified with Qiaquick Gel Extraction Kit (QIAGEN, Valencia, CA) following the manufacturer's instructions. Purified amplicons from Lake Geneva were combined in equimolar concentrations (20 ng of DNA per sample) and sequenced on Illumina NextSeq500 platform by USEQ, Utrecht as 2 x 150 bp paired end reads.

To estimate the concentration of total 18S rRNA gene copies per liter of lake water we carried out quantitative PCR (qPCR) using the same primers used for the 18S rRNA gene amplicon analysis and the same cycling

conditions as described above. qPCR analysis was performed on a Biorad CFX96TM Real-Time System/C1000 Thermal cycler equipped with CFX ManagerTM Software. Each reaction contained 9.25 µL deionized nuclease-free water, 5 µL 5X Phusion HF Buffer, 2 µL dNTPs (2.5 mM), 1 µL BSA (20 mg mL^{-1}), 0,25 µL Phusion DNA Polymerase (2 U μL^{-1}), 1.5 µL from each primer (10 µM) and 0.5 µL Sybr green and 4 µL of 100 time diluted DNA template. Reactions were performed on an iCycler iQTM 96-well plate (Bio-Rad). All qPCR reactions were performed in triplicate. Specificity of the qPCR was verified with melting curve analyses (50 °C to 95 °C).

Bioinformatic analyses

Most of the bioinformatic analyses of the 18S rRNA gene amplicon sequencing analyses were carried out using Quantitative Insight Into Microbial Ecology (QIIME) (Caporaso et al. 2010). A total of 51 862 159 raw Illumina forward reads and 57,186,747 reverse reads, with an average length of 150 bp, were obtained. Forward and reverse reads were paired using PEAR (Zhang et al. 2014) with a minimum length of 20 bp and a minimum overlap size of 7 bp. Paired reads were then extracted from the dataset based on the barcode sequences, demultiplexed into the different samples, and quality filtered using the QIIME scripts extract_barcode.py and split_libraries_fastq.py. Only reads with a phred quality ≥ 23 and a number of consecutive low quality base calls < 5 were retained for downstream analyses. The QIIME script pick_otus.py was used, based on uclust (Edgar 2010) algorithm, to identify and remove singletons (sequence identity 100 %). Chimera were then removed using the UCHIME algorithm (Edgar et al. 2011) within vsearch (https://github.com/torognes/vsearch) by comparison with the protist ribosomal database 2 (Guillou et al. 2013). Sequences were clustered into operational taxonomic units (OTUs) at 97 % identity using the QIIME script pick_otus.py. OTUs were then identified using command-line blast (Camacho et al. 2009) by comparison with the protist ribosomal database 2 (Guillou et al. 2013). The final dataset consisted of 9,533 OTUs and 3,688,575 good quality reads. Data were then converted to relative proportions and normalized by multiplying the contribution from each OTU in each sample to the number of gene copies calculated for that sample by qPCR.

We constructed a phylogenetic tree to identify the eustigmatophytes sequenced from Lake Geneva in more detail with respect to known freshwater eustigmatophytes. Specifically, we aligned the DNA sequences to the 74 18S rRNA gene sequences from cultured freshwater Eustigmatophyceae downloaded from the Genbank and 20 uncultured eustigmatophytes from the ARB database (Ludwig 2004). The sequences were aligned based on their secondary structure using ARB. (version 6.0.2, Tamura et al. 2007) was used to find the best nucleotide substitution model (great time reversible, GTR + gamma) and phylogeny was inferred using FastTree (Price et al. 2009) from a final alignment consisting of 134 sequences.

3 Results

3.1 Long-chain diols in Lake Geneva

LCDs were detected in all five SPM samples collected from Lake Geneva, in concentrations ranging from 3.4 ng L^{-1} in January to 34.3 and 36.2 ng L^{-1} in August and October, respectively (sum of all LCDs, Table 2, Fig. 3a). LCD concentrations exhibited intermediate concentrations in April and June (15.7 and 14.0 ng L^{-1}, respectively). LCD distributions changed throughout the year, and the most abundant LCD was the C_{30} 1,15-diol in August (accounting for 68 % of all LCDs at that time), the C_{28} 1,13-diol in October (27 %) and January (28 %), and the C_{32} 1,15-diol in April (65 %) and in June (42 %). The unsaturated $C_{32:1}$ 1,15-diol was detected in all months except in April (Table 2) with its highest abundance in June (1.1 ng L^{-1}). The C_{28} and C_{30} 1,14-diols were presents in all months and ranged from 0.3 ng L^{-1} in January to 2.5 ng L^{-1} in October. The C_{30} 1,16-diol was only present in August and October 2017 and January 2018 with concentration ranging from 0.5 to 4.4 ng L^{-1}. Overall, all LCDs peaked at different months, e.g. the 1,13- and 1,14-diols peaked in abundance in October while the C_{30} 1,15-diol maximum was in August and the C_{32} 1,15-diol in peaked April (Fig. 3a).

3.2 Labeling experiment in Lake Geneva

Incubation with ^{13}C-labelled bicarbonate successfully labelled the LCDs in all months except January (Fig. 3c). The C_{32} 1,15-diol had the highest (most ^{13}C-label uptake) $\delta^{13}C$ values in these months, ranging from 71 ± 0‰

to 633 ± 2‰. Lower values were found for the C_{30} 1,15-diol (-9 ± 4‰ to 256 ± 22‰), the C_{30} 1,13-diol (20 ± 4‰ to 253 ± 30‰) and the C_{28} 1,13-diol (67 ± 1‰ to 310 ± 3‰) (Table 3). In January, no ^{13}C label was detected in any of the measured diols ($\delta^{13}C_{C32\ 1,15}$ = -29.6‰, $\delta^{13}C_{C30\ 1,15}$ = -34.4‰, $\delta^{13}C_{C28\ 1,13}$ = -34.4‰). The $\delta^{13}C$ of the C_{28} 1,14- and C_{30} 1,14-diols could not be measured because of the low abundance of these compounds in Lake Geneva water.

3.3 Genetic analysis of eukaryotic plankton community in Lake Geneva

The 18S rRNA gene amplicon sequences obtained from Lake Geneva SPM were dominated by sequences affiliated to the subkingdom Hacrobia (15 – 61 %), the superkingdom Opisthokonta (2 – 71 %), the subkingdom Stramenopiles (6 – 34 %), kingdom Alveolata (2 – 20 %) and superkingdom Archaeplastida (5 – 17 %) (Fig. S1). Sequences attributed to Stramenopiles, which include all known LCD producers (Balzano et al. 2018), comprised 23 OTUs falling within the eustigmatophytes (0.04 to 0.32 % of all 18S rRNA gene reads). Phylogenetic analyses (Fig. S3) indicate the presence of 13 OTUs closely related to eustigmatophytes and 10 OTUs falling within different eustigmatophyte families. Of the 4,751 reads attributed by blast analysis to eustigmatophytes, 66 % (3,133 reads) correspond to 5 OTUs of the Monodopsidaceae family, 10 % (478 reads) belonging to 3 OTUs to the Goniochloridaceae family and 5 % (251 reads) belong to 2 OTUs of the Pseudocharaciopsidaceae family. Reads belonging to the Eustigmataceae family were not detected and the remaining 19 % (889 reads) belong to 13 unidentified OTUs closely related to eustigmatophytes (Fig. S3).

In general, 18S rRNA gene sequences closely related to *Monodus* spp. (Monodopsidaceae family) were dominant among the eustigmatophyte 18S rRNA gene sequences in all five months, followed by those attributed to *Nannochloropsis* spp. (Monodopsidaceae family, 7 % of eustigmatophyte 18S rRNA gene copies L^{-1} in June) and Goniochloridaceae family (23 % of eustigmatophyte 18S rRNA gene copies L^{-1} in January, 11 % in August and 8 % in October) and Pseudocharaciopsidaceae (8 % of eustigmatophyte 18S rRNA gene copies L^{-1} in April, Fig. 3b).

The total concentration of eukaryotic 18S rRNA ranged between 1.1 (± 0.1) x 10^6 gene copies per liter in January and 2.8 (± 0.2) x 10^6 gene copies L^{-1} in August. The abundance of 18S rRNA gene copies L^{-1} assigned to eustigmatophytes was highest in August (Fig. 3b) with a dominance of genes related to Monodus spp. (4.0 x 10^3 gene copies L^{-1}) followed by genes related to Goniochloridaceae (in August 6.7 x 10^2 gene copies L^{-1}). Finally, sequences related to radial centric diatoms were detected (Fig. S2) and ranged from 5.4 x 10^4 gene copies L^{-1} in June to 4.5 x 10^6 gene copies L^{-1} in April. However, no sequences related to the LCD producer *Proboscia* were detected.

3.4 Lake Chala

LCDs were detected in all 40 monthly sediment trap samples collected from Lake Chala between August 2011 and January 2015, but with varying distributions (Fig. 4c). The C_{30} and C_{32} 1,15-diols were most common overall (both ca 30 ± 20 %), while the C_{30} 1,14- and 1,13-diols were present in lower abundance (ca 10 ± 5 % and 3 ± 3 %, respectively), the C_{34} 1,17-diol was only detected during some periods, whereas C_{28} diols were not detected at all. The fluxes of the different LCDs showed a similar seasonal pattern. The flux of C_{30} 1,15-diols varied from 0.1 and 26.6 g m^{-2} d^{-1}, peaking in April 2012, 2013, and 2014, August 2013 and November 2013 and 2014. The flux of C_{32} 1,15-diols ranged from 0.05 to 22.1 g m^{-2} d^{-1} with peaks in April 2012 and 2013, May and November 2014 and smaller increases in August and November 2013. The C_{30} 1,13-, C_{30} 1,14- and C_{34} 1,17-diol fluxes peaked in the same periods, i.e. April 2012 and 2013, May and November 2014 and ranged from 0.04 to 0.9 g m^{-2} d^{-1}, from 0.02 to 2.5 g m^{-2} d^{-1}, and 0 to 4.2 g m^{-2} d^{-1} respectively.

4 Discussion

4.1 Controls on the production of long-chain diols

Lake Geneva

The LCD distribution in Lake Geneva agrees with previous findings from other lakes, where the C_{32} 1,15- and the C_{30} 1,15-diols were the most abundant LCDs (Rampen et al., 2014b). The proportion of the different LCDs varied seasonally (Fig. 3a) which might either indicate a change in LCDs producer(s) or a variation in

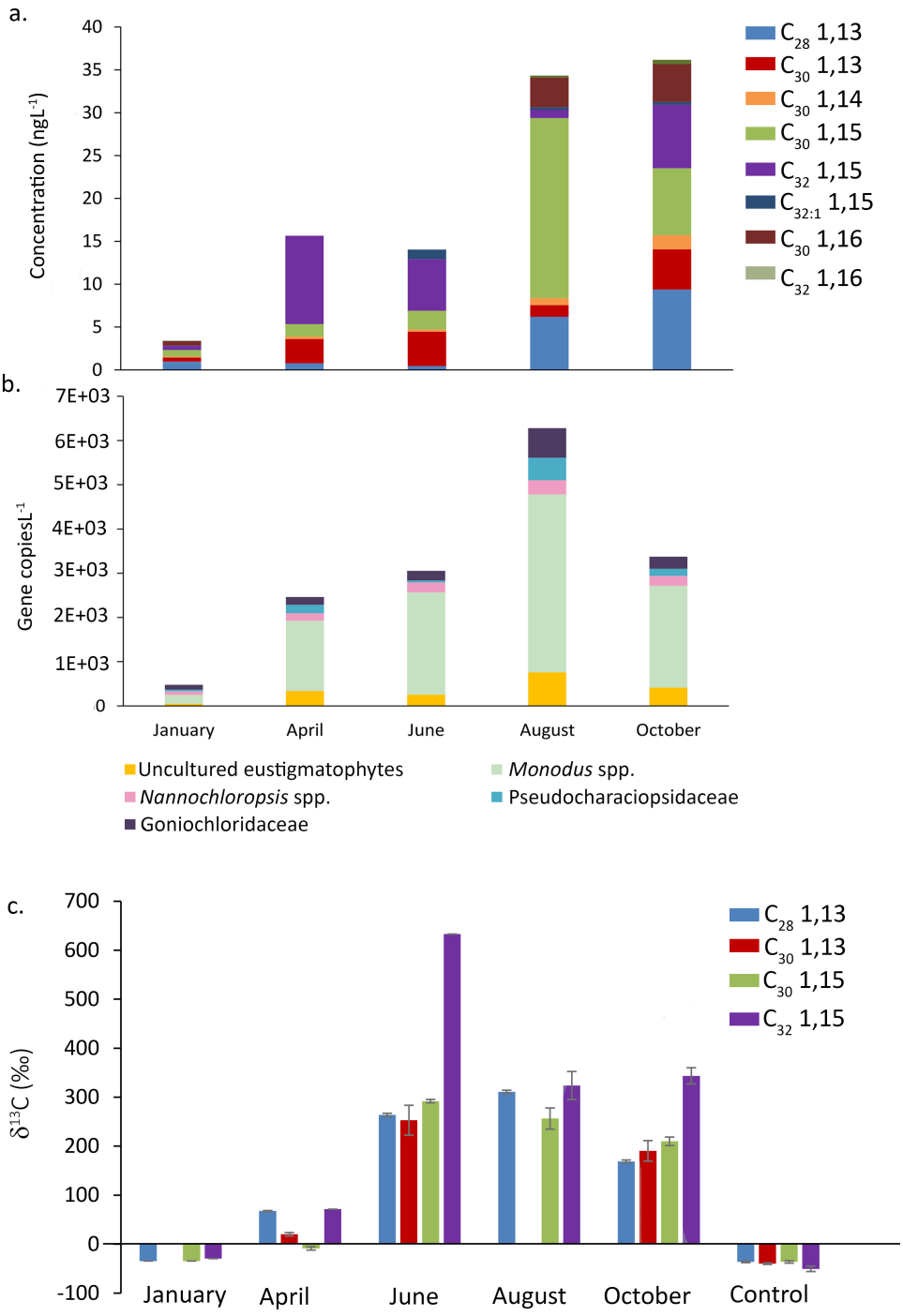

Figure 4: Seasonal variation in Lake Geneva of (a) abundance and composition of long-chain diols, (b) 18S rRNA gene copies affiliated to eustigmatophytes per liter, and (c) ^{13}C label incorporation in the different diols.

LCD production under different environmental conditions. Balzano et al. (2017) showed that, in cultures of the marine species *Nannochloropsis oceanica*, the proportion of LCDs is not sensitive to changes in cultivation conditions such as light irradiance (25 to 300 µE m^{-2} s^{-1}), salinity (10 to 50 g kg^{-1}) and nitrogen depletion (< 1 µM). However, Rampen et al. (2014a) found an increase in the proportion of the C_{32} 1,15-diol with temperature for the freshwater species *Goniochloris sculpta* and marine species *Nannochloropsis gaditana*. In Lake Geneva, we observe an opposite trend, as there is less C_{32} 1,15-diol in August and October (Fig. 3a), which are the warmest months (Fig. 2). Thus, temperature is unlikely to explain the seasonal change in LCD distributions in Lake Geneva.

Since LCDs can persist for long periods in the water column (Grossi et al. 2001; Reiche et al. 2018), and

can derive from fossil material (Balzano et al. 2018; Lattaud et al. 2018a), we evaluated in situ production of LCDs by performing incubation experiments with ^{13}C-labelled bicarbonate. The ^{13}C label was incorporated in the LCDs in all months except January, reflecting in situ production during these periods (Fig. 3c). It also suggests that the LCDs present in the lake in January likely originate from fossil material (c.f. Balzano et al. 2018). The relatively high degree of labelling (as shown by the high ^{13}C value) of the C_{32} 1,15-diol compared to that of the other LCDs indicates either a higher production rate of the C_{32} 1,15-diol or the presence of fast growing LCD producers that predominantly make the C_{32} 1,15-diol. Comparison of gene abundances with lipid abundances also suggests that most LCDs are produced in situ. A rough estimate of the LCD concentration per cell is 20 fg cell^{-1} for *Nannochloropsis* (Balzano et al. 2018). Hence, with one 18S rRNA gene copy per cell for *Nannochloropsis* (Zhu et al. 2005), 5 x 10^3 gene copies L^{-1} (total abundance of OTUs related to LCD producers) would translate to a LCD concentration of 10 ng L^{-1} which is comparable to what is detected in June (15 ng L^{-1}, Fig. 3a).

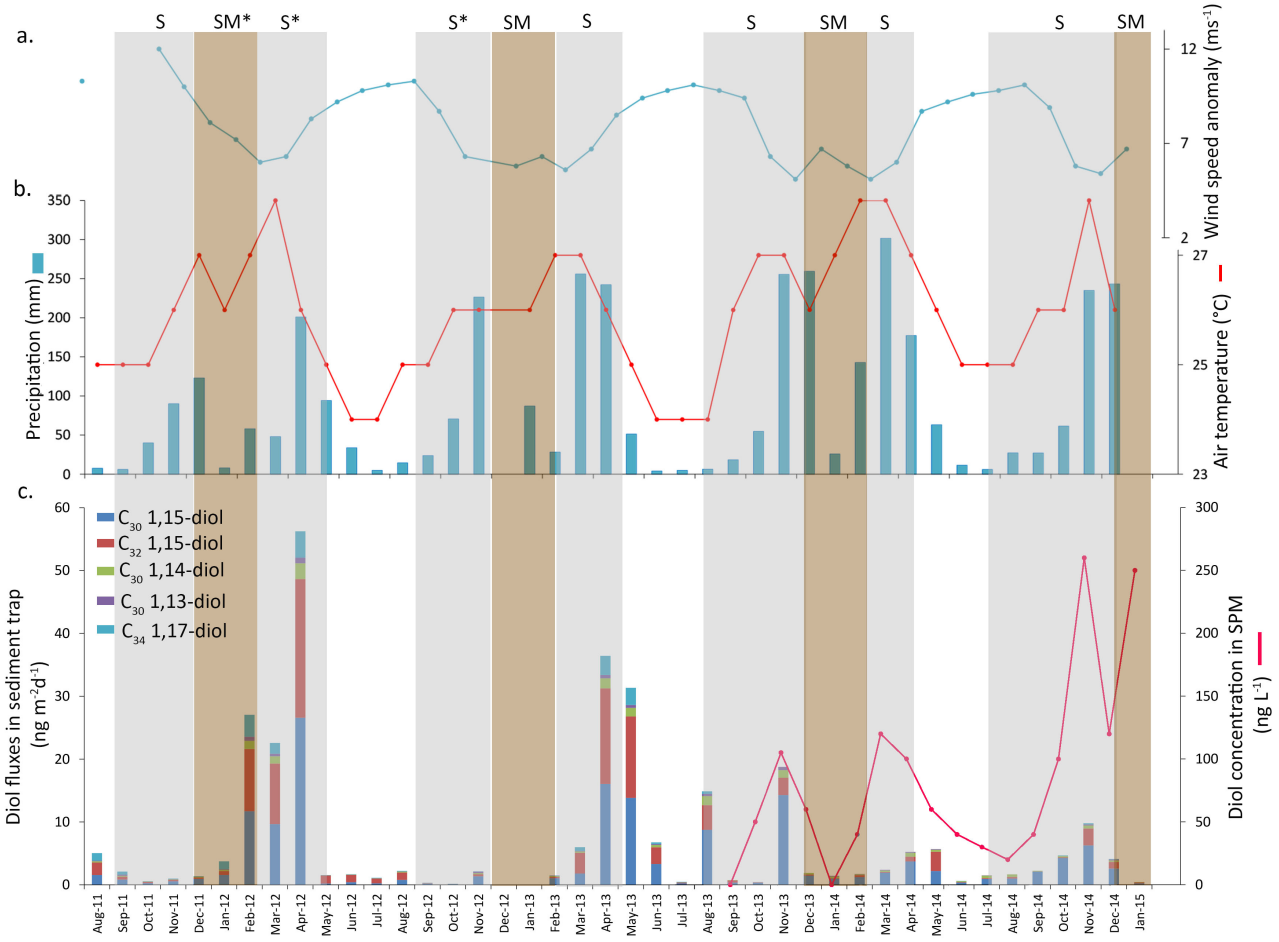

Figure 5: Monthly climatic average of (a) wind speed and (b) precipitation (bar plot) and air temperature (line) from Voi (Kenya) station (about 100 km away from Lake Chala, Buckles et al. 2013). (c) Long-chain diol fluxes in sediment traps (this study) and long chain diol concentrations of SPM (average of 0 to 15 m depth; sum of C_{30} and C_{32} diols; van Bree et al. 2018) of Lake Chala. Grey bars indicate periods of stratification (S) or shallow mixing (SM) in the water column (* indicates hypothesized periods of S or SM, from van Bree et al. 2018).

A thermocline is present in Lake Geneva between 7 to 25 m depth in all months except in January (Table 1). Interestingly, the LCD concentrations show a positive relation with the temperature of the epilimnion (lake temperature at 15 m depth, $r^2 = 0.90$, $p = 0.08$, $n = 5$), indicating that the production of LCDs is enhanced during periods with a stratified water column, particularly during summer months when stratification is the strongest (Fig. 3). Nevertheless, there is no correlation between chlorophyll-a concentration and LCD concentrations (data not shown), indicating that LCD producers only are a small proportion of the photosynthetic community.

Lake Chala

In Lake Chala, there is a strong increase in LCD fluxes during periods of low wind speed and relatively warm temperature i.e. April 2012, April 2013, May 2014, November 2014 and, to a lesser extent, August and November 2013 (Fig. 4). A previous study by Villanueva et al. (2014) on LCD fluxes from August 2009 to August 2010 showed a similar pattern and amounts of LCDs (sum of all LCDs from 10 to 206 µg m^{-2} d^{-1}), with a peak in April 2010. van Bree et al. (2018) showed that LCDs in the SPM of the upper 25 meters peaked during periods with stratified water column conditions in November 2013, May 2014 and November 2014 (Fig. 4). The periods of strong LCD increase, in both fluxes and concentrations, occur during times of strong stratification (temperature and oxygen) of the water column (Sinninghe Damsté et al. 2009; Buckles et al. 2014; Wolff et al. 2014; van Bree et al. 2018). The daily shallow (15-20 m) mixing is driven by wind, but deep (45-60 m) seasonal mixing happens during dry periods with high wind speed and lower lake surface temperature (Sinninghe Damsté et al. 2009; Buckles et al. 2014). Some increases of LCDs do not correspond to period of stratification as in February 2012 when LCDs fluxes are elevated before the stratification period. However, as the sediment trap collects material from a whole month while stratification starts at the end of the month (e.g. 17^{th} February 2012) it will already record a period of increased fluxes while the lake is not yet fully stratified. To the contrary, in some periods the LCD flux remained relatively high after stratification ended (e.g. May 2013 and 2014, Fig. 4). During these times, deep mixing happened and it is possible that part of the LCDs in the sediment trap may be from resuspended inking particles. Interestingly, in some periods with stratification there are no elevated fluxes of LCDs, such as from September to December 2012, indicating that stratification might not be the only parameter leading to enhanced LCD production.

Overall, LCDs in these two lakes, and potentially in other lakes, seem to be mainly produced during periods of thermal stratification in the water column. The stratification, and relatively higher water temperature in the surface, might enhance LCD production within the organisms or favour the bloom of the LCD producers. The latter is more likely, as eustigmatophyte algae in culture studies do not enhance LCD production when the medium temperature is changed (i.e. cold shock from Balzano et al. 2017), while phytoplankton blooms are generally enhanced in stratified waters (Peeters et al. 2007; Paerl and Huisman 2008; Wolff et al. 2014).

4.2 Sources of LCDs in lakes

DNA analysis showed that eustigmatophytes are present in Lake Geneva in all seasons but that their relative abundance is higher in June, August and October (3.1 x 10^3, 6.3 x 10^3 and 3.4 x 10^3 18S rRNA gene copies L^{-1}, respectively, Fig. 3b), and relatively low in January (4.8 x 10^2 18S rRNA gene copies L^{-1}). The low concentration of eustigmatophytes in January is in agreement with the absence of in situ production of LCDs and the low concentration of LCDs during this month (Fig. 3a). Hence, the link between the number of gene copies related to eustigmatophytes and LCD abundance (see above), strongly suggests that eustigmatophyte algae are the main producers of LCDs in Lake Geneva. In comparison, in Lake Chala, DNA sequencing of 18S rRNA in SPM collected in February 2010, showed the presence of several reads associated with eustigmatophyte families, including two new groups that could be associated with the presence of the C_{34} 1,17-diol (Villanueva et al. 2014). In our study, the flux of the C_{34} 1,17-diol follows a similar trend as the other diols (Fig. 4), indicating that either the LCD producers linked to this diol were always present with the other LCD producers, or that it is not specific to a certain group of eustigmatophytes. Villanueva et al. (2014) found similar abundances of gene copies (4 x 10^4 eustigmatophyte 18S rRNA gene copies L^{-1}) as found here for Lake Geneva, despite the use of different primers for the quantitative PCR assay indicating that the sequences obtained with general eukaryotic primers are reflecting the eustigmatophyte community. Collectively, our results together with that of Villanueva et al. (2014) suggest that eustigmatophytes are the major source of LCDs in lakes Geneva and Chala and likely in others.

As hypothesized above, the variations in the relative distribution of LCDs between April/June and August/October in lake Geneva (more C_{32} 1,15-diol in April/June and more C_{30} 1,15-diol in August/October, Fig. 3a) suggest a change in LCD producers. Indeed, in August and October, the number of gene copies related to the eustigmatophyte family Goniochloridaceae and Pseudocharaciopsidaceae increased (from 1.7 x 10^2 in April to 6.7 x 10^2 in August and from 1.9 x 10^2 in April to 5.1 x 10^2 in August 18S rRNA gene copies L^{-1}, respectively, Fig. 3b). This implies that species related to Goniochloridaceae or Pseudocharaciopsidaceae families could be responsible for the increased C_{30} 1,15-diol production at this time. However, although Rampen et al.

(2014a) found that freshwater species belonging to the Goniochloridaceae (*G. sculpta*, *Microtalis aquatica* and *P. enorme*) contain C_{30} 1,15-diol, they do so in only low relative abundance (5-20 %). Furthermore, species belonging to the Pseudocharaciopsidaceae family have not yet been analysed for their LCD composition, and thus we cannot assess if they are responsible for the high contribution of C_{30} 1,15-diol found in Lake Geneva.

With respect to the 1,14-diols detected in Lake Geneva, the diatoms *Proboscia* are an unlikely source as they primarily comprise marine species (Moita et al. 2003; Lassiter et al. 2006; Takahashi et al. 2011) and no sequences related to these diatoms were detected here. Furthermore, we do not observe similar trends between the abundance of sequences related to radial centric diatoms and the concentration of 1,14-diols in Lake Geneva (Fig. S2a). A more likely candidate could be species falling in the Goniochloridaceae family as one species has previously been shown to produce 1,14-diols (Rampen et al. 2014a). However, we do not observe a match between the abundance of sequences related Goniochloridaceae and the concentration of 1,14-diols (Fig. S2b) and, therefore, it remains unclear which organisms produce 1,14-diols in lakes.

Conclusions

We investigated two lakes for the occurrence of LCDs, the controls on their production, and their sources. In Lake Geneva, LCDs are produced in situ from spring to late summer. Their distribution is dominated by the C_{32} 1,15-diol in April/June and C_{30} 1,15-diol in August/October. The seasonal production of LCDs seems to be controlled by thermal stratification in the water column of Lake Geneva, which likely stimulates the bloom of LCD producers. Enhanced LCD fluxes in sediment traps of Lake Chala coincide with wet periods with low wind speed and relatively high temperature, and thus confirm previous findings that the production of LCDs occurs primarily under stratified water column conditions in this lake. 18S rRNA gene analysis of Lake Geneva revealed the presence of freshwater eustigmatophytes, of which several species are known to produce LCDs in cultures. Their abundance covary with that of LCD concentrations, suggesting that they are likely the major producers of these compounds in Lake Geneva, as was previously shown to be the case for LCDs in Lake Chala. seasonal changes in LCD distributions are most likely due to changes in eustigmatophyte composition rather than environmental conditions.

Acknowledgments

We thank Jort Ossebaar and Monique Verweij for analytical help, Pauline de Regt for lipid extraction of sediment trap sampled from Lake Chala, Maartje Brouwer for help during DNA analysis, Laura Schreuder, Jean-Christophe Hustache and the UMR CARRTEL for assistance during sampling of the Geneva Lake, and Alejandro Abdala for assistance in bioinformatics. Thanks to Wannes De Crop for providing stratification data of Lake Chala. C. M. Oluseno is thanked for conducting the monthly collection of sediment trap material from Lake Chala. Thanks to Dirk Verschuren for comments on a previous version of the manuscript. The environmental data from the Geneva Lake have been obtained thanks to © SOERE OLA-IS, AnaEE-France, INRA Thonon-les-Bains, CIPEL 7-12-18, developed by Eco-Informatics ORE INRA Team. We thank Utrecht Sequencing Facility for providing sequencing service and data. The Utrecht Sequencing Facility is subsidized by the University Medical Center Utrecht, Hubrecht Institute and Utrecht University.

This research has been funded by the European Research Council (ERC) under the European Union's Seventh Framework Program (FP7/2007-2013) ERC grant agreement [339206] to S. S. The work was further supported by funding from the Netherlands Earth System Science Center (NESSC) through a gravitation grant (NWO 024.002.001) from the Dutch Ministry for Education, Culture and Science to J. S. S. D. and S. S.
The authors declare that they have no conflict of interest.

Table 1: Physical water properties and biological parameters of Lake Geneva during the sampling period between October 2017 and June 2018.

Sampling date	Air temperature (°C)	Water temperature (°C) surface	Water temperature (°C) 10 m	Water temperature (°C) 15 m	Water temperature (°C) 30 m	pH	Chlorophyll concentration (ug/L)
01-08-2017	20,5	23	21,2	15,9	8,5	8,56	2,44
01-10-2017	10,6	16	16,5	16,2	9,3	8,17	2,42
01-01-2018	4,7	7	6,9	6,9	6,9	8,08	1,9
01-04-2018	12,1	16	7,5	7,1	6,5	8,6	2,34
01-06-2018	16,5	22	12,2	9	7,1	8,6	2,92

Table 2: Concentration (ng L^{-1}) of the long-chain diols in Lake Geneva during the period of October 2017 and June 2018. ND: not detected.

	Concentration (ng L^{-1})								
Sampling date	**C_{28} 1,13**	**C_{28} 1,14**	**C_{30} 1,13**	**C_{30} 1,14**	**C_{30} 1,15**	**C_{30} 1,16**	**$C_{32:1}$ 1,15**	**C_{32} 1,15**	**Sum Diol**
01-08-2017	5,84	0,36	1,35	0,82	20,99	3,48	0,29	0,97	34,1
01-10-2017	8,52	0,86	4,70	1,64	7,80	4,43	0,32	7,41	35,7
01-01-2018	0,81	0,16	0,48	0,10	0,78	0,51	0,04	0,47	3,4
01-04-2018	0,27	0,48	2,85	0,27	1,47	ND	ND	10,30	15,7
01-06-2018	0,24	0,21	4,01	0,23	2,21	ND	1,13	5,99	14,0

Table 3: $\delta^{13}C$ values of long-chain diols in ^{13}C bicarbonate incubation experiments with Lake Geneva water.

	$\delta^{13}C$ C_{32} 1,15-diol (‰)		$\delta^{13}C$ C_{30} 1,15-diol (‰)		$\delta^{13}C$ C_{30} 1,13-diol (‰)		$\delta^{13}C$ C_{28} 1,13-diol (‰)	
Sampling date	**Labeling exp**	**Control**	**Labeling exp**	**Control**	**Labeling exp**	**Control**	**Labeling exp**	**Control**
01-08-2017	324±29	-50±6	256±22	-36±1	ND	-40±2	311±3	-36±2
01-10-2017	344±16		210±9		190±21		169±3	
01-01-2018	-30±0		-34±0		ND		-34±0	
01-04-2018	71±0		-9±4		20±4		68±1	
01-06-2018	634±2		290±67		253±31		264±4	

Supplement

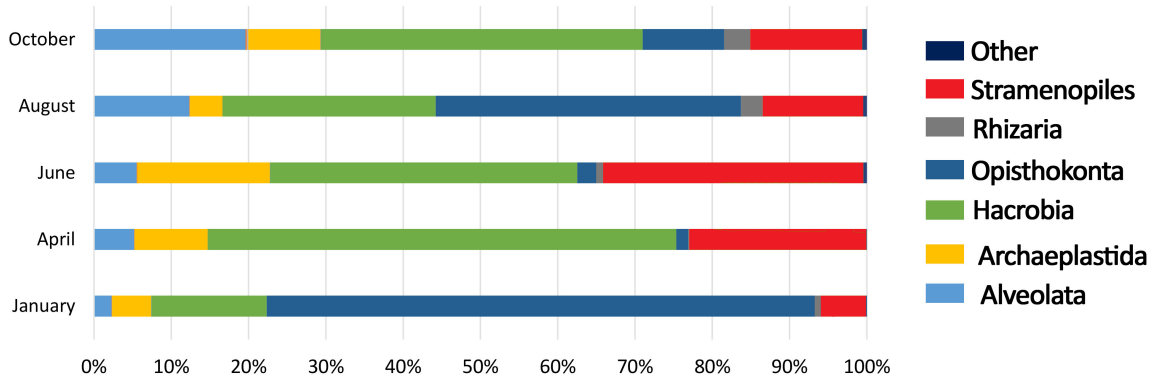

Figure 1: Results of the 18S rRNA sequencing of SPM collected from Lake Geneva.

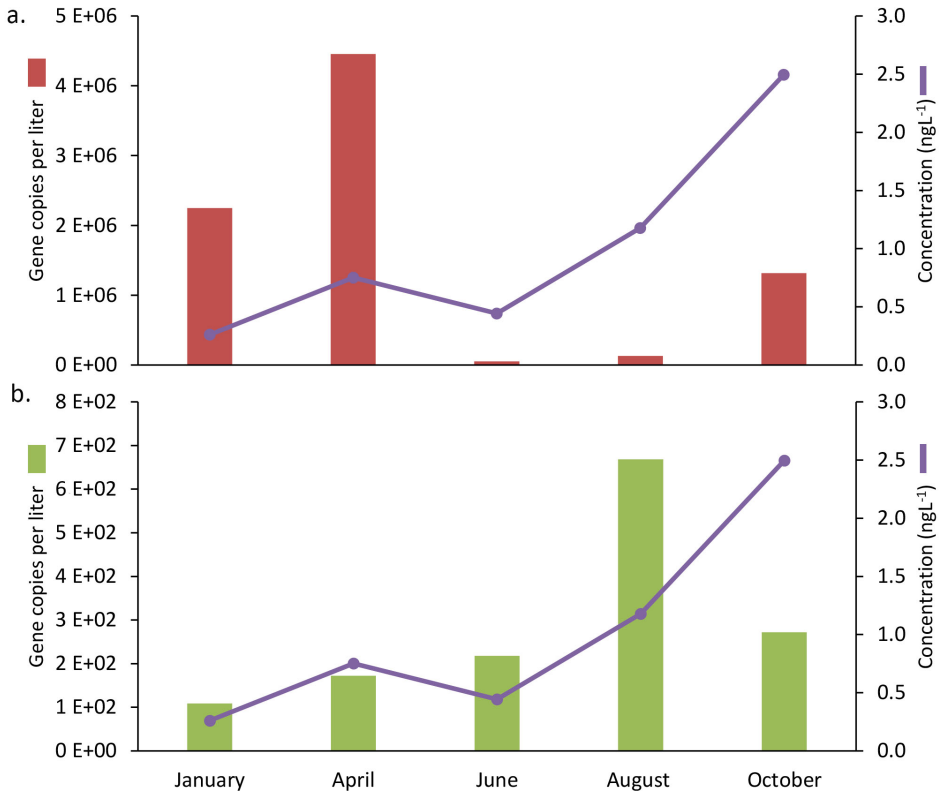

Figure 2: Seasonal variation in Lake Geneva of (a) 18S rRNA gene copies affiliated to radial centric diatoms and (b) 18S rRNA gene copies affiliated to Goniochloridaceae in relation to 1,14-diols concentrations.

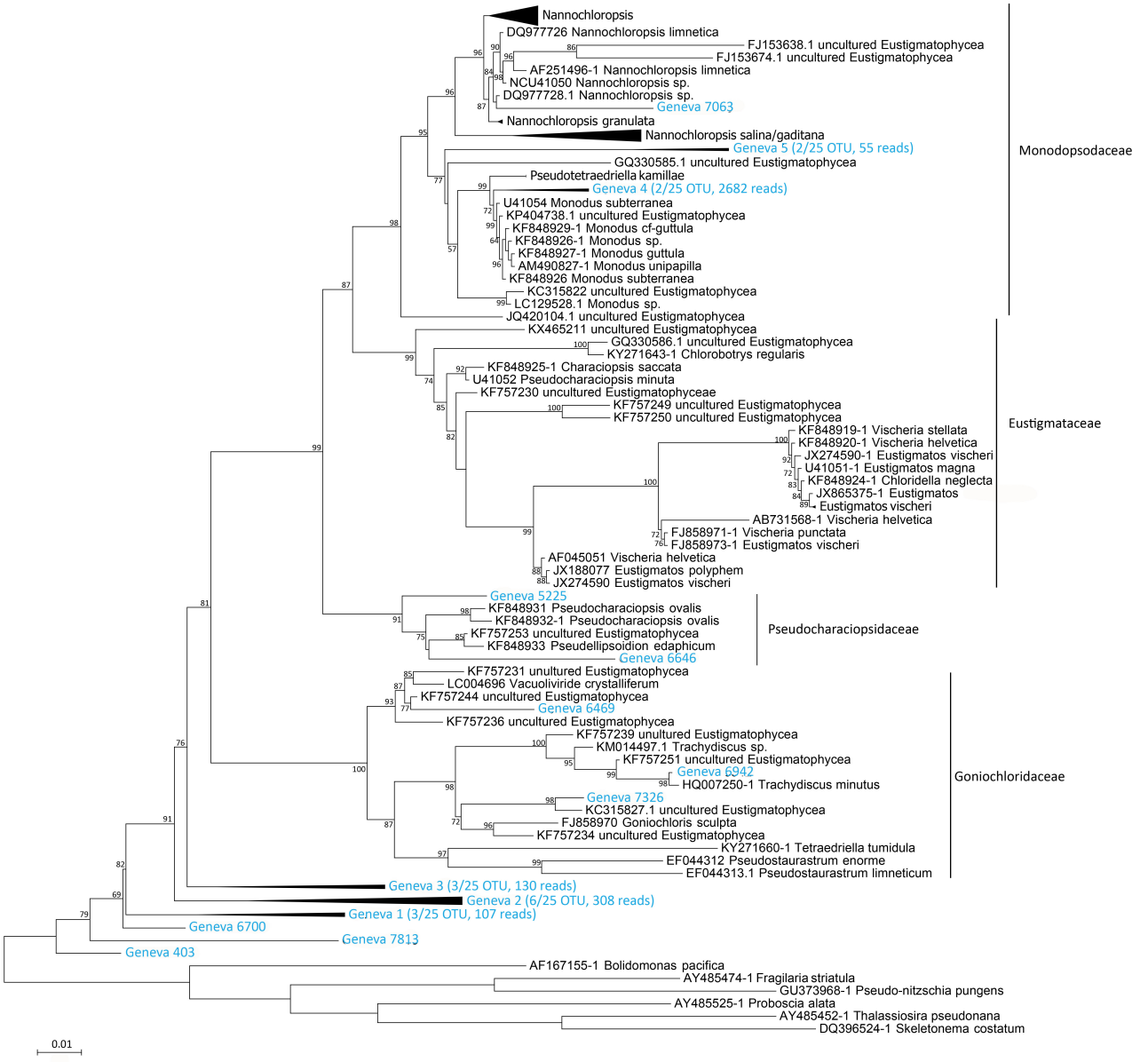

Figure 3: Phylogenetic tree comparing the 18S rRNA gene sequences of Lake Geneva (based on the 25 most abundant OTUs) with 18S rRNA gene sequences of cultured eustigmatophyte freshwater species. The tree was inferred by maximum likelihood based. Numbers next to the branches indicate bootstrap support (based on 1,000 replicates), and only values < 50% are shown. NCBI accession number is indicated next to the sequences of known eustigmatophytes. Classification is made following Fawley et al. (2014).

Sampling in Lake Geneva, April 2018

Part II

Paleo application of the long-chain diol proxies

Piston core sampling, cruise 64PE418, March 2017 Credit @Wouter Hoijmann

Chapter 6

The C_{32} alkane-1,15-diol as a proxy of late Quaternary riverine input in coastal margins

Climate of the Past 13 (2017) 1049–1061

Julie Lattaud [a,*], Denise Dorhout[a], Hartmut Schulz[b], Isla S. Castañeda[a,1], Enno Schefuß[c], Jaap S. Sinninghe Damsté[a,d], Stefan Schouten[a,d]

[a] NIOZ, Royal Netherlands Institute for Sea Research, Department of Marine Microbiology and Biogeochemistry (MMB), and Utrecht University, PO Box 59, 1790 AB Den Burg, The Netherlands
[b] University of Tübingen, Department of Geosciences, Hölderlinstrasse 12, D-72074 Tübingen, Germany
[c] MARUM Center for Marine Environmental Sciences, University of Bremen, Germany.
[d] Utrecht University, Department of Earth Sciences, Faculty of Geosciences, Princetonlaan 8a, 3584 CD Utrecht, The Netherlands.

[*] Corresponding author.
E-mail address: Julie.lattaud@nioz.nl (J. Lattaud).
[1] Current address: University of Massachusetts, Department of Geological sciences, 244 Morrill Science Center, Amherst, United States of America
https://doi.org/10.5194/cp-13-1049-2017

Abstract

The study of past sedimentary records from coastal margins allows us to reconstruct variations of terrestrial input into the marine realm and to gain insight into continental climatic variability. There are numerous organic proxies for tracing terrestrial input into marine environments but none that strictly reflect the input of river-produced organic matter. Here, we test the fractional abundance of the C_{32} alkane 1,15-diol relative to all 1,13- and 1,15-long-chain diols ($F_{C32\ 1,15}$) as a tracer of input of river-produced organic matter in the marine realm in surface and Quaternary (0-45 ka) sediments on the shelf off the Zambezi and nearby smaller rivers in the Mozambique Channel (western Indian Ocean). A Quaternary (0-22 ka) sediment record off the Nile River mouth in the Eastern Mediterranean was also studied for long-chain diols. For the Mozambique Channel, surface sediments of sites most proximal to Mozambique Rivers showed the highest $F_{C32\ 1,15}$ (up to 10 %). The sedimentary record shows high (15-35 %) pre-Holocene $F_{C32\ 1,15}$ and low (<10 %) Holocene $F_{C32\ 1,15}$ values, with a major decrease between 18 and 12 ka. $F_{C32\ 1,15}$ is significantly correlated (r^2 = 0.83, p<0.001) with the BIT index, a proxy for the input of soil and river-produced organic matter in the marine environment, which declines from 0.25-0.60 for the pre-Holocene to <0.10 for the Holocene. This decrease of both $F_{C321,15}$ and the BIT is interpreted to be mainly due to rising sea level, which caused the Zambezi River mouth to become more distal to our study site, thereby decreasing riverine input at the core location. Some small discrepancies are observed between the records of the BIT index and $F_{C32\ 1,15}$ for Heinrich Event 1 (H1) and Younger Dryas (YD), which may be explained by a change in soil sources in the catchment area rather than a change in river influx. Like for the Mozambique Channel, a significant correlation between $F_{C32\ 1,15}$ and the BIT index (r^2 = 0.38, p<0.001) is observed for the Eastern Mediterranean Nile record. Here also, the BIT index and $F_{C32\ 1,15}$ are lower in the Holocene than in the pre-Holocene, which is likely due to the sea level rise. In general, the differences between BIT index and $F_{C32\ 1,15}$ Eastern Mediterranean Nile records can be explained by the fact that the BIT index is not only affected by riverine runoff but also by vegetation cover with increasing cover leading to lower soil erosion. Our results confirm that $F_{C32\ 1,15}$ is a complementary proxy for tracing riverine input of organic matter into marine shelf settings and, in comparison with other proxies, it seems not to be affected by soil and vegetation changes in the catchment area.

Keywords: *Long chain diols; C_{32} 1,15-diol; River outflow; Terrigenous output*

1 Introduction

Freshwater discharge from river basins into the ocean has an important influence on the dynamics of many coastal regions. Terrestrial organic matter (OM) input by fluvial and aeolian transport represents a large source of OM to the ocean (Schlesinger and Melack 1981). Deltaic and marine sediments close to the outflow of large rivers form a sink of terrestrial OM and integrate a history of river, catchment, and oceanic variability (Hedges et al. 1997).

Terrestrial OM can be differentiated from marine OM using carbon to nitrogen (C/N) ratios and the bulk carbon isotopic composition (^{13}C) of sedimentary OM (e.g. Meyers 1994). The abundance of N-free macromolecules such as lignin or cellulose result in organic carbon-rich plant tissues that lead to an overall higher C/N ratio for terrestrial OM compared to aquatic organisms (Hedges et al. 1986). However, this ratio may be biased when plant-tissues gain nitrogen during bacterial degradation and when planktonic OM preferentially lose nitrogen over carbon during decay (Hedges and Oades 1997). Differences in the stable carbon isotopic composition may also be used to examine terrestrial input as terrestrial OM is typically depleted in ^{13}C ($\delta^{13}C$ of -28 to -25‰) compared to marine OM (-22 to -19‰). However, C_4 plants have $\delta^{13}C$ values of around -12‰ (Fry and Sherr 1989; Collister et al. 1994; Rommerskirchen et al. 2006) and thus a substantial C_4 plant contribution can make it difficult to estimate the proportion of terrestrial to marine OM in certain settings (Goni et al. 1997).

Biomarkers of terrestrial higher plants are also used to trace terrestrial OM input into marine sediments. For example, plant leaf waxes such as long-chain n-alkanes are transported and preserved in sediments (Eglinton and Eglinton 2008, and references cited therein) and can provide information on catchment-integrated vegetation or precipitation changes (e.g. Ponton et al. 2014), while soil specific bacteriohopanepolyols (BHP) are biomarkers

of soil bacteria and indicate changes in soil OM transport (Cooke et al. 2008). Similarly, branched glycerol dialkyl glycerol tetraethers (brGDGTs) are widespread and abundant in soils (Weijers et al. 2007, 2009) and can be used to trace soil OM input into marine settings via the branched and isoprenoid tetraether (BIT) Index (Hopmans et al. 2004). However, brGDGTs can also be produced in-situ in rivers (e.g. Jonge et al. 2015a) and thus the BIT index does not exclusively reflect soil OM input. Moreover, because the BIT index is the ratio of brGDGTs to crenarchaeol (an isoprenoidal GDGT predominantly produced by marine Thaumarchaeota; Sinninghe Damsté et al. 2002), the BIT index can also reflect changes in marine OM productivity instead of changes in terrestrial OM input in areas where primary productivity is highly variable, i.e. where the quantity of crenarchaeol is variable (Smith et al. 2012).

Although these terrestrial organic proxies are useful to trace soil, river or vegetation input into marine sediments, previously there were no organic geochemical proxies to specifically trace river-produced OM input. However, recently, the C_{32} 1,15-diol, relative to all 1,13- and 1,15-long-chain diols ($F_{C32\ 1,15}$), was proposed as a tracer for river-produced OM input (de Bar et al. 2016; Lattaud et al. 2017b). Long-chain diols (LCD), such as the C_{32} 1,15-diol, are molecules composed of a long alkyl chain ranging from 26 to 34 carbon atoms, an alcohol group at position C_1 and at a mid-chain position, mainly at positions 13, 14 and 15. They occur ubiquitously in marine environments (de Leeuw et al. 1981; Versteegh et al. 1997, 2000; Gogou and Stephanou 2004; Rampen et al. 2012, 2014b; Romero-Viana et al. 2012; Plancq et al. 2015; Zhang et al. 2011 and references therein), where the major diols are generally the C_{30} 1,15-diol, C_{28} and C_{30} 1,13-diols, and the C_{28} and C_{30} 1,14-diols. In marine environments the 1,14-diols are produced mainly by *Proboscia* diatoms (Sinninghe Damsté et al. 2003; Rampen et al. 2007) and the 1,13 and 1,15-diol are thought to be produced by eustigmatophyte algae (Volkman et al. 1999; Rampen et al. 2007, 2014a; Villanueva et al. 2014). Versteegh et al. (2000) showed that $F_{C321,15}$ was relatively higher closer to the mouth of the Congo River. Likewise, Rampen et al. (2012) observed that sediments from the estuarine Hudson Bay have a much higher $F_{C32\ 1,15}$ than open-marine sediments. More recent studies noted elevated amounts of $F_{C32\ 1,15}$ in coastal sediments, and even higher amounts in rivers indicating a continental source for this diol (de Bar et al. 2016; Lattaud et al. 2017b). Since the C_{32} 1,15-diol was not detected in soils distributed worldwide, production of this diol in rivers by freshwater eustigmatophytes is the most likely source of this compound which, therefore, can potentially be used as a proxy of river-produced OM input to marine settings.

Here we test the downcore application of this new proxy by analyzing $F_{C32\ 1,15}$ in a continental shelf record (0-45 ka) from the Mozambique Channel and a record (0-24 ka) from the Eastern Mediterranean Sea to reconstruct Holocene/Late Pleistocene changes in freshwater input of the Zambezi and Nile rivers, respectively. Analysis of surface sediments and comparison with previously published BIT index records (Castaneda et al. 2010; Kasper et al. 2015) allow us to assess the potential of the C_{32} 1,15-diol as a tracer for riverine runoff, or more precisely, river-produced organic matter, in these coastal margins.

2 Material an methods

2.1 Study sites

Mozambique margin and Zambezi River

The Mozambique Channel is located between the coasts of Mozambique and Madagascar between 11°S and 24°S and plays an important role in the global oceanic circulation by transporting warm Indian Ocean surface waters into the Atlantic Ocean. The Zambezi River is the largest river that delivers freshwater and suspended particulate matter to the Mozambique Channel (Walford et al. 2005). The Zambezi River has a drainage area of 1.4 x 10^6 km^2 and an annual runoff between 50 and 220 km^3 (Fekete et al. 1999). It originates in northern Zambia, flows through eastern Angola and Mozambique to reach the Indian Ocean. The Zambezi delta starts at Mopeia (Fasolato et al. 2006) and the Zambezi plume enters the Mozambique Channel and flows northwards along the coast (Nehama and Reason 2014). The rainy season in the catchment is in austral summer when the Intertropical convergence zone (ITCZ) is at its southernmost position (Beilfuss and Santos 2001; Gimeno et al. 2010; Nicholson 2009). The seasonal variation of the Zambezi runoff varies between 7000 m^3/s during the wet season to 2000 m^3/s during the dry season (Beilfuss and Santos 2001). A few smaller Mozambique rivers other than the Zambezi River flow into the Mozambique Channel (Fig. 1): the Ligonha, Licungo, Pungwe and Revue in Mozambique (together with the Zambezi River, they are collectively called “the Mozambique rivers” here).

Past studies have shown that the deposition pattern of the Zambezi riverine detritus is variable with sea level, i.e. most of the time material was deposited downstream of the river mouth but during high sea level it was deposited northeast of the river mouth due to a shore current (Schulz et al. 2011). During the last glacial period the Zambezi riverine detritus followed a more channelized path (Schulz et al. 2011). van der Lubbe et al. (2016) found that the relative influence of the Zambezi river compared to more northern rivers in the Mozambique Channel varied during Heinrich event 1 (H1) and the Younger Dryas (YD). Schefuß et al. (2011) studied the δ^{13}C and δD of n-alkanes, and the elemental composition (Fe content) of core GeoB9307-3, located close to the present day river mouth (Fig. 1), and reported higher precipitation and riverine terrestrial input in the Mozambique Channel during the Younger Dryas and H1. This is in agreement with more recent results from Just et al. 2014 on core GeoB9307-3 and Wang et al. 2013 on core GIK16160-3, further away from the actual river mouth; both studies also showed an increased riverine terrestrial input during H1 and YD. To summarize, during H1 and the YD, the Zambezi catchment is characterized by higher precipitation and enhanced riverine runoff due to a southward shift of the Intertropical Convergence Zone (ITZC) resulting from Northern Hemisphere cold events, whereas during the Holocene drier conditions prevailed (Schefuß et al. 2011; Wang et al. 2013; van der Lubbe et al. 2014; Weldeab et al. 2014). The Last Glacial Maximum (LGM) in the Zambezi catchment is also recognized as an extremely wet period (Wang et al. 2013).

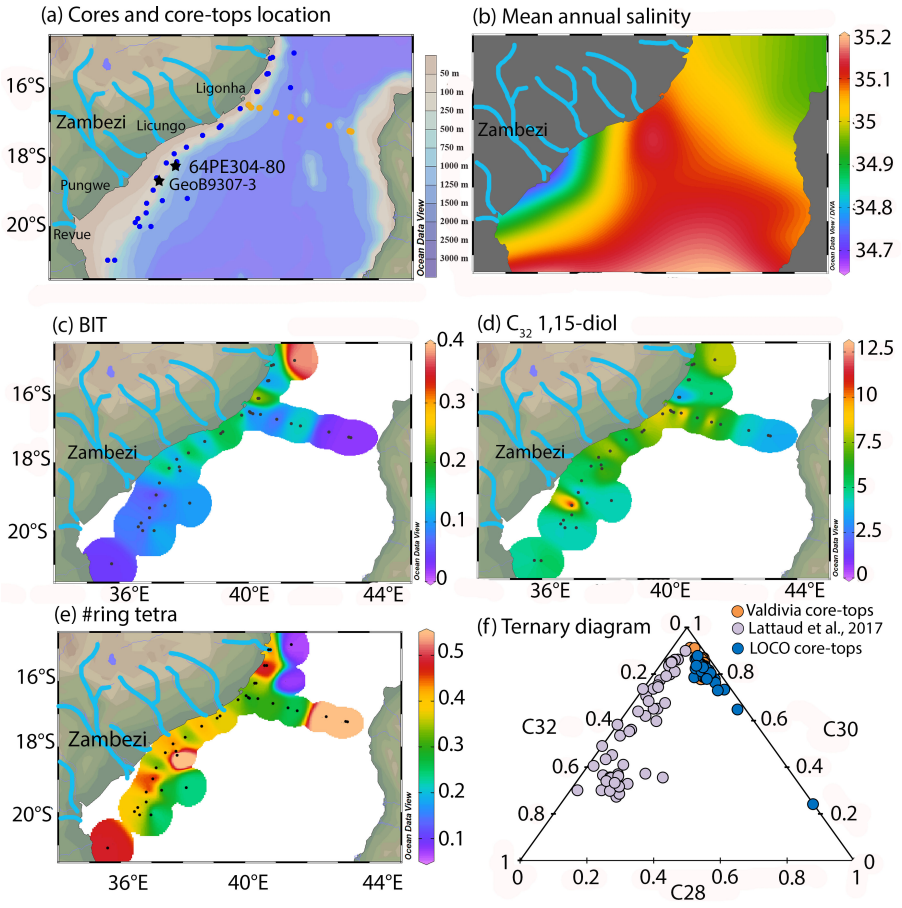

Figure 1: Map presenting (a) the location of the core-tops (LOCO transect in orange, VA core-tops in blue) and cores (stars), (b) the mean annual salinity (iridl.ldeo.columbia.edu), (c) the BIT index (LOCO transect values, VA core-tops from this study), (d) $F_{C32\ 1,15}$in the core-tops, (e) #ring tetra of the surface sediments (#ring tetra as defined by Sinninghe Damsté 2016), (f) Ternary diagram of C_{28} (sum of C_{28} 1,13 and C_{28} 1,14), C_{30} (sum of C_{30} 1,13, C_{30} 1,14 and C_{30} 1,15) and C_{32} (C_{32} 1,15) -diols (LOCO transect in orange, VA core-tops in blue, data from Lattaud et al. 2017b in purple). The maps were drawn using Ocean Data View.

Eastern Mediterranean Sea and Nile River

The Eastern Mediterranean Sea is influenced by the input of the Nile River, which is the main riverine sediment supply with annual runoff of 91 km^3 and a sediment load of about 60 x 10^9 $kg.yr^{-1}$ (Foucault and Stanley 1989; Weldeab et al. 2002). Offshore Israel, the Saharan aeolian sediment supply is very low (Weldeab et al. 2002). A strong north-eastern current distributes the Nile River sediment along the Israeli coast toward our study site. The Nile River consists of two main branches: the Blue Nile (sourced at Lake Tana, Ethiopia) and the White Nile (sourced at Lake Victoria, Tanzania, Uganda). Precipitation in the Nile catchment fluctuates widely with latitude with the area north of 18°N dry most of the year and the wettest areas at the source of the Blue Nile and White Nile (Camberlin 2009). This general distribution reflects the latitudinal movement of the ITCZ.

Castaneda et al. (2010) have shown that sea surface temperature (SST) (reconstructed with alkenones and TEX_{86}) at the study site was following Northern Hemisphere climate variations with a cooling during the LGM, H1 and the YD and warming during the early part of the deposition of sapropel 1 (S1). Associated H1 and LGM cooling, extreme aridity in the Nile catchment is observed as inferred from the δD of leaf waxes. In contrast, during the early Holocene S1 deposition, a more humid climate and enhanced Nile River runoff prevailed (Castaneda et al. 2016). Neodymium (ϵNd) and strontium ($^{87}Sr/^{88}Sr$) isotopes (Castaneda et al. 2016; Box et al. 2011, respectively) show a relative increase in the contribution of Blue Nile inputs when the climate is arid (H1, LGM) and an increased contribution of the White Nile inputs when the climate is humid (S1). This change also affects the soil input into the Nile River, as inferred from the distribution of branched GDGTs, with a more arid climate reducing the vegetation in the Ethiopian highlands (source of the Blue Nile) and favoring soil erosion while during a more humid climate, vegetation increasing and soil erosion is less (Krom et al., 2002). To summarize, the climate of the Nile catchment area was colder and drier (Castaneda et al. 2010, 2016) during the YD, H1 and the LGM. The LGM and H1 were extremely arid events with the likely desiccation of the Nile water sources, i.e. Lake Tana and Lake Victoria (Castaneda et al. 2016). To the contrary, the time period during S1 sapropel deposition was warmer and wetter resulting in an enhanced riverine runoff. The late Holocene is characterized by a decrease in precipitation (Blanchet et al. 2014).

2.2 Sampling and processing of the sediments

Mozambique Channel sediments

We analyzed 36 core-top sediments (from multi cores) along a transect from the Mozambique coast to Madagascar coast (LOCO transect, Fallet et al. 2012). The LOCO core-tops have been previously studied by XRF and grain-size analysis (van der Lubbe et al. 2014, 2016) as well as for inorganic ($\delta^{18}O$, Mg/Ca) and organic (TEX_{86}, $U^{k'}_{37}$) temperature proxies (Fallet et al. 2012). 25 core-top sediments (from grabs, gravity or trigger-weight corers) retrieved during the R/V Valdivia's Expeditions VA02 (1971) and VA06 (1973) (hereafter called VA; Schulz et al. 2011), comprising a north-south transect paralleling the East African coast, and spanning from 21°S to 15°N (Fig. 1) were also analyzed. These surface sediments have been studied previously for element content (TOC, TON), isotopic content ($\delta^{18}O$, $\delta^{13}C$) as well as for mineral and fossil (foraminifera) content (Schulz et al. 2011). Piston core 64PE304-80 was obtained from 1329 m water depth during the INATEX cruise by the RV Pelagia in 2009 from a site (18°14.44'S, 37°52.14'E) located on the Mozambique coastal margin, approximately 200 km north of the Zambezi delta (Fig. 1a). The age model of core 64PE304-80 is based on ^{14}C dating of planktonic foraminifera (see supplementary information, van der Lubbe et al. 2014; Kasper et al. 2015) and by correlation of log (Ti/Ca) data from XRF core scanning with those of nearby core GIK16160-3, which also has an age model based on ^{14}C dating of planktonic foraminifera (see van der Lubbe et al. 2014 for details).

The LOCO sediment core-tops were sliced into 0-0.25 and 0.25-0.5 cm slices and extracted as described by Fallet et al. (2012). Briefly, ultrasonic extraction was performed (x 4) with a solvent mixture of dichloromethane (DCM)/methanol (MeOH) (2 : 1 v/v). The total lipid extract (TLE) was then run through a Na_2SiO_4 column to remove water. The 25 VA core-tops from the Valdivia's expedition were freeze dried on board and stored at 4°C. They were extracted via Accelerator Solvent Extractor (ASE) using DCM: MeOH mixture 9:1 (v/v) and a pressure of 1000 psi at 100°C using three extraction cycles. We analyzed sediments of core 64PE304-80 for diols using solvent extracts that were previously obtained for determination of the BIT index and δD values of alkenones (Kasper et al. 2015). Briefly, the core was sliced into 2 cm thick slices and the sediments were ASE extracted using the method described above.

For all Mozambique Channel sediments, the total lipid extract (TLEs) were separated through an alumina pipette column into three fractions: apolar (Hexane : DCM, 9:1 v/v), ketone (Hexane : DCM, 1:1 v/v) and polar (DCM : MeOH, 1:1 v/v). The polar fractions, containing the diols and GDGTs, were dissolved into a mixture of 99:1 (v/v) Hexane : Isopropanol and filtered through a 0.45 µm PTFE filters.

Eastern Mediterranean sediment core

Gravity core GeoB 7702-3 was collected during the R/V Meteor cruise M52/2 in 2002 from the slope offshore Israel (31°91.1'N, 34°04.4'E) at 562 m water depth (Pätzold et al. 2003; Castaneda et al. 2010). The chronology of this sedimentary record is based on 15 planktonic foraminiferal ^{14}C AMS dates (for details see Supplementary Information, Castaneda et al. 2010). The sediments have previously been analyzed for GDGTs, alkenones, δD and δ^{13}C of leaf wax lipids, and bulk elemental composition (Castaneda et al. 2010, 2016). Sediments were sampled every 5 cm and are 1 cm thick, and previously extracted as described by Castaneda et al. (2010). Briefly, the freeze-dried sediment were ASE extracted and the TLEs were separated using an aluminum oxide column into 3 fractions as described above.

Analysis of long-chain diols

Diols were analyzed by silylation of the polar fraction with 10 µL N,O-Bis(trimethylsilyl)-trifluoroacetamide (BSTFA) and 10 µL pyridine, heated for 30 min at 60°C and adding 30 µL of ethyl acetate. Diol analysis was performed using a gas chromatograph (Agilent 7990B GC) coupled to a mass spectrometer (Agilent 5977A MSD) (GC-MS) and equipped with a capillary silica column (25 m x 320 µm; 0.12 µm film thickness). The oven temperature regime was as follows: held at 70°C for 1 min, increased to 130°C at 20°C/min, increased to 320°C at 4°C/min, held at 320°C during 25 min. Flow was held constant at 2 mL/min. The MS source temperature was held at 250 °C and the MS quadrupole at 150°C. The electron impact ionization energy of the source was 70 eV. The diols were quantified using selected ion monitoring (SIM) of ions *m/z* 299.4 (C_{28} 1,14-diol), 313.4 (C_{28} 1,13-diol, C_{30} 1,15-diol), 327.4 (C_{30} 1,14-diol), and 341.4 (C_{30} 1,13-, C_{32} 1,15-diol) (Versteegh et al., 1997; Rampen et al., 2012).

The fractional abundance of the C_{32} 1,15-diol is expressed as percentage of the total major diols as follows:

$$F_{C321,15} = \frac{[C_{32}1,15]}{[C_{28}1,13] + [C_{30}1,13] + [C_{30}1,15] + [C_{32}1,15]} \times 100 \quad (1)$$

Analysis of GDGTs

GDGTs in the polar fractions of the extracts of the VA and LOCO core-top sediments were analyzed on an Agilent 1100 series LC/MSD SL following the method described by Hopmans et al. (2016). The BIT index was calculated according to Hopmans et al. 2004. We calculated the # ring tetra as described by Sinninghe Damsté (2016) and the CBT index and soil pH as described by Peterse et al. (2012):

$$\#ringtetra = \frac{GDGTIb + 2 \times GDGTIc}{GDGTIa + GDGTIb + GDGTIc)} \quad (2)$$

$$CBT = \log(\frac{GDGTIb + GDGTIIb}{GDGTIa + GDGTIIa}) \quad (3)$$

$$pH = 7.9 - 1.97 \times CBT \quad (4)$$

3 Results

3.1 Surface sediments of the Mozambique Channel

$F_{C32\ 1,15}$ in surface sediments across the Mozambique Channel varies from 2.3 to 12.5 % (Fig. 1) with one of the highest value in front of the Zambezi River mouth (10 %). The core-tops located in front of other minor northern rivers (Licungo, Ligonha Rivers) are also characterized by values of $F_{C32\ 1,15}$ (>7.5 %) higher than

those further away from the coast (<5 %). The major diol in all Mozambique surface sediments is the C_{30} 1,15-diol (57.5 ± 9.9%) with lower amounts of the C_{30} 1,14-diol (21.1 ± 6.0 %) and C_{28} 1,14-diol (13.2 ± 4.9 %) (Fig. 1).

The values for the BIT index in surface sediments across the Mozambique Channel vary from 0.01 to 0.42 (Fig. 1). BIT values are highest in the most northern region (0.4) and in front of river mouths (0.2-0.3) compared to values found close to the coast of Madagascar (<0.04). Following Sinninghe Damsté 2016, we calculated the #ring tetra (the relative abundance of cyclopentane rings in tetramethylated branched GDGTs) to determine if the brGDGTs are in-situ produced in the surface sediments or derived from the continent. The #ring tetra has an average of 0.39 ± 0.03 with higher values in front of the river mouths (with the highest values close to the Madagascar Rivers) and shows a clear decrease towards the open ocean (Fig. 1). The low #ring tetra indicate that there is likely limited in-situ sedimentary production of brGDGTs in the sediments of the Mozambique coastal shelf area except for the samples closest to the Madagascar coast where high #ring tetra values and low BIT values indicate in-situ production of brGDGTs. However, for the Mozambique shelf, the brGDGTs are mostly derived from the continent, confirming the use of the BIT index as a tracer for riverine input in this region.

3.2 Holocene and Late Quaternary sediments of the Mozambique Channel and Nile River

In the sediments of the Mozambique Channel core 64PE304-80, $F_{C32\ 1,15}$ shows a wide range; it varies from 2.4 to 47.6 % (Fig. 2). Between 44 and 39 ka the values are relatively stable (average of 27.6 ± 4.5 %), then they rapidly decline between 39 and 36 ka to 11 %. From this point on they gradually increase, reaching 37.4 % at 17 ka. $F_{C32\ 1,15}$ is then rapidly decreasing until it reaches the lowest values of the record after 12 ka (average of 4.9 ± 1.4 %). Holocene sediments (0-11 ka) show relatively low and constant values of $F_{C32\ 1,15}$ (5 ± 1.5 %), similar to the values found in the surface sediments of the area, i.e. 3.5 ± 1.6 % (Figs. 1 and 2).

The BIT index record (data from Kasper et al. 2015) shows similar changes as that of $F_{C32\ 1,15}$. Between 44 and 39 ka the average BIT value is 0.43 ± 0.06, then the BIT value decreases to 0.36 at 36 ka, followed by an increase until 17 ka to reach a value of 0.6, while the Holocene values are constant and average at 0.1 ± 0.02. The #ring tetra of branched GDGTs is constantly low (average 0.15 ± 0.01; Fig. S1a) between 44 to 15.5 ka, then increases to 0.4 at 8 ka and stays constant until the end of the Holocene (average 0.34 ± 0.03). Overall, these values are low and do not approach the values (0.8-1.0) associated with in-situ production of branched GDGTs in coastal marine sediments (Sinninghe Damsté 2016). The #ring tetra also shows a negative correlation with the BIT index throughout the record (r^2 = 0.74, p<0.05), indicating that when BIT values are high, #ring tetra is low. Therefore, high BIT values can definitely be associated with terrestrial brGDGT input. If we assume that the in-situ production of brGDGTs in the river (e.g. Jonge et al. 2015a; Zell et al. 2015) is minimal, we can then infer sources of soils from the different catchment areas by reconstructing the soil pH via the CBT index (see equation 3 and 4, Peterse et al., 2012). This showed a constant soil pH (average 6.2 ± 0.1) from 43 to 15 ka followed by a slight increase to 7 at 8 ka and constant (average 6.8 ± 0.08) at the end of Holocene (Supplementary fig. 1).

In Eastern Mediterranean sediment core GeoB 7702-3, $F_{C32\ 1,15}$ ranges from 3.9 to 47.0 %. Between 24 and 15 ka the values are slowly decreasing from 41 % at 24 ka to 7 % at 15 ka. Subsequently, $F_{C32\ 1,15}$ raises sharply until 11.7 ka (44 %) followed by a sharp decrease down to 16 % at 10 ka. $F_{C32\ 1,15}$ increases again until 7.5 ka up to 30 %, followed by a slow decrease in the Late Holocene towards values as low as 6 % (Fig. 3). The BIT index (data from Castaneda et al. 2016) varies in a similar way as $F_{C32\ 1,15}$. It is constant between 24 and 17 ka (average 0.37 ± 0.05), then decreases to 0.13 at 14.5 ka. It subsequently increases between 15.6 and 9 ka, before it decreases after 9 ka and stays constant in the Holocene (average 0.17 ± 0.05). The #ring tetra of the brGDGTs (Supplementary fig. 1) is constant from 24 to 15 ka (0.37 ± 0.05) then shows lower values from 15 to 7 ka (0.29 ± 0.04) and, finally, increases again during the late Holocene (0.40 ± 0.05). The BIT index and #ring tetra do not show a clear negative correlation as observed for the Mozambique core. However, the values of #ring tetra values are well below 0.8-1.0, suggesting that in-situ production of brGDGTs does not play an important role, in line with the depth from which the core was obtained which is well below the zone of 100-300 m where in-situ production is most pronounced (Sinninghe Damsté 2016). During parts of the record, low #ring tetra are associated with high BIT values, indicating that between 24 and 7 ka the brGDGT are mainly terrigenous. For the oldest part of the core, the soil pH shows a stable period from 24 to 14.8 ka (average 6.94 ± 0.07) then increases to 7.3 at 15 ka, followed by a large decrease (pH reaching 6.5 at 8.5 ka). As the in-situ

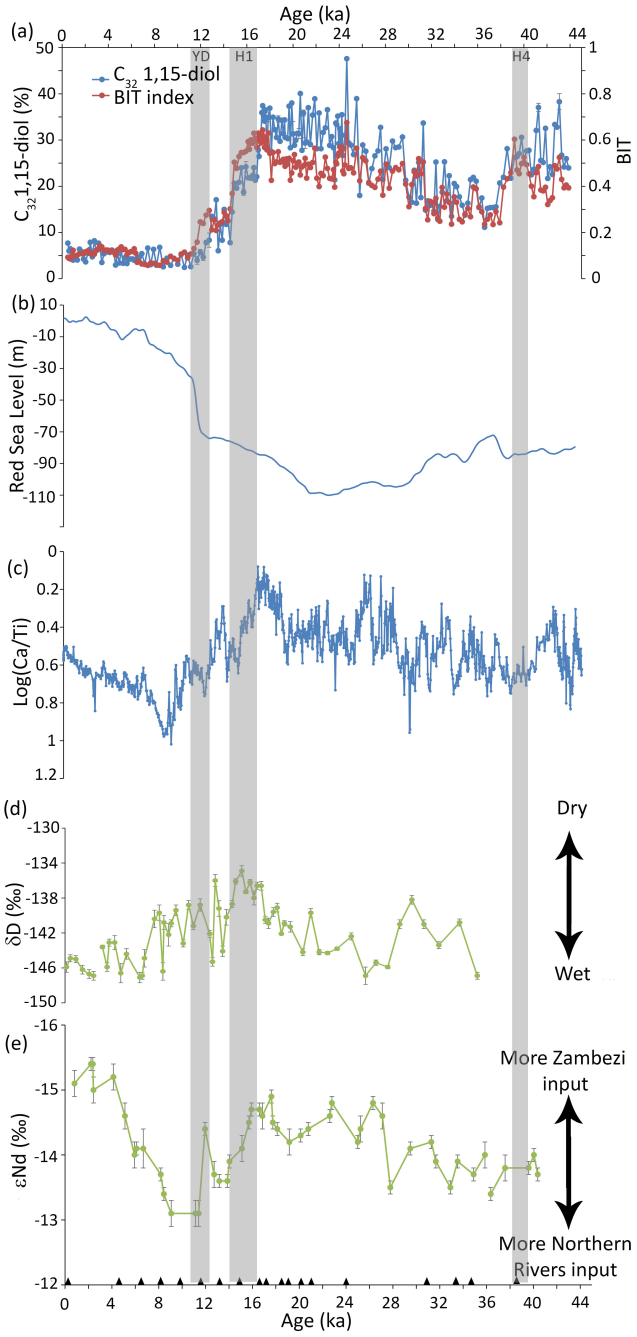

Figure 2: Organic and lithologic proxy records for core 64PE304-80 and parallel core GIK16160-3. (a) BIT index indicating soil and riverine input (Kasper et al. 2015) and $F_{C32\ 1,15}$ tracing riverine input (b) Red Sea Level changes (Grant et al. 2014) (c) log(Ca/Ti) indicating terrestrial input (van der Lubbe et al. 2014), (d) reconstruction of δD precipitation based on leaf wax n-C_{29} alkane of core GIK16160-3 (Wang et al. 2013), ϵNd signatures of the clay fraction document changes in riverine influence (van der Lubbe et al. 2016). The grey bars show the Younger Dryas (YD) and Heinrich event 1 (H1) and 4 (H4). Black triangles indicate positions where ^{14}C AMS dates were obtained (Kasper et al. 2015)

production of brGDGT is likely to be minimal in the latest part of the Holocene, and assuming that riverine production of brGDGTs is minimal, the soil pH can be reconstructed via the CBT index and shows a stable pH (average of 6.8 ± 0.1).

4 Discussion

4.1 Application of C_{32} 1,15-diol as a proxy for riverine input in the Mozambique shelf

In the surface sediments of the Mozambique Channel $F_{C32\ 1,15}$ is relatively low overall (<10 %) in comparison with other coastal regions with substantial river input (Fig. 1), where values can be as high as 65 % (de Bar et al. 2016; Lattaud et al. 2017b). Moreover, the BIT values are also relatively low at 0.01-0.42. Further confirmation of the low amount of terrestrial input in the analyzed surface sediments comes from the low C/N values (between 4.2 and 8.9 for the VA surface sediments; Schulz et al. 2011), characteristic of low terrestrial OM input (Meyers 1994). Nevertheless, the slightly higher values of both the BIT index and the $F_{C32\ 1,15}$ near the river mouths indicate that both proxies do seem to trace present day riverine input into the Mozambique Channel in line with earlier findings of other coastal margins influenced by river systems (de Bar et al. 2016; Lattaud et al. 2017b).

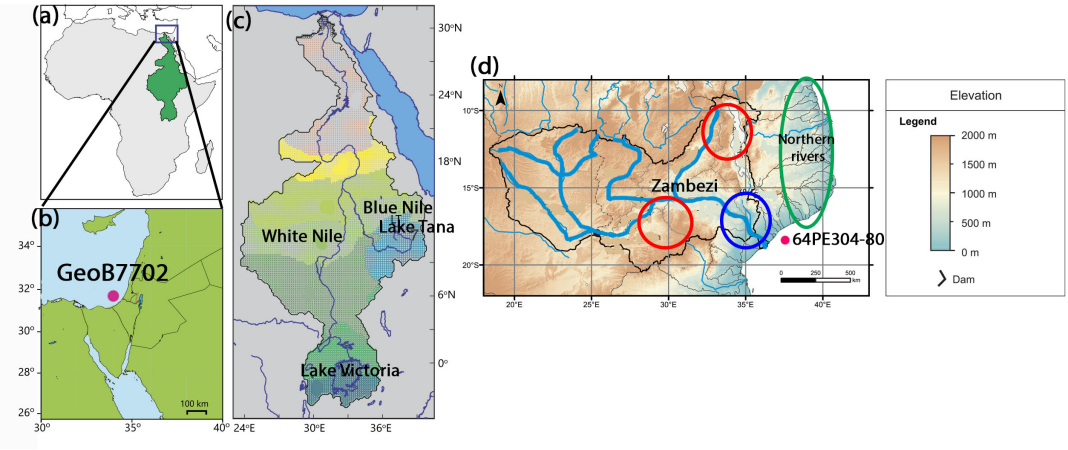

Figure 3: Sources of riverine input in both area, (a) Location of core GeoB7702-3 (b) Close up location of core GeoB7702-3 (adapted from Castaneda et al. 2016) (c) source of the Nile river sediments (from Castaneda et al. 2016) and (d) Location of core 64PE304-80 and the Mozambique Channel (red circles shows source areas of the Zambezi river during dry conditions, blue circle shows source area of the Zambezi river during wet conditions (Just et al. 2014), and green circle show northern rivers source area (van der Lubbe et al. 2016).

4.2 Past variations in riverine input in the Mozambique Channel

We compared the record of $F_{C32\ 1,15}$ with previously published proxy records, in particular the BIT index (Kasper et al. 2015) and log (Ca/Ti) (van der Lubbe et al. 2016). These two proxies show the same pattern as $F_{C32\ 1,15}$ (Fig. 2). Indeed, the BIT index and $F_{C32\ 1,15}$ are strongly correlated (r^2 =0.83, p<0.001). Since the #ring tetra of brGDGTs varies between 0.06 and 0.4 (Supplementary fig. 1), and is significantly negatively correlated with the BIT values, the brGDGTs are predominantly derived from the continent (cf. Sinninghe Damsté 2016) and thus the BIT is likely reflecting riverine input in the marine environment. Furthermore, $F_{C32\ 1,15}$ also shows a significant negative correlation with log(Ca/Ti) (r^2 = 0.43, p<0.0001, van der Lubbe et al. 2016). This is another proxy for riverine input since Ti is mainly derived from erosion of continental rocks transported to the ocean through rivers, whereas Ca derives predominantly from the marine environment.

The records of $F_{C32\ 1,15}$ and BIT index show three major variations: a steep drop from 19 to 10 ka, a slow increase from 38 to 21 ka during the Last Glacial and a steep decrease between 40 to 38 ka. The largest change in the BIT index and $F_{C32\ 1,15}$ is between 19 to 10 ka, i.e. a major drop which coincides with an interval of rapid sea level rise (Fig. 2). Following Menot et al. (2006), we explain the drop in the BIT index, and consequently also the drop in $F_{C32\ 1,15}$, by the significant sea level rise occurring during this period. Rising sea level flooded the Mozambique plateau, moving the river mouth further away from the core site and establishing more open-marine conditions. This most likely resulted in lower $F_{C32\ 1,15}$ and BIT values, conditions that remained throughout the Holocene. The decrease in the delivery of terrestrial matter is also seen in element ratios (Fe/Ca) and organic proxies (BIT) in nearby core GeoB9307-3 (Schefuß et al. 2011), which is located closer to the present day river mouth in the Mozambique plateau (Fig. 1). Likewise, the gradual increase in the

BIT index and $F_{C32\ 1,15}$ between 38 and 21 ka occurred at a time when sea-level was decreasing (Fig 2b., Grant et al. 2014; Rohling et al. 2014) and thus the river mouth came closer to our study site. The decrease of BIT values and $F_{C32\ 1,15}$ during 40-38 ka coincides with Heinrich event 4 (H4), a cold and dry event in this part of Africa (Partridge et al. 1997; Tierney et al. 2008; Thomas et al. 2009), with dry conditions likely leading to a reduced riverine input into the ocean and thus a reduced input of brGDGTs and the C_{32} 1,15-diol.

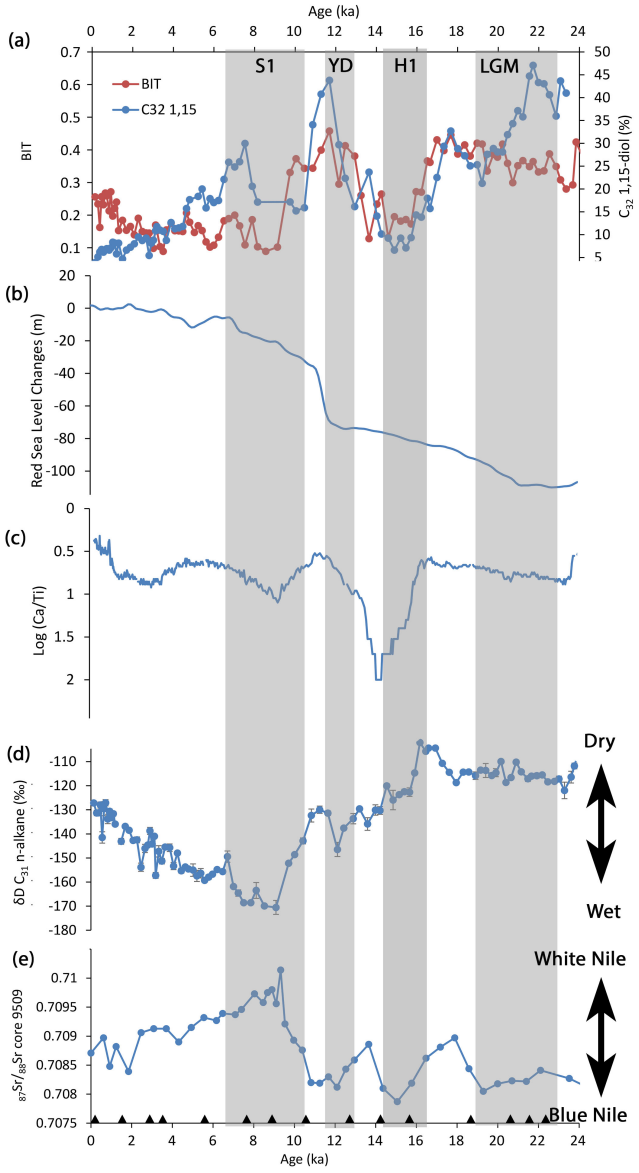

Figure 4: Organic and lithologic proxy records for core GeoB7702-3 and core 9509. (a) BIT index indicating soil and riverine input (Castaneda et al. 2010) and $F_{C32\ 1,15}$ tracing riverine input (b) Red Sea Level changes (Grant et al. 2014) (c) log(Ca/Ti) indicating terrestrial input (Castaneda et al. 2016), (d) reconstruction of δD precipitation based on leaf wax n-C_{31} alkane (Castaneda et al. 2016), (e) $^{87}Sr/^{86}Sr$ signatures of the sediment core 9509 (offshore the Israeli coast) document changes in riverine influence (Box et al. 2011). The grey bars show the sapropel layer (S1), Younger Dryas (YD), Heinrich event 1 (H1) and the Last Glacial Maximum (LGM). Black triangles indicate ^{14}C AMS dates (from Castaneda et al. 2010).

Interestingly, there are two periods where BIT and $F_{C32\ 1,15}$ records diverge (Fig. 2): during the Younger Dryas (YD; 12.7-11.6 ka) and Heinrich event 1 (H1; 17-14.6 ka) with the BIT index decreasing ca. 1 ky later than $F_{C32\ 1,15}$. Comparison with the Ca/Ti ratio shows that both during H1 and the YD, the Ca/Ti ratio increased at the same time as the C_{32} 1,15-diol but earlier than the BIT index, suggesting that the latter was influenced by other parameters. The BIT index is the ratio of brGDGTs (produced mostly in soil or in-situ in rivers in this area

based on the low values for #ring tetra; Sinninghe Damsté 2016) over crenarchaeol (produced mainly in marine environment; Schouten et al. 2013 and references cited therein). As both the Ti/Ca ratio and $F_{C32\ 1,15}$ indicate a decrease in riverine input, a constant BIT index can be explained by two options: a simultaneous decrease in crenarchaeol (marine) production or a change in soil input with higher brGDGT concentrations eroding into the river. The concentration of crenarchaeol during H1 is relatively stable but there is a slight decrease of crenarchaeol during YD (Supplementary fig. 2). Thus, the difference between BIT and $F_{C32\ 1,15}$ during YD can be partly explained by decreased crenarchaeol production together with a decrease in branched GDGTs due to a reduced river flow leading to relatively stable BIT values. In contrast, crenarchaeol and brGDGT concentrations are relatively stable during H1 and thus the lower river input, as indicated by the Ca/Ti and $F_{C32\ 1,15}$, apparently did not lead to a decrease in brGDGT input. This could be due to a shift of sources of soil which are eroded in the river, i.e. if in this period there is a shift towards soils with relatively higher brGDGT concentrations, the BIT index would remain high despite decreased river flow.

A shift in soil sources may be due to two major changes that happened during this period (and also during the YD), i.e. a shift in catchment area of the Zambezi River (Schefuß et al. 2011; Just et al. 2014) and a shift in the relative influence of the Zambezi River versus northern Mozambique rivers (van der Lubbe et al. 2016). The shift in catchment area is evident from the higher influx of kaolinite-poor soil into the marine system during H1 and YD (Just et al. 2014) coming from the Cover Sands of the coastal Mozambique area (Fig. 3, blue circle), relative to the kaolinite-rich soils of the hinterlands (Fig. 3, red circles). If the brGDGT concentrations from the latter region are higher, then this change of soil input could lead to a stable brGDGT flux into the marine environment, despite decreasing Zambezi River runoff. Support for a shift in soil sources comes from the soil pH record reconstructed from brGDGTs, which during the YD shows a shift towards more acidic soils. However, no change in soil pH are observed during H1.

The relative influence of other rivers (Lurio, Rovuma Rivers) relative to the Zambezi River (Fig. 3 green circle) was inferred from neodymium isotopes by van der Lubbe et al. (2016), i.e. more radiogenic rocks are found in the northern river catchments in comparison to the rocks in the Zambezi catchment (Fig. 2). These authors found that during H1 and YD, the relative contribution of the northern rivers is lower than normal, likely due to drought conditions north of the Zambezi catchment area (Tierney et al. 2008, 2011; Just et al. 2014). These northern rivers run through a catchment containing mainly humid highstand soils, which are different soil types than observed in the catchment area of the Zambezi River (van der Lubbe et al. 2016). We hypothesize that higher brGDGT concentrations in the soils of the catchment areas of the Zambezi River can potentially explain the discrepancy between BIT and $F_{C32\ 1,15}$, i.e. during H1 and YD there is more input of brGDGT-rich soils from the Zambezi than brGDGT-poor soils from the northern rivers leading to constant BIT values despite a dropping riverine input. Further research examining the brGDGT contents of soils in the different river catchment areas as well as surface sediments from offshore these northern rivers is required to distinguish between the different hypotheses.

4.3 Past variations in riverine input in the Eastern Mediterranean Sea

With the Eastern Mediterranean Sea core, we compared $F_{C32\ 1,15}$ in core GeoB7702 with other proxies including the BIT index, log (Ca/Ti) and strontium isotopes, the latter to infer the relative importance of the Blue Nile and the White Nile as source regions (Fig. 4). The BIT values (data from Castaneda et al. 2010) show a significant positive correlation with $F_{C32\ 1,15}$ (r^2 = 0.38, p<0.05), while log (Ca/Ti) shows an negative correlation to $F_{C32\ 1,15}$, again supporting a continental origin of the C_{32} 1,15-diol. $F_{C32\ 1,15}$ and BIT records show much lower Holocene values (12 ± 6 %) compared to pre-Holocene (27 ± 11 %), which again can be attributed to the sea level rise occurring during the last deglaciation, i.e. our study site was further away from the river mouth and the amount of continental-derived OM reaching the site decreased. Both records show low values during H1 comparable to the Holocene. These low values can be attributed to extreme aridity in the Nile River catchment (Castaneda et al. 2016), which we hypothesize led to a lack of vegetation and enhanced soil erosion but also leading to a severely reduced river flow, thereby decreasing the net amount of river borne OM reaching our core site.

In this core, there are 3 major discrepancies observed between the BIT index and $F_{C32\ 1,15}$: (1) during the LGM, between 22-19 ka, where the C_{32} 1,15-diol shows a decrease while the BIT index remains constant, (2) during the onset of the deposition of S1 (6.1-10.5 ka, Grant et al., 2016) where the BIT index decreases later than the C_{32} 1,15-diol, and (3) after 2 ka when the BIT index increases while the C_{32} 1,15-diol decreases. For

the LGM $F_{C32\ 1,15}$ is decreasing, log (Ca/Ti) is as well, but the BIT index remains constant (and the brGDGT concentration is also low; see supplementary fig. 3) indicating that there is no significant decrease in terrigenous OM reaching the core site at that time. During the LGM, there is no significant change in continental climate, based on the findings of Castaneda et al. (2016), suggesting no change in vegetation cover or river flux. This suggests that the change in $F_{C32\ 1,15}$ is not due to a change in the input of C_{32} 1,15-diol but in other, mainly marine derived, diols, in particular the C_{30} 1,15-diol. If this hypothesis is true then an increase in this marine diol will lower the $F_{C32\ 1,15}$ but if the amount of crenarchaeol is not changing at the same time, the BIT values will remain unaffected.

The deposition of S1 is described as a period of increased freshwater input leading to stratification and anoxia (Rossignol-Strick et al. 1982). However, an increased river input is neither reflected in $F_{C32\ 1,15}$ nor in the BIT index, in fact both of them are asynchronously decreasing. Castaneda et al. (2010) showed that the decrease in the BIT index is due to a large increase in crenarchaeol (Supplementary fig. 3), much larger than the increase in brGDGTs, due to increased productivity and preservation. A similar scenario may apply for the diols, i.e. the marine diols (in particular the C_{30} 1,15-diol, data not shown) are also increasing at that time more substantially than the C_{32} 1,15-diol, thus lowering $F_{C32\ 1,15}$. However, there is a difference in timing, i.e. the BIT index decreases slightly later than the C_{32} 1,15-diol (9.1 and 10.5 ka, respectively). The decrease in $F_{C32\ 1,15}$ coincides with a substantial increase in sea level (Fig. 4), which would cause the distance between the core site and the river mouth to increase, thereby decreasing the amount of terrigenous material reaching the site. This terrigenous decrease is also visible to some extent in the log (Ca/Ti) but not in the BIT index. Possibly, like with the Mozambique Channel, the brGDGT concentrations in the river were much higher at that time. Indeed, the Sr isotopic record suggest a major shift from a Blue Nile to a White Nile source at 10.5 ka, with the latter possibly containing more eroded soils with high brGDGT concentrations. This shift in soil sources is also shown in the change towards more acidic soil pH during that period based on the CBT index (Supplementary fig. 1).

For the most recent part of the record (0-5 ka), the BIT index increases, while $F_{C32\ 1,15}$ is slightly decreasing. The $\delta D_{leafwaxes}$ (Fig. 4) shows it was period of mild aridity which likely led to a decreased riverine runoff and thus decreased river input. The reason the BIT index is increasing rather than decreasing is due to an increase in brGDGT concentrations (Fig. 3), despite evidence for a decrease in river runoff. This can possibly be linked to the amount of vegetation in the Nile catchment, i.e. at that time there was a decrease in vegetation cover (Blanchet et al. 2014; Castaneda et al. 2016), which led to more soil erosion and thus potentially a higher brGDGT concentration in rivers and a higher BIT index. This hypothesis is supported by the log (Ca/Ti) (Fig. 4), which is decreasing at this time, suggesting that soil runoff was increasing.

Our results from both the Nile and Mozambique Channel cores illustrate that $F_{C32\ 1,15}$ provides a suitable proxy for reconstructing past riverine input into coastal seas. Although some discrepancies are noted with other terrigenous proxies for both cores, $F_{C32\ 1,15}$ generally agrees well with these proxies. However, our interpretation of the C_{32} 1,15-diol record relies on the assumption that production of this diol in rivers is not changing with different hydroclimate fluctuations on land, something that needs to be tested. However, de Bar et al. (2016) showed that $F_{C32\ 1,15}$ in the Tagus River in Portugal did not significantly change over the course of a year, suggesting that this assumption might be valid. Since the C_{32} 1,15-diol is mainly produced in rivers itself, it is not impacted by vegetation abundance and soil composition, in contrast to other proxies like the BIT index and lignin concentrations. This may make it a potentially more reliable proxy to trace past river input into marine environments.

Conclusion

We studied core-tops in the Mozambique Channel and two sediment cores, in the Mozambique Channel, off the Zambezi River mouth and in the Eastern Mediterranean Sea, offshore the Nile delta, to test $F_{C32\ 1,15}$ as a proxy for riverine input into the marine realm. The surface sediments show that the C_{32} 1,15-diol traces present day riverine input into the Mozambique Channel, supported by the BIT index. In both sediment records, $F_{C32\ 1,15}$ is significantly correlated with the BIT index showing the applicability of this proxy to trace riverine input, but also showed some discrepancies. This can be explained by the different sources of these proxies, i.e. the BIT index is reflecting soil and river-produced OM input and the C_{32} 1,15-diol is mainly reflecting river-produced OM input. Our multiproxy approach suggests that the timing of changes in the different terrestrial proxies

records can differ due to changes in catchment area or to shifting importance of the different source rivers.

Author contribution

S. S. and J. L. designed the study. J. Lattaud analyzed the surface sediments for diols and GDGTs and core GeoB 7702-3 for diols, I. C. sampled and extracted the surface sediments and the sediment cores 64PE304-80 and GeoB 7702-3, D. D. analyzed the sediment core 64PE304-80 for diols. H. S. collected the VA core-tops, E.S. collected core GeoB7702-3. J. L., S. S., I. C. and J.S.S.D. interpreted the data. J. L. wrote the manuscript with input of all authors.

The authors declare that they have no conflict of interest.

Acknowledgement

We thank Anchelique Mets and Jort Ossebaar for analytical help. This research has been funded by the European Research Council (ERC) under the European Union's Seventh Framework Program (FP7/2007-2013) ERC grant agreement [339206] to S.S. J.S.S.D. and S.S. received financial support from the Netherlands Earth System Science Centre and this work was in part carried out under the program of the Netherlands Earth System Science Centre (NESSC), financially supported by the Ministry of Education, Culture and Science (OCW). Sample material of core GeoB7702-3 has been provided by the GeoB Core Repository at the MARUM – Center for Marine Environmental Sciences, University of Bremen, Germany. The data reported in this paper are archived in Pangaea (www.pangaea.de).

Supplements

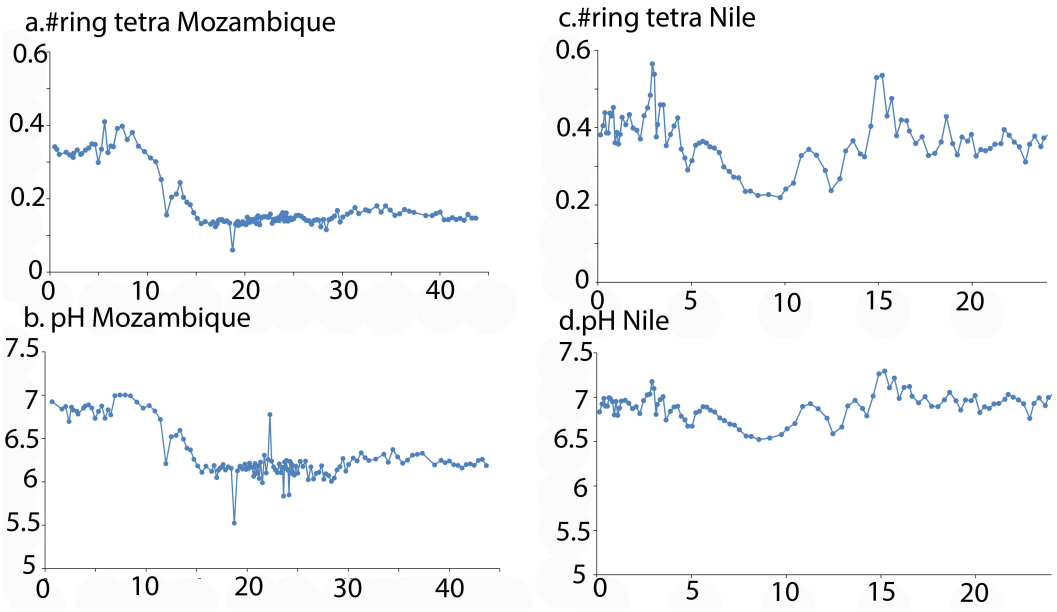

Figure 1: (a) #ring tetra of core 64PE304-80, (b) reconstructed pH of core 64PE304-80, (c) #ring tetra of core Geob7702-3 and (d) reconstructed pH of core GeoB7702-3.

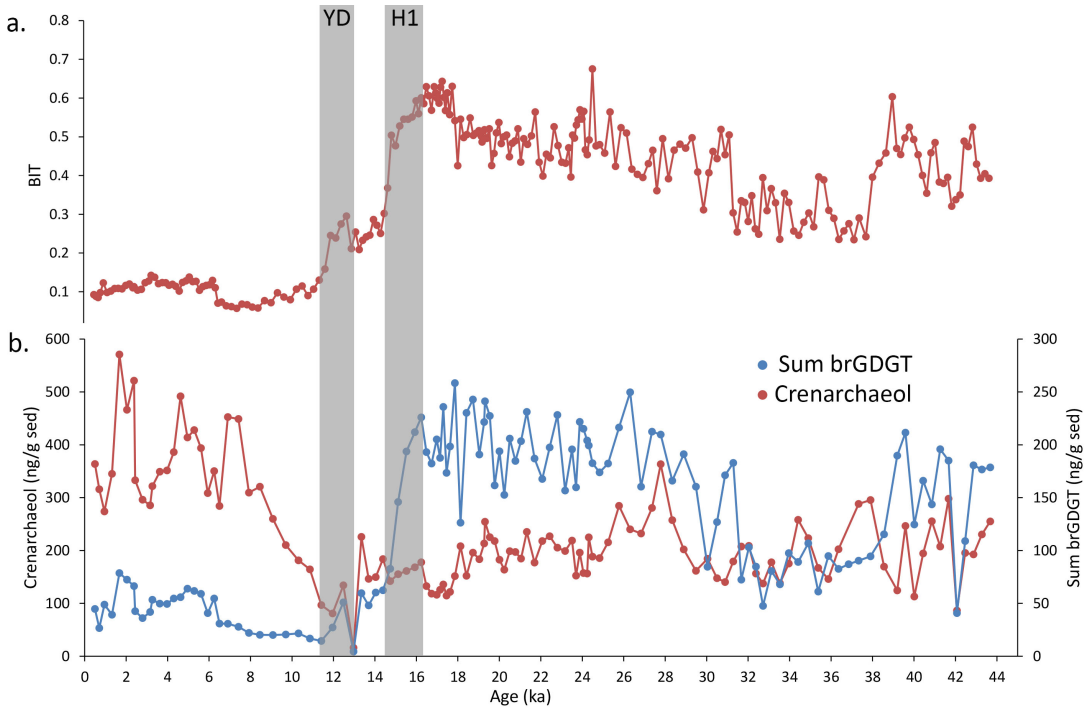

Figure 2: (a) BIT index of core 64PE304-60 (from Kasper et al. 2015) and (b) Crenarchaeol and brGDGT concentration in core 64PE304-60.

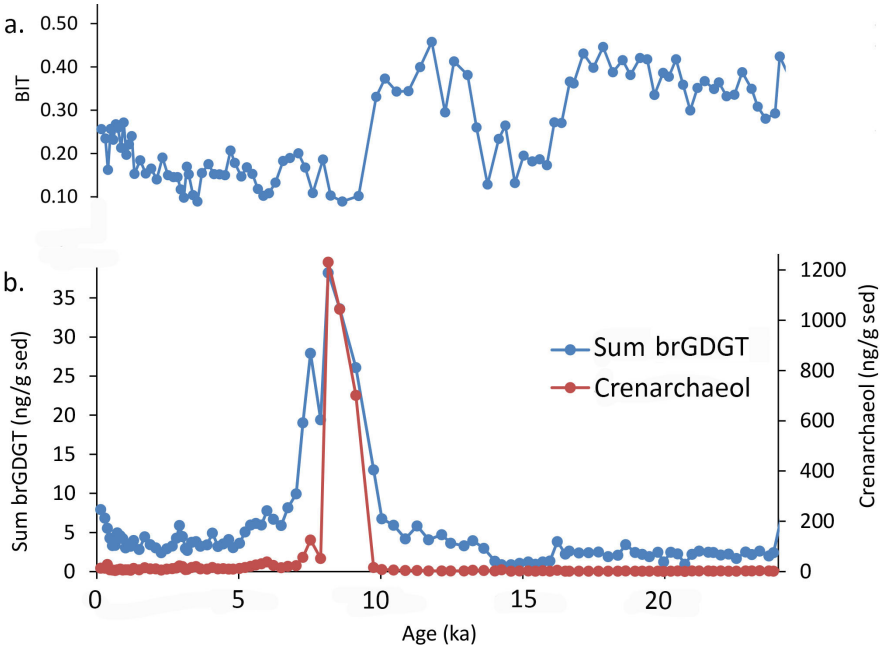

Figure 3: (a) BIT index if core GeoB7702-3 (from Castaneda et al. 2010) and (b) Crenarchaeol and brGDGT concentration in core GeoB7702-3.

Chapter 7

A comparison of Late Quaternary organic proxy-based paleotemperature records of the central Sea of Okhotsk

Paleoceanography Paleoclimatology, 33 (7), 732-744 (2018)

Julie Lattaud [a,*], Li Lo[b,c], Jyh-Jaan Huang[d,1], Yu-Min Chou[e], Sergey A. Gorbarenko[f], Jaap S. Sinninghe Damsté[a,g], Stefan Schouten[a,g]

[a] NIOZ, Royal Netherlands Institute for Sea Research, Department of Marine Microbiology and Biogeochemistry (MMB), and Utrecht University, PO Box 59, 1790 AB Den Burg, The Netherlands
[b] State Key Laboratory of Isotope Geochemistry, Guangzhou Institute of Geochemistry, Chinese Academy of Sciences, China
[c] Department of Earth Sciences, University of Cambridge, UK
[d] Department of Geosciences, National Taiwan University, Taiwan
[e] Department of Ocean Sciences and Engineering, Southern University of Science and Technology, China
[f] V.I. Il'ichev Pacific Oceanological Institute, Far East Branch Russian Academy of Science, Vladivostok 690041, Russia
[g] Utrecht University, Department of Earth Sciences, Faculty of Geosciences, Department of Earth Sciences, Princetonlaan 8A, 3584 CB Utrecht, The Netherlands

*Corresponding author.
E-mail address: Julie.lattaud@nioz.nl (J. Lattaud).
[1] Current address: Institute of Geology, University of Innsbruck, Austria
https://doi.org/10.1029/2018PA003388

Abstract

The long-chain diol index (LDI) is a new organic sea surface temperature (SST) proxy based on the distribution of long-chain diols. It has been applied in several environments but not yet in subpolar regions. Here, we tested the LDI on surface sediments and a sediment core from the Sea of Okhotsk, which is the southernmost seasonal sea ice covered region in the Northern Hemisphere, and compared it with other organic temperature proxies, i.e. $U^{k'}_{37}$ and TEX^{L}_{86}. In the surface sediments, the LDI is correlated with autumn sea surface temperature, similar to the $U^{k'}_{37}$ but different from the TEX^{L}_{86} that correlates best with summer sea subsurface temperature. Remarkably, the obtained local LDI calibration was significantly different from the global core-top calibration. We used the local LDI calibration to reconstruct past SST changes in the central Sea of Okhotsk. The LDI-SST record shows low glacial (Marine Isotope Stage, MIS 2, 4, 6) and high interglacial (MIS 1 and MIS 5) temperatures and follows the same pattern as the $U^{k'}_{37}$-SST and a previously published TEX^{L}_{86} temperature record. Similar to the modern situation, the reconstructed temperatures during the interglacials likely reflect different seasons, i.e. summer for the TEX^{L}_{86} and autumn for $U^{k'}_{37}$ and LDI. During glacials, the reconstructed temperatures of all three proxies are similar to each other, likely reflecting summer temperatures as this was the only season free of sea ice. Our results suggest that the LDI is a suitable proxy to reconstruct subpolar sea water temperatures.

Keywords: *LDI, TEX_{86}, $U^{k'}_{37}$, Sea of Okhotsk*

1 Introduction

Several organic proxies have been developed to reconstruct past sea surface temperatures (SST) in the geological record. The first organic SST proxy that was developed is the unsaturated ketone index ($U^{k'}_{37}$), based on alkenone lipids synthesized by haptophyte algae (Brassell et al. 1986; Prahl and Wakeham 1987). Culture studies showed that haptophyte algae adjust the degree of unsaturation of alkenones in response to growth temperature, with increased fractional abundances of the tri-unsaturated alkenone at lower temperatures. Subsequent work on surface sediments revealed that the $U^{k'}_{37}$ index is strongly related to annual mean SST (Prahl et al. 1988; Müller et al. 1998). Another organic paleothermometer, the tetraether index (TEX_{86}), uses Thaumarchaeotal membrane lipids, i.e. glyceryl dibiphytanyl glycerol tetraether lipids (GDGTs) (Schouten et al. 2002). These Archaea synthesize GDGTs with an increasing number of cyclopentane moieties when sea water temperatures are higher and the TEX_{86}, is strongly correlated with annual mean SST in global core top data sets (Kim et al. 2010, 2015; Tierney and Tingley 2015). However, both the $U^{k'}_{37}$ and TEX_{86}, proxies have their limitations. For example, the $U^{k'}_{37}$ might be affected by nutrient availability, lateral transport, or oxic degradation (e.g. Hoefs et al. 1998; Gong and Hollander 1999; Prahl et al. 2003; Sikes et al. 2005; Kim et al. 2009; Rontani et al. 2013) and the TEX_{86}, by subsurface production of GDGTs and input of terrestrial GDGTs (e.g. Weijers et al. 2006; Huguet et al. 2007; Shintani et al. 2011; Ho et al. 2014; Kim et al. 2015). Furthermore, studies comparing $U^{k'}_{37}$ and TEX_{86}, show that they can reflect temperatures of different seasons of production and not annual mean temperature (Huguet et al. 2006; dos Santos et al. 2013; Smith et al. 2013; Jonas et al. 2017).

Recently, a new SST proxy, the Long chain Diol Index (LDI), was developed based on the distribution of long chain diols (LCDs; Rampen et al. 2012), i.e. the ratio of the C_{30} 1,15-diol over the sum of C_{28} 1,13-, C_{30} 1,13- and C_{30} 1,15-diols, with higher fractional abundances of 1,15-diol observed at higher temperatures. The LDI seems to be independent from salinity, but is impacted by freshwater input (de Bar et al. 2016; Lattaud et al. 2017b) and oxic degradation (Rodrigo-Gámiz et al. 2016). Nevertheless, the reconstruction of past SST using the LDI has been successful in various marine environments, predominantly in temperate regions (Naafs et al. 2012; Rampen et al. 2012; Smith et al. 2013; Rodrigo-Gámiz et al. 2014; Plancq et al. 2015; Jonas et al. 2017). However, the LDI has, up to now, never been applied in subpolar regions. Rodrigo-Gámiz et al. (2015) tested the application of the LDI in the North Atlantic Ocean, around Iceland, but the large amount of 1,14-diols (>80% of all long-chain diols), derived from *Proboscia* diatoms (Sinninghe Damsté et al. 2003; Rampen et al. 2007) obscured the LDI dependence to SST since *Proboscia* diatoms also produce minor amounts of 1,13-diols (Rampen et al. 2007), biasing the LDI towards colder SST.

Here, we tested the applicability of the LDI in the Sea of Okhotsk. We generated high-resolution records of LDI-derived and $U^{k'}_{37}$ -derived SST for the past 180 ka from the central Sea of Okhotsk and compared this to a previously generated TEX_{86}-derived SST record (Lo et al. 2018). Furthermore, we also determined whether in the present-day environment the LDI, $U^{k'}_{37}$ and TEX_{86} are reflecting annual mean or seasonal temperatures by analyzing a set of surface sediments from the Sea of Okhotsk.

2 Setting

2.1 Study site

The Sea of Okhotsk is part of the Western Pacific Ocean and represents both the lowest-latitude and largest region with seasonal sea ice in the world (Harada et al. 2014). It is the second largest marginal subpolar sea of the Pacific after the Bering Sea. At present, in the Sea of Okhotsk, sea ice forms in the northwestern coastal area in November. Its maximum elongation goes as far south as northern Hokkaido, Japan, in March and disappears by June (Shimada and Hasegawa 2001). The Sea of Okhotsk has many characteristics of a polar ocean: severe winters with cold air and strong northern winds, mild but short summers, large seasonal variation of air and water temperatures, and a subarctic water column structure (Wakatsuchi and Martin 1991). The modern SST ranges from 13°C in summer to -1°C in winter (Fig. 1b). According to Harada et al. (2014), autumn SST, sea surface salinity and sea ice extent all impact the intensity of downwelling in the Sea of Okhotsk and, subsequently, control the formation of the Sea of Okhotsk Intermediate Water, which is a key component of the North Pacific Intermediate Water (itself an important carbon reservoir; Tsunogai et al. 1993). The Amur River in the northwest releases freshwater into the Sea of Okhotsk but most of its detrital loading does not reach the central part of the Sea of Okhotsk because the material is transported further to the south by lateral currents present in the Sea of Okhotsk (Yasuda et al. 2014).

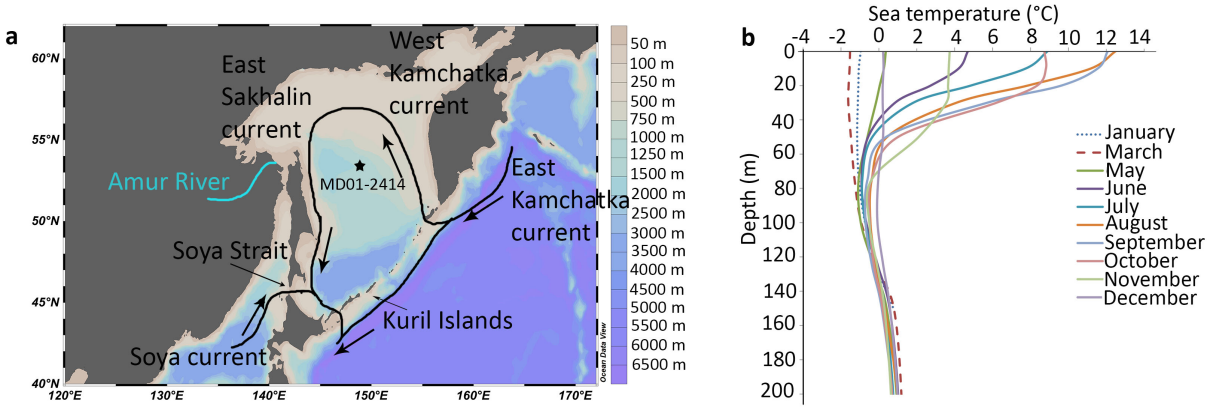

Figure 1: (a) Oceanographic setting of the Sea of Okhotsk and the location of core MD01 2414 and (b) monthly sea temperature (from NOAA, Locarnini et al. 2009) at this site.

2.2 Previous paleoceanographic studies

Several paleoceanographic studies on the Sea of Okhotsk have been performed. For example, Gorbarenko (1996), (2014) reconstructed periods of rapid warming and cooling during the Holocene and late Pleistocene, synchronous with the Greenland climatic cycles (glacial and interglacial stages as well as Heinrich events). SST reconstructions have been performed for the Holocene and the last glacial-interglacial interval using the $\delta^{18}O$ of planktonic foraminifera (Gorbarenko 1996), as well as the TEX_{86} (Harada et al., 2012; Seki et al., 2009, 2014; Lo et al., 2018) and $U^{k'}_{37}$ (Harada et al. 2004, 2006, 2014; Seki et al. 2004b) temperature proxies. The reconstructed temperatures range from 5-7°C to 8-12°C for the TEX_{86} and from 4-7°C to 8-12°C for the $U^{k'}_{37}$ for the last glacial maximum and the Holocene, respectively. These studies indicate that the alkenone and GDGT records reflect temperatures of different seasons, with the TEX_{86}-derived temperatures representing summer

subsurface temperature (Seki et al. 2009, 2014a; Lo et al. 2018) and the $U^{k'}_{37}$-derived temperatures representing autumn SST (Seki et al. 2007).

3 Material et methods

3.1 Sampling and age model

Giant piston core MD01-2414 (53°11.77'N, 149°34.80'E; Fig. 1) was collected during the IMAGES VII cruise from the central region of the Sea of Okhotsk (Deyugin basin) at a water depth of 1123 m in 2001 (Chou et al. 2011). This core has a length of 52.76 m but here we studied the upper 900 cm. This section was sampled every 10 cm, and the samples were stored frozen until freeze-dried. An age model for the core was established by Lo et al. (2018) based on the correlation of XRF data (log-ratios of (Ba/Ti)) with the global benthic foraminiferal δ^{18}O stack (LR04, Lisiecki and Raymo 2005) and 5 accelerator mass spectrometry radiocarbon (AMS ^{14}C) dates of picked planktonic foraminifera (*Neogloboquadrina pachyderma, sinistral*).

Thirteen surface sediments were collected from the Sea of Okhotsk as described by Lo et al. (2018) (Fig. 1).

3.2 Extraction and separation of lipids

The sediments were previously extracted by Lo et al. (2018). Briefly, sediment samples (1–10 g) were homogenized, freeze-dried and extracted using dichloromethane (DCM) : methanol (4 : 1 v/v) using an Accelerated Solvent Extractor (ASE). The extracts were separated into three fractions on a Pasteur pipette packed with activated Al_2O_3: an apolar fraction (hexane : DCM, 9:1 v/v), a ketone fraction (hexane : DCM, 1:1 v/v) containing alkenones, and a polar fraction containing the GDGTs and diols (DCM : MeOH, 1:1 v/v).

3.3 Alkenone analysis and determination of $U^{k'}_{37}$

Sedimentary alkenones were analyzed by dissolving the ketone fraction into 100 µL of hexane and using capillary gas chromatography (GC) with an Agilent 6890N GC equipped with a silica column coated with CP Sil-5 (50 m x 320 µm; film thickness 0.12 µm), equipped with an on-column injector. The initial oven temperature of 70°C increased with 20°C/min to 200°C and subsequently with 3 °C/min to 320°C, at which it was held for 25 min. The carrier gas was helium at constant flow at 30 mL/min. Alkenones were detected with a Flame Ionization Detector (FID) held at 330°C.

The alkenone unsaturation index $U^{k'}_{37}$ (Prahl and Wakeham 1987) was calculated as follows:

$$U^{k'}_{37} = \frac{[C_{37:2}]}{[C_{37:2}] + [C_{37:3}]} \tag{1}$$

Several correlations between $U^{k'}_{37}$ and water temperature have been reported (Prahl and Wakeham 1987; Prahl et al. 1988; Sikes et al. 1997; Müller et al. 1998). The most often used global calibration of $U^{k'}_{37}$ against annual mean SST is that of Müller et al. (1998)):

$$SST = \frac{U^{k'}_{37} - 0.044}{0.033} \tag{2}$$

We applied the Bayspline calibration from Tierney and Tingley (2018) but no remarkable difference in absolute temperatures or trends with the calibration of Müller et al. (1998) was observed (maximum 0.7°C).

3.4 LCD analysis and determination of LDI

LCDs were analyzed by silylation of an aliquot of the polar fraction with 10 µL BSTFA and 10 µL pyridine, heated for 30 min at 60°C and adding 30 µL of ethyl acetate. The analysis of diols was performed using a gas chromatograph (Agilent 7990B GC), equipped with a capillary silica column coated with CP Sil 5 (25 m x 0.32 mm; film thickness 0.12 µm) and coupled with a mass spectrometer (Agilent 5977A MSD; GC-MS). Oven temperature during injection was 70°C and increased thereafter to 130°C at 20°C/min and to 320°C at 20°C/min, at which it was maintained for 25 min. The flow of the carrier gas was held constant at 2 mL/min.

The MS source was held at 25°C and the MS quadrupole at 150°C. The electron impact ionization energy of the source was 70 eV. The LCDs were identified and quantified via SIM (Single Ion Monitoring) of the fragment ions m/z 299.3 (C_{28} 1,14-diol), 313.3 (C_{28} 1,13-diol; C_{30} 1,15-diol), 327.3 (C_{30} 1,14-diol) and 341.3 (C_{30} 1,13-diol; C_{32} 1,15-diol) following Versteegh et al. (1997) and Rampen et al. (2012). The abundance of the LCDs are expressed as fraction of the total LCDs quantified.

The Long-chain Diol Index (LDI) is the ratio of C_{30} 1,15-diol over the sum of C_{30} + C_{28} 1,13-diols as defined by Rampen et al. (2012):

$$LDI = \frac{[C_{30}1,15]}{[C_{30}1,15] + [C_{30}1,13] + [C_{28}1,13]} \tag{3}$$

The global calibration of LDI against annual mean SST (Rampen et al. 2012) is as follows:

$$SST = 0.033 \times LDI + 0.095 \tag{4}$$

3.5 GDGT analysis and determination of TEX_{86}

TEX_{86} (equation 5, Schouten et al. (2002) values of the surface sediments and of the sediment core between 0-130 ka have been previously reported by Lo et al. (2018). Here we extended this record to 180 ka by analyzing 20 additional sediment samples for GDGTs following the methods described by Lo et al. (2018).

$$TEX_{86} = \frac{GDGT-2 + GDGT-3 + Cren'}{GDGT-1 + GDGT-2 + GDGT-3 + Cren'} \tag{5}$$

A global calibration of the TEX_{86}^{L}, more suited for polar oceans, has been reported by Kim et al. (2010):

$$TEX_{86}^{L} = \log(\frac{GDGT-2}{GDGT-1 + GDGT-2 + GDGT-3}) \tag{6}$$

$$TEX_{86}^{L} - SST = 67.5 \times TEX_{86}^{L} + 46.9 \tag{7}$$

The Branched versus Isoprenoid Tetraether index (BIT) was calculated as described by Hopmans et al. 2004, (Hopmans et al. 2016) with the inclusion of the 6-methyl branched GDGT from Jonge et al. (2013) to infer if the GDGTs in the sediment core and surface sediments were affected by terrigenous input from the Amur River.

$$BIT = \frac{Ia + IIa + IIIa + IIa' + IIIa'}{Ia + IIa + IIIa + IIa' + IIIa' + IV} \tag{8}$$

4 Results and discussion

4.1 Proxy calibration

In all surface sediments alkenones, GDGTs and LCDs were detected. The $U_{37}^{k'}$ ranges from 0.05 to 0.39, while the LDI varies from 0.02 to 0.44 (Fig. 2). The TEX_{86} has previously been reported to vary from 0.18 to 0.34 (Lo et al. 2018). The BIT index is low in all surface sediments (0.02-0.12, Fig. 5) indicating relatively little input of terrestrial organic matter in these surface sediments (Hopmans et al. 2004; Weijers et al. 2006, 2009; Jonge et al. 2014b). The fractional abundance of the C_{32} 1,15-diol varies between 0.03 and 0.32 (Fig. 5), with higher fractional abundances close to the Soya Strait (0.20-0.32) compared to the northern and central part of the Sea of Okhotsk (0.03-0.10). This indicates input of riverine organic matter to the southern part of the Sea of Okhotsk but shows that the northern and central part of the Sea of Okhotsk are not influenced by riverine organic matter (cf. Lattaud et al. 2017b).

To determine if each proxies are reflecting seasonal or annual temperatures in modern days in the Sea of Okhotsk we correlated the values of $U_{37}^{k'}$, LDI and the TEX_{86}^{L} from 13 surface sediments (Fig. 2) with annual mean and seasonal SSTs (World Ocean Database 2009, Locarnini et al. 2009).

The $U_{37}^{k'}$ values are only weakly correlated with annual mean SST (Fig. 3, r^2 = 0.24, p = 0.08, n = 13) but the correlation obtained ($U_{37}^{k'}$ = 0.039 x SST + 0.0733) is statistically identical (homogeneity of slope, p = 0.98) to the global calibration of Müller et al. (1998) (eq. 2; Fig. 3). Indeed, the global calibration (Eq. 2) has

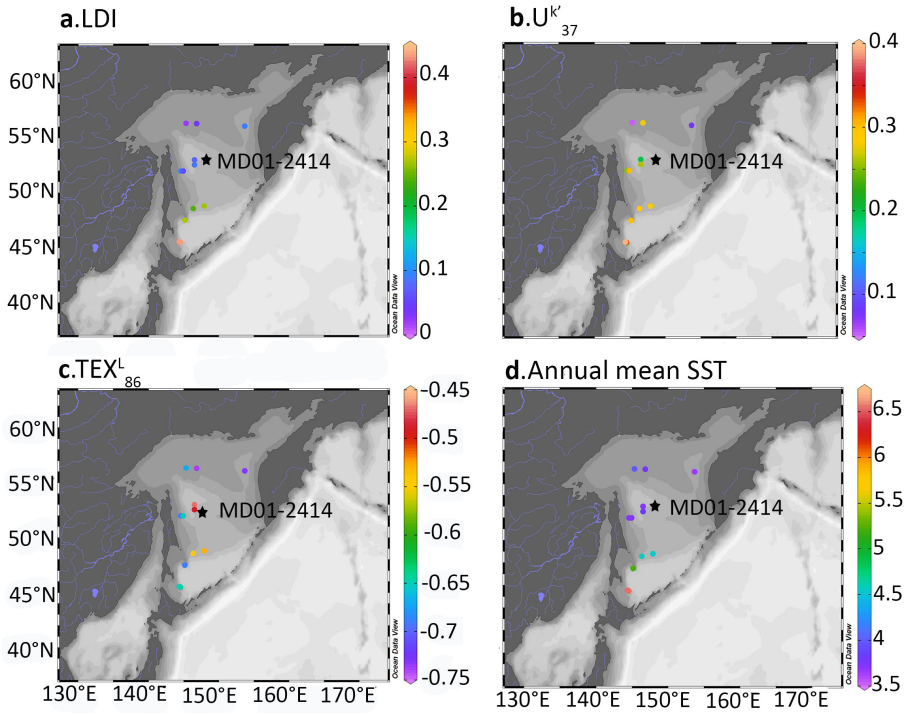

Figure 2: Geographical distribution of the values for (a) LDI, (b) $U^{k'}_{37}$, and (c) TEX^{L}_{86} of surface sediments and of (d) annual mean temperature (from NOAA, Locarnini et al. 2009).

been shown to be suitable for estimating past temperatures in the subarctic region of the North Pacific, where *Emiliana huxleyi* is the main alkenone producer (Broerse et al. 2000) and has been applied earlier in the Sea of Okhotsk (Harada et al. 2004, 2006). However, *E. huxleyi* has been reported to bloom in autumn (late November to early December) in the Sea of Okhotsk (Broerse et al. 2000). Moreover, Seki et al. (2007) reported peak fluxes of alkenones in descending particles in the water column in autumn in the central Sea of Okhotsk and showed that $U^{k'}_{37}$-derived temperature estimates from the collected sinking particles reflected autumn temperature of the shallow subsurface layer (20-30 m water depth). In the Sea of Okhotsk, autumn is a period with a strongly stratified water column and a warm and nutrient-depleted surface layer favoring the growth of *E. huxleyi* (Fig. 1). Indeed, we find a stronger correlation of the $U^{k'}_{37}$with late autumn SST (October-December, $U^{k'}_{37}$ = 0.046 x SST + 0.030, r^2 = 0.53, p<0.005, n = 13, Fig. 3) than with annual mean SST, suggesting that the $U^{k'}_{37}$, reflects autumn temperatures rather than annual mean temperature in the Sea of Okhotsk. The significance of correlation with autumn temperatures decreases with deeper water temperature (e.g. 50 m, r^2 = 0.29, p = 0.06, n = 13; Fig. 3), suggesting that $U^{k'}_{37}$reflects autumn SST in the Sea of Okhotsk. There is no significant (p=0.95) difference between the global calibration of Müller et al. (1998) (equation 2) and the local autumn SST calibration. Furthermore, because the global calibration of Müller et al. (1998) is statistically more robust (n = 149 for the global calibration vs n = 13 for the local calibration) we use the global calibration for reconstructing autumn SST thereby also making our study comparable with other studies (Harada et al. 2004; Seki et al. 2007).

The LDI values of the surface sediments are strongly correlated with annual mean SST (Fig. 3, LDI = 0.133 x SST - 0.416, r^2 = 0.93, p<0.005). This correlation is stronger than the correlation of $U^{k'}_{37}$ with annual mean or autumn SST. Furthermore, in contrast to the $U^{k'}_{37}$, this correlation differs significantly from the global core top calibration of Rampen et al. (2012) (homogeneity of slopes, p<0.05, Fig. 3). The LCD producers are likely phototrophic (eustigmatophyte) algae (Volkman et al. 1992, 1999; Gelin et al. 1997a; Méjanelle et al. 2003), which proliferate in the photic zone. The relative proportion of 1,14-diols is low to moderate (13-43%) so we do not expect *Proboscia* diatoms to be a major source of the 1,13-diols. As the Sea of Okhotsk is partially frozen during the year (Shimada and Hasegawa 2001), light penetration and nutrients will be limited during the winter and spring months, so it is likely that the LCDs are produced during a specific season rather than over the whole year and thus will likely reflect a seasonal rather than an annual mean signal. The LDI values are equally strongly correlated with autumn SST (Fig. 3, LDI = 0.103 x SST – 0.29, r^2 = 0.94, p<0.005) as

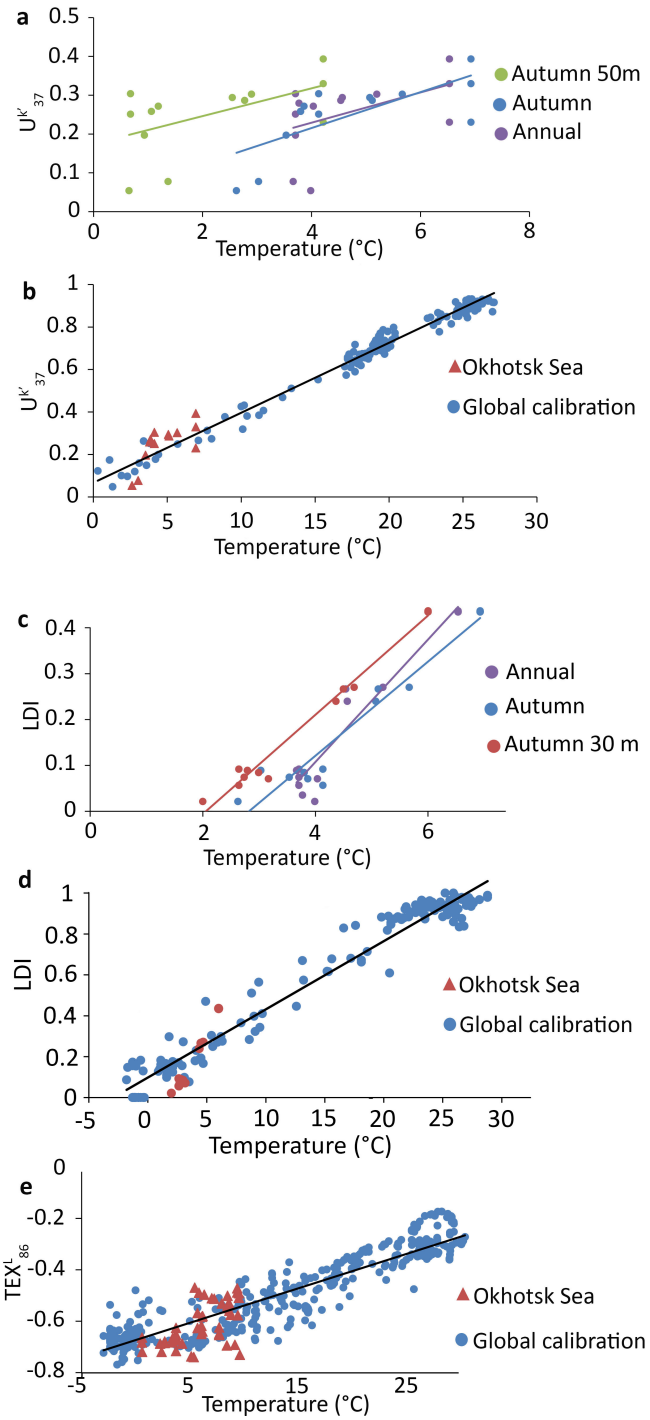

Figure 3: Correlation of observed sea temperature (from NOAA, Locarnini et al. 2009) with (a) $U^{k'}_{37}$, (b) $U^{k'}_{37}$ and the global dataset of Müller et al. (1998), (c) LDI, (d) LDI and global data set of Rampen et al. (2012) and (e) TEX^{L}_{86} including the data of Seki et al. (2014a) and the global data set of Kim et al. (2010).

with annual mean. In contrast to the $U^{k'}_{37}$, an even stronger correlation is observed with deeper water autumn temperatures, i.e. at 20 m depth (Fig. 3, LDI = 0.108 x SWT – 0.222, $r^2 = 0.98$, $p<0.005$, n = 13). However, the calibrations of the LDI for the autumn sea temperature at the surface and at 20 m are not statistically different ($p = 0.95$) and improvement of correlation coefficient is relatively small and thus it is not clear if the LDI is really reflecting SST or subsurface temperature. Based on the observation on phytoplankton dynamics in the Sea of Okhotsk, i.e. diatoms are blooming in June as soon as the sea ice melts and the water column is rich in nutrients (Seki et al. 2007), while coccolithophorids are blooming in autumn when the water column is well

stratified and nutrient-depleted (Seki et al. 2007), we assume that the LDI likely reflects autumn SST, when the competition with diatoms is less. Since the local calibration with autumn SST is significantly different from the global one we used the former to reconstruct autumn sea surface temperature (Fig. 3). This difference between the global and local calibration could be explained by the absence of Pacific surface sediments in the global calibration. Possibly, the diol producers in the Pacific Ocean might respond in their diol composition to temperature differently than those in the Atlantic Ocean.

We combined the reported TEX_{86}^{L} values of Lo et al. (2018) with those of Seki et al. (2014a) to infer if the TEX_{86}^{L} is reflecting seasonal or annual sea temperature. The TEX_{86}^{L} values correlate weakly with annual mean SST (r^2 = 0.09, p = 0.03). Seki et al. (2007) suggested that the Thaumarchaeota, producing the GDGTs, may be blooming in late summer in the Sea of Okhotsk when enhanced ammonium concentration is observed between 20 m and 45 m depth (in June 2000, Seki et al. 2014a). Since Thaumarchaeota are ammonium oxidizers (Wuchter et al. 2006; la Torre et al. 2008), this time and depth may be the optimal time to proliferate. Indeed, the TEX_{86}^{L} correlates more significantly with summer sea subsurface temperatures at 20 m depth (SST = 0.018 x TEX_{86}^{L} -0.719, r^2 = 0.33, p<0.005), while there is no significant correlation between TEX_{86}^{L} and summer SST (r^2 = 0.002, p = 0.4). There is a correlation between TEX_{86}^{L} and summer sea temperatures at 200 m depth (r^2 = 0.20, p<0.005) but this correlation is weaker than with the summer sea temperature at 20 m depth. Alternatively, instead of TEX_{86}^{L}, we can use the original TEX_{86} definition (Schouten et al. 2002). However, correlation of the TEX_{86} of the surface sediments with the annual mean SST showed a weak correlation (r^2 = 0.11, p = 0.02). We also correlated TEX_{86} with summer sea temperature at 20 m and found a weak correlation (r^2 = 0.20, p<0.005), weaker than with TEX_{86}^{L}. Therefore, it seems that TEX_{86}^{L} is best applicable for the Sea of Okhotsk. The regional calibration of TEX_{86}^{L} with summer sea temperatures at 20 m depth is not significantly different (homogeneity of slopes, p = 0.9) from the global core top calibration with annual mean SST of Kim et al. (2010) (Fig. 3). Hence, we will thus use the global calibration, which is statistically more robust, but are probably reconstructing a summer sea subsurface temperatures (around 20 m depth) signal.

4.2 Temperature variations over the last 180 ka as recorded by organic proxies

Using the global calibrations for $U_{37}^{k'}$ and TEX_{86}^{L} and the regional calibration of the LDI we reconstructed temperatures over the last 180 ka in the Sea of Okhotsk. The LDI varies from 0.06 to 0.62, the $U_{37}^{k'}$ varies from 0.07 to 0.72 and the TEX_{86}^{L} varies from -0.66 to -0.46 (TEX_{86} varies from 0.22 to 0.34). The three proxy records yield quite different absolute sea temperatures and trends (Fig. 4). Nevertheless, LDI-derived and $U_{37}^{k'}$-derived SST records show some significant correlation (r^2 = 0.13, p-value <0.005), but with considerable scatter, and both are not correlated with TEX_{86}^{L}-derived temperatures (r^2 = 0.03 and 0.04, p-value >0.05). This agrees with our findings for the surface sediments, i.e. both LDI and $U_{37}^{k'}$ are thought to reflect similar temperatures (autumn SST), while TEX_{86}^{L} reflects summer subsurface temperatures. However, a difference in seasonality cannot explain the lack of correlation between TEX_{86}^{L} and the other proxies, as we expect some correlation between seasonal temperatures. We also reconstructed temperatures using the BAYSPAR calibration (Tierney and Tingley 2015) of TEX_{86} but this yielded mostly temperatures well below 0 (-7 to 3°C), which seems unrealistic. LDI-derived SSTs also frequently differs from $U_{37}^{k'}$-derived SSTs, especially during MIS 1, 5 and MIS 6. These differences are often larger than the proxy calibration errors (2°C and 1.5°C, respectively).

A general cause for the difference in the LDI temperature record and those of the $U_{37}^{k'}$ could be input of LCDs from the Amur River as river input can affect the LDI (de Bar et al. 2016, Lattaud et al. 2017a, 2017b). The fractional abundance of C_{32} 1,15-diols (Fig. 5) in the sediment core is on average 0.33 ± 0.16, indicating some riverine input (cf. Lattaud et al. 2017b). It shows maxima at the start of Termination I and II, i.e. at the end of MIS 2 (~0.5) and MIS 6 (~0.6), likely because of the low sea level stand at that time, maximizing the influence of the Amur River. We also observe a generally higher fractional abundance of C_{32} 1,15-diols (Fig. 5) during MIS 4. However, at times of a high fractional abundance of C_{32} 1,15-diols no large variations in the LDI-SST record are observed, suggesting that river input of LCDs does not strongly affect the LDI (Fig. 6a). The record of the BIT index (Fig. 5), a proxy for input of continental derived GDGTs (Hopmans et al. 2004; Weijers et al. 2006, 2009; Jonge et al. 2014b) also peaks at the end of MIS 6 but not at the end of MIS 2. Overall, it remains <0.2 (average 0.08 ± 0.04), suggesting that application of the TEX_{86}^{L} is not affected by terrigenous input from the Amur River. Below we discuss potential causes for the difference between LDI reconstructed temperatures and those of other proxies in interglacial and glacial stages.

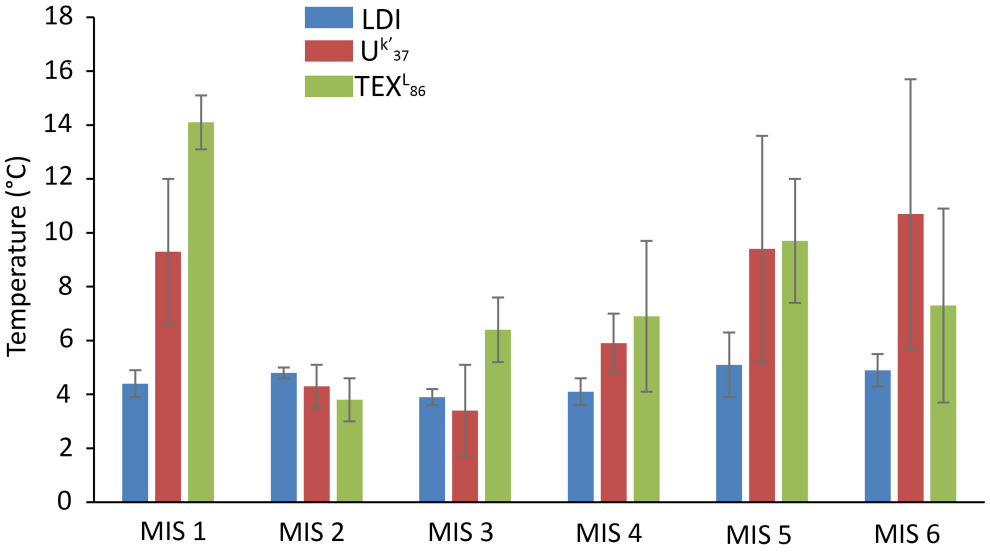

Figure 4: Average reconstructed temperature of the three paleothermometers and standard deviation during marine isotope stages (MIS 1: 0-14 ka, n = 16, MIS 2: 14-29 ka, n = 8, MIS 3: 28-57 ka, n = 8, MIS 4: 53-64 ka, n = 4, MIS 5: 64-130 ka, n = 26, MIS 6: 130-180 ka, n = 20).

4.3 Sea temperature reconstructions during interglacial stages

During the early phase of MIS 5 the LDI shows a drop in temperature from 8.8 to 3.5°C, while this drop for the $UU^{k'}_{37}$ record is from 16.0 to 2.8°C (Fig. 6a) and for the TEX^{L}_{86} record from 13.6 to 4.6°C. MIS 5e (130-115 ka, Shackleton et al. 2003; Martrat et al. 2014) is the warmest period of the LDI temperature record (6.6 ± 1.3°C), exceeding the modern day reconstructed LDI temperatures by 3°C.

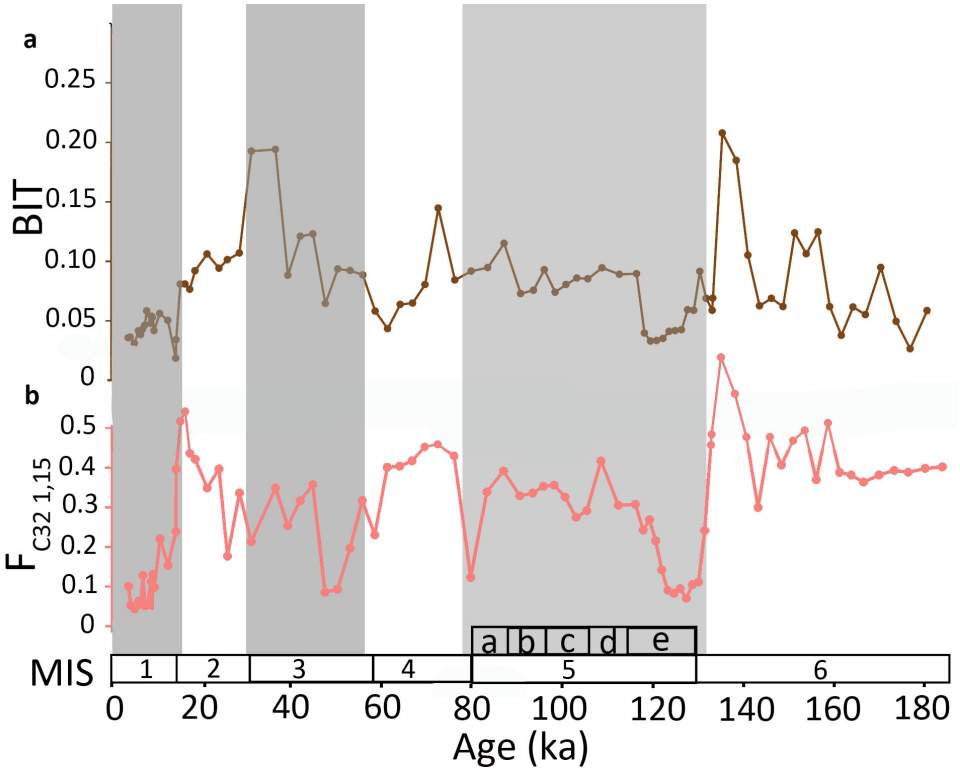

Figure 5: Terrigenous input proxies for core MD01-2414 (a) BIT index and (b) $F_{C32\ 1,15}$

During the Holocene, both $U^{k'}_{37}$ and LDI temperatures show a (sub)maximum at 9 ka, with $U^{k'}_{37}$-SST reaching 9°C, 4°C (Fig. 6) higher than LDI-SST, while TEX^{L}_{86} reflects higher temperatures from 12 ka to 9 ka (15°C). The warmest LDI and $U^{k'}_{37}$ temperature at 9 ka falls during the Holocene Thermal Maximum (9-5 ka, Ritchie et al. 1983). This warm thermal event corresponded with the maximum northern extension of the warm Kuroshio current (Tsushima Current, Kuroshio culmination event, Harada et al. (2004) and, like during MIS 5e, incurred permanent ice-free condition in the entire Sea of Okhotsk (Nürnberg et al. 2011; Lo et al. 2018). This optimum is also observed in the $U^{k'}_{37}$-SST records of Harada et al. (2004) and Martinez-Garcia et al. (2010) in the northwestern Pacific. Finally, there is a decrease of about 2°C in LDI-derived temperatures in the late Holocene until modern days, reflecting the Late Holocene cooling observed by e.g. Martrat et al. (2014) in the North Atlantic region using $U^{k'}_{37}$-derived SST reconstructions, and Russian terrestrial records (Salonen et al. 2011). This decrease is also observed in the Sea of Okhotsk and Northern Pacific records (via $U^{k'}_{37}$ by Harada et al. (2014). Overall, the LDI-derived SSTs for the late Holocene are quite low, i.e. we reconstructed the same temperatures for MIS 2 and the late Holocene. Potentially, these low temperatures could be explained by a shift in the season of production of the diols from summer (during MIS 2) towards autumn (during the Holocene). The $U^{k'}_{37}$-SST also shows a lowering of temperatures during the late Holocene but remains higher than those during MIS 2.

Although LDI and $U^{k'}_{37}$-SST records seem to match trend wise, in both interglacials MIS 1 and 5, there is a mismatch in absolute temperatures with $U^{k'}_{37}$ being generally higher than those of the LDI, while our surface sediment study suggests both could reflect autumn SST. This could be due to the enhanced presence of diol-producing diatoms, i.e. *Proboscia* (Sinninghe Damsté et al. 2003; Rampen et al. 2011) that produce 1,14-diols but also minor amounts of 1,13-diols that will biased the LDI temperatures towards colder values (Rodrigo-Gámiz et al. 2015). However, the amount of 1,14-diols is generally much lower than observed by Rodrigo-Gámiz et al. (2015) (up to 83 % in Icelandic SPM against 33 % for MIS 5 and for the Holocene in the Sea of Okhotsk), suggesting this effect may be less. Alternatively, sea ice limits the penetration of light in the water column, so absence of sea ice (like during MIS 5e and 5c, Lo et al. 2018) extended the time period of light availability for primary producer. Thus, the blooming period of the haptophyte algae may have shifted or was extended to include warmer periods, such as summer and the blooming period of the diol producers could be extended to colder periods, such as spring. Indeed, $U^{k'}_{37}$-SST temperatures are closer to TEX^{L}_{86}-temperatures, which reflect subsurface summer temperatures in the present-day Sea of Okhotsk, suggesting they might have been blooming earlier in the season in between fall and summer.

4.4 Sea temperature reconstructions during glacial stages

In contrast to the interglacial stages, during the glacial stages (MIS 2, 4 and 6), the three temperature proxies yield similar temperatures (within proxy error, with the exception of MIS 6 for the $U^{k'}_{37}$-SST, Fig. 4) indicating that the proxies likely reflect the same season of production. This season is most likely summer as the Sea of Okhotsk is frozen during the remaining part of the year during glacial stages (Nürnberg et al. 2011; Lo et al. 2018). The $U^{k'}_{37}$-derived SST record shows a continuous warming trend during MIS 6, in contrast to the other proxies (Fig. 6). During the late MIS 6, the $U^{k'}_{37}$-SST are unrealistically high, i.e. the $U^{k'}_{37}$-derived SST was up to 16°C higher than LDI-derived SST and TEX^{L}_{86} temperatures (Fig. 6). These temperatures are not plausible during a glacial stage that was much colder than modern day temperature (Nürnberg et al. 2011; Lo et al. 2018). These abnormally high $U^{k'}_{37}$-derived SST during late MIS 6 have also been observed by Martinez-Garcia et al. (2010) in sediments from the Northwestern Pacific and by Seki et al. (2009) in a core from the southern Sea of Okhotsk (51°N). These anomalous $U^{k'}_{37}$-derived SST values may be due to a contribution of allochtonous alkenones transported laterally (Mollenhauer et al. 2008), either from the warm Japan Sea via the Kuroshio current or from the relatively warmer Amur River delta further north. However, studies of sediment traps located 100 m above the sea floor in the present-day Sea of Okhotsk show no evidence for lateral transport of alkenones (Harada et al. 2006; Seki et al. 2007). These anomalous $U^{k'}_{37}$ values co-occur with an apparent input from the Amur River, as evidenced by the relatively higher BIT values (0.2, Fig. 5) and a high abundance of the C_{32} 1,15-diol between 140-134 ka (fractional abundance up to 0.7 of 1,13 and 1,15 LCDs at 134 ka, Fig. 5). This higher input is likely partly caused by the lower sea level during glacials which will have moved the mouth of the Amur River closer to the core site. However, it is unclear how this enhanced river input would affect the $U^{k'}_{37}$ to anomalously high values, while the LDI and TEX^{L}_{86} do not seem to be affected. MIS 4 is not

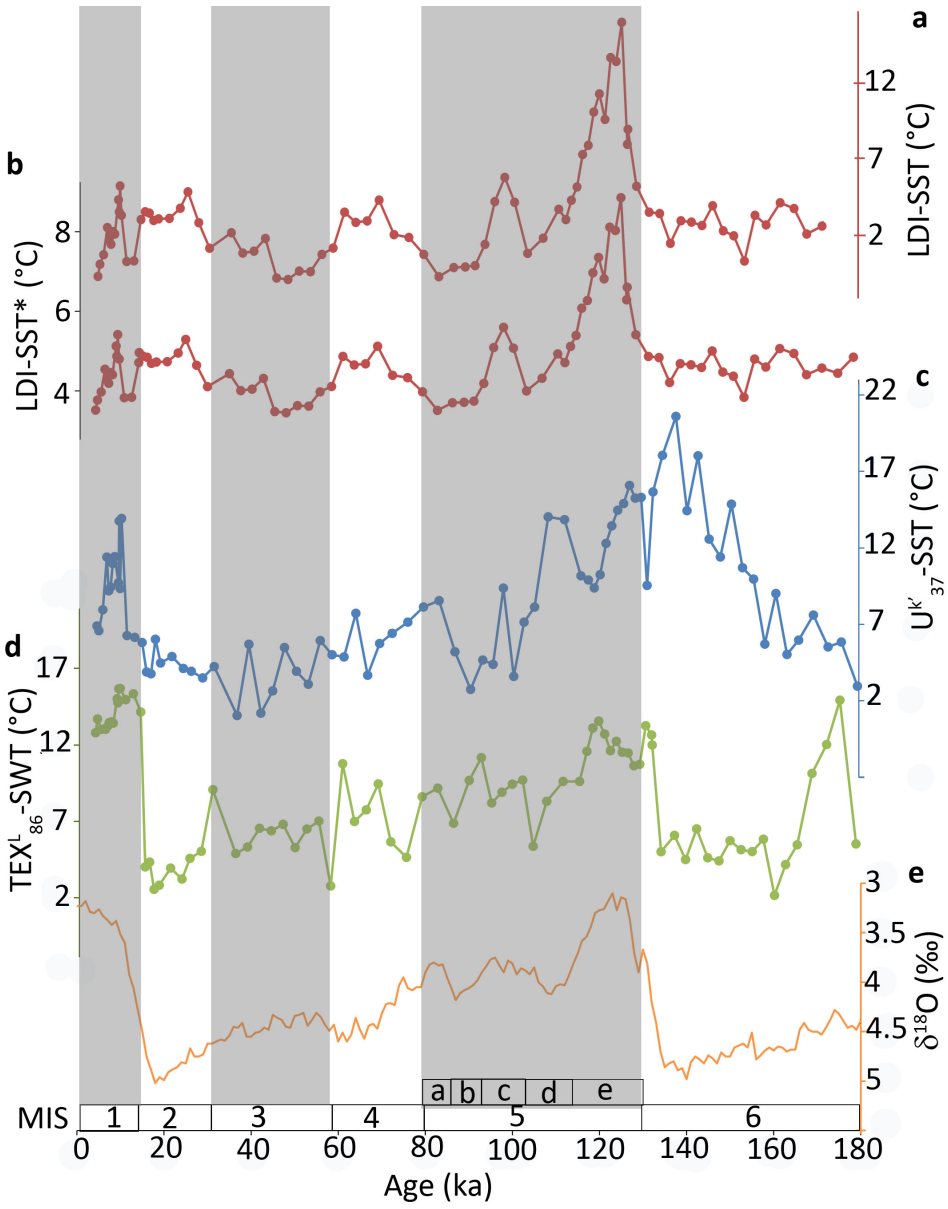

Figure 6: Reconstructed temperatures over the last 180 ka in comparison with the global LR04 stack. (a) LDI-SST (using the global calibration from Rampen et al. 2012) (b) LDI-SST* (using the local Okhotsk calibration), (c) $U^{k'}_{37}$-derived SST and (d) TEX^{L}_{86}-derived temperatures (partly from Lo et al. 2018), and (e) $\delta^{18}O$ from the LR04 stack (Lisiecki and Raymo 2005).

apparent as a strong glacial period in all three temperatures (Fig. 4), as observed in the $\delta^{18}O$ of the LR04 stack (Fig. 6d). The TEX^{L}_{86}-SST is particularly high (6.9 ± 2.8°C), which could be due to enhanced terrestrial input as suggested by the relatively higher BIT index (0.14, Fig. 5) during that period.

MIS 2 (30-17 ka) is reflected as a cold stable period in the LDI temperature record (4.7 ± 0.3°C, Fig. 4) and temperatures are similar to those of the $U^{k'}_{37}$ and TEX^{L}_{86} records. During this period the Sea of Okhotsk was almost totally closed because of the shallow depth of the Soya Strait and Kuril Islands passes that were emerged during the low sea level stand of MIS 2 (Fig. 1; Harada et al. 2004). This is similar to MIS 6, when sea ice also extended, and supported by relatively high IP_{25} concentrations, a proxy for seasonal ice cover (Belt et al. 2007; Knies et al. 2014), during MIS 2 (Lo et al. 2018). However, in contrast to MIS 6, the three temperature proxies all reveal similar temperatures, as would be expected if they are produced during the same season, i.e. summer being the only ice-free season with substantial biological activity. Also, in MIS 2, there seems to be an enhanced input from the Amur River, as suggested by elevated values of the BIT index (0.14) and of $F_{C321,15}$

(0.43), although these are lower than observed during MIS 6. The termination (16-12 ka) of MIS 2 shows increasing TEX_{86}^{L} temperatures but a relatively constant LDI and $U_{37}^{k'}$-SST. This may be caused by a deepening of the production of alkenones and diols in the water column resulting in colder temperatures, as explained above, or by a shift from summer towards autumn SST (as found present day) for the LDI and $U_{37}^{k'}$, which would results in apparent relatively constant temperatures despite overall global warming.

4.5 Diatom productivity in the Sea of Okhotsk

MIS 5e is characterized by a higher percentage of 1,14-diols (30 % of all LCDs, Fig. 7), derived from *Proboscia* diatoms (Sinninghe Damsté et al. 2003; Rampen et al. 2011) and a high opal content (up to 0.63 % at 129 ka, Fig. 7, from Liu et al. 2006), indicating increased diatom productivity (Leinen et al. 1986), and an increased TOC content (up to 0.81 % at 129 ka, Fig. 7), suggesting higher primary productivity and, hence, more nutrient-rich water. This is supported by opal records from other cores from the Sea of Okhotsk (core PC3B, Iwasaki et al. 2012; core GC09A, Khim et al. 2012; Bosin et al. 2015), with high opal content indicating high productivity during this time period. MIS 5e was characterized by open water conditions in the central Sea of Okhotsk with no sea ice formation all year (Nürnberg et al. 2011; Lo et al. 2018). The absence of sea ice during MIS 5e allowed nutrients coming from the Amur River and the Pacific Ocean to reach the Sea of Okhotsk, thereby stimulating productivity.

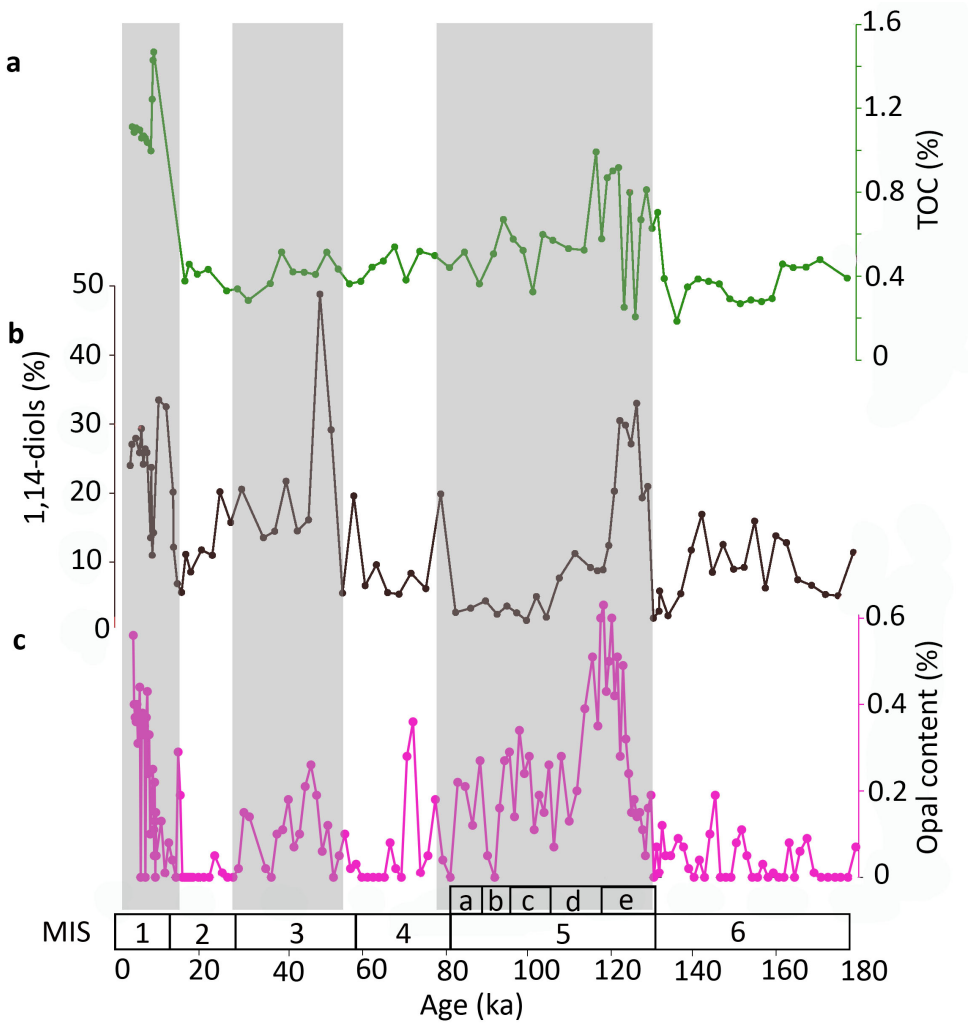

Figure 7: Productivity indicators in core MD01-2414 (a) TOC content, (b) Fractional abundance of 1,14-diols and (c) Opal content (from Liu et al. 2006).

Similar to MIS 5, there is evidence of an increase in diatomaceous production during the mid-Holocene with increase in biogenic opal content in the sediment (Fig. 7c, Liu et al. 2006), paleontological indications of

the remains of diatoms (Bosin et al. 2015) and increases in relative proportion of 1,14-diols (Fig. 7b; up to 33 %), as well as elevated TOC level (up to 1.5 %), all suggesting increased (diatom) productivity. This agrees with the findings of Bosin et al. 2015 who showed that diatoms are the main primary producers presently in the Sea of Okhotsk (Sorokin 1999) and that a phytoplankton transition occurred at the onset of the Holocene going from mainly haptophyte productivity towards a diatom productivity (Katsuki et al. 2010; Shiga and Koizumi 1999; Khim et al. 2012).

Conclusion

Our study shows the applicability of the LDI as a proxy for sea surface temperature in a polar region. The LDI-derived temperatures from surface sediments correlates well with autumn SST, similar to the $U^{k'}_{37}$ but different than the TEX^{L}_{86}, which likely reflects summer subsurface temperature. Interestingly, the LDI-SST correlation is substantially different from the global core top correlation, suggesting the importance of local calibrations. The LDI-derived SST record obtained from a sediment core in the central part of the Sea of Okhotsk shows temperature changes, generally in agreement with known global temperature changes during glacials and interglacials. The $U^{k'}_{37}$, LDI and TEX^{L}_{86} temperature proxies yield similar temperatures during glacials, likely indicating the same season of production, i.e. summer months as this was the only period without the presence of sea ice. In contrast, during interglacials when there is no sea ice, all three proxies yield different temperature representing different season and depth of production. Diatom productivity in the Sea of Okhotsk is reflected in the proportion of 1,14-diol and opal content of the sediment, showing increased productivity during terminations and during the Holocene.

Acknowledgments, Samples, and Data

Drs. J. L. Toney and J. Tierney are thanked for their constructive comments which improved the manuscript. We thank Denise Dorhout, Jort Ossebaar and Anchelique Mets for technical assistance. This research has been funded by the European Research Council (ERC) under the European Union's Seventh Framework Program (FP7/2007-2013) ERC grant agreement [339206] to S.S. The work was further supported by funding from the Netherlands Earth System Science Center (NESSC) through a gravitation grant (NWO 024.002.001) from the Dutch Ministry for Education, Culture and Science to J.S.S.D. and S.S. L.L. was supported by grants of the Ministry of Science and Technology (MOST), Taiwan ROC (10-2119-M-002-003, 104-2917-I-564-046, 105-2119-M-002-001), National Natural Science Foundation of China (41773116), State Key Laboratory of Isotope Geochemistry, Guangzhou Institute of Geochemistry, Chinese Academy of Sciences start-up fund and 135 project (SKLaBIG-QD-16-04 and 135 PY201605). Samples of core MD01-2414 and core-tops samples were generously provided by Taiwan Ocean Research Institute (TORI) and S.A. Gorbarenko, respectively. Data are available at Pangaea (doi:10.1594/PANGAEA.890820).

Piston core sampling, cruise 64PE418, March 2017

Chapter 8

Past environmental changes in the Sea of Okhotsk during the last 1.5 Ma using long-chain diol proxies

Organic Geochemistry, submitted

Julie Lattaud [a,*], Li Lo[b], Christian Zeeden[c], Ya-Jun Liu[d], Seng-Rong Song[d], Marcel T. J. van der Meeer [a], Jaap S. Sinninghe Damsté[a,e], Stefan Schouten[a,e]

[a] NIOZ, Royal Netherlands Institute for Sea Research, Department of Marine Microbiology and Biogeochemistry (MMB), and Utrecht University, PO Box 59, 1790 AB Den Burg, The Netherlands
[b]State Key Laboratory of Isotope Geochemistry, Guangzhou Institute of Geochemistry, Chinese Academy of Sciences, China
[c]LIAG - Leibniz Institute for Applied Geophysics, GEOZENTRUM Hannover, 30655 Hannover, Germany
[d]Department of Geosciences, National Taiwan University, Taiwan ROC
[e]Utrecht University, Department of Earth Sciences, Faculty of Geosciences, Department of Earth Sciences, Princetonlaan 8A, 3584 CB Utrecht, The Netherlands

*Corresponding author.
E-mail address: Julie.lattaud@nioz.nl (J. Lattaud).

Abstract

Long-chain diols have been detected in a wide range of environments and have been used to reconstruct past environmental changes, however only a few long-term records exist to date. Here we reconstructed past environmental changes in the central Sea of Okhotsk over the last 1.5 million years, covering the Mid-Pleistocene Transition (MPT). Sea surface temperatures (SST) reconstructed using the Long-chain Diol Index (LDI) reflects glacial/interglacial changes. However, when compared with other organic paleothermometers ($U^{k'}_{37}$ and TEX^{L}_{86}) the LDI-SST is lower during interglacials and similar or higher during glacials possibly suggesting a shift of diol production season during interglacials. The LDI-SST does not change in periodicity around the MPT as observed for the TEX^{L}_{86}, likely due to this seasonal shift. Diatom productivity, as recorded by 1,14-diols and biogenic opal content, increased during the main deglaciations with a succession from *Proboscia* diatoms to diatoms with a more heavily silicified shell, confirming that primary productivity in the central Sea of Okhotsk is driven by sea-ice progress and retreat. In contrast to the LDI-SST, the 1,14-diols record shows a change in periodicity around the MPT from 41- to 100-kyr cycle, suggesting an influence of orbital parameters on diatom productivity. In the central Sea of Okhotsk, the relative amount of C_{32} 1,15-diol ($F_{C32\ 1,15}$), a proxy for riverine input, correlates with sea-level changes with more riverine-derived material reaching the core site when the Amur River mouth is closer at lower sea-levels. In agreement, $F_{C32\ 1,15}$ shows a change in periodicity during the MPT, with the appearance of a 100-kyr cycle. Our results show that the long-chain diols can provide important paleoceanographic information in subpolar environments over long time scales, but that temperature reconstructions can be severely impacted by changes in seasonality.

Keywords: Sea of Okhotsk, Mid-Pleistocene Transition, LDI, TEX_{86}, $U^{k'}_{37}$, biogenic opal

Highlights

- LDI-reconstructed sea temperature is impacted by seasonality.
- $F_{C32\ 1,15}$ is influenced by sea-level changes in the Sea of Okhotsk.
- 1,14-diols and opal suggest that primary productivity is controlled by sea-ice cover.
- TEX^{L}_{86}-SWT shows a 100-kyr cyclicity after 1100 ka.

1 Introduction

The last 2 million years (Ma) in the Earth history cover an important climatic transition called the Mid-Pleistocene Transition (MPT) where the start of strong glacial/interglacial successions was initiated. This MPT occurred around 950 ka, with a change in the dominant periodicity from 41- to 100-kyr as seen in benthic foraminifera $\delta^{18}O$ records. At the same time, an overall positive isotope shift in these records is observed, suggesting more severe and longer glaciations (e.g. Hays et al. 1976; Shackleton and Opdyke 1976; Pisias and Moore 1981; Clark and Pollard 1998; Berger et al. 1999; Medina-Elizalde 2005; Clark et al. 2006; Elderfield et al. 2012; McClymont et al. 2013 and reference therein). The MPT was accompanied by a decrease in sea surface temperature (SST) in the northern Atlantic and an increase in aridity over the African and Asian peninsulas (Clark et al. 2006). A cold event at the start of the intensification of the glaciations (~900 ka) has been observed in several marine records (e.g. Schefuß et al. 2004; Medina-Elizalde 2005; Elderfield et al. 2012; McClymont et al. 2013). Furthermore, the high-latitude areas underwent major changes during the MPT as the Laurentide ice sheet became volumetrically larger (Clark and Pollard 1998), making it sensitive to changes in periodicity. Only a few records document changes in SST during the MPT in the northern Pacific (Raymo et al. 1990; McClymont et al. 2008).

The Sea of Okhotsk is a semi-enclosed marginal sea from the northwestern Pacific and is linked to the Sea of Japan and the Pacific Ocean, with the Amur River discharging terrigenous input into the eastern part. The oldest paleoceanographic record of the Sea of Okhotsk goes back to 1.1 Ma (Nürnberg and Tiedemann 2004) and showed that the sediments from the Sea of Okhotsk reflect glacial/interglacial variability that are

characteristic for the northern hemisphere (Lisiecki and Raymo 2005). However, most sediment records of the Sea of Okhotsk only cover the late Quaternary (Gorbarenko 1996; Sorokin 1999; Ternois et al. 2001; Gorbarenko et al. 2004, 2007, 2010, 2012, 2014; Harada et al. 2004, 2006, 2008, 2012, 2014; Seki et al. 2004a, 2004b, 2009, 2012, 2014a, 2014b; Sakamoto et al. 2005, 2006; Liu et al. 2006; Wang and Wang 2008; Ishiwatari et al. 2009; Malakhov et al. 2009; Katsuki et al. 2010; Nürnberg et al. 2011; Iwasaki et al. 2012; Khim et al. 2012; Nakanowatari et al. 2014; Bosin et al. 2015; Lembke-Jene et al. 2018).

Recently, Lattaud et al. (2018b) sshowed that organic proxies could be applied to reconstruct sea water temperatures in the Sea of Okhotsk until Marine Isotope Stage (MIS) 6 (~180 ka). In particular, they used long-chain diols (LCDs) to reconstruct past autumn SST via the Long-chain Diol Index or LDI (Rampen et al. 2012). The presence of LCDs in this core raises the possibility to reconstruct other parameters such as riverine input using the proportion of C_{32} 1,15-diol ($F_{C32\ 1,15}$, Lattaud et al. 2017b,2017a), upwelling intensity (with the Diol Index or DI, Willmott et al. 2010) and *Proboscia* diatom productivity (via the concentration of 1,14-diols; Rampen et al. 2014b). LCD proxies have rarely been applied on long time scales and the longest LDI-SST record is dating back to 3.3 Ma in sapropels from the Mediterranean Sea (Plancq et al. 2015) but most records do not go further back than 180 ka (dos Santos et al. 2013; Smith et al. 2013; Jonas et al. 2017; Kotthoff et al. 2017; Lattaud et al. 2017a, 2018b; Warnock et al. 2017; de Bar et al. 2018).

In this study we extended the LDI-SST record in the Sea of Okhotsk to 1.5 Ma to fully capture the MPT. Furthermore, we applied other LCD proxies, i.e $F_{C32\ 1,15}$ (to trace river input; Lattaud et al. 2017b), the DI and the 1,14-diols (as *Proboscia* diatom indicator),to reconstruct environmental changes during the MPT in the central Sea of Okhotsk. These LCD proxy records were compared with other sea water temperature proxies (TEX_{86}^{L} reflecting summer subsurface temperatures and $U_{37}^{k'}$ reflecting autumn SST; Lattaud et al. 2018b) as well as with productivity proxies such as biogenic opal content, and riverine input proxies such as the hydrogen isotopic composition of long chain alkenones, reflecting the hydrogen isotopic composition of the water and salinity, and the BIT index.

2 Material and Methods

2.1 Study site

The Sea of Okhotsk is part of the Western Pacific Ocean and it is the southernmost sea of the northern hemisphere with seasonal sea-ice cover (Harada et al. 2014). Nowadays, polynyas open up on the northeastern shelf area and can spread to cover up to 85% of the Sea of Okhotsk (Hays and Morley 2003). It is a highly productive sea with a major planktonic spring bloom and a smaller autumn bloom of diatoms (Hays and Morley 2003). In autumn there is also a major haptophyte bloom with *Coccolithus oceanicus* and *Emiliana huxleyi* (Broerse et al. 2000). In the Sea of Okhotsk, autumn SST, salinity and sea-ice extend, influence the intensity of downwelling that creates the Okhotsk Sea Intermediate Water (OSIW), which in turn is a key component of the North Pacific Intermediate Water (NPIW) (Tsunogai et al. 1993).

Giant piston core MD01-2414 (53°11.77'N, 149°34.80'E and water depth of 1123 m, Fig. 1) was collected during the IMAGES VII cruise from the central region of the Sea of Okhotsk (Deryugin basin) as described by Chou et al. (2011). This core has a length of 52.76 m and we studied the top 51 m. The age model is described in Lo et al. (2018) and was obtained by correlating the XRF core scanner data with the global $\delta^{18}O$ LR04 stack (Lisiecki and Raymo 2005). Furthermore, 5 radiocarbon ^{14}C ages of planktonic foraminifera (*Neogloboquadrina pachyderma*, sinistral) were determined by accelerator mass spectrometry (AMS). Together this shows that the core covers ages between 3.7 to 1520 ka (52.76 m) with sedimentation rates varying between 1 and 4 cm kyr^{-1}. The sediment core was sampled every 10 cm which corresponds to a time resolution of 3- to 10-kyr. The sediment was stored frozen until freeze-dried. Besides the piston core samples, thirteen surface sediments were collected from the Sea of Okhotsk as described by Lo et al. (2018).

2.2 Extraction and separation of lipids

The sediments were extracted following the procedures described by Lo et al. (2018). Briefly, sediment samples (1–10 g) were homogenized, freeze-dried and extracted using dichloromethane (DCM) : methanol (MeOH) (4 : 1, v/v) using an Accelerated Solvent Extractor (ASE). The extracts were separated into three fractions on a Pasteur pipette packed with activated Al_2O_3: an apolar fraction (hexane : DCM, 9 : 1 v/v), a ketone fraction

(hexane : DCM, 1 : 1 v/v) containing alkenones, and a polar fraction (DCM : MeOH, 1 : 1 v/v) containing Glycerol Dialkyl Glycerol Tetraethers (GDGTs) and long-chain diols were obtained.

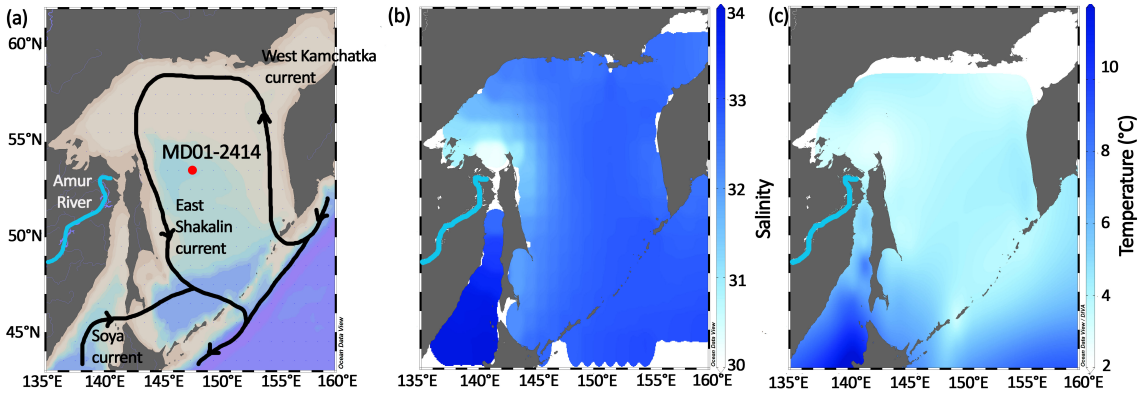

Figure 1: (a) Location of core MD01-2414 (Lo et al. 2018) and environmental parameters of the Sea of Okhotsk with (b) annual mean surface salinity (from NOAA, Antonov et al. 2010) and (c) annual mean sea surface temperature (from NOAA, Locarnini et al. 2009).

2.3 Analysis of biomarkers

The alkenone and LCDs were analysed as described in Lattaud et al. (2018b) and the GDGTs as described in Lo et al. (2018). A previous surface sediment study of the Sea of Okhotsk showed that TEXL86 values correlated strongly with summer sea water temperature (SWT) at 20 m depth (Lattaud et al. 2018b; Lo et al. 2018) and that the global calibration of Kim et al. (2010) (equation 1) could be used to reconstruct these temperature. The same surface sediments study showed that $U^{k'}_{37}$ the calibration from Prahl and Wakeham (1987) (equation 2), which is the one most commonly applied in the Sea of Okhotsk and which values correspond to autumn SST (Lattaud et al. 2018b) and that the $U^{k'}_{37}$ of Prahl and Wakeham (1987) (equation 2), which is the one most commonly applied in the Sea of Okhotsk, can be used. Finally, for the LDI, the regional core-top calibration to autumn-SST from Lattaud et al. 2018b (equation 3) was applied.

$$TEX^{L}_{86} - SWT = 67.5 \times TEX^{L}_{86} + 46.9 \quad (1)$$

$$U^{k'}_{37} - SST = \frac{U^{k'}_{37} - 0.044}{0.033} \quad (2)$$

$$LDI - SST = \frac{LDI + 0.29}{0.103} \quad (3)$$

The Branched Isoprenoid Tetraether index (BIT index, Hopmans et al. 2004), an indicator of terrigenous input transported by rivers into the marine environment, is based on the ratio of branched GDGTs (brGDGTs, produced in rivers and in soils, Weijers et al. 2009; Jonge et al. 2014b) over crenarchaeol (mainly produced in marine environments). The BIT index was calculated for the whole record to assess terrigenous input. Furthermore, two diol proxies were used, the $F_{C32\ 1,15}$ based on the fractional abundance of the C_{32} 1,15 diol over the C_{30} 1,15-, C_{30} 1,13- and C_{28} 1,13-diols (Lattaud et al. 2017b) and the DI based on the ratio of 1,14 diols over the C_{30} 1,13- and C_{28} 1,13-diols (Willmott et al. 2010) in order to reconstruct riverine input and nutrient conditions, respectively.

2.4 Analysis of δD of alkenones

47 samples contained alkenones in high enough abundance for hydrogen isotope measurements. To analyse the δD of alkenones, the ketone fractions were dissolved in ethyl acetate and analyzed for hydrogen isotopes as described by Kasper et al. (2015). Briefly, the ketone fractions were injected on a Thermo Finnigan Delta Plus XL Gas Chromatography Thermal Conversion isotope ratio Mass Spectrometer (GC/TC/irMS). The H^{3+} correction factor was determined daily and ranged between 3.56 and 3.9. Isotopic values for alkenones were

standardized against pulses of H^2 reference gas, which was injected three times at the beginning and two time at the end of each run. A set of standard n-alkanes with known isotopic composition (Mixture B, prepared by Arndt Schimmelmann, University of Indiana) was analyzed daily prior to each sample batch in order to monitor the system performance. Samples were only analyzed when the alkanes in Mix B had an average deviation from their off-line determined values of less than 5‰. The 47 hydrogen isotope values of alkenones (δD_{C37}) were measured as the combined peak of the $C_{37:2}$ and $C_{37:3}$ (van der Meer et al. 2013), which correlates best with salinity, and 0.2 µL of a standard mixture of known δD value, composed of squalane and C_{30} n-alkane, was coinjected to each sample. The samples were analyzed in duplicate and standard deviation of duplicate analyses varied from 0-5‰.

2.5 Biogenic opal analysis

The opal content was measured as described by Liu et al. (2006) to extend previous record (0-500 ka) reported by Liu et al. (2006) to 1550 ka. Briefly, freeze-dried sediment were homogenized in a mortar, and they were then smeared gently on glass slides for the mineralogical analysis. The mineralogy of the sediments was analyzed by using a Science Mxp III X-ray diffractometer (MAC) with CuKα radiation. Scans of bulk powders were run at 35 kV and 15 mA over a scanning range of 3°–70°.

2.6 Spectral analysis

The proxy records were linearly resampled to get an even spaced record and a 95% confidence level was chosen. A Morlet Wavelet analysis of the different records was realized with the PAST software (Hammer et al. 2001) t to study the changes of periodicity in the proxy records over time.

3 Results

3.1 Temperature proxies

Using the local LDI-autumn SST calibration of Lattaud et al. (2018b) we reconstructed SST using the LDI which varied from 3 to 12°C (Fig. 2b). The LDI temperatures were 5°C at 1520 ka, then increased to 11°C at 1300 ka, followed by a decrease until 3°C at 1100 ka. LDI-SST were then warming reaching 9°C at 1070 ka then decreased to 3°C at 970 ka. This was followed by two short-termed warming events (reaching 7°C at 960 and 930 ka, respectively). The LDI-SST was then varying by just 2°C over the next 600 ka, with some warming events at 860 ka (MIS 21), 800 ka (MIS 19) and 400 ka (MIS 11) (reaching 7°C, 8°C and 8°C, respectively). This was followed by two cycles of cooling/warming when temperatures reached a maximum of 7 and 8°C (at 340, i.e. MIS 9 and 245 ka, i.e. MIS 7, respectively) and minimums of 3 and 4°C. The last 180 ka (from Lattaud et al. 2018b), showed that MIS 6 was characterized by low temperatures (average 5 ± 1°C), that was followed by warmer temperatures, reaching 9°C at 130 ka (MIS 5e). After a cooling, the most recent part of the core varied around 4 to 5°C.

The $U^{k'}_{37}$-SST ranged from 1 to 23°C (Fig. 2c) over the whole record. At 1520 ka temperatures were around 6°C and increased to 20°C at 1320 ka, then decreased to 7°C around 1190 ka. The record was then characterized by several cooling/warming events, with the main warmings around 1160, 1070, 950, 880, 620 (MIS 15), 410 (MIS 11), 260 (MIS 8), 140 (MIS 6) and 9 ka, respectively. Late MIS 6 is characterized by relatively high temperatures (maximum of 20°C) that remain high throughout MIS 5e (15°C). $U^{k'}_{37}$-SST then decreased to 2.5°C at 90 ka (MIS 5b), followed by a warming (8°C at 80 ka). A cooling then occurred during MIS 4-2 (average of 4°C during 70-14 ka) and the Holocene is characterized by a warming to 7°C at 4 ka.

For TEX^L_{86} we used the global calibration of Kim et al. (2010) which in the Sea of Okhotsk has been shown to reflect summer subsurface sea water temperature (SWT). TEX^L_{86}-reconstructed sea water temperatures (TEX^L_{86}-SWT) varied from -3 to 18°C (Fig. 2d). At 1550 ka, the TEX^L_{86}-SWT were 4°C, increasing to 16°C until 1080 ka. This was followed by a decrease until 880 ka (TEX^L_{86}-SWT = 4°C), then a rapid warming happened with TEX^L_{86}-SWT reaching 14°C at 860 ka. This pattern of slow cooling and fast warming was repeated again between 860 to 620 ka and temperature ranged between 3°C at 640 ka to 14°C at 620 ka. This was followed by a period of relatively stable TEX^L_{86} temperatures (8.5 ± 2°C, n = 15) until 470 ka, followed by a steep cooling with TEX^L_{86}-SWT reaching -1°C at 460 ka (MIS 12). After MIS 12 a relatively fast warming was observed with

TEX_{86}^{L} temperatures increasing to the warmest temperature of the record of 18°C at 430 ka (MIS 11). This was followed by a slow cooling until 150 ka (4°C) (MIS 6). At 130 ka (MIS 5e) the TEX_{86}^{L} temperature reached 13°C which decreased until 3°C at 20 ka (MIS 2), respectively (Lo et al. 2018).

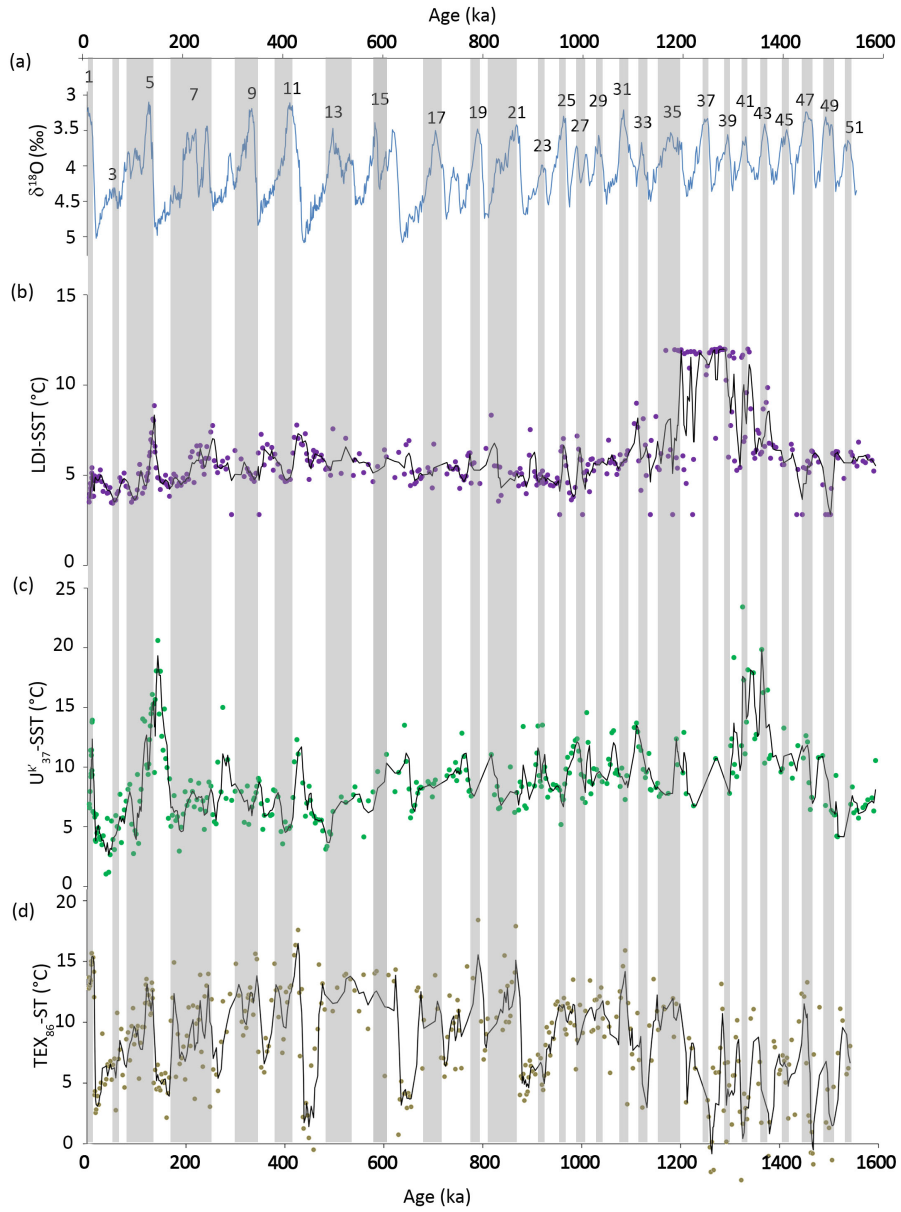

Figure 2: Paleotemperature records for the Sea of Okhotsk (a) global stack of $\delta^{18}O$ of benthic foraminifera (Lisiecki and Raymo 2005) with numbers indicating the different Marine Isotope Stages, and 3 point averaged temperature records of (b) LDI-SST, (c) $U_{37}^{k'}$-SST and (d) TEX_{86}^{L}-SWT from MD01-2414 core from the central Sea of Okhotsk.

3.2 Riverine input proxies

The $F_{C32\ 1,15}$, a proxy for riverine input (Lattaud et al. 2017b), ranged from 0.1 to 0.7 in the sediment core (Fig. 3). Between 1520 and 1250 ka, $F_{C32\ 1,15}$ was stable around 0.4 ± 0.1 (n = 73), except for a sharp drop (down to 0.2) at 1450 ka, then decreased to 0.1 between 1250 and 1150 ka, followed by an increase until 0.5 at 1140 ka. $F_{C32\ 1,15}$ decreased rapidly to 0.2 at 1070 ka before going back to higher values (0.4) between 1060 and 960 ka, followed by a rapid decrease at 950 ka (0.2). $F_{C32\ 1,15}$ was then varying between 0.3 and 0.7 with minima around 850, 760, 600, 420, 330, 120 ka (MIS 21, 19, 15, 11, 9 and 5, respectively) and the end of the Holocene. The BIT index (Fig. 3), a proxy for riverine terrigenous input (Hopmans et al. 2004; Zell et al. 2013a, 2015),had

values which were generally low with an average of 0.08 ± 0.05 (n = 384) and with 0.38 as maximum at 340 ka, and the record is characterized by several brief periods with relatively high values around 1450, 1120, 920, 430 (MIS 12), 340 (MIS 10), 190 (MIS 6), 130 (MIS 5) and 36 ka (MIS 3). For comparison $F_{C32\ 1,15}$ and the BIT index was also measured in surface sediments distributed around the Sea of Okhotsk (Table 1). In the surface sediments, $F_{C32\ 1,15}$ varied between 0.02 and 0.3 and the BIT index between 0.02 and 0.12 with no particular pattern (Table 1).

Table 1: LCD proxies Diol index and $F_{C32\ 1,15}$ and BIT index for the surface sediments in the Sea of Okhotsk.

Name	Latitude (°N)	Longitude (°E)	DI	$F_{C32\ 1,15}$	1,14-diols (%)	BIT
55-14-2	56.07	153.68	0.53	0.15	43.5	0.02
55-17-2	56.31	146.84	0.39	0.07	35.7	0.02
55-18-2	56.34	145.31	0.38	0.03	36.9	0.02
55-23-2	53.015	146.51	0.30	0.10	25.1	0.12
55-25-2	52.56	146.51	0.31	0.10	26.5	0.06
55-27-2	52.00	144.56	0.28	0.20	20.8	0.03
55-30-2	52.00	144.94	0.36	0.10	31.1	0.03
55-34-2	48.81	147.87	0.32	0.11	22.4	0.02
55-36-2	48.58	146.36	0.29	0.15	20.1	0.03
55-44-2	47.52	145.16	0.26	0.33	13.6	0.11
55-46-2	45.51	144.54	0.34	0.18	18.3	0.04
55-47-2	45.52	144.57	0.29	0.21	14.8	0.05

3.3 Diol index

The 1,14-diols, biomarkers for *Proboscia* diatoms (Sinninghe Damsté et al. 2003; Rampen et al. 2014b), were present throughout the record, and comprise on average 12 ± 0.1% of all diols (n = 409), with values ranging between 2 to 50 % (Fig. 3). At 1520 ka, the 1,14-diols were 10% of all LCDs, then increased briefly to 30% at 1450 ka before going back to 10%. At 1230 ka, a sharp and brief increase in the amount of 1,14-diols took place (reaching 50% of all LCDs) before going back to previous values of 10% until 1100 ka when it increased to 20%. The 1,14-diols showed maxima at around 950, 850, 750, 720, 430, 330, 130 and 50 ka (MIS 12, 9, 5 and 3, respectively, Fig. 3). The Diol Index (DI), an index used to reconstruct *Proboscia* productivity based on the amount of 1,14-diols versus 1,13-diols (Willmott et al. 2010), varied between 0.04 and 0.84 and showed a very similar trend as that of percentage of 1,14 diols except between 1300 and 1100 ka when the DI was continuously high (around 0.7). Between 1100 and 131 ka DI was on average 0.21 ± 0.09 (n = 228), after 131 ka the values were increasing to 0.48 at 125 ka then decreased and reached 0.04 at 100 ka. DI was then rising until the Holocene, reaching 0.32 at 4 ka. Maxima are observed at 440, 330, 130 and 50 (MIS 12, 9, 5 and 3, respectively, Fig. 3). Finally, in the surface sediments, DI varied between 0.26 and 0.53 and the 1,14-diols between 21 and 44 % with no particular spatial patterns (Table 1).

3.4 Hydrogen isotopic composition of C_{37} alkenones

The hydrogen isotopic composition of C_{37} alkenones (δD_{C37}), a proxy for salinity (Schouten et al. 2006), was obtained in a lower resolution than the other records due to the often relatively low abundance of alkenones, too low for hydrogen isotope analysis. The δD_{C37} varied from -215‰ to -172‰, with more depleted values during interglacials. At 1520 ka the value was -187‰ then it decreased to -197‰ at 1439 ka. It was followed by an increase up to -190‰ at 1280 ka, a decrease down to -205‰ at 1076 ka an increase up to -170‰ at 807 ka (MIS 20) followed by a steep decrease until -214‰ at 523 ka (MIS 13). A slow increase took place from 523 to 83 ka (MIS 13 to MIS 5), until the δD_{C37} reached -170‰. This increase was interrupted by a short event where values briefly decreased to -215‰ at 122 ka (MIS 5e). At the start of the Holocene at 12 ka the δD_{C37} shows a slow decrease, until -207‰ at 6 ka.

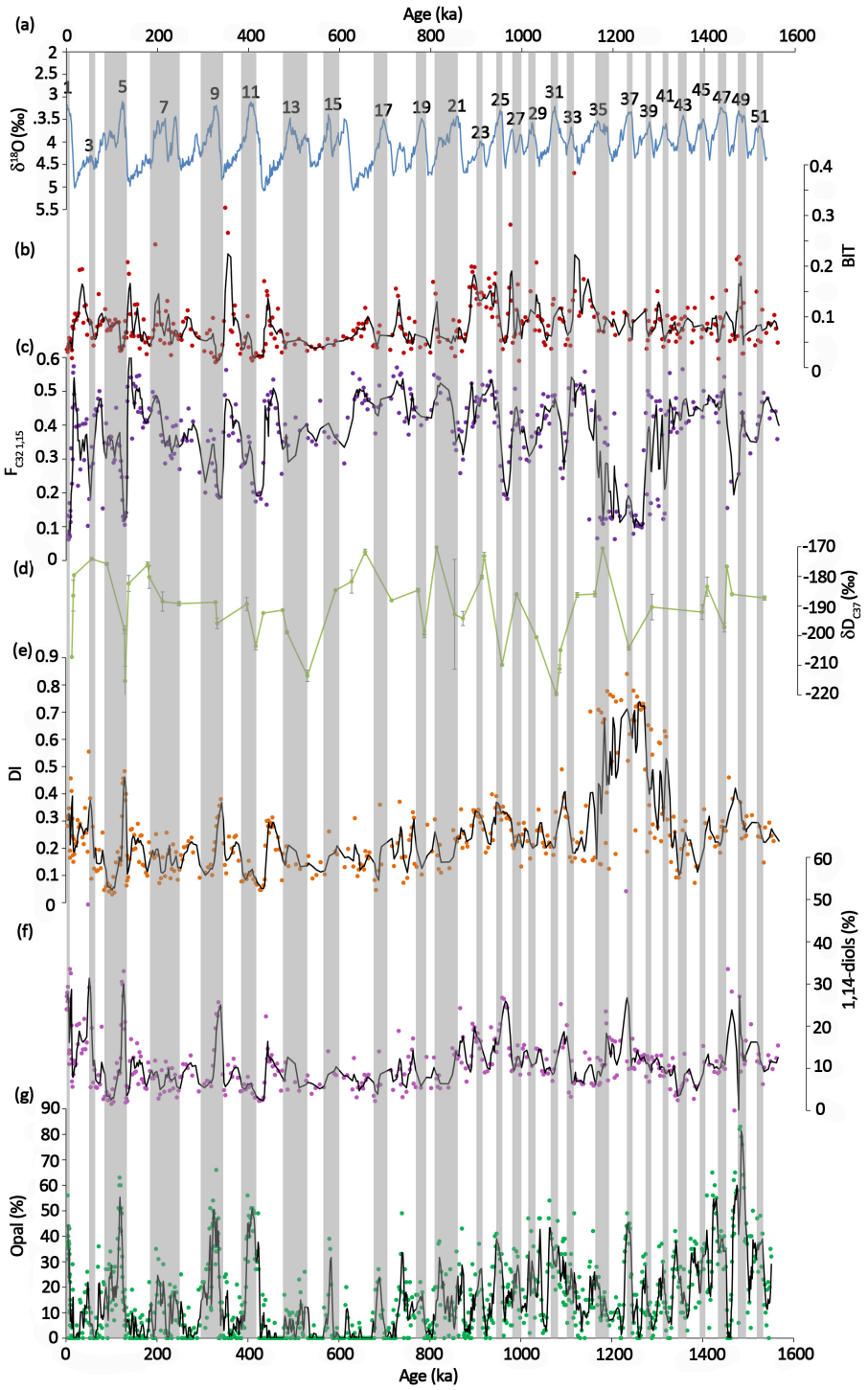

Figure 3: (a) The δ^{18}O benthic foraminifera global stack (Lisiecki and Raymo 2005) with numbers indicating the different Marine Isotope Stages, and proxy records of the Sea of Okhotsk (b) BIT index, (c) $F_{C32\ 1,15}$, (d) δD_{C37} (the grey bars represent the standard deviation of the replicate), (e) Diol Index (DI), (f) 1,14-diols in fractional abundance of all diols and (g) opal percentage (Liu et al. 2006 and this study). The black lines represents a running mean of 3 points.

3.5 Spectral analysis

We performed wavelet analysis (using a Morlet wavelet) on nearly all of our records (Fig. 4) and for comparison also on the LR04 benthic foraminifera stack (Lisiecki and Raymo 2005; reflecting global ice volume changes), and a $U^{k'}_{37}$-SST record from the northern Pacific (Martinez-Garcia et al. 2010). The TEX_{86}-ST record shows

changes from a dominant 41-kyr cyclicity in the oldest part of the core to a dominant 100-kyr cycle in the most recent part of the core, similar to the LR04 benthic δ^{18}O stack (Fig. 4). The LDI-SST does not show any significant cycle over the record, and the $U^{k'}_{37}$-SSTrecord has two periods with a significant cycle of 100-kyr (around 300 to 0 ka and 1300 to 1100 ka). The riverine input proxy $F_{C32\ 1,15}$ shows a significant 100-kyr cycle in the younger part of the core (after 1100 ka), similar to the LR04 benthic δ^{18}O stack while for the BIT index, a 100-kyr cycle is apparent before 1100 ka. For the opal content and 1,14-diols, a 100-kyr cycle is observed after 600 ka and for the opal content record, a 41-kyr cycle is present in the periods older than 1100 ka.

4 Discussion

4.1 Sea water temperature evolution of the Okhotsk Sea over the last 1.5 Ma

Comparison of sea water temperature proxies

Lattaud et al. (2018b) showed, using surface sediments from the Sea of Okhotsk, that the three temperature proxies, LDI, $U^{k'}_{37}$, and TEX^{L}_{86}, all reflect a different season and/or depth of production, i.e. summer subsurface temperature for TEX^{L}_{86} and autumn SST for LDI and $U^{k'}_{37}$. With this in mind we compared the three temperature records. The LDI-SST is significantly correlated with $U^{k'}_{37}$-SST (r^2 = 0.15, p<0.005) over the whole record but not with TEX^{L}_{86}-SWT (r^2 = 0.01, p = 0.09). Moreover, there is no correlation between TEX^{L}_{86}-SWT and $U^{k'}_{37}$-SST (r^2 = 0.0002, p = 0.71). This indicates that $U^{k'}_{37}$-SST and LDI-SST are following a similar pattern likely reflecting autumn SST, as shown previously in Lattaud et al. (2018b). The TEX^{L}_{86}-SWT is often higher than the other two proxy temperatures, except before 1200 ka when TEX^{L}_{86}-SWT are lower than the other two.

Despite the significant correlation there is still quite some discrepancy between SSTs derived from the $U^{k'}_{37}$ and LDI with the latter often being lower (Fig. 2). Potential biases that could explain lower LDI-SSTs values compared to $U^{k'}_{37}$ are 1,13-diol production by *Proboscia* diatoms (Rodrigo-Gámiz et al. 2015), the influence of riverine LCDs (de Bar et al. 2016; Lattaud et al. 2017b), and a shift in the season of production toward colder months (e.g. early spring) during ice-free interglacials. Examination of the SST records shows that colder LDI temperatures are not linked with elevated amount of 1,14-diols or higher values of $F_{C32\ 1,15}$ (Fig. 3c and 3f) indicating no influence of *Proboscia* diatoms or riverine input, respectively. This suggests that observed differences might be linked to a shift of production of long-chain diols towards a colder season like early spring or late autumn due to longer summer and ice-free conditions during interglacials. This hypothesis was also used to explain the colder LDI-SST compared to $U^{k'}_{37}$-SST observed in the last 180 ka of the sediment record (Lattaud et al. 2018b). Alternatively, some mismatches between LDI and $U^{k'}_{37}$ can be explained by the presence of allochtonous input of alkenones (Rosell-Melé et al. 1995; Thomsen et al. 1998; Mollenhauer et al. 2003). This is supported by the observation of Broerse et al. (2000) who find subtropical haptophytes (like *G. oceanica*, *U. sibogae*, and *Coronosphaera* spp.) in sediment traps in the Sea of Okhotsk just after the sea-ice retreated. This suggests that periods of extensive sea-ice coverage in the Sea of Okhotsk are likely to bring alkenones from subtropical regions and, combined with low in-situ alkenone production, yield higher $U^{k'}_{37}$-SSTs.

During MIS 12 and 16 (ca. 450 and 650 ka, respectively), TEX^{L}_{86}-SWT is low (1.5 ± 1°C and 3 ± 1°C respectively, n = 7) in comparison with the other two proxies (5.5 ± 0.5°C and 8 ± 1°C for the $U^{k'}_{37}$-SST and 5 ± 0.5°C and 5 ± 0°C for LDI-SST, n = 7 for each). As explained above, the TEX^{L}_{86} is reflecting summer subsurface SWT, explaining the mismatch with LDI and $U^{k'}_{37}$. However, it can also be biased by terrigenous input of GDGTs (Weijers et al. 2009). Examination of the BIT record shows that it was nearly always below 0.3, suggesting limited riverine input (Weijers et al. 2009). Alternatively, there may have been shifts in season and in depths of production of GDGTs leading to differences between TEX^{L}_{86} and the SST proxies. For example, due to limited primary productivity in glacials, the source organisms of the GDGTs might also have thrived in spring and autumn due to reduced competition for ammonia (cf. Hurley et al. 2016; Junium et al. 2018) and thus TEX^{L}_{86} would yield lower temperatures. Thus, all proxy temperature records seem to be affected by multiple factors such that possibly none of them are reflecting consistently annual mean SST of the Sea of Okhotsk.

Orbital scale forcing of SSTs

Wavelet analysis of the proxy temperature records shows that the LDI-SST has a weak 100-kyr cycle corresponding to eccentricity (Fig. 4). The impact of orbital forcing may have been weakened by the changes in season

of production (see above), thereby minimizing SST contrasts between glacial and interglacials. Similarly, the $U^{k'}_{37}$ shows only a weak 100-kyr cycle (Fig. 4) and spectral analysis using Redfit (Fig. S1) of the latest 900 ka do not yield any significant periodicity, indicating that the $U^{k'}_{37}$ is possibly impacted by allochtonous input. In contrast, the TEX^{L}_{86}-temperature shows a significant 100-kyr cycle and a weak 41-kyr cycle (Fig. S1) linked to eccentricity and obliquity, respectively. Wavelet analysis shows that the 100-kyr periodicity appears after the MPT, i.e. after 1000 ka, and the 41-kyr is strong before 1000 ka (Fig. 4c), similar to the LR04 benthic $\delta^{18}O$ stack and $U^{k'}_{37}$-SST from the northern Pacific (Fig. 4i, Martinez-Garcia et al. 2010). This strongly suggests that TEX^{L}_{86} represents global temperature trends in the Sea of Okhotsk that are (at least partly) orbitally forced, which is also observed in the northern Pacific.

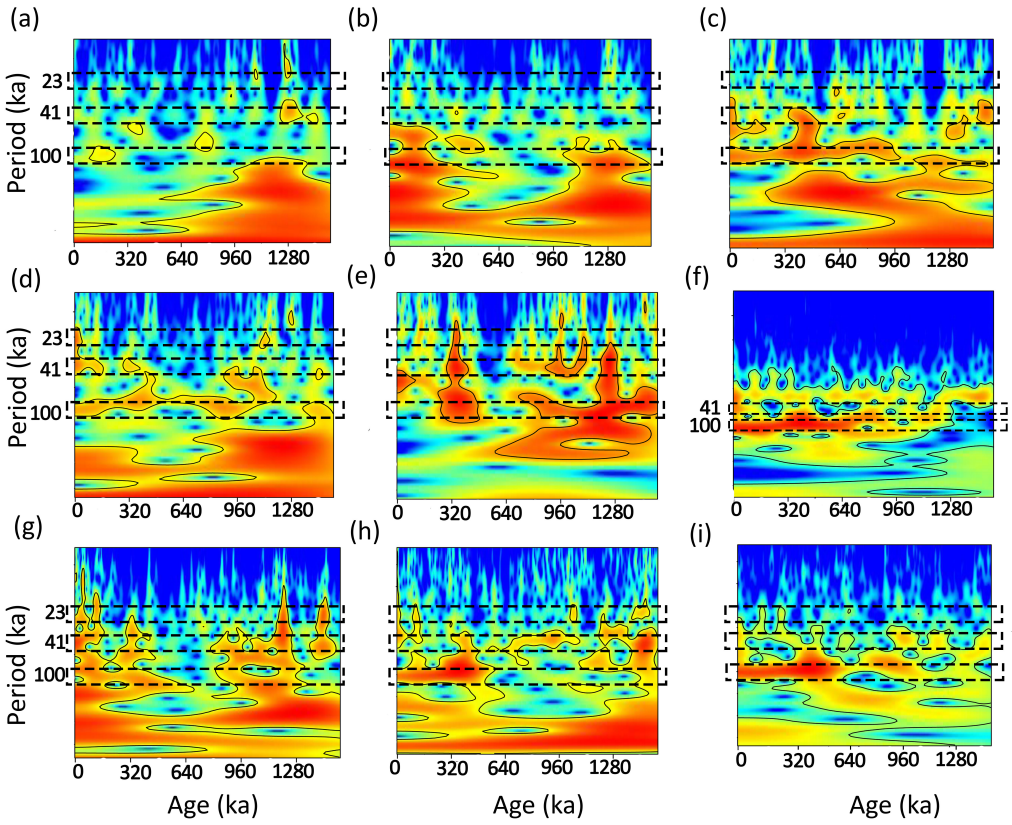

Figure 4: Spectral analysis (Wavelet) for (a) LDI-SST, (b) $U^{k'}_{37}$-SST, (c) TEX^{L}_{86}-SWT, (d) $F_{C32\ 1,15}$, (e) BIT, (f) $\delta^{18}O$ benthic foraminifera global stack (Lisiecki and Raymo 2005), (g) 1,14-diols, (h) opal content and (i) $U^{k'}_{37}$-SST from the northern Pacific ODP Hole 806B (Martinez-Garcia et al. 2010). The black boxes show the three main orbital cycles, i.e. 23-, 41- and 100-kyr.

4.2 Riverine input and salinity variation

The core site in the central Sea of Okhotsk is in the middle of the basin at 1123 m deep, far removed from the Amur River which is discharging mainly in the eastern part of the basin, bringing with it terrigenous material (Nakatsuka 2004; Seki et al. 2004b and reference cited therein). Indeed, core tops from the central part of the Sea of Okhotsk have a low $F_{C32\ 1,15}$ (0.03 to 0.12, Table 1) and a low BIT value (0.06 to 0.1, Table 1). However, in the sediment record these values were at certain times higher than present day (Fig. 3). Furthermore, a significant positive correlation between BIT index and $F_{C32\ 1,15}$ is observed (r^2 = 0.18, p <0.05, n = 395), in contrast with surface sediments of the Sea of Okhotsk where no correlation is observed (Lattaud et al., 2018). In the oldest part of the record (1500-1200 ka) this relation seems to be absent. The higher values compared to present day, as well as the correlation between BIT and $F_{C32\ 1,15}$, suggest that, in the past, riverine input was more noticeable in the central part of the Sea of Okhotsk. This can be explained by sea-level changes, i.e. during glacial periods the low sea-level (Siddall et al. 2006; Gorbarenko et al. 2014) brought the Amur River

mouth closer to the core site, thereby increasing the input of brGDGTs as well as C_{32} 1,15-diol. A previous study by Lattaud et al. (2017a) in the Mozambique Channel and the eastern Mediterranean showed a similar pattern with elevated BIT index and $F_{C32\ 1,15}$ during sea-level low stands for the late Quaternary. Changes in Amur River input are unlikely to explain the observed patterns as during glacials the Amur River is covered by an ice-cap and its input into the Sea of Okhotsk is reduced (Nürnberg and Tiedemann 2004). Furthermore, spectral analysis of the $F_{C32\ 1,15}$ record shows that a 100-kyr cycle (linked to eccentricity) initiated after the MPT (Fig. 4, Lisiecki and Raymo 2005) suggesting a link to changes in sea-level.

The δD_{C37} record likely reflects the salinity and the δD of sea water in the Sea of Okhotsk. The latter factor is controlled, amongst others, by global ice volume while salinity and the δD of sea water may be affected by input of freshwater from either the Amur River or melting ice. The δD_{C37} record (Fig.3d) shows a significant negative correlation with the $U^{k'}_{37}$-reconstructed SST (r^2 = 0.31, p<0.005, n = 47), indicating that warm interglacial stages are characterized by low δD_{C37}. These depleted δD_{C37} values during interglacials are partly linked to the change in ice volume, with a decrease in ice volume leading to an decreased δD of sea water and therefore an decrease in the δD_{C37}. During the transition between MIS 6/5, there is a global increase of 1‰ in $\delta^{18}O_{sea\ water}$ (obtained from Waelbroeck et al. 2002) which corresponds to a global increase in $\delta D_{sea\ water}$ of 18‰ (using the global meteoritic water line from Rozanski et al. 1993). However, in the Sea of Okhotsk, the difference in δD_{C37} between glacial and interglacial stages are much higher (up to 30‰, fig. 3d), and cannot be explained by ice volume alone. Therefore, a substantial part of the change must be due to salinity changes (cf. Kasper et al. 2015). This change in salinity can be due to variations in sea-ice, with increasing sea-ice buildup leading to increased salinity and vice versa, and/or changing freshwater input from the Amur River. Indeed, as discussed above, the Amur River is covered by an ice-cap and its input into the Sea of Okhotsk is reduced during glacials (Nürnberg and Tiedemann 2004) leading to increase salinity which would further increase due to extensive sea-ice formation. These combined factors may have led to more saline surface waters during glacials.

4.3 Diatom productivity in the Sea of Okhotsk

The DI (Fig. 3e) and the relative amount of 1,14-diols (Fig. 3f) can be used as qualitative indicators for *Proboscia* diatom productivity. They are both higher at the end of glacial stages (e.g. stages 2/1, 3/2, 6/5, 10/9, 16/15 and during MIS 12). Furthermore, there is also an increase in biogenic opal content which slightly lagged the 1,14-diols maxima, indicating that paleoproductivity was higher during deglaciations (Fig. 3). Biogenic opal in the Sea of Okhotsk is thought to be mainly representing diatoms as other siliceous organisms are less abundant in the Sea of Okhotsk (Iwasaki et al. 2012). However, since *Proboscia* diatoms have a weak silicified shell which are easily dissolved (Haake et al. 1993; Sakka et al. 1999; Koning et al. 2001; Rampen et al. 2011), they likely do not contribute substantially to the opal content. The succession of and opal maxima after a 1,14-diols maxima is likely due to the competition between *Proboscia* diatoms and other, more heavily silicified diatoms (like *Chaetoceros* in the modern Sea of Okhotsk, Tsoy et al. 2009; Riegman 1995, 1996) that will outcompete the *Proboscia* when silica is not limiting (Riegman et al. 1996; Ragueneau et al. 2006; Zhu et al. 2018). The increases in DI followed by increased in opal content is also observed in an offshore core from the Peru upwelling margin (de Bar et al. 2018) but, in contrast to of the Peru margin, there is no systematic upwelling in the Sea of Okhotsk. Here, the presence of *Proboscia* is more likely linked to nutrient availability as noticed by Willmott et al. (2010) for coastal Antarctica. The wavelet analysis shows for the opal content and 1,14-diols a 100-kyr cycle linked to eccentricity after the MPT, suggesting that diatom productivity is impacted by glacial/interglacial changes. This is in agreement with the idea that primary productivity in the Sea of Okhotsk is regulated by the progress and retreat of sea-ice (Seki et al. 2004a; Iwasaki et al. 2012; Bosin et al. 2015) with the retreat and melting of sea-ice providing more light for algal blooming, increased vertical mixing supplying silica to the surface layer and enhanced silica input by the Amur River.

5 Conclusions

In this study we analyzed a variety of long-chain diol proxies in a 1.5 Ma sediment core from the central Sea of Okhotsk. The LDI-SST seems to represent autumn SST during interglacials and possibly summer SST during glacials. In contrast, TEX^{L}_{86} seems to consistently represent summer subsurface sea temperature. The LDI-SST

and $U^{k'}_{37}$ do not show any significant periodicity, while the TEX^{L}_{86} has a dominant 100-kyr cycle appearing after the MPT. The lack of periodicity in the LDI and $U^{k'}_{37}$ is likely due to seasonal bias in the LDI and input of lateral transported alkenones for the $U^{k'}_{37}$.

The DI, the relative abundance of 1,14-diols and opal content in the sediment are all elevated during deglaciations and show a 100-kyr cyclicity in their records after the MPT. The recurrent lag between maxima of 1,14-diols and opal content suggests a competition for silica availability between *Proboscia* diatoms and heavily silica-shelled diatoms (recorded via the biogenic opal content of the sediment). The $F_{C32\ 1,15}$ as a proxy for river input is mainly linked with sea-level variation as it shows a 100-kyr cyclicity after the MPT. This is likely because during lower sea-level stands, i.e. during glacials, more riverine C_{32} 1,15-diol will be brought to the core site than during interglacials. In conclusion, this study shows that proxies based on long chain diols can be of use to reveal long term paleoceanographic changes in subpolar oceans.

Acknowledgments

We thank Denise Dorhout, Jort Ossebaar and Anchelique Mets for technical assistance and Rick Hennekam for discussion on the spectral analysis. This research has been funded by the European Research Council (ERC) under the European Union's Seventh Framework Program (FP7/2007-2013) ERC grant agreement [339206] to S.S. The work was further supported by funding from the Netherlands Earth System Science Center (NESSC) through a gravitation grant (NWO 024.002.001) from the Dutch Ministry for Education, Culture and Science to JSSD and SS. L.L. was supported by grants of National Natural Science Foundation of China (41773116), State Key Laboratory of Isotope Geochemistry, Guangzhou Institute of Geochemistry, Chinese Academy of Sciences start-up fund and 135 project (SKLaBIG-QD- 16-04 and 135PY201605) and the Ministry of Science and Technology (MOST), Taiwan ROC (104-2917-I-564-046). Samples of core MD01-2414 were generously provided by Taiwan Ocean Research Institute (TORI).
Data are available at Pangaea (doi.pangaea.de/10.1594/PANGAEA.896775).
The authors declare that they have no conflict of interest.

Supplement

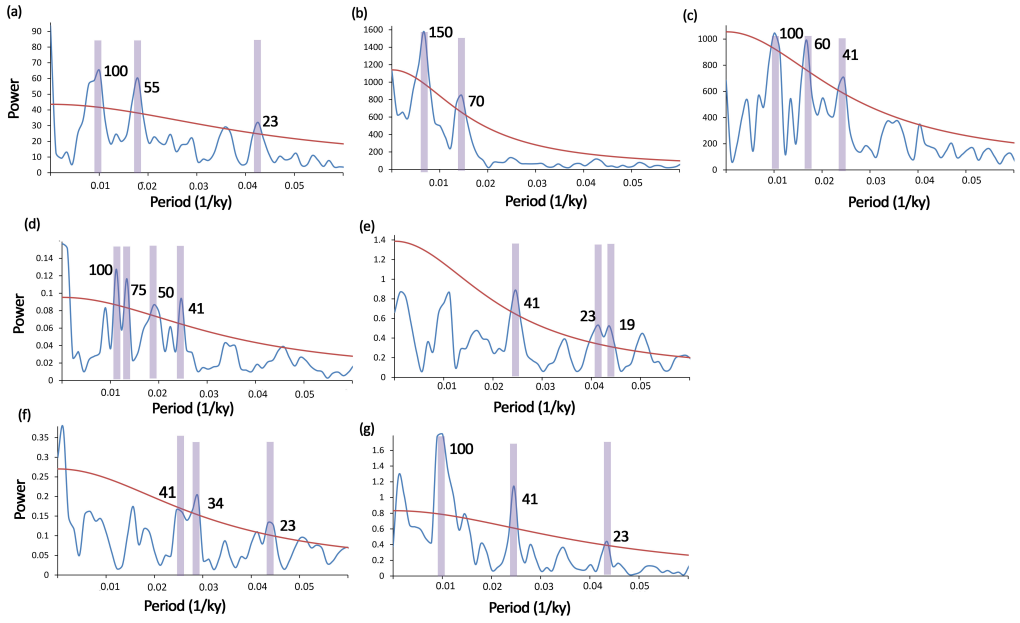

Figure 1: Spectral analysis (Redfit) of (a) LDI-SST, (b) $U^{k'}_{37}$-SST, (c) TEX^{L}_{86}-SWT, (d) BIT index, (e) $F_{C32\ 1,15}$, (f) 1,14-diols and (g) biogenic opal percentage. The red line indicates 90 % confidence.

References

Agatha, S., Struder-Kypke, M. C., and Beran, A. (2004). Morphologic and genetic variability in the marine planktonic ciliate Laboea strobila Lohmann, 1908 (Ciliophora, Oligotrichia), with notes on its ontogenesis. *The Journal of Eukaryotic Microbiology*, 51(3):267–281.

Altschul, S. F., Gish, W., Miller, W., Myers, E. W., and Lipman, D. J. (1990). Basic local alignment search tool. *Journal of Molecular Biology*, 215(3):403–410.

Andersen, R. A., Brett, R. W., Potter, D., and Sexton, J. P. (1998). Phylogeny of the Eustigmatophyceae based upon 18S rDNA, with emphasis on Nannochloropsis. *Protist*, 149:61–74.

Anneville, O., Souissi, S., Ibanez, F., Ginot, V., Druart, J. C., and Angeli, N. (2002). Temporal mapping of phytoplankton assemblages in Lake Geneva: Annual and interannual changes in their patterns of succession. *Limnology and Oceanography*, 47(5):1355–1366.

Antonov, J. I., Seidov, D., Boyer, T. P., Locarnini, R. A., Mishonov, A. V., and Garcia, H. E. (2010). *World Ocean Atlas 2009, Volume 2: Salinity.* NOAA Atlas NESDIS 69.

Arar, E. J. and Collins, G. B. (1997). In vitro determination of chlorophyll-a and pheophytin-a in marine and freshwater algae by fluorescence. *Environmental Protection Agency*.

Arifin, Z. and Koesmawati, T. A. (2007). Spatial distribution of trace metals (Pb, Cr, Cu and Zn) in sediments of the Berau delta, East Kalimantan and their accumulation in benthic biota. *Marine Research Indonesia*, 32(2):89–9.

Atwood, A. R., Volkman, J. K., and Sachs, J. P. (2014). Characterization of unusual sterols and long chain diols, triols, keto-ols and n-alkenols in El Junco Lake, Galápagos. *Organic Geochemistry*, 66:80–89.

Balakrishna, K. and Probst, J. L. (2007). Organic carbon transport and C/N ratio variations in a large tropical river: Godavari as a case study, India. *Biogeochemistry*, 73:457–473.

Bale, N. J., Hopmans, E. C., Zell, C., Sobrinho, R. L., Kim, J.-H., Damsté, J. S. S., Villareal, T. A., and Schouten, S. (2015). Long chain glycolipids with pentose head groups as biomarkers for marine endosymbiotic heterocystous cyanobacteria. *Organic geochemistry*, 81:1–7.

Bale, N. J., Villareal, T. A., Hopmans, E. C., Brussaard, C. P. D., Besseling, M., Dorhout, D., Damsté, J. S. S., and Schouten, S. (2018). C_5 glycolipids of heterocystous cyanobacteria track symbiont abundance in the diatom Hemiaulus hauckii across the tropical north Atlantic. *Biogeosciences*, 15:1229–1241.

Balzano, S., Abs, E., and Leterme, S. C. (2015). Protist diversity along a salinity gradient in a coastal lagoon. *Aquatic Microbiology Ecology*, 74:263–277.

Balzano, S., Lattaud, J., Villanueva, L., Rampen, S., Brussaard, C. P. D., van Bleijswijk, J., Bale, N., Damsté, J. S. S., and Schouten, S. (2018). A quest for the biological sources of the ubiquitous long chain alkyl diols in the marine realm. *Biogeosciences Discussions*, pages 1–40.

Balzano, S., Pancost, R. D., Lloyd, J. R., and Statham, P. J. (2011). Changes in fatty acid composition in degrading algal aggregates. *Marine Chemistry*, 124(1-4):2–13.

Balzano, S., Villanueva, L., de Bar, M., Sinninghe Damsté, J. S., and Schouten, S. (2017). Impact of culturing conditions on the abundance and composition of long chain alkyl diols in species of the genus Nannochloropsis. *Organic Geochemistry*, 108:9–17.

Becker, K. W., Lipp, J. S., Versteegh, G. J. M., Wörmer, L., and Hinrichs, K.-U. (2015). Rapid and simultaneous analysis of three molecular sea surface temperature proxies and application to sediments from the Sea of Marmara. *Organic Geochemistry*, 85:42–53.

Beilfuss, R. and Santos, D. D. (2001). Patterns of hydrological change in the Zambezi Delta. Mozambique, Programm for the Sustainable Management of Cahora Bassa Dam and the Lower Zambezi Valley Working Paper 2.

Belt, S. T., Massé, G., Rowland, S. J., Poulin, M., Michel, C., and LeBlanc, B. (2007). A novel chemical fossil of palaeo sea ice: IP_{25}. *Organic Geochemistry*, 38(1):16–27.

Benjamini, Y. and Hochberg, Y. (1995). Controlling the false discovery rate: a practical and powerful approach to multiple testing. *Journal of the Royal Statistical Society. Series B (Methodological*, 57(1):289–300.

Berger, A., Li, X. S., and Loutre, M. F. (1999). Modelling northern hemisphere ice volume over the last 3Ma. *Quaternary Science Reviews*, 18(1):1–11.

Bergesch, M., Odebrecht, C., and Moestrup, Ø. (2008). Nanoflagellates from coastal waters of southern Brazil (32°S). *Botanica Marina*, 51(1).

Biksham, G. and Subramanian, V. (1988). Sediment transport of the Godavari River basin and its controlling factors. *Journal of Hydrology*, 101(1-4):275–290.

Blanchet, C. L., Frank, M., and Schouten, S. (2014). Asynchronous changes in vegetation, runoff and erosion in the Nile River watershed during the Holocene. *PLoS ONE*, 9(12):e115958.

Booij, K., Arifin, Z., and Purbonegoro, T. (2012). Perylene dominates the organic contaminant profile in the Berau delta, East Kalimantan, Indonesia. *Marine Pollution Bulletin*, 64(5):1049–1054.

Bosin, A., Gorbarenko, S., Xuefa, S., Liu, Y., and Zou, J. (2015). Regionalized primary paleoproduction variability in the sea of Okhotsk during late Pleistocene and Holocene. *Journal of Asian Earth Sciences*, 114:534–540.

Box, M. R., Krom, M. D., Cliff, R. A., Bar-Matthews, M., Almogi-Labin, A., Ayalon, A., and Paterne, M. (2011). Response of the Nile and its catchment to millennial-scale climatic change since the LGM from Sr isotopes and major elements of East Mediterranean sediments. *Quaternary Science Reviews*, 30(3-4):431–442.

Boyer, T. P., Antonov, J. I., Baranova, O. K., Coleman, C., Garcia, H. E., Grodsky, A., Johnson, D. R., Locarnini, R. A., Mishonov, A. V., O'Brien, T. D., et al. (2013). World ocean database 2013. *NOAA Atlas NESDIS 72*.

Brassell, S. C., Eglinton, G., Marlowe, I. T., Pflaumann, U., and Sarnthein, M. (1986). Molecular stratigraphy: a new tool for climatic assessment. *Nature*, 320(6058):129–133.

Brassell, S. C., Eglinton, G., and Maxwell, J. R. (1981). Preliminary lipid analysis of two Quaternary sediment from the middle America trench, Southern Mexico transect. *Deep Sea Drilling Project leg 661*.

Broerse, A. T. C., Ziveri, P., and Honjo, S. (2000). Coccolithophore ($-CaCO_3$) flux in the Sea of Okhotsk: seasonality, settling and alteration processes. *Marine Micropaleontology*, 39(1-4):179–200.

Buckles, L. K., Villanueva, L., Weijers, J. W. H., Verschuren, D., and Damsté, J. S. S. (2013). Linking isoprenoidal GDGT membrane lipid distributions with gene abundances of ammonia-oxidizing Thaumarchaeotaand uncultured crenarchaeotal groups in the water column of a tropical lake (Lake Challa, East Africa). *Environmental Microbiology*, 15(9):2445–2462.

Buckles, L. K., Weijers, J. W. H., Verschuren, D., and Damsté, J. S. S. (2014). Sources of core and intact branched tetraether membrane lipids in the lacustrine environment: Anatomy of Lake Challa and its catchment, equatorial East Africa. *Geochimica et Cosmochimica Acta*, 140:106–126.

Buschhaus, C., Peng, C., and Jetter, R. (2013). Very-long-chain 1,2- and 1,3-bifunctional compounds from the cuticular wax of Cosmos bipinnatus petals. *Phytochemistry*, 91:249–256.

Callede, J., Kosuth, P., Loup, J., and Guimaraes, V. S. (2000). Discharge determination by Acoustic Doppler Current Profilers (ADCP): a moving bottom error correction method and its application on the River Amazon at óbidos. *Hydrological Sciences Journal*, 45(6):911–924.

Camacho, C., Coulouris, G., Avagyan, V., Ma, N., Papadopoulos, J., Bealer, K., and Madden, T. L. (2009). BLAST: architecture and applications. *BMC Bioinformatics*, 10(1):421.

Camberlin, P. (2009). *The Nile*, chapter Nile basin climates, pages 307–333. Springer Netherlands, Dordrecht.

Caporaso, J. G., Kuczynski, J., Stombaugh, J., Bittinger, K., Bushman, F. D., Costello, E. K., Fierer, N., Pena, A. G., Goodrich, J. K., Gordon, J. I., Huttley, G. A., Kelley, S. T., Knights, D., Koenig, J. E., Ley, R. E., Lozupone, C. A., McDonald, D., Muegge, B. D., Pirrung, M., Reeder, J., Sevinsky, J. R., Turnbaugh, P. J., Walters, W. A., Widmann, J., Yatsunenko, T., Zaneveld, J., and Knight, R. (2010). QIIME allows analysis of high-throughput community sequencing data. *Nature Methods*, 7(5):335–336.

Castaneda, I. S., Schefuß, E., Pätzold, J., Damsté, J. S. S., Weldeab, S., and Schouten, S. (2010). Millennial-scale sea surface temperature changes in the eastern Mediterranean (Nile River Delta region) over the last 27,000 years. *Paleoceanography*, 25(1).

Castaneda, I. S. and Schouten, S. (2011). A review of molecular organic proxies for examining modern and ancient lacustrine environments. *Quaternary Science Reviews*, 30(21-22):2851–2891.

Castaneda, I. S., Schouten, S., Pätzold, J., Lucassen, F., Kasemann, S., Kuhlmann, H., and Schefuß, E. (2016). Hydroclimate variability in the Nile River Basin during the past 28,000 years. *Earth and Planetary Science Letters*, 438:47–56.

Castaneda, I. S., Werne, J. P., Johnson, T. C., and Powers, L. A. (2011). Organic geochemical records from Lake Malawi (East Africa) of the last 700 years, part II: Biomarker evidence for recent changes in primary productivity. *Palaeogeography, Palaeoclimatology, Palaeoecology*, 303(1-4):140–154.

Chou, Y.-M., Lee, T.-Q., Song, S.-R., and Chen, K.-J. (2011). Magnetostratigraphy of marine sediment core MD01-2414 from Okhotsk Sea and its paleoenvironmental implications. *Marine Geology*, 284(1-4):149–157.

Christaki, U., Kormas, K. A., Genitsaris, S., Georges, C., Sime-Ngando, T., Viscogliosi, E., and Monchy, S. (2013). Winter summer succession of unicellular Eukaryotes in a meso-eutrophic coastal system. *Microbial Ecology*, 67(1):13–23.

Clark, P. U., Archer, D., Pollard, D., Blum, J. D., Rial, J. A., Brovkin, V., Mix, A. C., Pisias, N. G., and Roy, M. (2006). The middle Pleistocene transition: characteristics, mechanisms, and implications for long-term changes in atmospheric pCO_2. *Quaternary Science Reviews*, 25(23-24):3150–3184.

Clark, P. U. and Pollard, D. (1998). Origin of the Middle Pleistocene Transition by ice sheet erosion of regolith. *Paleoceanography*, 13(1):1–9.

Collister, J. W., Rieley, G., Stern, B., Eglinton, G., and Fry, B. (1994). Compound-specific $\delta\ ^{13}C$ analyses of leaf lipids from plants with differing carbon dioxide metabolisms. *Organic Geochemistry*, 21(6-7):619–627.

Comeau, A. M., Li, W. K. W., Tremblay, J.-É., Carmack, E. C., and Lovejoy, C. (2011). Arctic Ocean microbial community structure before and after the 2007 record sea ice minimum. *PLoS ONE*, 6(11):e27492.

Comet, P. A. and Eglinton, G. (1987). The use of lipids as facies indicators. *Geological Society, London, Special Publications*, 26(1):99–117.

Contreras, S., Lange, C. B., Pantoja, S., Lavik, G., Rincón-Martínez, D., and Kuypers, M. M. M. (2010). A rainy northern Atacama Desert during the last interglacial. *Geophysical Research Letters*, 37(23).

Cooke, M. P., Talbot, H. M., and Wagner, T. (2008). Tracking soil organic carbon transport to continental margin sediments using soil-specific hopanoid biomarkers: a case study from the Congo fan (ODP site 1075). *Organic Geochemistry*, 39(8):965–971.

Cranwell, P. A., Eglinton, G., and Robinson, N. (1987). Lipids of aquatic organisms as potential contributors to lacustrine sediments—II. *Organic Geochemistry*, 11(6):513–527.

de Bar, M. W., Dorhout, D. J. C., Hopmans, E. C., Rampen, S. W., Damsté, J. S. S., and Schouten, S. (2016). Constraints on the application of long chain diol proxies in the Iberian Atlantic margin. *Organic Geochemistry*, 101:184–195.

de Bar, M. W., Stolwijk, D. J., McManus, J. F., Damste, J. S. S., and Schouten, S. (2018). A late Quaternary climate record based on long chain diol proxies from the Chilean margin. *Climate of the Past Discussions*, pages 1–34.

de Leeuw, J. W., Irene, W., Rijpstra, C., and Schenck, P. A. (1981). The occurrence and identification of C_{30}, C_{31} and C_{32} alkan-1, 15-diols and alkan-15-one-1-ols in Unit I and Unit II Black Sea sediments. *Geochimica et Cosmochimica Acta*, 45(11):2281–2285.

de Leeuw, J. W., Rijpstra, W. I. C., and Mur, L. R. (1992). The absence of long-chain alkyl diols and alkyl keto-1-ols in cultures of the cyanobacterium Aphanizomenon flos-aquae. *Organic Geochemistry*, 18(4):575–578.

de Leeuw, J. W., van der Meer, F. W., Rijpstra, W. I. C., and Schenck, P. A. (1980). On the occurrence and structural identification of long chain unsaturated ketones and hydrocarbons in sediments. *Physics and Chemistry of the Earth*, 12:211–217.

de Leeuw, J. W., Versteegh, G. J. M., and van Bergen, P. F. (2006). Biomacromolecules of algae and plants and their fossil analogues. *Plant Ecology*, 182(1-2):209–233.

de Madron, X. D., Abassi, A., Heussner, S., Monaco, A., Aloisi, J. C., Radakovitch, O., Giresse, P., Buscail, R., and Kerherve, P. (2000). Particulate matter and organic carbon budgets for the Gulf of Lions (NW Mediterranean). *Oceanologica Acta*, 23(6):717–730.

de Vargas, C., Audic, S., Henry, N., Decelle, J., Mahe, F., Logares, R., Lara, E., Berney, C., Bescot, N. L., Probert, I., Carmichael, M., Poulain, J., Romac, S., Colin, S., Aury, J. M., Bittner, L., Chaffron, S., Dunthorn, M., Engelen, S., Flegontova, O., Guidi, L., Horak, A., Jaillon, O., Lima-Mendez, G., Luke, J., Malviya, S., Morard, R., Mulot, M., Scalco, E., Siano, R., Vincent, F., Zingone, A., Dimier, C., Picheral, M., Searson, S., Kandels-Lewis, S., Acinas, S. G., Bork, P., Bowler, C., Gorsky, G., Grimsley, N., Hingamp, P., Iudicone, D., Not, F., Ogata, H., Pesant, S., Raes, J., Sieracki, M. E., Speich, S., Stemmann, L., Sunagawa, S., Weissenbach, J., Wincker, P., Karsenti, E., Boss, E., Follows, M., Karp-Boss, L., Krzic, U., Reynaud, E. G., Sardet, C., Sullivan, M. B., and and, D. V. (2015). Eukaryotic plankton diversity in the sunlit ocean. *Science*, 348(6237):1261605–1261605.

Demicco, R. V., Lowenstein, T. K., and Hardie, L. A. (2003). Atmospheric pCO_2 since 60 Ma from records of seawater pH, calcium, and primary carbonate mineralogy. *Geology*, 31(9):793.

Derenne, S. and Largeau, C. (2001). A review of some important families of refractory macromolecules: composition, origin, and fate in soils and sediments. *Soil Science*, 166(11):833–847.

Dixon, P. (2003). VEGAN, a package of R functions for community ecology. *Journal of Vegetation Science*, 14(6):927–930.

dos Santos, A. L., Gourvil, P., Tragin, M., Noël, M.-H., Decelle, J., Romac, S., and Vaulot, D. (2016). Diversity and oceanic distribution of prasinophytes clade VII, the dominant group of green algae in oceanic waters. *The ISME Journal*, 11(2):512–528.

dos Santos, R. A. L., Prange, M., Castaneda, I. S., Schefuß, E., Mulitza, S., Schulz, M., Niedermeyer, E. M., Damsté, J. S. S., and Schouten, S. (2010). Glacial-interglacial variability in Atlantic meridional overturning circulation and thermocline adjustments in the tropical North Atlantic. *Earth and Planetary Science Letters*, 300(3-4):407–414.

dos Santos, R. A. L., Spooner, M. I., Barrows, T. T., Deckker, P. D., Damsté, J. S. S., and Schouten, S. (2013). Comparison of organic (UK'_{37}, TEX^{H}_{86}, LDI) and faunal proxies (foraminiferal assemblages) for reconstruction of late Quaternary sea surface temperature variability from offshore southeastern Australia. *Paleoceanography*, 28(3):377–387.

dos Santos, R. A. L., Wilkins, D., Deckker, P. D., and Schouten, S. (2012). Late Quaternary productivity changes from offshore Southeastern Australia: a biomarker approach. *Palaeogeography, Palaeoclimatology, Palaeoecology*, 363-364:48–56.

Dunne, T., Mertes, L. A. K., Meade, R. H., Richey, J. E., and Forsberg, B. R. (1998). Exchanges of sediment between the flood plain and channel of the Amazon River in Brazil. *Geological Society of America Bulletin*, 110(4):0450.

Edgar, R. C. (2010). Search and clustering orders of magnitude faster than BLAST. *Bioinformatics*, 26(19):2460–2461.

Edgar, R. C., Haas, B. J., Clemente, J. C., Quince, C., and Knight, R. (2011). UCHIME improves sensitivity and speed of chimera detection. *Bioinformatics*, 27(16):2194–2200.

Egge, E. S., Johannessen, T. V., Andersen, T., Eikrem, W., Bittner, L., Larsen, A., Sandaa, R.-A., and Edvardsen, B. (2015). Seasonal diversity and dynamics of haptophytes in the Skagerrak, Norway, explored by high-throughput sequencing. *Molecular Ecology*, 24(12):3026–3042.

Eglinton, G. and Hamilton, R. J. (1963). The distribution of alkanes. In *Chemical Plant Taxonomy*, pages 187–217. Elsevier.

Eglinton, G. and Hamilton, R. J. (1967). Leaf epicuticular waxes. *Science*, 156(3780):1322–1335.

Eglinton, T. I. and Eglinton, G. (2008). Molecular proxies for paleoclimatology. *Earth and Planetary Science Letters*, 275(1-2):1–16.

Ehleringer, J. R., Thure, T. E., and Helliker, B. R. (1997). C_4 photosynthesis, atmospheric CO_2, and climate. *Oecologia*, 112(3):285–299.

Elderfield, H., Ferretti, P., Greaves, M., Crowhurst, S., McCave, I. N., Hodell, D., and Piotrowski, A. M. (2012). Evolution of ocean temperature and ice volume through the Mid-Pleistocene Climate Transition. *Science*, 337(6095):704–709.

Elias, V. O., Simoneit, B. R. T., and Cardoso, J. N. (1997). Even n-alkane predominances on the Amazon shelf and a Northeast Pacific hydrothermal system. *Naturwissenschaften*, 84(9):415–420.

Epstein, S., Buchsbaum, R., Lowenstam, H. A., and Urey, H. C. (1953). Revised carbonate-water isotopic temperature scale. *Geological Society of America Bulletin*, 64(11):1315.

Erez, J. and Luz, B. (1983). Experimental paleotemperature equation for planktonic foraminifera. *Geochimica et Cosmochimica Acta*, 47(6):1025–1031.

Fallet, U., Castaneda, I. S., Henry-Edwards, A., Richter, T. O., Boer, W., Schouten, S., and Brummer, G.-J. (2012). Sedimentation and burial of organic and inorganic temperature proxies in the Mozambique Channel, SW Indian Ocean. *Deep Sea Research Part I: Oceanographic Research Papers*, 59:37–53.

Fasolato, G., Ronco, P., and Silvio, G. D. (2006). The case of the Zambezi River in Mozambique. In *River Flow 2006*. Taylor Francis.

Fawley, K. P., Eliáš, M., and Fawley, M. W. (2014). The diversity and phylogeny of the commercially important algal class Eustigmatophyceae, including the new clade Goniochloridales. *Journal of Applied Phycology*, 26(4):1773–1782.

Fawley, K. P. and Fawley, M. W. (2007). Observations on the diversity and ecology of freshwater Nannochloropsis (Eustigmatophyceae), with descriptions of new taxa. *Protist*, 158(3):325–336.

Fekete, B. M., Vörösmarty, C. J., and Grabs, W. (1999). Global, composite runoff fields based on observed river discharge and simulated water balances. Fed. Inst. of Hydrology.

Ficken, K. J., Li, B., Swain, D. L., and Eglinton, G. (2000). An n-alkane proxy for the sedimentary input of submerged/floating freshwater aquatic macrophytes. *Organic Geochemistry*, 31(7-8):745–749.

Filley, T. R., Minard, R. D., and Hatcher, P. G. (1999). Tetramethylammonium hydroxide (TMAH) thermochemolysis: proposed mechanisms based upon the application of ^{13}C-labeled TMAH to a synthetic model lignin dimer. *Organic Geochemistry*, 30(7):607–621.

Foucault, A. and Stanley, D. J. (1989). Late Quaternary palaeoclimatic oscillations in East Africa recorded by heavy minerals in the Nile delta. *Nature*, 339(6219):44–46.

Freymond, C. V., Kündig, N., Stark, C., Peterse, F., Buggle, B., Lupker, M., Plötze, M., Blattmann, T. M., Filip, F., Giosan, L., and Eglinton, T. I. (2018). Evolution of biomolecular loadings along a major river system. *Geochimica et Cosmochimica Acta*, 223:389–404.

Freymond, C. V., Peterse, F., Fischer, L. V., Filip, F., Giosan, L., and Eglinton, T. I. (2017). Branched GDGT signals in fluvial sediments of the Danube River basin: Method comparison and longitudinal evolution. *Organic Geochemistry*, 103:88–96.

Fry, B. and Sherr, E. B. (1989). δ ^{13}C measurements as indicators of carbon flow in marine and freshwater ecosystems. In *Stable Isotopes in Ecological Research*, pages 196–229. Springer New York.

Gal, J.-K., Kim, J.-H., and Shin, K.-H. (2018). Distribution of long chain alkyl diols along a south-north transect of the northwestern Pacific region: insights into a paleo sea surface nutrient proxy. *Organic Geochemistry*, 119:80–90.

Gelin, F., Boogers, I., Noordeloos, A. A. M., Damste, J. S. S., Riegman, R., and Leeuw, J. W. D. (1997a). Resistant biomacromolecules in marine microalgae of the classes Eustigmatophyceae and Chlorophyceae: geochemical implications. *Organic Geochemistry*, 26(11-12):659–675.

Gelin, F., Volkman, J. K., Leeuw, J. W. D., and Damsté, J. S. S. (1997b). Mid-chain hydroxy long-chain fatty acids in microalgae from the genus Nannochloropsis. *Phytochemistry*, 45(4):641–646.

Gimeno, L., Drumond, A., Nieto, R., Trigo, R. M., and Stohl, A. (2010). On the origin of continental precipitation. *Geophysical Research Letters*, 37(13):n/a–n/a.

Gliozzi, A., Relini, A., and Chong, P. L.-G. (2002). Structure and permeability properties of biomimetic membranes of bolaform archaeal tetraether lipids. *Journal of Membrane Science*, 206(1-2):131–147.

Gliozzi, A., Rolandi, R., Rosa, M. D., and Gambacorta, A. (1983). Monolayer black membranes from bipolar lipids of archaebacteria and their temperature-induced structural changes. *The journal of Membrane Biology*, 75(1):45–56.

Gobarenko, S. A., Artenova, A. V., Golberg, E. L., and Vasilenko, Y. P. (2014). The response of the Okhotsk Sea environment to the orbital-millennium global climate changes during the Last Glacial Maximum, deglaciation and Holocene. *Global and planetary change*, 116:76–90.

Gogou, A. and Stephanou, E. G. (2004). Marine organic geochemistry of the Eastern Mediterranean. *Marine Chemistry*, 85(1-2):1–25.

Gong, C. and Hollander, D. J. (1999). Evidence for differential degradation of alkenones under contrasting bottom water oxygen conditions: implication for paleotemperature reconstruction. *Geochimica et Cosmochimica Acta*, 63(3-4):405–411.

Goni, M. A., Ruttenberg, K. C., and Eglinton, T. I. (1997). Sources and contribution of terrigenous organic carbon to surface sediments in the Gulf of Mexico. *Nature*, 389(6648):275–278.

Gorbarenko, S. A. (1996). Stable isotope and lithologic evidence of late-glacial and Holocene oceanography of the Northwestern Pacific and its marginal seas. *Quaternary Research*, 46(03):230–250.

Gorbarenko, S. A., Artemova, A. V., Goldberg, E. L., and Vasilenko, Y. P. (2014). The response of the Okhotsk Sea environment to the orbital-millennium global climate changes during the Last Glacial Maximum, deglaciation and Holocene. *Global and Planetary Change*, 116:76–90.

Gorbarenko, S. A., Goldberg, E. L., Kashgarian, M., Velivetskaya, T. A., Zakharkov, S. P., Pechnikov, V. S., Bosin, A. A., Psheneva, O. Y., and Ivanova, E. D. (2007). Millennium scale environment changes of the Okhotsk Sea during last 80 kyr and their phase relationship with global climate changes. *Journal of Oceanography*, 63(4):609–623.

Gorbarenko, S. A., Harada, N., Malakhov, M. I., Vasilenko, Y. P., Bosin, A. A., and Goldberg, E. L. (2010). Orbital and millennial-scale environmental and sedimentological changes in the Okhotsk Sea during the last 350kyr. *Global and Planetary Change*, 72(1-2):79–85.

Gorbarenko, S. A., Harada, N., Malakhov, M. I., Velivetskaya, T. A., Vasilenko, Y. P., Bosin, A. A., Derkachev, A. N., Goldberg, E. L., and Ignatiev, A. V. (2012). Responses of the Okhotsk Sea environment and sedimentology to global climate changes at the orbital and millennial scale during the last 350kyr. *Deep Sea Research Part II: Topical Studies in Oceanography*, 61-64:73–84.

Gorbarenko, S. A., Southon, J. R., Keigwin, L. D., Cherepanova, M. V., and Gvozdeva, I. G. (2004). Late Pleistocene–Holocene oceanographic variability in the Okhotsk Sea: geochemical, lithological and paleontological evidence. *Palaeogeography, Palaeoclimatology, Palaeoecology*, 209(1-4):281–301.

Goulding, M., Barthem, R., Ferreira, E. F. G., and Duenas, R. (2003). *The Smithsonian atlas of the Amazon*. Smithsonian Books Washington.

Grant, K. M., Rohling, E. J., Ramsey, C. B., Cheng, H., Edwards, R. L., Florindo, F., Heslop, D., Marra, F., Roberts, A. P., Tamisiea, M. E., and Williams, F. (2014). Sea-level variability over five glacial cycles. *Nature Communications*, 5(1).

Grossi, V., Blokker, P., and Damsté, J. S. S. (2001). Anaerobic biodegradation of lipids of the marine microalga Nannochloropsis salina. *Organic Geochemistry*, 32(6):795–808.

Guillou, L., Bachar, D., Audic, S., Bass, D., Berney, C., Bittner, L., Boutte, C., Burgaud, G., de Vargas, C., Decelle, J., del Campo, J., Dolan, J. R., Dunthorn, M., Edvardsen, B., Holzmann, M., Kooistra, W. H. C. F., Lara, E., Bescot, N. L., Logares, R., Mahé, F., Massana, R., Montresor, M., Morard, R., Not, F., Pawlowski, J., Probert, I., Sauvadet, A.-L., Siano, R., Stoeck, T., Vaulot, D., Zimmermann, P., and Christen, R. (2013). The Protist Ribosomal Reference database (PR2): a catalog of unicellular eukaryote Small Sub-Unit rRNA sequences with curated taxonomy. *Nucleic Acids Research*, 41(D1):D597–D604.

Guillou, L., Viprey, M., Chambouvet, A., Welsh, R. M., Kirkham, A. R., Massana, R., Scanlan, D. J., and Worden, A. Z. (2008). Widespread occurrence and genetic diversity of marine parasitoids belonging to Syndiniales(Alveolata). *Environmental Microbiology*, 10(12):3349–3365.

Gupta, L. P., Subramanian, V., and Ittekkot, V. (1997). Biogeochemistry of particulate organic matter transported by the Godavari River, India. *Biogeochemistry*, 38(2):103–128.

Haake, B., Ittekkot, V., Rixen, T., Ramaswamy, V., Nair, R. R., and Curry, W. B. (1993). Seasonality and interannual variability of particle fluxes to the deep Arabian sea. *Deep Sea Research Part I: Oceanographic Research Papers*, 40(7):1323–1344.

Hammer, O., Harper, D. A. T., and Ryan, P. D. (2001). PAST: Paleontological statistics software package for education and data analysis. *Palaeontologia Electronica*, 4(1):9.

Harada, N., Ahagon, N., Sakamoto, T., Uchida, M., Ikehara, M., and Shibata, Y. (2006). Rapid fluctuation of alkenone temperature in the southwestern Okhotsk Sea during the past 120 ky. *Global and Planetary Change*, 53(1-2):29–46.

Harada, N., Ahagon, N., Uchida, M., and Murayama, M. (2004). Northward and southward migrations of frontal zones during the past 40 kyr in the Kuroshio-Oyashio transition area. *Geochemistry, Geophysics, Geosystems*, 5(9):n/a–n/a.

Harada, N., Katsuki, K., Nakagawa, M., Matsumoto, A., Seki, O., Addison, J. A., Finney, B. P., and Sato, M. (2014). Holocene sea surface temperature and sea ice extent in the Okhotsk and Bering Seas. *Progress in Oceanography*, 126:242–253.

Harada, N., Sato, M., and Sakamoto, T. (2008). Freshwater impacts recorded in tetraunsaturated alkenones and alkenone sea surface temperatures from the Okhotsk Sea across millennial-scale cycles. *Paleoceanography*, 23(3):n/a–n/a.

Harada, N., Sato, M., Seki, O., Timmermann, A., Moossen, H., Bendle, J., Nakamura, Y., Kimoto, K., Okazaki, Y., Nagashima, K., Gorbarenko, S. A., Ijiri, A., Nakatsuka, T., Menviel, L., Chikamoto, M. O., Abe-Ouchi, A., and Schouten, S. (2012). Sea surface temperature changes in the Okhotsk Sea and adjacent North Pacific during the last glacial maximum and deglaciation. *Deep Sea Research Part II: Topical Studies in Oceanography*, 61-64:93–105.

Harger, J. (1995). Air-temperature variations and ENSO effects in Indonesia, the Philippines and El Salvador. ENSO patterns and changes from 1866–1993. *Atmospheric Environment*, 29(16):1919–1942.

Hatch, M. D. (1992). C_4 photosynthesis: an unlikely process full of surprises. *Plant and cell physiology*, 33(4):333–342.

Haven, H. L. T., Leeuw, J. W. D., Peakman, T. M., and Maxwell, J. R. (1986). Anomalies in steroid and hopanoid maturity indices. *Geochimica et Cosmochimica Acta*, 50(5):853–855.

Haven, H. L. T., Peakman, T. M., and Rullkötter, J. (1992). Early diagenetic transformation of higher-plant triterpenoids in deep-sea sediments from Baffin Bay. *Geochimica et Cosmochimica Acta*, 56(5):2001–2024.

Hays, J. D., Imbrie, J., and Shackleton, N. J. (1976). Variations in the Earth's orbit: pacemaker of the ice ages. *Science*, 194(4270):1121–1132.

Hays, J. D. and Morley, J. J. (2003). The Sea of Okhotsk: A window on the Ice Age Ocean. *Deep Sea Research Part I: Oceanographic Research Papers*, 50(12):1481–1506.

Hedges, J. I., Clark, W. A., Quay, P. D., Richey, J. E., Devol, A. H., and Santos, M. (1986). Compositions and fluxes of particulate organic material in the Amazon River. *Limnology and Oceanography*, 31(4):717–738.

Hedges, J. I., Keil, R. G., and Benner, R. (1997). What happens to terrestrial organic matter in the ocean? *Organic Geochemistry*, 27(5-6):195–212.

Hedges, J. I. and Oades, J. M. (1997). Comparative organic geochemistries of soils and marine sediments. *Organic Geochemistry*, 27(7-8):319–361.

Hemp, A. (2006). Continuum or zonation? Altitudinal gradients in the forest vegetation of Mt. Kilimanjaro. *Plant Ecology*, 184(1):27–42.

Ho, S. L., Mollenhauer, G., Fietz, S., Martínez-Garcia, A., Lamy, F., Rueda, G., Schipper, K., Méheust, M., Rosell-Melé, A., Stein, R., and Tiedemann, R. (2014). Appraisal of TEX_{86} TEX_{86}^{L} thermometries in subpolar and polar region. *Geochimica et Cosmochimica Acta*, 131:213–226.

Hoefs, M. J. L., Versteegh, G. J. M., Rijpstra, W. I. C., de Leeuw, J. W., and Damsté, J. S. S. (1998). Postdepositional oxic degradation of alkenones: implications for the measurement of palaeo sea surface temperatures. *Paleoceanography*, 13(1):42–49.

Hoffmann, T., Erkens, G., Gerlach, R., Klostermann, J., and Lang, A. (2009). Trends and controls of Holocene floodplain sedimentation in the Rhine catchment. *CATENA*, 77(2):96–106.

Holm-Hansen, O., Lorenzen, C. J., Holmes, R. W., and Strickland, J. D. H. (1965). Fluorometric determination of chlorophyll. *ICES Journal of Marine Science*, 30(1):3–15.

Hopmans, E. C., Schouten, S., and Damsté, J. S. S. (2016). The effect of improved chromatography on GDGT-based palaeoproxies. *Organic Geochemistry*, 93:1–6.

Hopmans, E. C., Weijers, J. W. H., Schefuß, E., Herfort, L., Damsté, J. S. S., and Schouten, S. (2004). A novel proxy for terrestrial organic matter in sediments based on branched and isoprenoid tetraether lipids. *Earth and Planetary Science Letters*, 224(1-2):107–116.

Huang, Y., Lockheart, M. J., Collister, J. W., and Eglinton, G. (1995). Molecular and isotopic biogeochemistry of the Miocene Clarkia Formation: hydrocarbons and alcohols. *Organic Geochemistry*, 23(9):785–801.

Huguet, C., Hopmans, E. C., Febo-Ayala, W., Thompson, D. H., Damsté, J. S. S., and Schouten, S. (2006). An improved method to determine the absolute abundance of glycerol dibiphytanyl glycerol tetraether lipids. *Organic Geochemistry*, 37(9):1036–1041.

Huguet, C., Schimmelmann, A., Thunell, R., Lourens, L. J., Damsté, J. S. S., and Schouten, S. (2007). A study of the TEX_{86} paleothermometer in the water column and sediments of the Santa Barbara Basin, California. *Paleoceanography*, 22(3).

Hurley, S. J., Elling, F. J., Könneke, M., Buchwald, C., Wankel, S. D., Santoro, A. E., Lipp, J. S., Hinrichs, K.-U., and Pearson, A. (2016). Influence of ammonia oxidation rate on thaumarchaeal lipid composition and the TEX86 temperature proxy. *Proceedings of the National Academy of Sciences*, 113(28):7762–7767.

Ishiwatari, R., Fujino, N., Brincat, D., Yamamoto, S., Takahara, H., Shichi, K., and Krivonogov, S. K. (2009). A 35kyr record of organic matter composition and δ13C of n-alkanes in bog sediments close to Lake Baikal: Implications for paleoenvironmental studies. *Organic Geochemistry*, 40(1):51–60.

Iwasaki, S., Takahashi, K., Maesawa, T., Sakamoto, T., Sakai, S., and Iijima, K. (2012). Paleoceanography of the last 500 kyrs in the central Okhotsk Sea based on geochemistry. *Deep Sea Research Part II: Topical Studies in Oceanography*, 61-64:50–62.

Jetter, R. (2000). Long-chain alkanediols from Myricaria germanica leaf cuticular waxes. *Phytochemistry*, 55(2):169–176.

Jetter, R. and Riederer, M. (1999). Long-chain alkanediols, ketoaldehydes, ketoalcohols and ketoalkyl esters in the cuticular waxes of Osmunda regalis fronds. *Phytochemistry*, 52(5):907–915.

Jetter, R., Riederer, M., Seyer, A., and Mioskowski, C. (1996). Homologous long-chain alkanediols from Papaver leaf cuticular waxes. *Phytochemistry*, 42(6):1617–1620.

Jonas, A.-S., Schwark, L., and Bauersachs, T. (2017). Late Quaternary water temperature variations of the Northwest Pacific based on the lipid paleothermometers TEX^{H}_{86}, UK'_{37} and LDI. *Deep Sea Research Part I: Oceanographic Research Papers*, 125:81–93.

Jonge, C. D., Hopmans, E. C., Stadnitskaia, A., Rijpstra, W. I. C., Hofland, R., Tegelaar, E., and Damsté, J. S. S. (2013). Identification of novel penta- and hexamethylated branched glycerol dialkyl glycerol tetraethers in peat using HPLC–MS2, GC–MS and GC–SMB-MS. *Organic Geochemistry*, 54:78–82.

Jonge, C. D., Hopmans, E. C., Zell, C. I., Kim, J.-H., Schouten, S., and Damsté, J. S. S. (2014a). Occurrence and abundance of 6-methyl branched glycerol dialkyl glycerol tetraethers in soils: implications for palaeoclimate reconstruction. *Geochimica et Cosmochimica Acta*, 141:97–112.

Jonge, C. D., Stadnitskaia, A., Fedotov, A., and Damsté, J. S. S. (2015a). Impact of riverine suspended particulate matter on the branched glycerol dialkyl glycerol tetraether composition of lakes: the outflow of the Selenga River in Lake Baikal (Russia). *Organic Geochemistry*, 83-84:241–252.

Jonge, C. D., Stadnitskaia, A., Hopmans, E. C., Cherkashov, G., Fedotov, A., and Damsté, J. S. S. (2014b). In situ produced branched glycerol dialkyl glycerol tetraethers in suspended particulate matter from the Yenisei River, Eastern Siberia. *Geochimica et Cosmochimica Acta*, 125:476–491.

Jonge, C. D., Stadnitskaia, A., Hopmans, E. C., Cherkashov, G., Fedotov, A., Streletskaya, I. D., Vasiliev, A. A., and Damsté, J. S. S. (2015b). Drastic changes in the distribution of branched tetraether lipids in suspended matter and sediments from the Yenisei River and Kara Sea (Siberia): implications for the use of brGDGT-based proxies in coastal marine sediments. *Geochimica et Cosmochimica Acta*, 165:200–225.

Junium, C. K., Meyers, S. R., and Arthur, M. A. (2018). Nitrogen cycle dynamics in the Late Cretaceous Greenhouse. *Earth and Planetary Science Letters*, 481:404–411.

Just, J., Schefuß, E., Kuhlmann, H., Stuut, J.-B. W., and Pätzold, J. (2014). Climate induced sub-basin source-area shifts of Zambezi River sediments over the past 17 ka. *Palaeogeography, Palaeoclimatology, Palaeoecology*, 410:190–199.

Kasper, S., van der Meer, M. T. J., Castaneda, I. S., Tjallingii, R., Brummer, G.-J. A., Damsté, J. S. S., and Schouten, S. (2015). Testing the alkenone D/H ratio as a paleo indicator of sea surface salinity in a coastal ocean margin (Mozambique Channel). *Organic Geochemistry*, 78:62–68.

Katsuki, K., Khim, B.-K., Itaki, T., Okazaki, Y., Ikehara, K., Shin, Y., Yoon, H. I., and Kang, C. Y. (2010). Sea-ice distribution and atmospheric pressure patterns in southwestern Okhotsk Sea since the Last Glacial Maximum. *Global and Planetary Change*, 72(3):99–107.

Khim, B.-K., Sakamoto, T., and Harada, N. (2012). Reconstruction of surface water conditions in the central region of the Okhotsk Sea during the last 180 kyrs. *Deep Sea Research Part II: Topical Studies in Oceanography*, 61-64:63–72.

Kim, J.-H., Buscail, R., Fanget, A.-S., Eyrolle-Boyer, F., Bassetti, M.-A., Dorhout, D., Baas, M., Berné, S., and Damsté, J. S. S. (2014). Impact of river channel shifts on tetraether lipids in the Rhône prodelta (NW Mediterranean): implication for the BIT index as an indicator of palaeoflood events. *Organic Geochemistry*, 75:99–108.

Kim, J.-H., Ludwig, W., Schouten, S., Kerhervé, P., Herfort, L., Bonnin, J., and Damsté, J. S. S. (2007). Impact of flood events on the transport of terrestrial organic matter to the ocean: a study of the Têt River (SW France) using the BIT index. *Organic Geochemistry*, 38(10):1593–1606.

Kim, J.-H., Schouten, S., Buscail, R., Ludwig, W., Bonnin, J., Damsté, J. S. S., and Bourrin, F. (2006). Origin and distribution of terrestrial organic matter in the NW Mediterranean (Gulf of Lions): exploring the newly developed BIT index. *Geochemistry, Geophysics, Geosystems*, 7(11):n/a–n/a.

Kim, J.-H., Schouten, S., Rodrigo-Gámiz, M., Rampen, S., Marino, G., Huguet, C., Helmke, P., Buscail, R., Hopmans, E. C., Pross, J., Sangiorgi, F., Middelburg, J. B. M., and Damsté, J. S. S. (2015). Influence of deep-water derived isoprenoid tetraether lipids on the TEX_{86}^{H} paleothermometer in the Mediterranean Sea. *Geochimica et Cosmochimica Acta*, 150:125–141.

Kim, J.-H., van der Meer, J., Schouten, S., Helmke, P., Willmott, V., Sangiorgi, F., Koç, N., Hopmans, E. C., and Damsté, J. S. S. (2010). New indices and calibrations derived from the distribution of crenarchaeal isoprenoid tetraether lipids: implications for past sea surface temperature reconstructions. *Geochimica et Cosmochimica Acta*, 74(16):4639–4654.

Kim, J. H., Zarzycka, B., Buscail, R., Peterse, F., Bonnin, J., Ludwig, W., Schouten, S., and Damsté, J. S. S. (2009). Contribution of river-borne soil organic carbon to the Gulf of Lions (NW Mediterranean). *Limnology and Oceanography*, 55(2):507–518.

Kim, J.-H., Zell, C., Moreira-Turcq, P., Pérez, M. A. P., Abril, G., Mortillaro, J.-M., Weijers, J. W. H., Meziane, T., and Damsté, J. S. S. (2012). Tracing soil organic carbon in the lower Amazon River and its tributaries using GDGT distributions and bulk organic matter properties. *Geochimica et Cosmochimica Acta*, 90:163–180.

Knies, J., Cabedo-Sanz, P., Belt, S. T., Baranwal, S., Fietz, S., and Rosell-Melé, A. (2014). The emergence of modern sea ice cover in the Arctic Ocean. *Nature Communications*, 5(1).

Koning, E., van Iperen, J. M., van Raaphorst, W., Helder, W., Brummer, G.-J. A., and van Weering, T. C. E. (2001). Selective preservation of upwelling-indicating diatoms in sediments off Somalia, NW Indian Ocean. *Deep Sea Research Part I: Oceanographic Research Papers*, 48(11):2473–2495.

Kotthoff, U., Groeneveld, J., Ash, J. L., Fanget, A.-S., Krupinski, N. Q., Peyron, O., Stepanova, A., Warnock, J., Helmond, N. A. G. M. V., Passey, B. H., Clausen, O. R., Bennike, O., Andrén, E., Granoszewski, W., Andrén, T., Filipsson, H. L., Seidenkrantz, M.-S., Slomp, C. P., and Bauersachs, T. (2017). Reconstructing Holocene temperature and salinity variations in the western Baltic Sea region: a multi-proxy comparison from the Little Belt (IODP Expedition 347, Site M0059). *Biogeosciences*, 14(23):5607–5632.

Kusch, S., Rethemeyer, J., Hopmans, E. C., Wacker, L., and Mollenhauer, G. (2016). Factors influencing ^{14}C concentrations of algal and archaeal lipids and their associated sea surface temperature proxies in the Black Sea. *Geochimica et Cosmochimica Acta*, 188:35–57.

Kusch, S., Rethemeyer, J., Schefuß, E., and Mollenhauer, G. (2010). Controls on the age of vascular plant biomarkers in Black Sea sediments. *Geochimica et Cosmochimica Acta*, 74(24):7031–7047.

la Torre, J. R. D., Walker, C. B., Ingalls, A. E., Könneke, M., and Stahl, D. A. (2008). Cultivation of a thermophilic ammonia oxidizing archaeon synthesizing crenarchaeol. *Environmental Microbiology*, 10(3):810–818.

Lammers, R. B. and Shiklomanov, A. I. (2000). R-ArcticNet, a regional hydrographic data network for the Pan-Arctic Region. *Water Systems Analysis Group, University of New Hampshire, distributed by the National Snow and Ice Data Center (data available at http://www. R-ArcticNET. sr. unh. edu), Durham*.

Lassiter, A. M., Wilkerson, F. P., Dugdale, R. C., and Hogue, V. E. (2006). Phytoplankton assemblages in the CoOP-WEST coastal upwelling area. *Deep Sea Research Part II: Topical Studies in Oceanography*, 53(25-26):3063–3077.

Lattaud, J., Dorhout, D., Schulz, H., Castaneda, I. S., Schefuß, E., Damsté, J. S. S., and Schouten, S. (2017a). The C_{32} alkane-1,15-diol as a proxy of late Quaternary riverine input in coastal margins. *Climate of the Past*, 13(8):1049–1061.

Lattaud, J., Kim, J.-H., Jonge, C. D., Zell, C., Damsté, J. S. S., and Schouten, S. (2017b). The C_{32} alkane-1,15-diol as a tracer for riverine input in coastal seas. *Geochimica et Cosmochimica Acta*, 202:146–158.

Lattaud, J., Kirkels, F., Peterse, F., Freymond, C. V., Eglinton, T. I., Hefter, J., Mollenhauer, G., Balzano, S., Villanueva, L., van der Meer, M. T. J., Hopmans, E. C., Damsté, J. S. S., and Schouten, S. (2018a). Long-chain diols in rivers: distribution and potential biological sources. *Biogeosciences*, 15(13):4147–4161.

Lattaud, J., Lo, L., Huang, J.-J., Chou, Y.-M., Gorbarenko, S. A., Damsté, J. S. S., and Schouten, S. (2018b). A comparison of Late Quaternary organic proxy-based paleotemperature records of the Central Sea of Okhotsk. *Paleoceanography and Paleoclimatology*.

Legendre, P. and Gallagher, E. D. (2001). Ecologically meaningful transformations for ordination of species data. *Oecologia*, 129(2):271–280.

Leinen, M., Cwienk, D., Heath, G. R., Biscaye, P. E., Kolla, V., Thiede, J., and Dauphin, J. P. (1986). Distribution of biogenic silica and quartz in recent deep-sea sediments. *Geology*, 14(3):199.

Lembke-Jene, L., Tiedemann, R., Nürnberg, D., Gong, X., and Lohmann, G. (2018). Rapid shift and millennial-scale variations in Holocene North Pacific Intermediate Water ventilation. *Proceedings of the National Academy of Sciences*, 115(21):5365–5370.

Lisiecki, L. E. and Raymo, M. E. (2005). A Pliocene-Pleistocene stack of 57 globally distributed benthic ^{18}O records. *Paleoceanography*, 20(1).

Liu, Y.-J., Song, S.-R., Lee, T.-Q., Lee, M.-Y., Chen, Y.-L., and Chen, H.-F. (2006). Mineralogical and geochemical changes in the sediments of the Okhotsk Sea during deglacial periods in the past 500 kyrs. *Global and Planetary Change*, 53(1-2):47–57.

Lo, L., Belt, S. T., Lattaud, J., Friedrich, T., Zeeden, C., Schouten, S., Smik, L., Timmermann, A., Cabedo-Sanz, P., Huang, J.-J., Zhou, L., Ou, T.-H., Chang, Y.-P., Wang, L.-C., Chou, Y.-M., Shen, C.-C., Chen, M.-T., Wei, K.-Y., Song, S.-R., Fang, T.-H., Gorbarenko, S. A., Wang, W.-L., Lee, T.-Q., Elderfield, H., and Hodell, D. A. (2018). Precession and atmospheric CO_2 modulated variability of sea ice in the central Okhotsk Sea since 130,000 years ago. *Earth and Planetary Science Letters*, 488:36–45.

Locarnini, R. A., Mishonov, A. V., Antonov, J. I., Boyer, T. P., and Garcia, H. E. (2009). World ocean atlas 2009, volume 1: Temperature. *NOAA Atlas NESDIS 68*.

Logares, R., Audic, S., Santini, S., Pernice, M. C., de Vargas, C., and Massana, R. (2012). Diversity patterns and activity of uncultured marine heterotrophic flagellates unveiled with pyrosequencing. *The ISME Journal*, 6(10):1823–1833.

Ludwig, C. H. (1971). *Lignins: occurrence, formation, structure and reactions*. Wiley intersciences.

Ludwig, W. (2004). ARB: a software environment for sequence data. *Nucleic Acids Research*, 32(4):1363–1371.

Malakhov, M. I., Gorbarenko, S. A., Malakhova, G. Y., Harada, N., Vasilenko, Y. P., Bosin, A. A., Gol'dberg, E. L., and Derkachev, A. N. (2009). Petromagnetic parameters of bottom sediments as indicators of the climatic and environmental changes in the central zone of the Sea of Okhotsk during the last 350 kyr. *Russian Geology and Geophysics*, 50(11):973–982.

Mao, S., Zhu, X., Wu, N., Jia, G., Sun, Y., Guan, H., and Wu, D. (2016). Alcohol compounds in Azolla imbricata and potential source implication for marine sediments. *Science China Earth Sciences*, 60(2):348–359.

Marie, D., Simon, N., and Vaulotl, D. (2005). Phytoplankton cell counting by flow cytometry. *Algal culturing techniques*, 1:253–267.

Martinez-Garcia, A., Rosell-Mele, A., McClymont, E. L., Gersonde, R., and Haug, G. H. (2010). Subpolar link to the emergence of the modern equatorial pacific cold tongue. *Science*, 328(5985):1550–1553.

Martrat, B., Jimenez-Amat, P., Zahn, R., and Grimalt, J. O. (2014). Similarities and dissimilarities between the last two deglaciations and interglaciations in the North Atlantic region. *Quaternary Science Reviews*, 99:122–134.

Massana, R., Gobet, A., Audic, S., Bass, D., Bittner, L., Boutte, C., Chambouvet, A., Christen, R., Claverie, J.-M., Decelle, J., Dolan, J. R., Dunthorn, M., Edvardsen, B., Forn, I., Forster, D., Guillou, L., Jaillon, O., Kooistra, W. H. C. F., Logares, R., Mahé, F., Not, F., Ogata, H., Pawlowski, J., Pernice, M. C., Probert, I., Romac, S., Richards, T., Santini, S., Shalchian-Tabrizi, K., Siano, R., Simon, N., Stoeck, T., Vaulot, D., Zingone, A., and de Vargas, C. (2015). Marine protist diversity in European coastal waters and sediments as revealed by high-throughput sequencing. *Environmental Microbiology*, 17(10):4035–4049.

McClymont, E. L., Rosell-Melé, A., Haug, G. H., and Lloyd, J. M. (2008). Expansion of subarctic water masses in the North Atlantic and Pacific oceans and implications for mid-Pleistocene ice sheet growth. *Paleoceanography*, 23(4).

McClymont, E. L., Sosdian, S. M., Rosell-Melé, A., and Rosenthal, Y. (2013). Pleistocene sea-surface temperature evolution: early cooling, delayed glacial intensification, and implications for the mid-Pleistocene climate transition. *Earth-Science Reviews*, 123:173–193.

Medina-Elizalde, M. (2005). The Mid-Pleistocene Transition in the tropical Pacific. *Science*, 310(5750):1009–1012.

Méjanelle, L., Sanchez-Gargallo, A., Bentaleb, I., and Grimalt, J. O. (2003). Long chain n -alkyl diols, hydroxy ketones and sterols in a marine eustigmatophyte, Nannochloropsis gaditana , and in Brachionus plicatilis feeding on the algae. *Organic Geochemistry*, 34(4):527–538.

Menot, G., Bard, E., Rostek, F., Weijers, J. W. H., Hopmans, E. C., Schouten, S., and Damste, J. S. S. (2006). Early reactivation of European rivers during the last deglaciation. *Science*, 313(5793):1623–1625.

Meyers, P. A. (1994). Preservation of elemental and isotopic source identification of sedimentary organic matter. *Chemical Geology*, 114(3-4):289–302.

Middelburg, J. J., Vlug, T., Jaco, F., and van der Nat, W. A. (1993). Organic matter mineralization in marine systems. *Global and Planetary Change*, 8(1-2):47–58.

Milliman, J. D. and Meade, R. H. (1983). World-wide delivery of river sediment to the oceans. *The Journal of Geology*, 91(1):1–21.

Müller, P. J., Kirst, G., Ruhland, G., von Storch, I., and Rosell-Melé, A. (1998). Calibration of the alkenone paleotemperature index $U_{37}K'$ based on core-tops from the eastern South Atlantic and the global ocean (60°N-60°S). *Geochimica et Cosmochimica Acta*, 62(10):1757–1772.

Moernaut, J., Verschuren, D., Charlet, F., Kristen, I., Fagot, M., and Batist, M. D. (2010). The seismic-stratigraphic record of lake-level fluctuations in Lake Challa: Hydrological stability and change in equatorial East Africa over the last 140kyr. *Earth and Planetary Science Letters*, 290(1-2):214–223.

Moita, M. T., Oliveira, P. B., Mendes, J. C., and Palma, A. S. (2003). Distribution of chlorophyll a and Gymnodinium catenatum associated with coastal upwelling plumes off central Portugal. *Acta Oecologica*, 24:S125–S132.

Mollenhauer, G., Eglinton, T. I., Hopmans, E. C., and Damsté, J. S. S. (2008). A radiocarbon-based assessment of the preservation characteristics of crenarchaeol and alkenones from continental margin sediments. *Organic Geochemistry*, 39(8):1039–1045.

Mollenhauer, G., Eglinton, T. I., Ohkouchi, N., Schneider, R. R., Müller, P. J., Grootes, P. M., and Rullkötter, J. (2003). Asynchronous alkenone and foraminifera records from the Benguela Upwelling System. *Geochimica et Cosmochimica Acta*, 67(12):2157–2171.

Molleri, G. S. F., de M. Novo, E. M. L., and Kampel, M. (2010). Space-time variability of the Amazon River plume based on satellite ocean color. *Continental Shelf Research*, 30(3-4):342–352.

Morris, R. J. and Brassell, S. C. (1988). Long-chain alkanediols: biological markers for cyanobacterial contributions to sediments. *Lipids*, 23(3):256–258.

Naafs, B. D. A., Hefter, J., and Stein, R. (2012). Application of the long chain diol index (LDI) paleothermometer to the early Pleistocene (MIS 96). *Organic Geochemistry*, 49:83–85.

Nakanowatari, T., Nakamura, T., Uchimoto, K., Uehara, H., Mitsudera, H., Ohshima, K. I., Hasumi, H., and Wakatsuchi, M. (2014). Causes of the multidecadal-scale warming of the Intermediate Water in the Okhotsk Sea and Western Subarctic North Pacific. *Journal of Climate*, 28(2):714–736.

Nakatsuka, T. (2004). Dissolved and particulate organic carbon in the Sea of Okhotsk: Transport from continental shelf to ocean interior. *Journal of Geophysical Research*, 109(C9).

Nehama, F. P. J. and Reason, C. J. C. (2014). Morphology of the Zambezi River plume in the Sofala Bank, Mozambique. *Western Indian Ocean Journal of Marine Science*, 13(1):1–10.

New, M., Lister, D., Hulme, M., and Makin, I. (2002). A high-resolution data set of surface climate over global land areas. *Climate Research*, 21:1–25.

Nicholson, S. E. (2009). A revised picture of the structure of the monsoon and land ITCZ over West Africa. *Climate Dynamics*, 32(7-8):1155–1171.

Nielsen, K. M., Johnsen, P. J., Bensasson, D., and Daffonchio, D. (2007). Release and persistence of extracellular DNA in the environment. *Environmental Biosafety Research*, 6(1-2):37–53.

Nieto-Moreno, V., Martínez-Ruiz, F., Willmott, V., García-Orellana, J., Masqué, P., and Damsté, J. S. S. (2013). Climate conditions in the westernmost Mediterranean over the last two millennia: an integrated biomarker approach. *Organic Geochemistry*, 55:1–10.

Not, F., del Campo, J., Balagué, V., de Vargas, C., and Massana, R. (2009). New insights into the diversity of marine picoeukaryotes. *PLoS ONE*, 4(9):e7143.

Nürnberg, D., Dethleff, D., Tiedemann, R., Kaiser, A., and Gorbarenko, S. A. (2011). Okhotsk Sea ice coverage and Kamchatka glaciation over the last 350 ka: evidence from ice-rafted debris and planktonic ^{18}O. *Palaeogeography, Palaeoclimatology, Palaeoecology*, 310(3-4):191–205.

Nürnberg, D. and Tiedemann, R. (2004). Environmental change in the Sea of Okhotsk during the last 1.1 million years. *Paleoceanography*, 19(4):n/a–n/a.

Oesch, D. C., Jaquet, J.-M., Hauser, A., and Wunderle, S. (2005). Lake surface water temperature retrieval using advanced very high resolution radiometer and moderate resolution imaging spectroradiometer data: validation and feasibility study. *Journal of Geophysical Research*, 110(C12).

Olivier, J.-M., Carre, G., Lamouroux, N., Dole-Olivier, M.-J., Malard, F., Bravard, J.-P., and Amoros, C. (2009). *Rivers of Europe*, chapter The Rone River basin, pages 247–295. Amsterdam: Academic Press.

Paerl, H. W. and Huisman, J. (2008). CLIMATE: Blooms like it hot. *Science*, 320(5872):57–58.

Pagani, M. (1999). Late Miocene atmospheric CO_2 concentrations and the expansion of C_4 grasses. *Science*, 285(5429):876–879.

Pancost, R. D., Boot, C. S., Aloisi, G., Maslin, M., Bickers, C., Ettwein, V., Bale, N., and Handley, L. (2009). Organic geochemical changes in Pliocene sediments of ODP Site 1083 (Benguela Upwelling System). *Palaeogeography, Palaeoclimatology, Palaeoecology*, 280(1-2):119–131.

Partridge, T. C., Demenocal, P. B., Lorentz, S. A., Paiker, M. J., and Vogel, J. C. (1997). Orbital forcing of climate over South Africa: A 200,000-year rainfall record from the pretoria saltpan. *Quaternary Science Reviews*, 16(10):1125–1133.

Payne, B. R. (1970). Water balance of Lake Chala and its relation to groundwater from tritium and stable isotope data. *Journal of Hydrology*, 11(1):47–58.

Peeters, F., Straile, D., Lorke, A., and Livingstone, D. M. (2007). Earlier onset of the spring phytoplankton bloom in lakes of the temperate zone in a warmer climate. *Global Change Biology*, 13(9):1898–1909.

Peterse, F., Hopmans, E. C., Schouten, S., Mets, A., Rijpstra, W. I. C., and Damsté, J. S. S. (2011). Identification and distribution of intact polar branched tetraether lipids in peat and soil. *Organic Geochemistry*, 42(9):1007–1015.

Peterse, F., Kim, J.-H., Schouten, S., Kristensen, D. K., Koç, N., and Damsté, J. S. S. (2009). Constraints on the application of the MBT/CBT palaeothermometer at high latitude environments (Svalbard, Norway). *Organic Geochemistry*, 40(6):692–699.

Peterse, F., van der Meer, J., Schouten, S., Weijers, J. W. H., Fierer, N., Jackson, R. B., Kim, J.-H., and Damsté, J. S. S. (2012). Revised calibration of the MBT–CBT paleotemperature proxy based on branched tetraether membrane lipids in surface soils. *Geochimica et Cosmochimica Acta*, 96:215–229.

Pfister, L., Kwadijk, J., Musy, A., Bronstert, A., and Hoffmann, L. (2004). Climate change, land use change and runoff prediction in the Rhine–Meuse basins. *River Research and Applications*, 20(3):229–241.

Pisias, N. G. and Moore, T. C. (1981). The evolution of Pleistocene climate: a time series approach. *Earth and Planetary Science Letters*, 52(2):450–458.

Pitcher, A., Villanueva, L., Hopmans, E. C., Schouten, S., Reichart, G.-J., and Damsté, J. S. S. (2011). Niche segregation of ammonia-oxidizing archaea and anammox bacteria in the Arabian Sea oxygen minimum zone. *The ISME Journal*, 5(12):1896–1904.

Plancq, J., Grossi, V., Pittet, B., Huguet, C., Rosell-Melé, A., and Mattioli, E. (2015). Multi-proxy constraints on sapropel formation during the late Pliocene of central Mediterranean (southwest Sicily). *Earth and Planetary Science Letters*, 420:30–44.

Plancq, J., Mattioli, E., Pittet, B., Simon, L., and Grossi, V. (2014). Productivity and sea-surface temperature changes recorded during the late Eocene–early Oligocene at DSDP Site 511 (South Atlantic). *Palaeogeography, Palaeoclimatology, Palaeoecology*, 407:34–44.

Ponton, C., West, A. J., Feakins, S. J., and Galy, V. (2014). Leaf wax biomarkers in transit record river catchment composition. *Geophysical Research Letters*, 41(18):6420–6427.

Pradhan, U. K., Wu, Y., Shirodkar, P. V., Zhang, J., and Zhang, G. (2014). Multi-proxy evidence for compositional change of organic matter in the largest tropical (peninsular) river basin of India. *Journal of Hydrology*, 519:999–1009.

Prahl, F. G., Muehlhausen, L. A., and Zahnle, D. L. (1988). Further evaluation of long-chain alkenones as indicators of paleoceanographic conditions. *Geochimica et Cosmochimica Acta*, 52(9):2303–2310.

Prahl, F. G., Sparrow, M. A., and Wolfe, G. V. (2003). Physiological impacts on alkenone paleothermometry. *Paleoceanography*, 18(2).

Prahl, F. G. and Wakeham, S. G. (1987). Calibration of unsaturation patterns in long-chain ketone compositions for palaeotemperature assessment. *Nature*, 330(6146):367–369.

Price, M. N., Dehal, P. S., and Arkin, A. P. (2009). FastTree: Computing large minimum evolution trees with profiles instead of a distance matrix. *Molecular Biology and Evolution*, 26(7):1641–1650.

Pätzold, J., Bohrmann, G., and Hübscher, C. (2003). Black Sea–Mediterranean–Red Sea: Cruise No. 52, Meteor-Beer. Univ. Hamburg.

Racovita, R. C. and Jetter, R. (2016). Identification of in-chain-functionalized compounds and methyl-branched alkanes in cuticular waxes of Triticum aestivum cv. Bethlehem. *PLOS ONE*, 11(11):e0165827.

Ragueneau, O., Schultes, S., Bidle, K., Claquin, P., and Moriceau, B. (2006). Si and C interactions in the world ocean: importance of ecological processes and implications for the role of diatoms in the biological pump. *Global Biogeochemical Cycles*, 20(4).

Ramasubramanian, R., Gnanappazham, L., Ravishankar, T., and Navamuniyammal, M. (2006). Mangroves of Godavari – analysis through remote sensing approach. *Wetlands Ecology and Management*, 14(1):29–37.

Rampen, S. W., Datema, M., Rodrigo-Gámiz, M., Schouten, S., Reichart, G.-J., and Damsté, J. S. S. (2014a). Sources and proxy potential of long chain alkyl diols in lacustrine environments. *Geochimica et Cosmochimica Acta*, 144:59–71.

Rampen, S. W., Schouten, S., and Damsté, J. S. S. (2011). Occurrence of long chain 1,14-diols in Apedinella radians. *Organic Geochemistry*, 42(5):572–574.

Rampen, S. W., Schouten, S., Koning, E., Brummer, G.-J. A., and Damsté, J. S. S. (2008). A 90 kyr upwelling record from the northwestern Indian Ocean using a novel long-chain diol index. *Earth and Planetary Science Letters*, 276(1-2):207–213.

Rampen, S. W., Schouten, S., Schefuß, E., and Damsté, J. S. S. (2009). Impact of temperature on long chain diol and mid-chain hydroxy methyl alkanoate composition in Proboscia diatoms: results from culture and field studies. *Organic Geochemistry*, 40(11):1124–1131.

Rampen, S. W., Schouten, S., Wakeham, S. G., and Damsté, J. S. S. (2007). Seasonal and spatial variation in the sources and fluxes of long chain diols and mid-chain hydroxy methyl alkanoates in the Arabian Sea. *Organic Geochemistry*, 38(2):165–179.

Rampen, S. W., Willmott, V., Kim, J.-H., Rodrigo-Gámiz, M., Uliana, E., Mollenhauer, G., Schefuß, E., Damsté, J. S. S., and Schouten, S. (2014b). Evaluation of long chain 1,14-alkyl diols in marine sediments as indicators for upwelling and temperature. *Organic Geochemistry*, 76:39–47.

Rampen, S. W., Willmott, V., Kim, J.-H., Uliana, E., Mollenhauer, G., Schefuß, E., Damsté, J. S. S., and Schouten, S. (2012). Long chain 1,13- and 1,15-diols as a potential proxy for palaeotemperature reconstruction. *Geochimica et Cosmochimica Acta*, 84:204–216.

Rao, K. N., Saito, Y., Nagakumar, K. C. V., Demudu, G., Rajawat, A. S., Kubo, S., and Li, Z. (2015). Palaeogeography and evolution of the Godavari delta, east coast of India during the Holocene: an example of wave-dominated and fan-delta settings. *Palaeogeography, Palaeoclimatology, Palaeoecology*, 440:213–233.

Raymo, M. E., Ruddiman, W. F., Shackleton, N. J., and Oppo, D. W. (1990). Evolution of Atlantic-Pacific δ13C gradients over the last 2.5 m.y. *Earth and Planetary Science Letters*, 97(3-4):353–368.

Reiche, S., Rampen, S. W., Dorhout, D. J. C., Damsté, J. S. S., and Schouten, S. (2018). The impact of oxygen exposure on long-chain alkyl diols and the long chain diol index (LDI) – a long-term incubation study. *Organic Geochemistry*, 124:238–246.

Riegman, R. (1995). Nutrient-related selection mechanisms in marine phytoplankton communities and the impact of eutrophication on the planktonic food web. *Water Science and Technology*, 32(4).

Riegman, R., de Boer, M., and de Senerpont Domis, L. (1996). Growth of harmful marine algae in multispecies cultures. *Journal of Plankton Research*, 18(10):1851–1866.

Rîmbu, N., Boroneanţ, C., Buţă, C., and Dima, M. (2002). Decadal variability of the Danube river flow in the lower basin and its relation with the North Atlantic Oscillation. *International Journal of Climatology*, 22(10):1169–1179.

Rimet, F., Bouchez, A., and Montuelle, B. (2015). Benthic diatoms and phytoplankton to assess nutrients in a large lake: Complementarity of their use in Lake Geneva (France–Switzerland). *Ecological Indicators*, 53:231–239.

Ritchie, J. C., Cwynar, L. C., and Spear, R. W. (1983). Evidence from north-west Canada for an early Holocene Milankovitch thermal maximum. *Nature*, 305(5930):126–128.

Robinson, N., Cranwell, P. A., Finlay, B. J., and Eglinton, G. (1984). Lipids of aquatic organisms as potential contributors to lacustrine sediments. *Organic Geochemistry*, 6:143–152.

Robinson, N., Eglinton, G., Cranwell, P. A., and Zeng, Y. B. (1989). Messel oil shale (western Germany): Assessment of depositional palaeoenvironment from the content of biological marker compounds. *Chemical Geology*, 76(1-2):153–173.

Rodrigo-Gámiz, M., Martínez-Ruiz, F., Rampen, S. W., Schouten, S., and Damsté, J. S. S. (2014). Sea surface temperature variations in the western Mediterranean Sea over the last 20 kyr: a dual-organic proxy (UK' $_{37}$ and LDI) approach. *Paleoceanography*, 29(2):87–98.

Rodrigo-Gámiz, M., Rampen, S. W., de Haas, H., Baas, M., Schouten, S., and Damsté, J. S. S. (2015). Constraints on the applicability of the organic temperature proxies $U_{37}k'$, TEX_{86} and LDI in the subpolar region around Iceland. *Biogeosciences*, 12(22):6573–6590.

Rodrigo-Gámiz, M., Rampen, S. W., Schouten, S., and Damsté, J. S. S. (2016). The impact of oxic degradation on long chain alkyl diol distributions in Arabian Sea surface sediments. *Organic Geochemistry*, 100:1–9.

Rohling, E. J., Foster, G. L., Grant, K. M., Marino, G., Roberts, A. P., Tamisiea, M. E., and Williams, F. (2014). Sea-level and deep-sea-temperature variability over the past 5.3 million years. *Nature*, 508(7497):477–482.

Romero-Viana, L., Kienel, U., and Sachse, D. (2012). Lipid biomarker signatures in a hypersaline lake on Isabel Island (Eastern Pacific) as a proxy for past rainfall anomaly (1942–2006AD). *Palaeogeography, Palaeoclimatology, Palaeoecology*, 350-352:49–61.

Rommerskirchen, F., Plader, A., Eglinton, G., Chikaraishi, Y., and Rullkötter, J. (2006). Chemotaxonomic significance of distribution and stable carbon isotopic composition of long-chain alkanes and alkan-1-ols in C_4 grass waxes. *Organic Geochemistry*, 37(10):1303–1332.

Rontani, J.-F., Volkman, J. K., Prahl, F. G., and Wakeham, S. G. (2013). Biotic and abiotic degradation of alkenones and implications for paleoproxy applications: a review. *Organic Geochemistry*, 59:95–113.

Rosell-Melé, A. (1998). Interhemispheric appraisal of the value of alkenone indices as temperature and salinity proxies in high-latitude locations. *Paleoceanography*, 13(6):694–703.

Rosell-Melé, A., Eglinton, G., Pflaumann, U., and Sarnthein, M. (1995). Atlantic core-top calibration of the U37K index as a sea-surface palaeotemperature indicator. *Geochimica et Cosmochimica Acta*, 59(15):3099–3107.

Rossignol-Strick, M., Nesteroff, W., Olive, P., and Vergnaud-Grazzini, C. (1982). After the deluge: Mediterranean stagnation and sapropel formation. *Nature*, 295(5845):105–110.

Rozanski, K., Araguás-Araguás, L., and Gonfiantini, R. (1993). Isotopic patterns in modern global precipitation. In *Climate Change in Continental Isotopic Records*, pages 1–36. American Geophysical Union.

Ruan, J., Xu, Y., Ding, S., Wang, Y., and Zhang, X. (2017). A biomarker record of temperature and phytoplankton community structure in the Okinawa Trough since the last glacial maximum. *Quaternary Research*, 88(01):89–97.

Sabatier, F., Maillet, G., Provansal, M., Fleury, T.-J., Suanez, S., and Vella, C. (2006). Sediment budget of the Rhône delta shoreface since the middle of the 19th century. *Marine Geology*, 234(1-4):143–157.

Sakamoto, T., Ikehara, M., Aoki, K., Iijima, K., Kimura, N., Nakatsuka, T., and Wakatsuchi, M. (2005). Ice-rafted debris (IRD)-based sea-ice expansion events during the past 100kyrs in the Okhotsk Sea. *Deep Sea Research Part II: Topical Studies in Oceanography*, 52(16-18):2275–2301.

Sakamoto, T., Ikehara, M., Uchida, M., Aoki, K., Shibata, Y., Kanamatsu, T., Harada, N., Iijima, K., Katsuki, K., and Asahi, H. (2006). Millennial-scale variations of sea-ice expansion in the southwestern part of the Okhotsk Sea during the past 120 kyr: Age model and ice-rafted debris in IMAGES core MD01-2412. *Global and Planetary Change*, 53(1-2):58–77.

Sakka, A., Legendre, L., Gosselin, M., Leblanc, B., Delesalle, B., and Price, N. (1999). Nitrate, phosphate, and iron limitation of the phytoplankton assemblage in the lagoon of Takapoto Atoll (Tuamotu Archipelago, French Polynesia). *Aquatic microbial ecology*, 19:149–161.

Salonen, J. S., Seppä, H., Väliranta, M., Jones, V. J., Self, A., Heikkilä, M., Kultti, S., and Yang, H. (2011). The Holocene thermal maximum and late-Holocene cooling in the tundra of NE European Russia. *Quaternary Research*, 75(03):501–511.

Santoferrara, L. F., Alder, V. V., and McManus, G. B. (2017). Phylogeny, classification and diversity of Choreotrichia and Oligotrichia (Ciliophora, Spirotrichea). *Molecular Phylogenetics and Evolution*, 112:12–22.

Sarma, V. V. S. S., Gupta, S. N. M., Babu, P. V. R., Acharya, T., Harikrishnachari, N., Vishnuvardhan, K., Rao, N. S., Reddy, N. P. C., Sarma, V. V., Sadhuram, Y., Murty, T. V. R., and Kumar, M. D. (2009). Influence of river discharge on plankton metabolic rates in the tropical monsoon driven Godavari estuary, India. *Estuarine, Coastal and Shelf Science*, 85(4):515–524.

Sarma, V. V. S. S., Prasad, V. R., Kumar, B. S. K., Rajeev, K., Devi, B. M. M., Reddy, N. P. C., Sarma, V. V., and Kumar, M. D. (2010). Intra-annual variability in nutrients in the Godavari estuary, India. *Continental Shelf Research*, 30(19):2005–2014.

Schefuß, E., Damsté, J. S. S., and Jansen, J. H. F. (2004). Forcing of tropical Atlantic sea surface temperatures during the mid-Pleistocene transition. *Paleoceanography*, 19(4).

Schefuß, E., Kuhlmann, H., Mollenhauer, G., Prange, M., and Pätzold, J. (2011). Forcing of wet phases in southeast Africa over the past 17,000 years. *Nature*, 480(7378):509–512.

Schlesinger, W. H. and Melack, J. M. (1981). Transport of organic carbon in the world's rivers. *Tellus*, 33(2):172–187.

Schlitzer, R. (2002). Interactive analysis and visualization of geoscience data with Ocean Data View. *Computers & Geosciences*, 28(10):1211–1218.

Schmidt, F., Hinrichs, K.-U., and Elvert, M. (2010). Sources, transport, and partitioning of organic matter at a highly dynamic continental margin. *Marine Chemistry*, 118(1-2):37–55.

Scholz, M. J., Weiss, T. L., Jinkerson, R. E., Jing, J., Roth, R., Goodenough, U., Posewitz, M. C., and Gerken, H. G. (2014). Ultrastructure and composition of the Nannochloropsis gaditana cell wall. *Eukaryotic Cell*, 13(11):1450–1464.

Schouten, S., Hopmans, E. C., and Damsté, J. S. S. (2013). The organic geochemistry of glycerol dialkyl glycerol tetraether lipids: a review. *Organic Geochemistry*, 54:19–61.

Schouten, S., Hopmans, E. C., Schefuß, E., and Damsté, J. S. S. (2002). Distributional variations in marine crenarchaeotal membrane lipids: a new tool for reconstructing ancient sea water temperatures? *Earth and Planetary Science Letters*, 204(1-2):265–274.

Schouten, S., Ossebaar, J., Schreiber, K., Kienhuis, M. V. M., Langer, G., and Bijma, J. (2006). The effect of temperature and salinity on the stable hydrogen isotopic composition of long chain alkenones produced by Emiliania huxleyi and Gephyrocapsa oceanica. *Biogeosciences Discussions*, 2(6):1681–1695.

Schulz, H., Lückge, A., Emeis, K.-C., and Mackensen, A. (2011). Variability of Holocene to Late Pleistocene Zambezi riverine sedimentation at the upper continental slope off Mozambique, 15°–21°S. *Marine Geology*, 286(1-4):21–34.

Seki, O., Bendle, J. A., Harada, N., Kobayashi, M., Sawada, K., Moossen, H., Inglis, G. N., Nagao, S., and Sakamoto, T. (2014a). Assessment and calibration of TEX_{86} paleothermometry in the Sea of Okhotsk and sub-polar North Pacific region: implications for paleoceanography. *Progress in Oceanography*, 126:254–266.

Seki, O., Ikehara, M., Kawamura, K., Nakatsuka, T., Ohnishi, K., Wakatsuchi, M., Narita, H., and Sakamoto, T. (2004a). Reconstruction of paleoproductivity in the Sea of Okhotsk over the last 30 kyr. *Paleoceanography*, 19(1).

Seki, O., Kawamura, K., Ikehara, M., Nakatsuka, T., and Oba, T. (2004b). Variation of alkenone sea surface temperature in the Sea of Okhotsk over the last 85 kyrs. *Organic Geochemistry*, 35(3):347–354.

Seki, O., Mikami, Y., Nagao, S., Bendle, J. A., Nakatsuka, T., Kim, V. I., Shesterkin, V. P., Makinov, A. N., Fukushima, M., Moossen, H. M., and Schouten, S. (2014b). Lignin phenols and BIT index distributions in the Amur River and the Sea of Okhotsk: Implications for the source and transport of particulate terrestrial organic matter to the ocean. *Progress in Oceanography*, 126:146–154.

Seki, O., Nakatsuka, T., Kawamura, K., Saitoh, S.-I., and Wakatsuchi, M. (2007). Time-series sediment trap record of alkenones from the western Sea of Okhotsk. *Marine Chemistry*, 104(3-4):253–265.

Seki, O., Sakamoto, T., Sakai, S., Schouten, S., Hopmans, E. C., Damste, J. S. S., and Pancost, R. D. (2009). Large changes in seasonal sea ice distribution and productivity in the Sea of Okhotsk during the deglaciations. *Geochemistry, Geophysics, Geosystems*, 10(10).

Seki, O., Schmidt, D. N., Schouten, S., Hopmans, E. C., Damsté, J. S. S., and Pancost, R. D. (2012). Paleoceanographic changes in the Eastern Equatorial Pacific over the last 10 Myr. *Paleoceanography*, 27(3).

Seoane, S., Laza, A., Urrutxurtu, I., and Orive, E. (2005). Phytoplankton assemblages and their dominant pigments in the Nervion River Estuary. *Hydrobiologia*, 549(1):1–13.

Shackleton, N. J. and Opdyke, N. D. (1973). Oxygen isotope and palaeomagnetic stratigraphy of equatorial Pacific core V28-238: Oxygen isotope temperatures and ice volumes on a 105 year and 106 year scale. *Quaternary Research*, 3(01):39–55.

Shackleton, N. J. and Opdyke, N. D. (1976). Oxygen-isotope and paleomagnetic stratigraphy of Pacific core V28-239 Late Pliocene to Latest Pleistocene. In *Geological Society of America Memoirs*, pages 449–464. Geological Society of America.

Shackleton, N. J., Sánchez-Goni, M. F., Pailler, D., and Lancelot, Y. (2003). Marine Isotope Substage 5e and the Eemian Interglacial. *Global and Planetary Change*, 36(3):151–155.

Shanchun, J., O'Leary, T., Volkman, J. K., Huizhi, Z., Rongfen, J., Suhua, Y., Yan, W., Zuofeng, L., Zuoqing, S., and Ronghua, J. (1994). Origins and simulated thermal alteration of sterols and keto-alcohols in deep-sea marine sediments of the Okinawa Trough. *Organic Geochemistry*, 21(3-4):415–422.

Shi, X. L., Marie, D., Jardillier, L., Scanlan, D. J., and Vaulot, D. (2009). Groups without cultured representatives dominate Eukaryotic picophytoplankton in the oligotrophic South East Pacific Ocean. *PLoS ONE*, 4(10):e7657.

Shiga, K. and Koizumi, I. (1999). Latest Quaternary oceanographic changes in the Okhotsk Sea based on diatom records. *Marine Micropaleontology*, 38(2):91–117.

Shimada, C. and Hasegawa, S. (2001). Paleoceanographic implications of a 90,000 year long diatom record in piston core KH94-3, LM-8 off NE Japan. *Marine Micropaleontology*, 41(3-4):153–166.

Shimokawara, M., Nishimura, M., Matsuda, T., Akiyama, N., and Kawai, T. (2010). Bound forms, compositional features, major sources and diagenesis of long chain, alkyl mid-chain diols in Lake Baikal sediments over the past 28,000 years. *Organic Geochemistry*, 41(8):753–766.

Shintani, T., Yamamoto, M., and Chen, M.-T. (2011). Paleoenvironmental changes in the northern South China Sea over the past 28,000years: a study of TEX_{86}-derived sea surface temperatures and terrestrial biomarkers. *Journal of Asian Earth Sciences*, 40(6):1221–1229.

Sicre, M.-A., Bard, E., Ezat, U., and Rostek, F. (2002). Alkenone distributions in the North Atlantic and Nordic sea surface waters. *Geochemistry, Geophysics, Geosystems*, 3(2):1–13.

Siddall, M., Bard, E., Rohling, E. J., and Hemleben, C. (2006). Sea-level reversal during Termination II. *Geology*, 34(10):817.

Sikes, E. L., O'Leary, T., Nodder, S. D., and Volkman, J. K. (2005). Alkenone temperature records and biomarker flux at the subtropical front on the chatham rise, SW Pacific Ocean. *Deep Sea Research Part I: Oceanographic Research Papers*, 52(5):721–748.

Sikes, E. L., Volkman, J. K., Robertson, L. G., and Pichon, J.-J. (1997). Alkenones and alkenes in surface waters and sediments of the Southern Ocean: implications for paleotemperature estimation in polar regions. *Geochimica et Cosmochimica Acta*, 61(7):1495–1505.

Sinniger, F., Pawlowski, J., Harii, S., Gooday, A. J., Yamamoto, H., Chevaldonné, P., Cedhagen, T., Carvalho, G., and Creer, S. (2016). Worldwide analysis of sedimentary DNA rrveals major gaps in taxonomic knowledge of deep-sea benthos. *Frontiers in Marine Science*, 3.

Sinninghe Damsté, J. S. (2016). Spatial heterogeneity of sources of branched tetraethers in shelf systems: the geochemistry of tetraethers in the Berau River delta (Kalimantan, Indonesia). *Geochimica et Cosmochimica Acta*, 186:13–31.

Sinninghe Damsté, J. S., Ossebaar, J., Abbas, B., Schouten, S., and Verschuren, D. (2009). Fluxes and distribution of tetraether lipids in an equatorial African lake: Constraints on the application of the TEX86 palaeothermometer and BIT index in lacustrine settings. *Geochimica et Cosmochimica Acta*, 73(14):4232–4249.

Sinninghe Damsté, J. S., Rampen, S., Irene, W., Rijpstra, C., Abbas, B., Muyzer, G., and Schouten, S. (2003). A diatomaceous origin for long-chain diols and mid-chain hydroxy methyl alkanoates widely occurring in quaternary marine sediments: indicators for high-nutrient conditions. *Geochimica et Cosmochimica Acta*, 67(7):1339–1348.

Sinninghe Damsté, J. S., Schouten, S., Hopmans, E. C., van Duin, A. C. T., and Geenevasen, J. A. J. (2002). Crenarchaeol the characteristic core glycerol dibiphytanyl glycerol tetraether membrane lipid of cosmopolitan pelagic crenarchaeota. *Journal of Lipid Research*, 43(10):1641–1651.

Slapeta, J., Moreira, D., and Lopez-Garcia, P. (2005). The extent of protist diversity: insights from molecular ecology of freshwater eukaryotes. *Proceedings of the Royal Society B: Biological Sciences*, 272(1576):2073–2081.

Sluijs, A., van Roij, L., Frieling, J., Laks, J., and Reichart, G.-J. (2018). Single-species dinoflagellate cyst carbon isotope ecology across the Paleocene-Eocene Thermal Maximum. *Geology*, 46(1):79–82.

Smith, D. J., Eglinton, G., and Morris, R. J. (1983). The lipid chemistry of an interfacial sediment from the Peru Continental Shelf: Fatty acids, alcohols, aliphatic ketones and hydrocarbons. *Geochimica et Cosmochimica Acta*, 47(12):2225–2232.

Smith, M., Deckker, P. D., Rogers, J., Brocks, J., Hope, J., Schmidt, S., dos Santos, R. L., and Schouten, S. (2013). Comparison of TEX_{86}, and LDI temperature proxies for reconstruction of south-east Australian ocean temperatures. *Organic Geochemistry*, 64:94–104.

Smith, R. W., Bianchi, T. S., and Li, X. (2012). A re-evaluation of the use of branched GDGTs as terrestrial biomarkers: implications for the BIT Index. *Geochimica et Cosmochimica Acta*, 80:14–29.

Smith, R. Y., Greenwood, D. R., and Basinger, J. F. (2010). Estimating paleoatmospheric pCO_2 during the Early Eocene Climatic Optimum from stomatal frequency of Ginkgo, Okanagan Highlands, British Columbia, Canada. *Palaeogeography, Palaeoclimatology, Palaeoecology*, 293(1-2):120–131.

Sorokin, Y. (1999). Production in the Sea of Okhotsk. *Journal of Plankton Research*, 21(2):201–230.

Speelman, E. N., Reichart, G.-J., de Leeuw, J. W., Rijpstra, W. I. C., and Damsté, J. S. S. (2009). Biomarker lipids of the freshwater fern Azolla and its fossil counterpart from the Eocene Arctic Ocean. *Organic Geochemistry*, 40(5):628–637.

Stock, A., Jürgens, K., Bunge, J., and Stoeck, T. (2009). Protistan diversity in suboxic and anoxic waters of the Gotland Deep (Baltic Sea) as revealed by 18S rRNA clone libraries. *Aquatic Microbial Ecology*, 55:267–284.

Stoeck, T., Bass, D., Nebel, M., Christen, R., Jones, M. D. M., Breiner, H.-W., and Richards, T. A. (2010). Multiple marker parallel tag environmental DNA sequencing reveals a highly complex eukaryotic community in marine anoxic water. *Molecular Ecology*, 19:21–31.

Stoeck, T., Behnke, A., Christen, R., Amaral-Zettler, L., Rodriguez-Mora, M. J., Chistoserdov, A., Orsi, W., and Edgcomb, V. P. (2009). Massively parallel tag sequencing reveals the complexity of anaerobic marine protistan communities. *BMC Biology*, 7(1):72.

Syvitski, J. P. M. and Saito, Y. (2007). Morphodynamics of deltas under the influence of humans. *Global and Planetary Change*, 57(3-4):261–282.

Takahashi, K., Jordan, R., and Priddle, J. (1994). The diatom genus Proboscia in subartic waters. *Diatom Research*, 9(2):411–428.

Takahashi, K., Revelo, A. C., and Zarikian, C. A. A. (2011). Expedition 323 summary. In *Proceedings of the IODP, 323*. Integrated Ocean Drilling Program.

Tamura, K., Dudley, J., Nei, M., and Kumar, S. (2007). MEGA4: Molecular Evolutionary Genetics Analysis (MEGA) Software Version 4.0. *Molecular Biology and Evolution*, 24(8):1596–1599.

Tegelaar, E. W., de Leeuw, J. W., Derenne, S., and Largeau, C. (1989). A reappraisal of kerogen formation. *Geochimica et Cosmochimica Acta*, 53(11):3103–3106.

Telang, S. A., Pocklington, R., Naidu, A. S., Romankevich, E. A., Gitelson, I. I., and Gladyshev, M. I. (1991). *Biogeochemistry of major world rivers*, chapter Carbon and mineral transport in major North American, Russian, and Siberian rivers: the St Lawrence, the Mackenzie, the Yukon, the Arctic Alaskan rivers, the Arctic Basin rivers, and the Yenisei, pages 75–104. Wiley & Sons.

Ternois, Y., Kawamura, K., Keigwin, L., Ohkouchi, N., and Nakatsuka, T. (2001). A biomarker approach for assessing marine and terrigenous inputs to the sediments of Sea of Okhotsk for the last 27,000 years. *Geochimica et Cosmochimica Acta*, 65(5):791–802.

Thill, A., Moustier, S., Garnier, J.-M., Estournel, C., Naudin, J.-J., and Bottero, J.-Y. (2001). Evolution of particle size and concentration in the Rhône river mixing zone:. *Continental Shelf Research*, 21(18-19):2127–2140.

Thomas, D. S. G., Bailey, R., Shaw, P. A., Durcan, J. A., and Singarayer, J. S. (2009). Late Quaternary highstands at Lake Chilwa, Malawi: frequency, timing and possible forcing mechanisms in the last 44ka. *Quaternary Science Reviews*, 28(5-6):526–539.

Thomsen, C., Schulz-Bull, D. E., Petrick, G., and Duinker, J. C. (1998). Seasonal variability of the long-chain alkenone flux and the effect on the U37k′-index in the Norwegian Sea. *Organic Geochemistry*, 28(5):311–323.

Tierney, J. E., Russell, J. M., Damsté, J. S. S., Huang, Y., and Verschuren, D. (2011). Late Quaternary behavior of the East African monsoon and the importance of the Congo Air Boundary. *Quaternary Science Reviews*, 30(7-8):798–807.

Tierney, J. E., Russell, J. M., Huang, Y., Damste, J. S. S., Hopmans, E. C., and Cohen, A. S. (2008). Northern hemisphere controls on tropical Southeast African climate during the past 60,000 years. *Science*, 322(5899):252–255.

Tierney, J. E. and Tingley, M. P. (2015). A TEX_{86} surface sediment database and extended Bayesian calibration. *Scientific Data*, 2:150029.

Tierney, J. E. and Tingley, M. P. (2018). BAYSPLINE: a new calibration for the alkenone paleothermometer. *Paleoceanography and Paleoclimatology*, 33(3):281–301.

Tolmazin, D. (1985). Changing coastal oceanography of the Black Sea. I: Northwestern shelf. *Progress in Oceanography*, 15(4):217–276.

Tsoy, I. B., Obrezkova, M. S., and Artemova, A. V. (2009). Diatoms in surface sediments of the Sea of Okhotsk and the northwest Pacific Ocean. *Oceanology*, 49(1):130–139.

Tsunogai, S., Ono, T., and Watanabe, S. (1993). Increase in total carbonate in the western North Pacific water and a hypothesis on the missing sink of anthropogenic carbon. *Journal of Oceanography*, 49(3):305–315.

Usman, M. O., Kirkels, F. M. S. A., Zwart, H. M., Basu, S., Ponton, C., Blattmann, T. M., Ploetze, M., Haghipour, N., McIntyre, C., Peterse, F., Lupker, M., Giosan, L., and Eglinton, T. I. (2018). Reconciling drainage and receiving basin signatures of the godavari river system. *Biogeosciences*, 15(11):3357–3375.

van Bree, L. G. J., Peterse, F., van der Meer, M. T. J., Middelburg, J. J., Negash, A. M. D., Crop, W. D., Cocquyt, C., Wieringa, J. J., Verschuren, D., and Sinninghe Damsté, J. S. (2018). Seasonal variability in the abundance and stable carbon-isotopic composition of lipid biomarkers in suspended particulate matter from a stratified equatorial lake (Lake Chala, Kenya/Tanzania): Implications for the sedimentary record. *Quaternary Science Reviews*, 192:208–224.

van der Lubbe, H. J. L., Frank, M., Tjallingii, R., and Schneider, R. R. (2016). Neodymium isotope constraints on provenance, dispersal, and climate-driven supply of Zambezi sediments along the Mozambique Margin during the past ~45,000 years. *Geochemistry, Geophysics, Geosystems*, 17(1):181–198.

van der Lubbe, J. J. L., Tjallingii, R., Prins, M. A., Brummer, G.-J. A., Jung, S. J. A., Kroon, D., and Schneider, R. R. (2014). Sedimentation patterns off the Zambezi River over the last 20,000years. *Marine Geology*, 355:189–201.

van der Meer, M. T. J., Benthien, A., Bijma, J., Schouten, S., and Damsté, J. S. S. (2013). Alkenone distribution impacts the hydrogen isotopic composition of the $C_{37:2}$ and $C_{37:3}$ alkan-2-ones in Emiliania huxleyi. *Geochimica et Cosmochimica Acta*, 111:162–166.

Verschuren, D., Sinninghe Damsté, J. S., Moernaut, J., Kristen, I., Blaauw, M., Fagot, M., and Haug, G. H. (2009). Half-precessional dynamics of monsoon rainfall near the East African Equator. *Nature*, 462(7273):637–641.

Versteegh, G. J. M., Bosch, H.-J., and Leeuw, J. W. D. (1997). Potential palaeoenvironmental information of C_{24} to C_{36} mid-chain diols, keto-ols and mid-chain hydroxy fatty acids: a critical review. *Organic Geochemistry*, 27(1-2):1–13.

Versteegh, G. J. M., Jansen, J. H. F., Schneider, R. R., and Leeuw, J. W. D. (2000). Mid-chain diols and keto-ols in se atlantic sediments: a new tool for tracing past sea surface water masses? *Geochimica et Cosmochimica Acta*, 64(11):1879–1892.

Villanueva, L., Besseling, M., Rodrigo-Gámiz, M., Rampen, S. W., Verschuren, D., and Damsté, J. S. S. (2014). Potential biological sources of long chain alkyl diols in a lacustrine system. *Organic Geochemistry*, 68:27–30.

Volkman, J. K. (1986). A review of sterol markers for marine and terrigenous organic matter. *Organic Geochemistry*, 9(2):83–99.

Volkman, J. K., Barrett, S. M., and Blackburn, S. I. (1999). Eustigmatophyte microalgae are potential sources of C_{29} sterols, C_{22} - C_{28} n-alcohols and C_{28} - C_{32} n-alkyl diols in freshwater environments. *Organic Geochemistry*, 30(5):307–318.

Volkman, J. K., Barrett, S. M., Dunstan, G. A., and Jeffrey, S. W. (1992). C_{30}-C_{32} alkyl diols and unsaturated alcohols in microalgae of the class Eustigmatophyceae. *Organic Geochemistry*, 18(1):131–138.

Volkman, J. K., Eglinton, G., Corner, E. D. S., and Forsberg, T. E. V. (1980). Long-chain alkenes and alkenones in the marine coccolithophorid Emiliania huxleyi. *Phytochemistry*, 19(12):2619–2622.

Waelbroeck, C., Labeyrie, L., Michel, E., Duplessy, J. C., McManus, J. F., Lambeck, K., Balbon, E., and Labracherie, M. (2002). Sea-level and deep water temperature changes derived from benthic foraminifera isotopic records. *Quaternary Science Reviews*, 21(1-3):295–305.

Wakatsuchi, M. and Martin, S. (1991). Water circulation in the kuril basin of the Okhotsk Sea and its relation to eddy formation. *Journal of the Oceanographical Society of Japan*, 47(4):152–168.

Walford, H., White, N., and Sydow, J. (2005). Solid sediment load history of the Zambezi Delta. *Earth and Planetary Science Letters*, 238(1-2):49–63.

Walsh, E. M., Ingalls, A. E., and Keil, R. G. (2008). Sources and transport of terrestrial organic matter in Vancouver Island fjords and the Vancouver-Washington margin: a multiproxy approach using δ ^{13}Corg, lignin phenols, and the ether lipid BIT index. *Limnology and Oceanography*, 53(3):1054–1063.

Wang, W.-L. and Wang, L.-C. (2008). Reconstruction of oceanographic changes based on the diatom records of the Central Okhotsk Sea over the last 500000 years. *Terrestrial, Atmospheric and Oceanic Sciences*, 19(4):403.

Wang, Y. V., Larsen, T., Leduc, G., Andersen, N., Blanz, T., and Schneider, R. R. (2013). What does leaf wax δD from a mixed C_3/C_4 vegetation region tell us? *Geochimica et Cosmochimica Acta*, 111:128–139.

Ward, N. D., Keil, R. G., Medeiros, P. M., Brito, D. C., Cunha, A. C., Dittmar, T., Yager, P. L., Krusche, A. V., and Richey, J. E. (2013). Degradation of terrestrially derived macromolecules in the Amazon River. *Nature Geoscience*, 6(7):530–533.

Warnock, J. P., Bauersachs, T., Kotthoff, U., Brandt, H.-T., and Andrén, E. (2017). Holocene environmental history of the ångermanälven estuary, northern Baltic Sea. *Boreas*, 47(2):593–608.

Weijers, J. W. H., Panoto, E., van Bleijswijk, J., Schouten, S., Rijpstra, W. I. C., Balk, M., Stams, A. J. M., and Damsté, J. S. S. (2009). Constraints on the biological source(s) of the orphan branched tetraether membrane lipids. *Geomicrobiology Journal*, 26(6):402–414.

Weijers, J. W. H., Schouten, S., Hopmans, E. C., Geenevasen, J. A. J., David, O. R. P., Coleman, J. M., Pancost, R. D., and Damste, J. S. S. (2006). Membrane lipids of mesophilic anaerobic bacteria thriving in peats have typical archaeal traits. *Environmental Microbiology*, 8(4):648–657.

Weijers, J. W. H., Schouten, S., van den Donker, J. C., Hopmans, E. C., and Damsté, J. S. S. (2007). Environmental controls on bacterial tetraether membrane lipid distribution in soils. *Geochimica et Cosmochimica Acta*, 71(3):703–713.

Weldeab, S., Emeis, K.-C., Hemleben, C., and Siebel, W. (2002). Provenance of lithogenic surface sediments and pathways of riverine suspended matter in the Eastern Mediterranean Sea: evidence from $^{143}Nd/^{144}Nd$ and $^{87}Sr/^{86}Sr$ ratios. *Chemical Geology*, 186(1-2):139–149.

Weldeab, S., Lea, D. W., Oberhänsli, H., and Schneider, R. R. (2014). Links between southwestern tropical Indian Ocean SST and precipitation over southeastern Africa over the last 17kyr. *Palaeogeography, Palaeoclimatology, Palaeoecology*, 410:200–212.

Wen, M., Au, J., Gniwotta, F., and Jetter, R. (2006). Very-long-chain secondary alcohols and alkanediols in cuticular waxes of Pisum sativum leaves. *Phytochemistry*, 67(22):2494–2502.

Willmott, V., Rampen, S. W., Domack, E., Canals, M., Damsté, J. S. S., and Schouten, S. (2010). Holocene changes in Proboscia diatom productivity in shelf waters of the north-western Antarctic Peninsula. *Antarctic Science*, 22(01):3.

Wolff, C., Kristen-Jenny, I., Schettler, G., Plessen, B., Meyer, H., Dulski, P., Naumann, R., Brauer, A., Verschuren, D., and Haug, G. H. (2014). Modern seasonality in Lake Challa (Kenya/Tanzania) and its sedimentary documentation in recent lake sediments. *Limnology and Oceanography*, 59(5):1621–1636.

Wuchter, C., Abbas, B., Coolen, M. J. L., Herfort, L., van Bleijswijk, J., Timmers, P., Strous, M., Teira, E., Herndl, G. J., Middelburg, J. J., Schouten, S., and Damste, J. S. S. (2006). Archaeal nitrification in the ocean. *Proceedings of the National Academy of Sciences*, 103(33):12317–12322.

Xu, Y. and Jaffé, R. (2009). Geochemical record of anthropogenic impacts on Lake Valencia, Venezuela. *Applied Geochemistry*, 24(3):411–418.

Xu, Y., Simoneit, B. R. T., and Jaffé, R. (2007). Occurrence of long-chain n-alkenols, diols, keto-ols and sec-alkanols in a sediment core from a hypereutrophic, freshwater lake. *Organic Geochemistry*, 38(6):870–883.

Yamamoto, M., Ficke, K., Baas, M., and de Leeuw, J. W. (1996). Molecular paleontology of the earliest danian at Geulhemmerberg (the Netherlands). *Geology Mijnbouw*, 75:255–267.

Yasuda, T., Asahara, Y., Ichikawa, R., Nakatsuka, T., Minami, H., and Nagao, S. (2014). Distribution and transport processes of lithogenic material from the Amur River revealed by the Sr and Nd isotope ratios of sediments from the Sea of Okhotsk. *Progress in Oceanography*, 126:155–167.

Zell, C., Kim, J.-H., Abril, G., Sobrinho, R. L., Dorhout, D., Moreira-Turcq, P., and Damsté, J. S. S. (2013a). Impact of seasonal hydrological variation on the distributions of tetraether lipids along the Amazon River in the central Amazon basin: implications for the MBT/CBT paleothermometer and the BIT index. *Frontiers in Microbiology*, 4.

Zell, C., Kim, J.-H., Dorhout, D., Baas, M., and Damsté, J. S. S. (2015). Sources and distributions of branched tetraether lipids and crenarchaeol along the Portuguese continental margin: implications for the BIT index. *Continental Shelf Research*, 96:34–44.

Zell, C., Kim, J.-H., Hollander, D., Lorenzoni, L., Baker, P., Silva, C. G., Nittrouer, C., and Damsté, J. S. S. (2014). Sources and distributions of branched and isoprenoid tetraether lipids on the Amazon shelf and fan: implications for the use of GDGT-based proxies in marine sediments. *Geochimica et Cosmochimica Acta*, 139:293–312.

Zell, C., Kim, J.-H., Moreira-Turcq, P., Abril, G., Hopmans, E. C., Bonnet, M.-P., Sobrinho, R. L., and Damsté, J. S. S. (2013b). Disentangling the origins of branched tetraether lipids and crenarchaeol in the lower Amazon River: implications for GDGT-based proxies. *Limnology and Oceanography*, 58(1):343–353.

Zeng, Y. B., Eglinton, G., Robinson, N., and Cassani, F. M. (1988). Long-chain alkane-diol and alkan-keto-1-ol components of the Messel kerogen. *Courier Forschungsinstitut Senckenberg*, 107:53–71.

Zhang, J., Kobert, K., Flouri, T., and Stamatakis, A. (2014). PEAR: a fast and accurate Illumina Paired-End reAd mergeR. *Bioinformatics*, 30(5):614–620.

Zhang, Z., Metzger, P., and Sachs, J. P. (2011). Co-occurrence of long chain diols, keto-ols, hydroxy acids and keto acids in recent sediments of Lake El Junco, Galápagos Islands. *Organic Geochemistry*, 42(7):823–837.

Zhu, F., Massana, R., Not, F., Marie, D., and Vaulot, D. (2005). Mapping of picoeucaryotes in marine ecosystems with quantitative PCR of the 18S rRNA gene. *FEMS Microbiology Ecology*, 52(1):79–92.

Zhu, X., Jia, G., Mao, S., and Yan, W. (2018). Sediment records of long chain alkyl diols in an upwelling area of the coastal northern South China Sea. *Organic Geochemistry*, 121:1–9.

Aknowledgments

I want to thanks the person without whom all that would not have happened, Stefan I am so grateful for the chance of doing my PhD with you. You have been a great guide throughout the years and you taught me to work hard but efficiently, to be curious of everything, critical about my work (and others') and happy of all results. Let's say that your corrections of my manuscripts were necessary and I hope I got a bit better at my grammar than before... You were always available which is more than I expected, either for little stupid questions or longer talks, I could always pass by. I also want to thanks Jaap Sinninghe Damsté for his great help and guidance, either during conferences or with my papers. I had the chance to supervise a master student thanks to you, it was such an interesting experience. Discussions with you are always intense and I got out of them knowing so much more than before. I hope your health will improve soon.

I want to thanks all the BGC and later on MMB department for the help and support during these 4 years. A special thanks to Jort who have supplied me with endless precolumn changing and beer talks, Marcel for the interesting isotope conversations, Anchelique and Denise for the guidance through the lab. I am grateful to Ellen, Monique, Caglar, and the whole MMB team for all their technical help. Thank you Sergio, Maartje and Laura for your help in the molecular lab. Jan, thank you for taking the time to help me with the introduction of this thesis and the English and Dutch summaries.

I am also thankful to the people I got to meet during conferences, for the exciting debates, the inspiring stories and new ideas, especially, Sabine, Cindy, Helen, Marisa, Julia and Rich. Also a big thanks to all my collaborators without whom this work would have been much reduced, Francien, thanks to you I had the opportunity to work on so many great samples, this thesis would have been much more reduced without you. Our shared container during the GoMex cruise was sure the most efficient!

I would like to thanks my committee for taking the time to review this thesis.

I had the chance to go on three scientific cruises during my PhD and I warmly thanks the chief scientists for these amazing opportunities and the Pelagia crew for the help and fun. I also met some amazing persons during these cruises, Niels, Wytze, Olga, Tim, Wim-Jan, Inno, Peter L. and Peter K., thanks for the card games and great time.

Laura, dear deskmate, citymate, partymate... I could not have had a better person to share my office with, I will miss our science talk but also our drama chat. You are a great scientist and an even greater person, thank you for showing me Den Helder, the Netherlands and to have always been there for me. You will forever be my princess Av.

Gabs, darling, what could I say that I did not tell you? Thanks to be my friend, my paranymph and to share so much time with me, and as much science. Let's not forget all the dragrace, biking, beer festivals and more that we have shared. From Destiny, with love.

Darci, you are the sunshine in my life. I wish I could not leave you but you have been such an inspiration that I want to continue and succeed in science to meet you again for collaborations and conferences. You are always welcomed to join me for the wine festival, you know the dates. Please continue challenging yourself!

Alice, merci ma belle. The year we shared that house was amazing, we were there at the same time maybe 4 months in total but they were full of laughter, smile, songs, wines, beers, tears... all what you need to live. You are an amazing person, I envy your flamboyance, you know how to live! Notre bar était le meilleur...

Nicole, Saara, Diana, Alejandro I am so happy to have known you, please continue to be so friendly and chitchatting, and also thanks for all the special dinners. Thanks for the hugs, thanks for your warm smile anytime I saw you.

Zeynep, Marijke my diol ladies, thanks for helping me throughout my PhD, our discussions were always interesting and necessary. Zeynep, 2 cruises, conferences, beds and some years together made me realize the amazing person that you are, I wish you all luck with your proposals. I hope we can still share a house in the

future for conferences or holidays. Marijke, be confident! You're so good =) I also won't forget your love of wine.

Didier, let's go diving!! And also drinking, biking, boxing and talking. I had such funny times with you, for me your name equals a little house lost in France, as well as the Red Sea, the Caribbean and a house full of random things, quite a good mix! Let's continue diving, I still miss the mantas.

Thanks to the Den Helder people for the fun evenings, Sabine, Wim, Michelle, Rob, Marine... and to the Texel people for the occasions to stay on the island and nice time, Esmée, Rick, Yvo...

Merci maman, papa d'avoir toujours été là pour moi et de m'avoir poussé à réussir. Vous m'avez donné l'occasion de faire ce que je voulais. Merci d'être venu me voir si loin et si froid, je pense que ça vous a plu à la fin. Papi, mamie, Catherine, merci des petits mots, des encouragements et de m'avoir toujours ouvert la porte si je passais en voiture dans le coin. Vous m'avez beaucoup manqué pendant ces 4 ans.

Hugues, alors quoi, elle est pas fini ta thèse ? Va falloir écrire un peu plus ! Bon courage pour la fin, j'attends avec impatience ta soutenance.

Céline, Jean, Fanny, Thibault, Ulysse, nos emails matinaux ont été une motivation pour me lever pendant tout ce temps. Vous êtes des personnes extraordinaires, et même si le travail nous éloigne peu à peu, vous êtes toujours présents dans mes pensées. Amélie, on se voit peu mais je t'ai toujours dans mes pensées lors des rangements de soirées... Je te souhaite plein de réussite dans ta fin de thèse.

Sylvain, merci de m'avoir toujours encouragée et supportée.

Lissie, sweet darling, we met on a cold island, during a stressing moment, with only clouds at the horizon but we managed! You can do anything and be the sweetest person. Thanks for always answering your phone for me, even if we call each other every other month. I really value our friendship and the time we spend together. Robin!! I am so happy to have met you, you are so interesting and even though your moving to the end of the world (yes that's Koudekerk) made things harder to see each other we continued during *gezellig* BBQs and beer festivals. Let's keep that up. Nikolas, Ségolène, PY, Kemal, Gizem, meeting you was great and resulted on quite crazy times. I have such great memories from the Potvis and our amazing parties. I hope we can all meet up again on Texel, let's plan a reunion!

Oscar, missing you everyday...

About the author

Photo credit @ Wim-Jan Boon

Julie Lattaud was born on December 2^{nd} 1990 by a cold winter day in Chalon sur Sâone, France. She graduated from high school in 2008 and integrated the classes prépa at the Lycée du Parc, after three intense years she eventually entered the Ecole Normale Supérieure de Lyon (ENSL) and Université Claude Bernard Lyon 1 and obtained her Bachelor (2012) and Master (2014). Her specialty was paleontology, paleoclimate and paleoenvironments, she did several internships and her master thesis was on the reconstruction of the paleoclimatic history of the Lac Pavin (France) using biomarkers. She followed her master by a traineeship at the Royal Netherlands Institute for Sea Research (NIOZ) on the paleoclimatic reconstruction of the Okhotsk Sea using biomarkers. Her PhD was entitled "Source and proxy potential of long-chain diols in marine and continental settings" under the supervision of Stefan Schouten and Jaap Sinninghe Damsté.

List of publications:

- Balzano S.*, Lattaud J., Rampen S., Villanueva L., Brussaard C., van Bleijsweijk J., Bale N., Sinninghe Damsté J. S., and Schouten S. (2018): A quest for the biological sources of long chain alkyl diols in the western tropical North Atlantic Ocean. Biogeosciences, 15, 5951-5968.

- Lattaud J.*, Lo L., Huang J. -J., Chou Y-M., Gorbarenko S. A., Sinninghe Damsté J. S., and Schouten S. (2018): A comparison of Late Quaternary paleotemperature records of the central Okhotsk Sea based on organic proxies. Paleoceanography and Paleoclimatology, 33, 732–744.

- Lattaud J.*, Kirkels F., Peterse F., Freymond C., Eglinton T. I., Mollenhauer G., Balzano S., Villanueva L., van der Meer M. T. J., Hopmans E. C., Sinninghe Damsté J. S., and Schouten S. (2018): Distribution and sources of long chain diols in rivers. Biogeosciences, 15, 4147-4161.

- Lo L.*, Belt S., Lattaud J., Friedrich T., Zeeden C., Schouten S., Smik L., Timmermann A., Cabedo-Sanz P., Huand J. -J., Zhou L., Ou T. -H., Chang Y. -P., Wang L.-C., Chou Y. -M., Shen C. -C., Chen M. -T., Wei K. -Y., Son S. -R., Fang T. -H., Gobarenko S. A., Wang W. -L., Lee T. -Q., Elderfield H., and Hodell D. A. (2018): Precession and atmospheric CO_2 modulated variability of sea ice in the central Okhotsk Sea since 130,000 years ago. Earth and Planetary Science Letter, 488, 36-45.

- Lattaud J.*, Kim J. -H., De Jonge C., Zell C., Sinninghe Damsté J. S., and Schouten S. (2017): The C_{32} alkane-1,15-diol as a tracer for riverine input in coastal seas. Geochimica and Cosmochimica Acta, 202, 146-158.

- Lattaud J.*, Dorhout D., Schulz H., Schefuss E., Castaneda I., Sinninghe Damsté J. S., and Schouten S. (2017): The C_{32} alkane-1,15-diol as a proxy of late Quaternary riverine input in coastal margins. Climate of the Past, 13, 1049-1061.

Submitted:

- Lattaud J.*, Lo L., Zeeden C., Liu, Y. -L., Song S. -R., van der Meer M. T .J., Sinninghe Damsté J. S., and Schouten S. : Past environmental changes in the Sea of Okhotsk during the last 1.5 Ma reconstructed using long-chain diol proxies. Submitted to Organic Geochemistry.
- De Bar M. W.*, Weiss G.M., Yildiz C., Rampen S., Lattaud J., Bale N., Mienis F., Brummer G. -J., Schulz H., Rush D., Kim J.-H., Donner B., Knies J., Luckge A., Stuut J. -B., Sinninghe Damsté J. S. and Schouten S.: Global temperature calibration of the long chain diol index in marine surface sediments. Submitted to Geochimica and Cosmochimica Acta.
- Metzger E. M.*, van Erk M., Schouten S., Lattaud J., Erdem Z., and Reichart G. -J.: Arabian Sea salinity and temperature changes over the last glacial cycle and impact on the oxygen minimum zone. Submitted to Palaeogeography, Palaeoclimatology, Palaeoecology.

In preparation:

- Erdem Z.*, Lattaud J., van Erk M., Mezger E., Reichart G. -J., Luckge A., Sinninghe Damsté J. S., and Schouten S.: Applicability of the long chain diols as sea surface temperature and upwelling proxies in the Arabian Sea. To be submitted Paleoceanography and Paleoclimatology.
- Lattaud J.*, van Bree L., Balzano S., Peterse F., van der Meer M. T. J., Hopmans E. C., Villanueva L, Sinninghe Damsté J.S., and Schouten S.: Production of long-chain diols in lakes: sources and controls. To be submitted to Biogeosciences.
- Schreuder L.*, van der Linden A., Lattaud J., van Erk M., van der Meer M., Reichart G. -J, Hopmans E. C., Sinninghe Damsté J. S., and Schouten S.: Constraints on levoglucosan as a biomass burning marker in marine sediments: A case study from the Arabian Seas. To be submitted to Climate of the Past.

Now time for another adventure